Advancements of free fall penetrometer data-processing and their ground proving in regional sediment (re-) mobilisation studies in New Zealand

Doctoral Thesis

Submitted for the doctoral degree in natural science at the Faculty of Geoscience
at University of Bremen

By

Roko Robert Roskoden

University of Bremen January 2020

Abstract

In the last century, the necessity to understand geotechnical soil parameters has become of significance importance; not only for fundamental research questions but also for every day civil engineering purposes. While there are theoretical geotechnical soil mechanics as well as numerical assessments, most geotechnical investigations of the soils are based on empirical studies. The later is categorising the soil and correlating it to its physical properties. The cone penetration test has been recognised as an established testing techniques, developing over the last century. Developments have occurred in the technical department, including a transition from a mechanical to electrical cone penetration tests and the integration of side friction as well as pore pressure measurements. Additionally, the interpretational capabilities have been extended by the usage of controlled testing for example by the development of cone penetration calibration chamber tests. The numerous empirical studies in the cone penetration testing has enabled the correlation of the primary measurements of the cone penetration (cone resistance, sleeve friction, and pore pressure etc.) to other geotechnical properties like undrained shear strength, friction angle and shear wave velocity. Besides developments in the standard cone penetration tests, it has also become clear that the cone penetration test can be combined with many other data acquisition procedures. Common combinations include the seismic, magnetic, electric resistivity, video, and sampler cone penetration tests. Significant progress with the penetration testing was achieved in the 1970's when the need for off-shore $CPTu$ applications emerged.

The deployment of standard marine cone penetration devices requires an off-shore sea rig to provide the necessary force for seafloor soil penetration. Research has demonstrated that the standard marine devices deform the uppermost deposits, whose physical properties are vital to aquatic related objectives. Such objectives are: (1) coastal protection projects, (2) sedimentary transport, (3) mining, (4) drilling foundations, (5) underwater pipelines as well as cables and tubes, (6) failure mechanism, (7) channel dredging, and (8) anchoring (other factors exist). Hence, dynamic penetration systems have been developed, which penetrate the aquatic soil with its own momentum via a free fall or semi-free fall mode. Evidently, the biggest advantage of such penetration campaigns is the enhanced deployment rate when compared with the standard cone penetration test resulting in financial benefits. In particular, the deployment via the pogo-style decreases acquisition time and thus research costs.

Following the given list from above and considering the dangers of local sea level rise in the course of climate change, the most prominent objective will be the geotechnical investigation of coastal areas. Unfortunately, neither standard nor the free fall cone penetration systems are capable to test remotely in logistically challenging areas such as intertidal areas. Only the portable free fall cone penetration systems are able to overcome the restriction of the standard and free fall cone penetration lances. However, portable penetration lances have one big disadvantage: Most portable lances cannot measure the resistance forces directly. Consequently, many geotechnical analyses like standard soil behaviour type estimations are not possible with portable penetration lances. The total resistance estimated via the measurement of the penetrometers acceleration or deceleration. Additionally to the shortcomings in the measurements of the resistance forces, all free fall penetration systems show clear disadvantages

in the pore pressure data acquisition. Firstly, the pore pressure data is yet uncorrected for penetration rate effects. Secondly, the dissipation test is often not applied in a free fall campaign because it enhances the data acquisition time especially when during deployments in low permeability soils.

In this dissertation, five first author manuscripts, of which four have already been submitted or published, investigate the shortcomings mentioned above. Hence, this thesis aims to improve the processing procedures of free fall penetration tests to assess sediment (re-) mobilisation processes. Furthermore, this dissertation aims to identify geotechnical soil properties, which can be used as a proxy to monitor the remobilisation potential of sediments in coastal areas.

For this purpose, a free fall calibration test has been designed to develop a processing technique, which 1) allows the estimation of cone resistance and sleeve friction from acceleration data, and 2) approaches the issues of the pore pressure rate corrections in a first attempt. The results from the free fall calibration tests have been utilised and verified in a local field study in the Firth of Thames, New Zealand. This includes first attempts to estimate the (re-)mobilisation potential of the local sediment by correlating the portable resistance forces to the geotechnical properties such as the coefficient of consolidation. In particular, the change in the consolidation potential was used to identify the interplay between the local floras (the mangrove forest) and the dewatering processes in the soil.

Furthermore, a sophisticated and autonomous dissipation test model was developed to extrapolate short time dissipation tests in the field instantaneously. The autonomous model is termed *ad hoc model*. Its advantages lay up on its extrapolation potential and its autonomous variable analysis of the rigidity index and the coefficient of consolidation without any prior estimation of soil properties. The model was tested in the field on the peninsula Omokoroa at the Bramley Drive landslide, New Zealand. Four dissipation tests were carried out at depth of ~19, ~22, ~23, and ~26 m. The tests have been utilised and truncated to test the actual extrapolation potential and to identify the hydrogeological properties of the study area. The four different dissipation depths represent three different dominating halloysite morphologies (tubular, spheroidal and polyhedrons/plates) and have been chosen in order to study the influence of the halloysite morphology microstructure on the hydrogeological behaviour. Here, again, the coefficient of consolidation was used as a proxy to identify the sediment (re-)mobilization potential for the different designated depths.

Zusammenfassung

Im letzten Jahrhundert ist die Notwendigkeit, geotechnische Bodenparameter zu verstehen, nicht nur für grundlegende Forschungsfragen, sondern auch für den Alltag im Bauwesen von Bedeutung geworden. Die geotechnische Beurteilung der Böden basiert auf empirischen Untersuchungen, wobei der Boden kategorisiert und mit physikalischen Eigenschaften in Beziehung gesetzt wird. Der Kegelpenetrationstest ($CPTu$) ist als eine etablierte Prüftechniken anerkannt, die sich im Laufe des letzten Jahrhunderts immer weiterentwickelt hat. Die wichtigsten technischen Weiterentwicklungen waren z.B. der Übergang von einem mechanischen zu einem elektrischen Kegelpenetrationstest und die Integration von Seitenreibungsmessungen. Zusätzlich wurden die Interpretationsmöglichkeiten durch die Entwicklung von Kegelpenetrationskammertests erweitert. Die hierdurch entwickelten zahlreichen empirischeren Studien haben es ermöglicht, die primären Messungen der Kegelpenetration (Kegelwiderstand, Seitenreibung und Porendruck etc.) mit anderen geotechnischen Größen wie der undrainierten Scherfestigkeit, dem Reibungswinkel und der Scherwellengeschwindigkeit zu korrelieren. Neben der Entwicklung in den Standard-Kegelpenetrationstests hat sich gezeigt, dass der Kegelpenetrationstest mit vielen anderen Datenerfassungsverfahren kombiniert werden kann. Gängige Kombinationen sind die seismischen, magnetischen, Widerstands-, Video- und Proben-Kegelpenetrationstests. Bedeutende Fortschritte bei den Penetrationstests wurden in den 1970er Jahren erzielt, als der Bedarf an Offshore $CPTu$-Messungen aufkam.

Der Einsatz von Standard-Marine-$CPTu$ erfordert einen stabilen Unterwasserträger, um die $CPTu$ an den Messort zu fixieren und die erforderliche Kräfte für das Eindringen unter Wasser zu gewährleisten. Studien haben gezeigt, dass die Standard-Marine-$CPTu$s die obersten Ablagerungen mit ihren Eigengewicht verformen und somit deren physikalische Eigenschaften in den gemessenen Daten falsch widerspiegeln. Jedoch sind die geotechnischen Informationen der obersten Ablagerungsschichten für aquatische Ziele von entscheidender Bedeutung. Solche Ziele sind unter anderem: (1) Küstenschutzprojekte, (5) Sedimenttransport, (2) Unterwasser Bergbau- und Bohrfundamente, (3) Unterwasserpipelines sowie Kabel und Rohre, (4) Bodenversagensmechanismen, (6) Kanalausbaggerung und (7) Installation von Verankerungsvorrichtungen (um nur die wichtigsten zu benennen). Daher wurden dynamische Eindringsysteme entwickelt, die im freien oder halbfreien Fall mit Eigenmomentum in die obersten Bodenschichten eindringen. Der größte Vorteil solcher dynamischen Penetrationskampagnen ist offensichtlich die erhöhte Einsatzsrate im Vergleich zum Standard-Kegeleindringungstest. Insbesondere der Einsatz im Pogo-Stil verringert die allgemeine Messzeit und damit die Forschungskosten.

In Anlehnung an die vorher beschriebene Auflistung von oben und unter Berücksichtigung der Gefahren des lokalen Meeresspiegelanstiegs im Zuge des Klimawandels sollte das vorrangige Ziel die geotechnische Untersuchung von Küstengebieten sein. Leider sind weder die Standard- noch die dynamischen Penetrationssysteme in der Lage, abgelegene und logistisch anspruchsvolle geotechnische Ziele wie die Tidengebiete zu testen. Nur der Leichtbau des kinematische Penetrationssystems ist in der Lage, die Beschränkung der Standard- und Freifall-Kegelpenetrationslanzen zu überwinden, und kann somit in jenen abgelegenen Studienorten eigesetzt werden. Kinematische Penetrationslanzen haben aber leider einen großen Nachteil. Viele

geotechnische Analysen, wie z.B. die Abschätzung des geotechnischen Bodentyps und die Korrelationen zwischen dem Kegelwiderstand und z.B. der undrainierten Scherfestigkeit, sind aufgrund der indirekten Abschätzung des Gesamtwiderstandes über die Messung der Penetrationsbeschleunigung bzw. -entschleunigung nicht möglich. Zuzüglich zu jenen Unzulänglichkeiten bei der Messung der Widerstandskräfte weisen alle dynamischen und kinematischen Penetrationssysteme deutliche Nachteile bei der Porendruckerfassung auf. Zum einen sind die Penetrationsrateneffekte bei Porendruckdaten noch nicht korrigiert. Zum anderen ist einer der wichtigsten Tests einer Kegelpenetration der Dissipationstest. Dieser Test ist aufgrund der üblicherweise erhöhten Messrate und der damit verbundenen reduzierten Messzeit in gering durchlässigen Böden oft nicht in einer Freifallkampagne eingeplant.

In dieser Dissertation befassen sich fünf Erstautorenmanuskripte, von denen vier bereits eingereicht oder veröffentlicht wurden, mit den oben genannten Versäumnisse der kinematischen Penetrationslanzen. Ziel der Doktorarbeit ist es daher, die Datenverarbeitung der dynamischen und kinematischen Penetrationstests zu verbessern, um Sediment (Re-)mobilisierungsprozesse besser analysieren und evaluieren zu können. Darüber hinaus sollen im Rahmen dieser Arbeit geotechnische Bodeneigenschaften identifiziert werden, die als Proxy zur Untersuchung des Remobilisierungspotentials von Sedimenten im Küstenbereich verwendet werden können.

Zu diesem Zweck wurde ein Freifall-Kalibrierungstest entwickelt, um die Datenverarbeitungstechnik weiter zu entwickeln, um die 1) die Abschätzung des Kegelwiderstands und der Seitenreibung aus Beschleunigungsdaten zu ermöglichen und 2) die Korrektur des Rateneffekts auf die Porendruckdaten in einem ersten Versuch anzugehen. Die Ergebnisse der Freifallkalibrierungstests wurden in einer lokalen Feldstudie im Firth of Thames, Neuseeland, genutzt und verifiziert. Hier wurden erste Versuche unternommen, das (Re-)Mobilisierungspotential des lokalen Sediments abzuschätzen, indem die kinematischen Widerstandskräfte mit den geotechnischen Eigenschaften wie dem Konsolidierungskoeffizienten korreliert wurden. Insbesondere wurde die Veränderung des Konsolidierungspotentials genutzt, um das Zusammenspiel zwischen der lokalen Flora (dem Mangrovenwald) und den Entwässerungsprozessen im Boden zu identifizieren.

Darüber hinaus wurde ein ausgeklügeltes und autonomes Dissipationstestmodell entwickelt, um Kurzzeit-Dissipationstests im Feld instantan zu extrapolieren. Das autonome Modell wird als *Ad-hoc-Modell* bezeichnet. Seine Vorteile liegen in seinem Extrapolationspotential und in der autonomen variablen Analyse des Steifigkeitsindexes und des Konsolidierungskoeffizienten ohne vorherige Abschätzung der Bodeneigenschaften. Das Modell wurde im Feld auf der Halbinsel Omokoroa am Bramley Drive Erdrutsch, Neuseeland, getestet. Es wurden vier Dissipationstests in einer Tiefe von ~19, ~22, ~23 und ~26 m durchgeführt. Die verschiedene Dissipationtestsdatensätze wurden auf verschiedene Längen gestutzt, um das tatsächliche Extrapolationspotential zu testen. Zusätzlich wurden die hydrogeologischen Eigenschaften des Untersuchungsgebietes ermittelt. Die vier verschiedenen Dissipationstiefen repräsentieren drei verschiedene dominierende Halloysitmorphologien (röhrenförmig, kugelförmig und Polyeder/Platten) und wurden ausgewählt, um den Einfluss der Mikrostruktur der Halloysitmorphologie auf das hydrogeologische Verhalten zu untersuchen. Auch hier wurde der Konsolidierungskoeffizient als Proxy verwendet, um das (Re-) Mobilisierungspotential der Sedimente für die verschiedenen vorgesehenen Tiefen zu ermitteln.

Table of Contents

Prefix

Affiliation of this dissertation

This dissertation was part of the international graduate school between the *Waikato University* (New Zealand) and the *University of Bremen* (Germany). The collaboration was founded in 2009 as the *Integrated Coastal Zone and Shelf-Sea Research* project and is called '*Intercoast'* (*IC*). *IC* is the umbrella for an international research-training group and was funded by the *Deutsche Forschungsgeschellschaft* (*DFG*) until October 2018. The scientific goals in this collaboration are of geoscientific, socio-economic, and legal interest. *IC's* objective is to investigate climate and global changes and their geoscientific, socio-economic, and legal effects on costal and shelf-sea areas. The doctoral thesis at hand, with the project name *IC29*, was hosted in the research group *Marine Geotechnics* and is incorporated into the framework of the research faculty *MARUM – Centre of Marine Environmental Sciences*.

Integration of this dissertation in a scientific framework and its main objective

The *IC*-proposal initially entitled the *IC29*-project '*Sediment stability and (re)mobilisation in coastal areas of Germany and New Zealand*' and integrates the project in the defined overall theme '*Pulses of Coastal Sediment Mobilisation – Causes, Consequences and Mitigation*'. The project, as suggested by the proposal, is related to the projects of the second *InterCoast*-cohort *IC28, 30, 31,* and *IC40_NZ*. The proposal description states the following tasks:

- To investigate short-term extraordinary events such as rainfall or spring tide events in coastal areas and their strong impact on coastal depositional processes and budgets.
- To acquire *in situ* data to reveal important insights into the seabed stability and its environmental impacts to support the numerical studies with *in situ* data to improve modelling results.
- To assess such issues via numerical simulations.

IC29 was supposed to build on its predecessors *IC10_I* ('*Effects on the strain rates effects on pore pressure signals*') and *IC10_II* ('*Rate-dependent geotechnical testing in areas of marine bedforms and mass transport*') to focus on two main objectives:

- To gain a deeper insight into temporal and seasonal variations of extraordinary events.
- To get a reliably assess of their impact on coastal depositional processes and budgets, in estuarine ecosystems.

However, given that the earlier projects *IC10_I* and *IC10_II* changed their research foci, the objectives for *IC29* were also slightly adjusted to the following title:

'*Processing advancements of the pore pressure and free fall penetrometer data and its ground proving in two regional studies in New Zealand'*.

The three sub-projects of this dissertation are therefore:

1) The free fall penetration rate corrections and acceleration analysis,

2) The evaluation of the effect of the mangrove forest on the sediment stability, the consolidation processes, and the drowning risk assessment of the mangrove forest in the Firth of Thames, New Zealand, and,
3) The integration of a new dissipation test model for the analysis of the dissipation behaviour of the different halloysite morphologies and its trigger mechanism on slope failure in Omokoroa, New Zealand.

Admittedly, if all sub-projects are considered independently, one is to dismiss easily the constructional framework, which ties these three inherently different studies together.

The scientific objectives of *IC29* are to improve free fall penetration tests and to assess climate and global changes in local field studies in New Zealand. The improvements of the free fall penetration tests result in a geometrical algorithm to differentiate the total sediment resistance, into the sediment cone resistance and side friction, and in a numerical model to extrapolate and interpret short-term dissipation data in an *ad hoc* mode. Consequently, the field studies, besides their own single contributions to investigate global and climate effects on a local scale, are there to ground prove the new free fall analysis tools. Hence, the new advancements are considered to be the groundwork for a *new sediment penetration lance*. A penetration lance, which could unite two separate penetration tests, both developed at *MARUM*:

- The Bremer Heat Probe (an in-house development of a Lister-type marine heat probe) to measure heat flows in the sediment and
- *NIMROD*, a kinematic free fall penetrometer, measuring the instrumental acceleration to calculate the ultimate bearing capacity of the sediment

Structure of the thesis

The introduction in this thesis is separated into five parts:

I. *A general motivation* of why geotechnical information of soils and sediments are important for scientific and engineering objectives.

II. *A brief historical review* of cone penetration testing, while introducing the measuring technique itself.

III. The review of the *state of the arts,* a short comparison of standard cone penetration tests versus dynamic free fall penetration tests. Here, emphasis is given to the penetration rate effect. The focus in the end of this section will be laid on the introduction of kinematic penetrometer such as *NIMROD* and the *LIRMETER*, two penetration lances developed at *MARUM*.

    Note: Technical details about the lances such as logger frequencies or sensor sensibilities will not be discussed in detail here to avoid reputational work. For further details about the penetration lances, please see the references given in the corresponding sections.

IV. *The resulting motivation* for this doctoral-thesis. This part will be complemented by addressing the following questions:

    i) Why do we need lightweight penetration tests?

    ii) What are the current needs to improve kinematic penetration tests?

V. *Outline of the Manuscripts*. This part will shortly emphasise the goal of the different studies and indicate the author's responsibilities and contributions for each project.

The five manuscripts themselves will follow directly the introduction. Each manuscript will have a short transitional descriptions (one to two pages), which will relate the manuscript to the current research. Moreover, the descriptions will link each manuscript to the manuscript before, ensuring the overall common theme is not lost. Afterwards, the common conclusions are drawn out of conclusions from each single manuscript. Finally yet importantly, the outlook of this thesis will emphasise how to incorporate the technical advancements in the data processing in current and future free fall penetration devices.

In order to clarify the exact status of each manuscript in a condensed manner I am attaching this additional dissertational publication list, including all given reference numbers, and the status of publication for each manuscript.

1. Manuscript 1
   Analysis of acceleration and excess pore pressure data of laboratory impact penetrometer experiments in remolded overconsolidated cohesive soils
   (first author, published at the CPT'18 (Cone Penetration Testing 2018), 2018, p. 545-550, CRC Press/Balkema, Leiden, NL, ISBN 978-1-138-58449-5)
2. Manuscript 2
   Rapid transition of sediment consolidation across an expanding mangrove fringe in the Firth of Thames New Zealand
   (first author, published at the Geo-Marine Letters, 2019, p. 1-14, DOI:10.1007/s00367-019-00589-9)
3. Manuscript 3
   The usage of incomplete and metadata. Why failing is part of succeeding
   (first author, In Proceedings of the 8th International Geoscience Student Conference, Uppsala, Sweden, 2019. (forthcoming), diva2:1383507, DOI: 10.33063/diva-401520)
4. Manuscript 4
   Evaluation of a new dissipation test model with field data from a slide prone coastal area, New Zealand
   (first author, submitted 02.01.2020 at Canadian Geotechnical Journal, Manuscript ID cgj-2020-0004)
5. Manuscript 5
   Evaluating the hydrogeological properties of the Bramley Drive slide, New Zealand
   (first author, in co-author review process)

Chapter 1:

Introduction

I. The purpose of Cone Penetration Tests

Geotechnical soil parameters as the *ultimate bearing capacity* (q_u, the maximum amount of load of a soil before failure) are of great importance for not only fundamental research questions, but also for every day civil engineering purposes (Nordlund, 1963). The *Tilted Tower of Pisa* best illustrates the importance of thorough soil investigation (or the lack of it). The tower, which was a witness to Galileo Galilei's free fall experiments, became a world heritage site because of differential compaction of the ground causing the tilted nature of the building. The engineers of that time did not acknowledge or know about the significance of the *geotechnical soil properties*, which are indispensable for sustainable infrastructure. Furthermore, and even more important, geotechnical soil properties are not only related to sediment stability questions. Soil properties also help to understand sediment (re-) mobilisation, which may lead to disastrous natural hazards such as sediment mass transports and sediment erosion. Mass transports, as for example landslides, can in turn result into even bigger hazards such as tsunamis if they happen under water, as has highlighted for examples in Canada (Krastel et al., 2016) and New Zealand (Power et al., 2005). Therefore, geotechnical investigations, especially in the aquatic and sub-aquatic realm, are of importance for civil engineering acts (e.g. offshore wind parks), and governmental costal protection projects.

Geotechnical assessments of the soils are based mostly on empirical studies, categorising the soil and correlating its physical properties (e.g. grain size, pore space, or the soils plasticity) to its soil mechanical parameters (e.g. critical slope angle, cohesion and friction) (Casagrande and Fadum, 1940). The soil-stability was found to mostly depend on physical and geotechnical properties such as grain size, coefficient of consolidation, overconsolidation ratio, rigidity index, undrained shear strength, shear modulus, pore pressure, permeability, primary and secondary on the properties cementation, mineralogy and mineral morphology - to only name a few.

Thus, soil properties need to be examined before the design and construction phase of civil engineering projects. The examination should be a combination of *ex situ* (via laboratory experiments), *in situ* and numerical studies. Standard Cone Penetration Tests (*CPTu*) are very feasible, efficient and sophisticated means for *in situ* soil investigations (Lunne, Powell, et al., 1997; Lunne, Robertson, et al., 1997; Robertson, 1990; Stark, 2011; Steiner, 2013). During penetration, the *CPTu* measures the soils sleeve friction (f_s), cone resistance (q_c) and pore pressure (u) [kPa] at given position (u_1, u_2 or u_2, P. Figure 1).

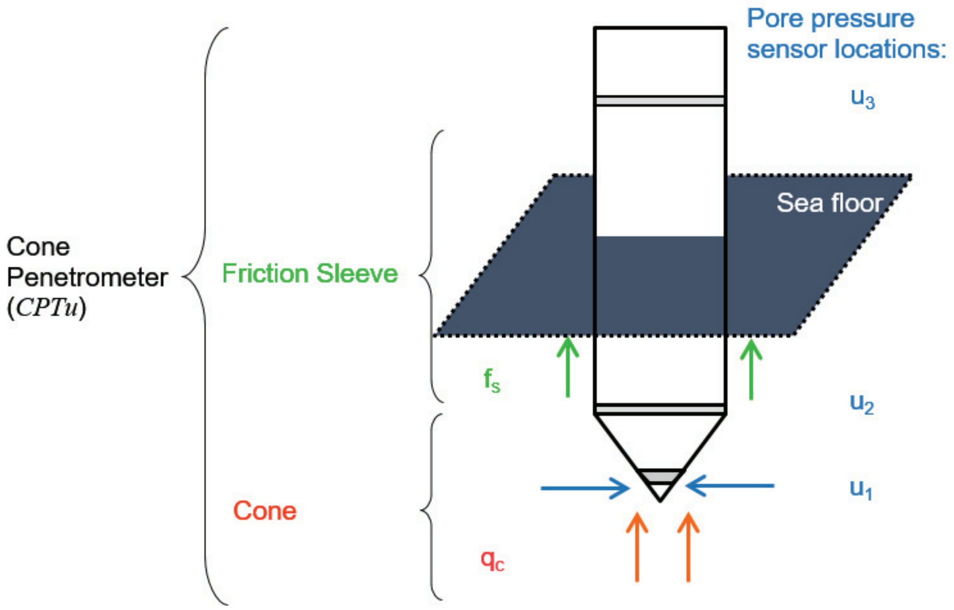

P. Figure 1 Schematic representation of a CPTu *and its nomenclature:* q_c*, cone resistance,* f_s *sleeve friction and* u *the pore pressure and its index numbers one to three, which indicate the possible pore pressure sensor positions (modified after Roskoden (2016))*

The primary measuring parameters yield secondary parameters such as the *friction ratio* (R_f), the *undrain shear strength* (s_u), which are needed to assess for example the soil stability. These parameters will be introduced in the upcoming chapter.

II. Cone Penetration Test (*CPT*) - a historical review

The first *CPT*, simply driven by mechanical forces, was developed at the *Department of Civil Works* in the Netherlands in 1936, and was designed by the Dutch mechanical engineer Barentsen (1936) (Massarsch, 2014; Stegmann, 2007). The device needed men-power to drive the cone into the sediment, while a hydraulic meter was measuring the cone resistance only (Lunne, Powell, et al., 1997). The cone resistance (P. Figure 1) was calculated as the force needed to drive the *CPT* into the soil, divided by the cone area, equation (*EQ*) 1:

$$q_c = \frac{Q_c}{A_c} \qquad 1$$

Where q_c is the cone resistance in [kPa], Q_c is the resistance force at the cone in [N], and A_c is the projected-area of the cone in [m²].

The resistance force was initially measured with a hydraulic meter. The change from mechanical *CPT*- to the electrical *CPT-meters* was done in Berlin by the '*Deutsche Forschungsgesellschaft für Bodenmechanik*' (*Dgebo*) during the Second World War (de Ruiter, 1971; Lunne, Powell, et al., 1997; Stegmann, 2007). The change resolved many uncertainties by enabling a constant penetration rate. Furthermore, the change from analogue to digital cones improved the sensitivity of the instruments. However, the issue of the soil friction was discovered early on by Barentsen (1936) who already described the effects of the friction in his measurement. It took merely another 20 years to utilise the friction as a *CPT* soil parameter. It was Begemann (1953), who added the first ‘adhesion jacket’. It is called *friction sleeve* (P. Figure 1) and hence, the *sleeve friction/skin friction* could be calculated as:

$$f_s = \frac{F_s}{A_s} \tag{2}$$

Where f_s is the sleeve friction in [kPa], F_s is the resistance force at the sleeve in [N] and A_s is the area of the sleeve in [m²]. The possibility to measure the sediment friction gave Begemann (01 August 2018) the opportunity to classify the soil by plotting cone resistance as a function of the sleeve friction. Begemann (01 August 2018) also introduced the *friction ratio* R_f (in %) *EQ* 3:

$$R_f = \frac{f_s}{q_c} * 100 \tag{3}$$

The Dutch company *Fugro*, founded in 1962, developed a new *CPT* in 1965, which set the benchmarks for reference test procedures and standards for further *CPTs*, including for example the *standard penetration rate* (2 cm s^{-1}) and the *standard cone dimensions* (cone area 10cm² or 15 cm², cone angle 60° Lunne, Powell, et al. (1997); Stegmann (2007)).

Because of the introduction of this new parameter and the references procedures, first *CPT* correlations have been possible (Begemann, 01 August 2018; Sanglerat, 1973). These correlations define *soil types* via the *geotechnical soil properties* q_c, f_s, and R_f. The first classification chart correlates the skin friction versus the cone resistance and was developed by Begemann (01 August 2018) (P. Figure 2).

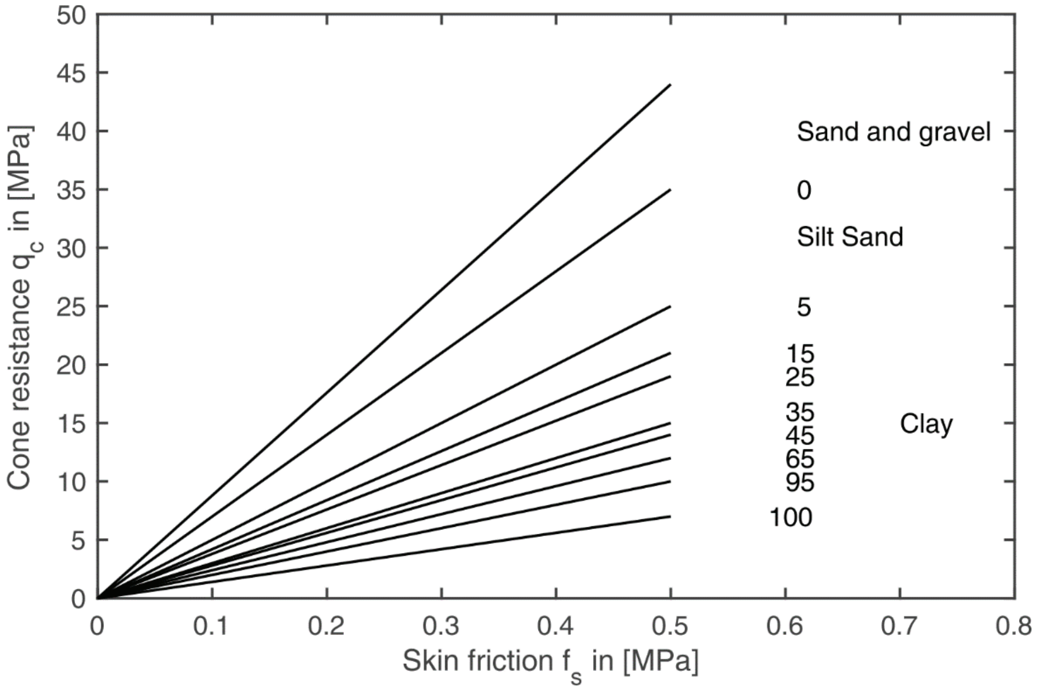

P. Figure 2 First soil classification chart altered after Begemann (1965). The numbers next to each curve indicated the percentage of clay.

Other classification charts followed thereafter, but will be discussed in the chapter $CPTu$ Soil classification below. In 1974, piezometers were integrated for the first time into $CPTs$, which are called $CPTu$ (Lunne, Powell, et al., 1997). The incorporation of the piezometer led to the formulation of the correction of the cone resistance due to pore pressure effects:

$$q_t = q_c + u_2(1 - a) \tag{4}$$

Where q_t is the pore pressure corrected cone resistance in [kPa], u_2 is the measured pore pressure – here at the position 2, behind the cone (P. Figure 1) in [kPa], and a, the net area ratio determined from laboratory calibration test with a typical value between 0.70 and 0.85 (Robertson and Cabal, 2010). From here on $CPTs$ have been modularised many times to combine different tip geometries or measuring techniques. One example is the work of Prof. Campanella in the 1980's, who introduced the seismic CPT ($SCPT$). Further examples can be found in Lunne, Powell, et al. (1997) and Burns and Mayne (1998). A big advancement was introduced in the 1970's when the need for off-shore $CPTu$ applications emerged. Aquatic related applications include: (1) coastal protection projects, (2) sedimentary transport, (3) mining, (4) drilling foundations, (5) underwater pipelines as well as cables and tubes, (6) sediment stability, (7) failure mechanism, (8) sedimentary transport, (9) channel dredging, and (10) anchoring, (11) man-made islands, (other factors exist) (Stegmann, 2007). Due to the different target penetration depths, two general principles have been established: a) the rig based deep penetration $CPTu$ devices, and b) the free fall (also called dynamic) lances shaped $CPTu$ devices for shallow applications.

III. State of the Art

After a brief comparison of the standard $CPTu$ the focus will lie on the kinematic penetration devices, their applications and dynamic processing strategies.

A brief comparison of aquatic static versus dynamic $CPTu$ applications

Comparing both $CPTu$ systems, one should keep in mind that both systems have their advantages and disadvantages. Therefore, the scientific objectives, the time, and the budget at hand determine which system to use best.

The static penetrometer system

The aquatic static $CPTu$ penetrates the soil with a constant velocity of ~2 cm s^{-1}. This allows a coherent data processing similar to land-based applications and facilitates correlation to standard in field or laboratory methods such as *vane shear, full cone, triaxle* or the *undrained shear tests*. Additionally, the data is logged in real-time, which allows an immediate raw-data review during penetration. After lowering the rig to the seabed, the quasi-static penetrometer is then pushed with hydraulic forces into the soil (Lunne, Powell, et al., 1997). The penetration depth can be up to several tens of meters (Lunne, Powell, et al., 1997; Stegmann, 2007). Hence, regarding deep penetration and data reliability, *in situ* static $CPTu$ deployments are the first choice. Therefore, questions about *slope stability* (as long as the slope is not too steep), *ground water influx measurements*, as well as *foundation or anchor installations* are best answered via the static $CPTu$ (Stegmann, 2007). However, the deployment of the static $CPTu$ system in the aquatic realm requires:

1) *A survey vessel* with a crane to deploy the static *CPTu*,
2) *Space on the survey vessel* to store the static *CPTu* and its seabed-rig,
3) *Time*, since, the deployment for one static *CPTu* position includes the controlled, but slow lowering-process of the seabed-rig to the seafloor as well as the slow standard penetration velocity of 2 cm s^{-1},
4) *Enhanced logistical planning*, not only because of 1) to 3), but also due to transporting issues to and from the research vessel, and
5) *The analysis of metocean conditions,* because the deployment via the crane is only safe during a calm sea.

Given the above, the static *CPTu* can be cost- and time-consuming and its deployment is definitely weather dependant (Stark et al., 2014). Furthermore, because of the weight of the static *CPTu*, there can be artefacts in the strength properties in the upper meters of the sediment (Stegmann, 2007; Steiner, 2013). These disadvantages do not apply to dynamic penetrometers.

The free fall penetrometers systems

The free fall penetrometers are lance-shaped (Dayal and Allen, 1973) and vary in size and weight. The length-range is between decimetres (Stoll and Akal, 1999) and a couple of meters as well as between a few kilogram to a couple of hundred kilogram (Kopf et al., 2007). The penetrometer lances are deployed only via a single winch. The deployment is either in a *free fall mode* or in a velocity controlled falling-like mode often referred to as '*winch-mode'*. Thus, the data acquisition for one *CPTu* position is very fast and if the device is deployed in a '*pogo-mode'* (lifting the device only half way up through the water column while transitioning to the next *CPTu*-position) several positions can be tested in half an hour. Furthermore, due to the penetration of the soil via the momentum of the free fall *CPTu* the self-weight artefacts from the standard marine deployment via the seabed rig are averted (Stegmann, 2007). The penetration depth depends on the length of the free fall CPTu-system, the length-weight ratio, and the sediment type, but penetration depth have been reported of up to 10 meters (Stegmann, 2007). Therefore, free fall CPT's are utilised for *marine pipeline* and *cable installations, pockmark investigation, shallow mass wasting triggers* (such as methane hydrate blow outs, or the aforementioned tsunami events e.g. in Canada (Krastel et al., 2016)) or the *investigation of surface mass wasting deposits*. Clear disadvantages are:

1) Most free fall devices have a *concluded data logging system* inside a self-contained pressure housing, allowing no real time data review (Stegmann, 2007).
2) *Penetration rate effects*, due to the enhanced penetration velocity. These effects need to be corrected to create a comparable data outcome to the standard acquisition, because many of the acquired parameters are rate-dependent.
3) *Non-linear penetration-rate profile,* which complicates the penetration correction
4) *Impeded/ more complicated processing* procedures, due to points 2) and 3), but also because of the need to manually pick the soil penetration-times and to apply offset-, penetration velocity and depth analyses with help of the acceleration data (s. Impeded processing procedures for free fall penetration data),
5) *Lack of control* of penetration depth

6) The biggest disadvantage might be the reduced *penetration depth* compared to the static system.

The kinematic/ portable penetration system

Besides the just described free fall penetration lances there also lightweight (mass < 15 kg) penetration lances such as the *XBP-tool* (Stoll and Akal, 1999) *NIMROD* (Stark, 2011), *BlueDrop* (Stark et al., 2014) or *FluMu* (developed at the *MARUM*). Such devices do not measure cone resistance or sleeve friction directly (besides the *FluMu, which has an ultra-sensitive tip resistance sensor*) via strain gauges as the free fall *CPTu* does. Therefore, these lances are also referred to as *portablel kinematic penetrometers*. Kinematic penetrometers, due to their lightweight, are most suitable for extreme time-, cost-efficient, or logistical challenged geotechnical targets. Therefore, their objectives are the *mapping of remote, difficult to access areas* or the *investigation of superficial sediment dynamics and permafrost soils* (Stark et al., 2014; Stark and Kopf, 2011). Disadvantages of the free fall *CPTu* also apply to kinematic penetrometers. Additionally kinematic penetrometers require even a more challenging processing procedure and do not measure side friction.

The most common resistance parameter, which can be derived from the kinematic penetrometer, is the *ultimate dynamic bearing capacity*. Using Newton's second law of motion, the *total resistance force* (F_T), which is needed to decelerate kinematic penetration lances, is:

$$F_T = m * dec \tag{5}$$

with m, the mass of the instrument in [kg] and dec, the deceleration in [m s^{-2}]. The *ultimate dynamic bearing capacity* (q_{ud}) is then derived similar to the cone resistance (*EQ* 1) by dividing the *total resistance force* by the projected cone area *EQ* 6.

$$q_{ud} = \frac{F_T}{A_c} \tag{6}$$

For convenience, *pro* and *cons* of the static and dynamic penetrometers are listed in the following P. Table 1.

P. Table 1 Pros and cons for the three introduced penetration test techniques.

Penetrometer	***Pros***	***Cons***
1. Static	• Real time raw-data review • Direct correlations to standard methods • Reliable data • Depth control • Deeper penetration • No rate correction needed	• In need of a survey vessel with a crane • Usage of a lot of storage space • Time consuming deployment • Logistical issues for instrument transportation • Cost-consuming (due to space, time and logistics) • Weather dependant • Smear of thin layers, • self-weight destroys upper soil information
2. Dynamic	• No logistical issues • More cost-efficient • Fast deployment • Single-winch deployment • Independent of weather conditions • More sensitive to smaller layers,	• In need of a winch • Data logging is concluded • ***Impeded processing procedures,*** ○ Estimation of penetration depth via acceleration data instead of direct measurement of the depth ○ Penetration rate effects ○ Non-linear penetration-rate profile • Lack of control of penetration depth • Small penetration depth compared to the static system.
3. Kinematic	***Same as dynamic, additionally*** • No need of a winch • Access to remote areas due to lightweight	***Same as dynamic, additionally*** • Even greater impediment for processing • No direct measurements of resistance forces • No measurement of side friction

Impeded processing procedures for free fall penetration data

It is important to introduce the processing procedures for the free fall penetrometers. Due to the concluded data logging system and the dependency on the acquisition time, the amount of data produced in one field campaign can be quite big. Hence, on a side note, free fall *CPTu* data can be regarded already as *big data*, which is important to keep in mind for later on. However, the amount of data demands an *acquisition journal* similar to the one shown in P. Table 2 Example table for data journal for a dynamic free fall penetration test campaign..

P. Table 2 Example table for data journal for a dynamic free fall penetration test campaign.

Campaign		***Cruise #***		***Date***	***Scientist***	
Name	***Drop #***	***Time***	***Latitude***	***longitude***	***Winch velocity***	***Notes***

The journal allows the scientist to find the important penetration data in the discrete millisecond time data-pool. The exact processing schema is shown in P. Figure 3.

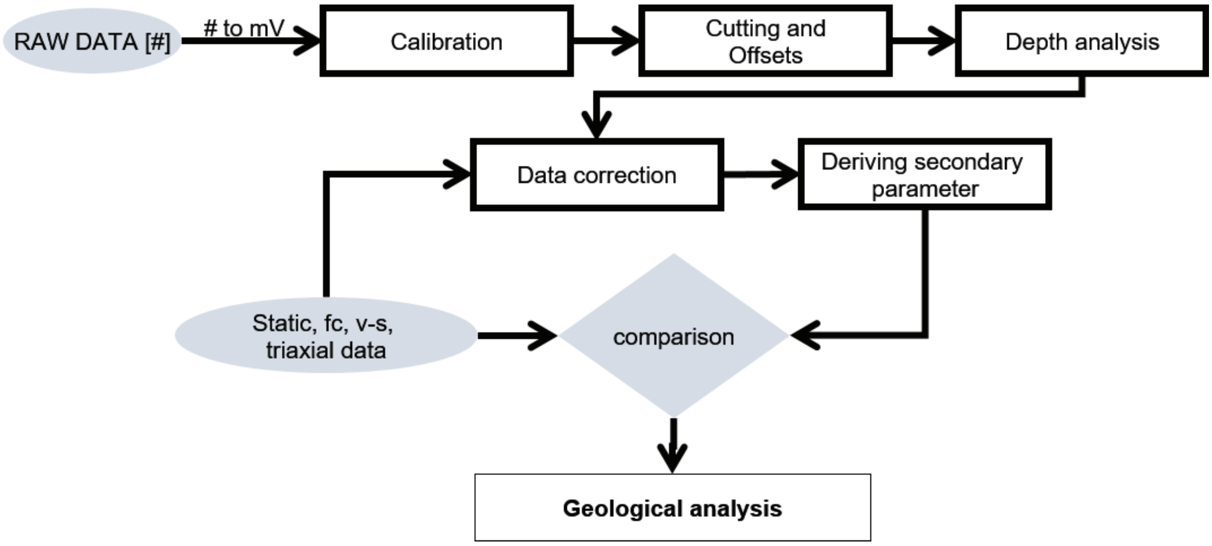

P. Figure 3 Processing schemata for the free fall CPTu. After the data correction via the reference literature data or ex situ data, secondary parameters such as the undrained shear strength, the normalised resistance forces and resistance ratios (to only name a few) are derived and compared to the geotechnical soil parameters (either literature values or laboratory data).

The first processing step is to convert the data from its raw binary state to an ascii-file output. Afterwards, the data must be recalculated from [mV] to soil related physical SI units via specific linear calibration functions, which are either given by the providing company or are tested for in a calibration test. The third step is to cut the data into the right amount of data blocks and to remove offsets. The offsets, such as the hydrostatic water pressure or any artefacts, which may come from the fall through the water column up on penetration, must be subtracted because they obscure the data analysis later on. Nevertheless, no geological information is valid if not connected to a depth profile. Standard *CPTu* are equipped with depth-meter while free fall lances are reduced to analysing accelerometers to determine the penetration velocity (1st integration) and depth (2nd integration) to eventually assign any data point to its corresponding depth.

Penetration depth analysis

In order to receive penetration depth information, the accelerometer-data of the free fall *CPTu* needs to be processed. A double integration of the de/acceleration data over time will first result in information about the penetration velocity and second in a depth profile as shown in

$$d = \iint_{t1}^{t2} dec(t)dt \qquad 7$$

Where d is the penetration depth in [m], dec is the deceleration data and t the time in [s], while t_1 in the start of the penetration and t_2 in the end of the penetration where the de/acceleration should be zero. In order to receive a trustworthy velocity and depth profile, one has to make sure to pick the right t_1 and t_2 values otherwise the penetration depth will be unrealistic. The reliability depends strongly on the metocean conditions, given that the free fall *CPTu* is attached to the recovery cable, the swell might pull on the instrument. Also, and maybe more importantly, low sediment densities may obscure accuracy of the actual t_1 value.

Further acceleration processing

In case of the portable penetrometers, the acceleration data are not only important to generate a depth profile, but also to obtain any soil resistance information as explained above. It is important to differentiate between the various parameters. F_T (*EQ* 5), the total resistance force, is not Q_c, the resistance force at the cone from *EQ* 1, but the total soil resistance force measured for the whole penetration system. This means, that the sediment friction is also included in the estimation of the total resistance F_T, whereas Q_c regards only the forces at the cone itself. Albatal and Stark (2017); Lucking et al. (2017); Mulukutla et al. (2011); Stark et al. (2014) and other argue to neglect the differences between F_T and Q_c due to the small dimensions of the kinematic penetration lances and therefore regard them often as the same for further analysis purposes. As this might be true for the dimensions of the *Bluedrop* (Albatal and Stark, 2017); Lucking et al., 2017), it is not for *NIMROD* (Stark et al., 2014) or other portable penetrometers (Chow et al., 2017).

This is an important and interesting topic, because it also concerns the major application of penetration testing: the *soil classification*. The argumentation from above excludes the kinematic penetrometers from standard soil classification, because the sediment side friction is not considered. Also soil classification charts based on the normalised cone resistance and pore water pressure can hardly be applied for free fall penetrometers (Roskoden, 2016), because the measured pore water pressure is also effected by penetration rate effects (s. subchapter Penetration Rate Correction). Furthermore, the portable lances, which do not measure the cone resistance directly, may additionally overestimate the normalised cone resistance due to the included friction force. The current standard workaround of these kinematic classification issues will be reviewed later on in Free fall *CPTu* soil classification. Furthermore, the topic of kinematic sediment friction is reviewed later in the chapters *Manuscript 1* and *2*. It may be noted here already that the scientific conclusion from these chapters suggests that F_T and Q_c are indeed very different and that F_T can be separated in Q_c and F_s.

Note: Even though, the free fall *CPTu* may measure the cone resistance directly, it should still be considered to also use the acceleration data in order to calculate the resistance forces. The acceleration data logging is not subject to external forces, which might obscure the data or create data gaps. Data gaps may occur in the sleeve friction measurements due the skin effect (Seifert, 2011). However, because the accelerometers are built into the interior part of the penetration lance and not the exterior part data gaps can be filled with the estimated resistance forces from the acceleration data.

Strain or Penetration Rate Correction (PRC)

One of the biggest issues of the dynamic and kinematic penetration lances is the impeded processing procedure and especially its required *penetration rate correction* (*PRC*). Thus, *PRC*-issues are emphasised and discussed in the following sub-chapters.

Empirical studies, incorporating different soil behaviour theories, correlate single geotechnical parameters, for example, the *cone resistance, sleeve friction*, or the *undrained shear strength*, to different strain rates. Such empirical correlations result in analytical regressions, which comprise the strain rate relation in different mathematical formulations. All formulas calculate the *Penetration* or *Strain Rate Factor* (*PRF/SRF*), which is used for the back calculation of increased soil properties to soil properties measured at standard strain rates. For example, the *quasi static cone resistance* is then derived as:

$$q_{\text{c-qst}} = \frac{q_{\text{c-dy}}}{PRF} \qquad 8$$

with $q_{c\text{-}qst}$, quasi static cone resistance and $q_{c\text{-}dy}$, dynamic cone resistance.

Note: The form of *EQ* 8 is also valid for other soil properties.

What is a Strain Rate Effect (SRE)?

The dynamic *CPTu* momentum results in an increased penetration velocity, which in turn will result in *Strain Rate Effects* (*SRE*). Rate effects are a change of resistance forces due to an increase of kinetic energy. Hence, any increased penetration velocity will result in increased soil resistance properties. The first *SRE* have been reported by Richardson and Whitman (1963) and Mitchell (1964). From this point onward, many studies have classified and corrected these *SRE* for the penetration test properties. Evidently, many solutions have been found, but not all penetration properties (for example the pore pressure data) are yet corrected for their *SRE* as shown for example by Roskoden (2016). Therefore, one of the major current focuses of the *SRE* is the correction of the pore pressure values generated by the free fall penetrometers (Chow et al., 2017; Roskoden, 2016; Seifert et al., 2008; Steiner, 2013).

Soil specific Rate coefficients (SSRC)

A soil specific rate coefficient (*SSRC*) is a soil parameter proxy. The proxy reflects the influence of the soil on the correction formula. Therefore, the *SSRCs* work as a mathematical function, which changes the curving of the correlation in relation to the actual soil. Mostly the *SSRC* is lower than one and tends to be higher for more coarse soils.

A list of current studies will be shown after the introduction to three common correction methods. Current correlation laws are the *log-, power-* and *arcsinh-law*. All corrections refer to normalizations of strength ($q_{c\text{-}dy}/q_{c\_ref}$) and velocity parameters ($v_{dy}/v_{\_ref}$), where the index *ref* stands for the reference parameter e.g.

reference velocity 2 cm s^{-1} and *dy* stands for the dynamic penetration data. The common practice for the *PRC* are:

The log-law

The most common *PRC* is the *log-law* developed by Dayal and Allen (1975) *EQ* 9:

$$PRF = \frac{q_{c\text{-}dy}}{q_{c\text{-}qst}} = \mu \, log_{10}\left(\frac{v}{v_{st}}\right) + 1 \quad 9$$

with μ, the non-dimensional soil coefficient, v, velocity during penetration in [m s^{-1}], v_{st}, standard velocity (0.002 m s^{-1}). Note that the *SSRC* not only depends on the soil but also on the considered *CPTu*-parameter (Dayal and Allen, 1975; Steiner, 2013). For example, the *SSRC* for the cone resistance is different than for the undrained shear strength even so the same soil is considered. The correlation is based on the *soil bearing capacity* theory after Terzaghi (1943). The *log-law* is tested and applied on *in situ* and *ex situ* laboratory penetrometer tests (Mulhearn, 2002), and centrifuge and vane shear tests (Aubeny and Shi, 2006; Randolph and Hope, 2004). The downside of the mathematic *log-law* is the divergent behaviour of the *PRF* if $v/v_{\_ref} \leq 1$.

The power-law

The *power-law EQ* 10

$$PRF = \frac{q_{c\text{-}dy}}{q_{c\text{-}qst}} = \left(\frac{v}{v_{st}}\right)^{\beta} \quad 10$$

was introduced by Perlow and Richards (1977) and was shown to work for laboratory experiments such as centrifuges and undrained shear tests (Biscontin and Pestana, 2001; Steiner, 2013). β, similar to μ, is the soil proxy and changes with the investigated soil and with the considered soil parameter at hand. The rheological model, which defines the *power-law* is the *stress-strain-strain rate* relation after Leroueil et al. (1985) (Steiner, 2013).

The arcsinh-law

The *arcsinh-law* is based on studies, which dealt with shear viscosity and chemical reaction rates (Eyring, 1936). The theory was introduced to soil mechanics by Casagrande and Wilson (1951). It is formulated similar to the *log-low* as:

$$PRF = \frac{q_{c\text{-}dy}}{q_{c\text{-}qst}} = \frac{\mu}{ln(10)} \, arcsinh\left(\frac{v}{v_{st}}\right) + 1 \quad 11$$

EQ 10 and 11result in very similar *PRF* values as long as $v/v_{\_ref} > 1$. The formula was shown to work well for free fall *CPTu* rate corrections but is also often applied to centrifuge and vane shear data (Mitchell and Soga, 2005; Randolph and Hope, 2004; Steiner, 2013).

The choosing of the right *SSRC* is either done due to estimations based on a known soil type or via reference or literature data. The reference data can either be *in situ* from for example van shear or static *CPTu*, or *ex situ* from laboratory testing. An estimation in relation to a single reference point or geological information can also help to determine the correct *SSRC*. An iterative approach, as described in Steiner

(2013), to match the reference and free fall data is best to estimate the $SSRC$. Steiner (2013)'s schematic iterative approach is emulated in P. Figure 4.

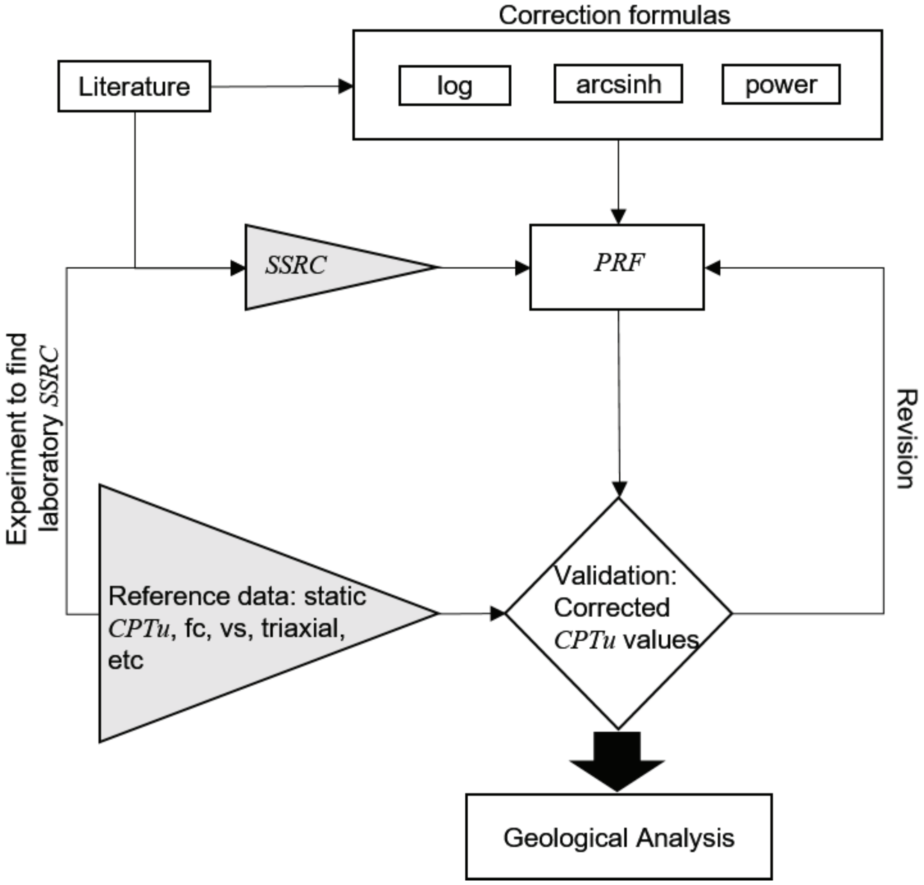

P. Figure 4 Schmeatic overview how to choose the right SSRC to correct the strain rate effects on the dynamoic cone penetration tests altered after Steiner (2013). The SSRC is either estimated in the laboratory or via literature data.

P. Table 3 illustrates that the processor must choose the right correction formula for the study at hand. This is done via the literature research and depends strongly on the reference method. Afterwards, the penetration rate factor is calculated by choosing the right $SSRC$. The strain rate corrected penetration parameters are validated via the data from the chosen or available reference method. If the difference is too severe, the penetration rate factor calculation will be repeated with a different $SSRC$. The new $SSRC$ value can either be a different literature or an experimental ascertained value. In case of a satisfying correction, a geological analysis can be initiated.

P. Table 3 Specific soil rate coefficients listed for different soil types, their reference test and its corresponding parameter to correct from. List from Steiner (2013) altered and extended.

Soil type	***Test type***	***To correcting parameter***	***SSRC μ***	***Reference***
Remoulded clay	*CPT*	q_c	0.03 - 1.50	Dayal and Allen (1975)
Remoulded clay	*CPT*	f_s	0.38 - 0.93	Dayal and Allen (1975)
Kaolinite Clay	*CPT*	q_n	0.10 - 0.15	Randolph and Hope (2004)
Water saturated sand	*CPT*	q_c	0.70 - 1.50	Stoll et al. (2007a)
Quartz and carbonate sand	*Nimrod*	q_u	1.00 – 1.5	Stark et al. (2009)
Clay to silty clay	*CPTu*	q_t	0.13	Steiner et al. (2012)
Clay	*CPTu*	f_s	0.45	Young et al. (2011)
Silt	vane shear	s_u	0.11	Perlow and Richards (1977)
Bentonite – Kaolinite clay	vane shear	s_u	0.15	Biscontin and Pestana (2001)
clay	*XBP*	s_u	0.15	Aubeny and Shi (2006)
Syntactical altered clay from the Hemelinger Marsh	*Free fall calibration test*	Q_c	0.31 and 0.74 (for consolidation pressure 32 kPa and 64 kPa, respectively)	Roskoden et al. (2018)
Soil type	***Test type***	***To correcting parameter***	***SSRC β***	***Reference***
sensitive clay, organic silt, peat	*oedometer*	*pre-consolidation pressure*	0.025 - 0.10	Mesri and Godlewski (1977)
Silt	*vane shear*	s_u	0.080 - 0.13	Perlow and Richards (1977)
Bentonite – Kaolinite clay	*vane shear*	s_u	0.055	Biscontin and Pestana (2001)
Kaolin clay	*centrifuge*	s_u	0.050	Rattley et al. (2008)

Challenges of the PRC

The challenges of the *PRC* are threefold:

1. There is the need of ground proving the dynamic *CPTu*-data (via either laboratory or literature data) to verify that the *PRC* was correct.
2. Undeniably, *CPTu*-lances penetrate not only one, but several different layers of soil, especially if penetration-depths are not superficial as lightweight penetrations are. However, in practice

PRCs are only done with one *PRF* for one penetration site. Hence, the change of layers is not accounted for. Therefore, if corrections are done with only one *PRF*, sediment layers might be under- or overestimated.

3. The biggest issue might be the validation choosing of the right *SSCR* and its validation via either laboratory or literature data.

PRC -Suggestions

A possible, but yet not realised workaround is the *segmentation* of the dynamic *CPTu*-data-sets. Here, the different layers need to be identified before the *PRC* to apply different *PRF* to the penetration site.

CPTu Soil classification

As mentioned before, the major application of cone penetration testing in the classification and identification of soil types. The first real classification started Begemann (01 August 2018) using the cone resistance versus the side friction to determine the soils clay percentages (P. Figure 2).

Standard CPTu *soil classification charts*

The most common *CPTu* soil classification was created by Robertson et al. (1986) and refers to a non-normalized classification chart where the cone resistance and the friction ratio are plotted in a semi-logarithmic plot against each other as shown by P. Figure 5. Note that a tabular description of all soil behaviour types is given in P. Table 4.

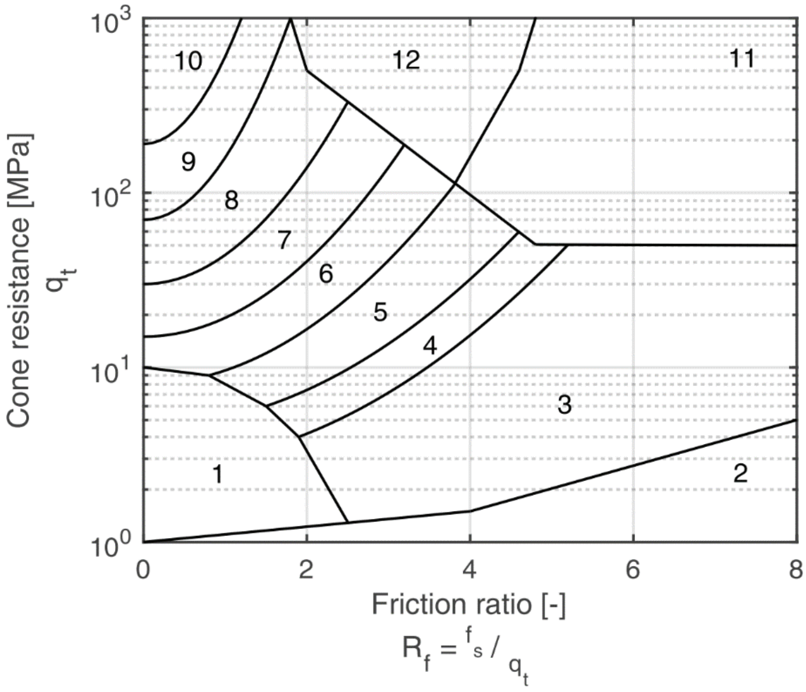

P. Figure 5 Corrected cone resistance plotted over the friction ratio. The figure is the non-normalized soil classification chart by Robertson et al. (1986).

The chart of Robertson et al. (1986) was developed on the base global standard cone penetration data and provides reasonable predictions for *CPTu* sounding up to 20 m penetration depth. Here Robertson et al. (1986) defined 12 different *soil behaviour types,* which also identify general trends in the soil like a change in the *over consolidation ratio, the sediment sensitivity, relative density* and *void ratio*. Later on Robertson (1990) defined a normalised version of his soil behaviour chart. The *normalized cone resistance*, Q_t, is calculated as:

$$Q_t = \frac{q_t - \sigma_{v0}}{\sigma'_{v0}} \qquad 12$$

With σ_{v0}, the vertical overburden stress, σ'_{v0}, the effective vertical overburden stress and q_t, the corrected cone resistance from *EQ* 1. The numerator for *EQ* 12 is termed the *net cone resistance*, q_n. The normalisation makes it easier to compare deeper laying soils with shallow deposited sediments, because the cone resistance is viewed in relation to the effective overburden stress (P. Figure 6). Note that the normalised cone resistance and friction ratio are plotted in double logarithmic chart.

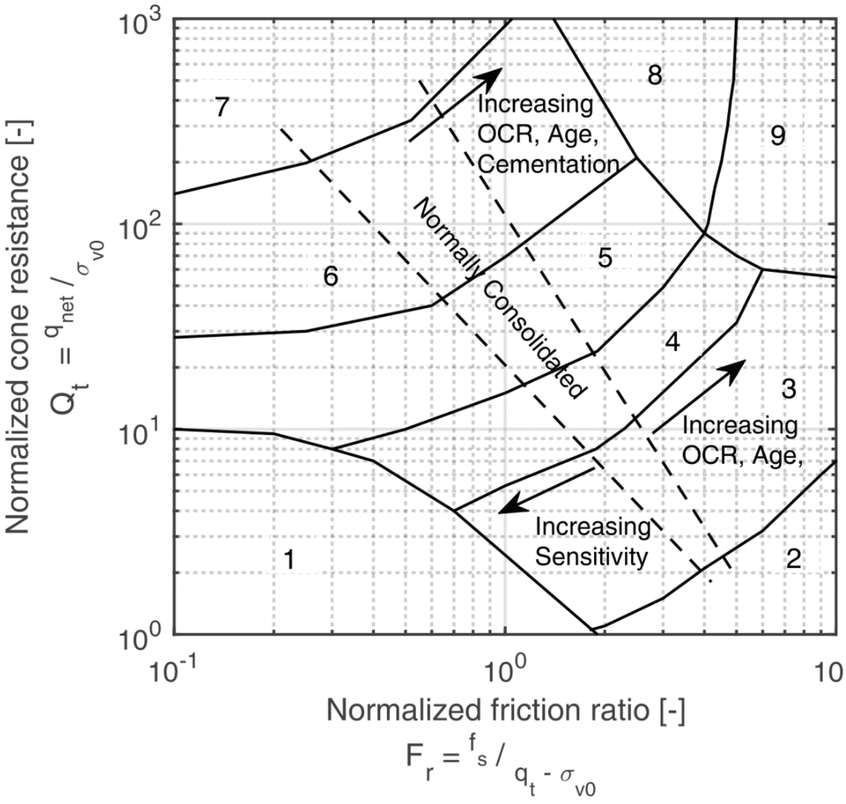

P. Figure 6 Normalised cone resistance plotted over the normalised friction ratio. The figure is the normalized soil classification chart by Robertson (1990). Indicated by arrows are increasing soil properties such as: Sensitivity, overconsolidation ratio (OCR), Age, and Cementation.

For the normalised classification chart, there are only nine soil types defined, but the chart also shows trends for cementation, over consolidation ratio, age, and sensitivity. Besides the utilisation of the friction ratio, Robertson (1990) also introduced the soil characterisation via the *normalised pore water pressure*, B_q, instead of the friction ratio. However, this chart is rarely used because of its low repeatability of the pore pressure measurements. The excess pore water pressure is here normalised by the net cone resistance

$$B_q = \frac{\Delta u}{q_n} \qquad 13$$

with Δu being the excess pore water pressure, which in turn follows

$$\Delta u = u_2 - u_o \qquad 14$$

where u_0 is the equilibrium pore water pressure and u_2 the measured pore water pressure at the pressure sensor position two. The chart plots the normalised cone resistance in a double logarithmic plot over the normalised pore pressure ratio as shown by P. Figure 7.

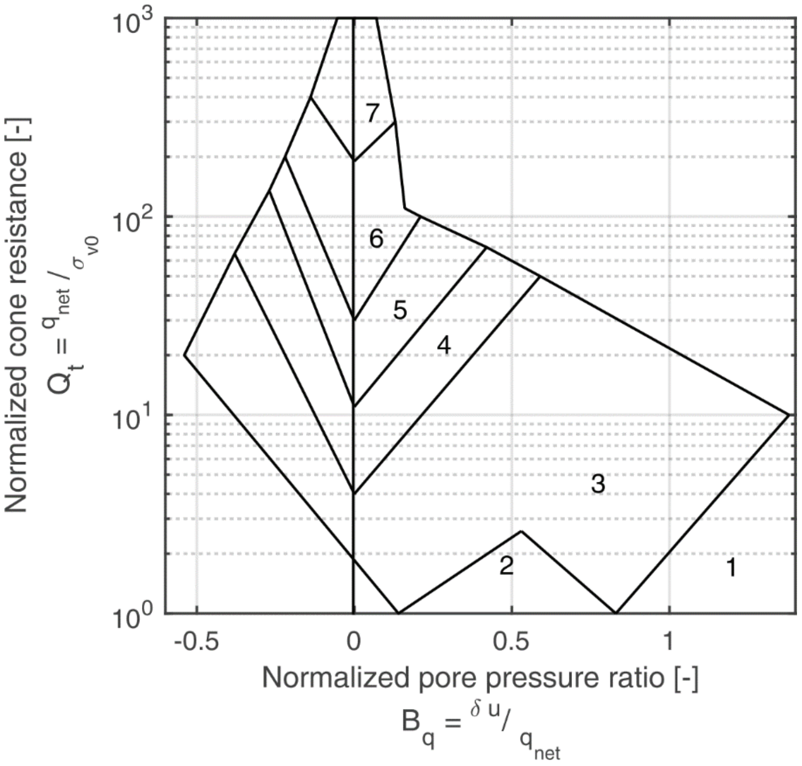

P. Figure 7 Normalised cone resistance plotted over the normalised pore pressure ratio. The figure is the -normalized soil classification chart by Robertson (1990).

Here there are only seven defined soil types, but the soil types are the same as for the normalised cone resistance - friction ratio chart. The recommendation of Robertson and Cabal (2010) is to use both charts if possible. Evidently, both charts my result in different soil classifications. However, Robertson and Cabal (2010) argue that the defined classes are *soil behaviour types* and therefore not the same as the soil classes defined by other geological disciplines such as sedimentology. This means a certain soil behaviour type will react as indicated by the charts, even though grain size analysis may suggest a different sedimentological description of the soil itself. It also means that both charts may suggest different soil behaviour types. These different classifications are not exclusive, but are to be used in parallel. So as an example if one charts suggests soil type four and the other five, than the answer would be a clayey silt sand mixture (compare P. Figure 6, P. Figure 7 and P. Table 4).

P. Table 4 Soil behaviour type description after Robertson et al. (1986) and Robertson (1990).

No.	***Non-normalised***	***Normalised***
1	Sensitive fine grained	Sensitive fine grained
2	Organic material	Organic soils - peat
3	Clay	Clay – silty clay to clay
4	Silty clay to clay	Silt mixtures – clayey silt to silty clay
5	Clayey silt to silty clay	Sand mixtures – silty sand to sandy silt
6	Sandy silt to clayey silt	Sands – clean sand to silty sand
7	Silty sand to sandy silt	Gravelly sand to dense sand
8	Sand to silty sand	Very stiff sand to clayey sand#
9	Sand	Very stiff, fine grained#
10	Gravelly sand to sand	
11	Very stiff to fine grained*	
12	Sand to clayey sand*	

*Overconsolidated or cemented; # Heavily overconsolidated or cemented

Alternative CPTu *soil classification charts*

Besides the classification charts of Robertson (1990), which are all based on a globally distributed database, which again is the usage of big data in the geoscience, there are also other charts available, which are based on more local soil and data samples. One of these classification charts is the one from Ramsey (2002). Similar to Robertson, Ramsey also used the friction and pore pressure ratio in order to define his soil classes; however, his database is based on North Sea sediments only. Statistically speaking global data bases make more sense for classification schemes, however, many studies relay only on regional to local comparisons, because the relative changes can here be more more emphasized (Roskoden, 2016).

Free fall CPTu *soil classification*

Even though, the classification charts after Robertson (1990) and Ramsey (2002) are based on standard cone penetration tests, Steiner (2013) and Roskoden (2016) showed that after correcting for the strain rate effects the soil classifications are applicable to free fall tests. However, Roskoden (2016) also shows that the pore pressure classification is just not yet really applicable to dynamic soil classifications, because of the strain rate effects on the pore water pressure, which have no correction formula yet.

Kinematic penetrometer soil classification

Unfortunately, due to the lack of friction information and the uncorrected dynamic pore water pressure, the soil classification after Robertson (1990) and Ramsey (2002) are not really applicable to kinematic cone penetration tests (Roskoden, 2016). Alternative solutions have been established by Mulukutla et al. (2011) and Albatal and Stark (2017). Mulukutla et al. (2011) for example defined new dynamic penetration test parameters such as the factor of firmness, which is plotted against the normalised embedded depth. The *factor of firmness*, FF, is defined as:

$$FF = \frac{a_{max}}{v_i * t_p * g} \tag{15}$$

where a_{max}, is the maximum acceleration of the instrument in [m/s²], v_i, is the impact velocity in [m/s] and t_p, the total penetration time in [s] and g, the gravitational constant (9.81 m/s²). The factor increases with a decrease of grain size and decreases with the embedded instrument depth. The *normalised embedded depth,* d_n, is defined as:

$$d_n = \frac{z}{D} \tag{16}$$

Where z is the embedded depth in [m], and D the diameter of the cone in [m]. In the work of Mulukutla et al. (2011), the authors stress the fact that the factor of firmness depends on the acceleration, the diameter of the probe and its mass. An increase in mass of the kinematic penetrometer will lead to an increase of the factor of firmness while increase of the diameter will lead to a decrease of the factor of firmness. The classification model, unlike to models of Robertson (1990) and Ramsey (2002), directly links the soil classification to the grain sizes as shown by P. Figure 8. The classification has four different classes and is plotted in a double logarithmic figure. The classes range from very fine sand to coarse silt or softer sediments and therefore cover more coarse material.

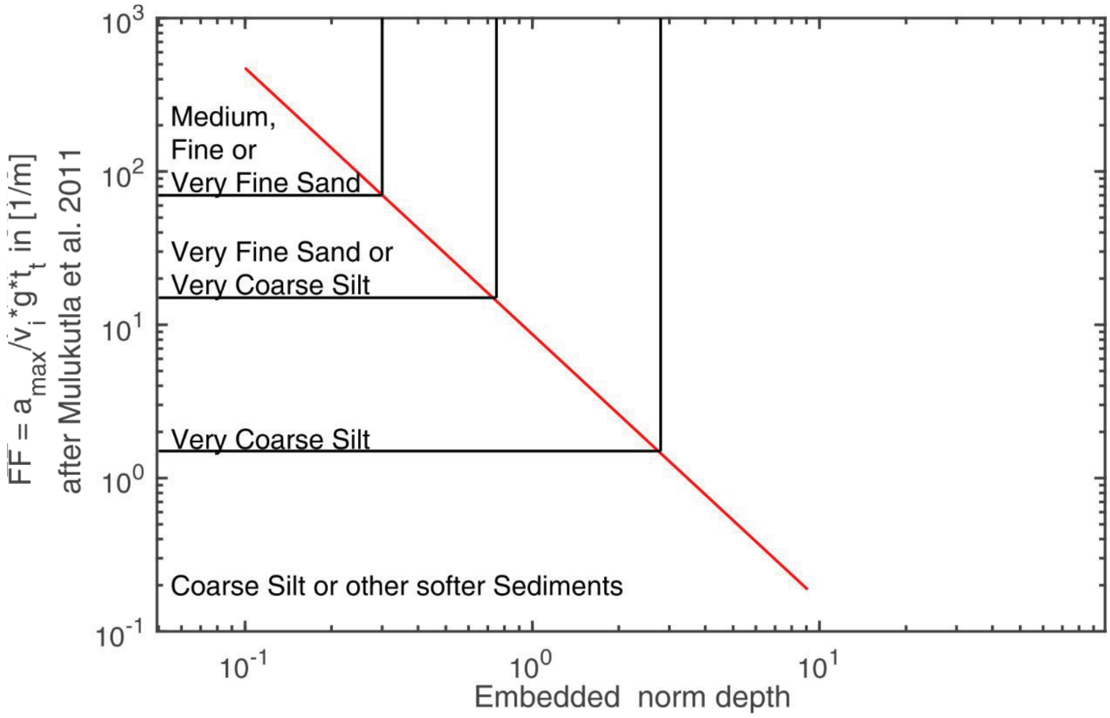

P. Figure 8 Kinematic soil classification chart after Mulukutla et al. (2011). The factor of firmness (FF) is plotted in a double logarithmic plot over the embedded normalised depth.

Albatal and Stark (2017) utilised the factor of firmness as well but plot it against the quasi static bearing capacity (q_{scb}, so the ultimate dynamic capacity corrected by *EQ* 8, P. Figure 9). Here the soil classification in a double logarithmic plot has only the sedimentological descriptions of clay, silt, and sand, but covers a larger range of sediment types or grain sizes.

Both mentioned classification charts are based on locally acquired data and mostly correspond to the field studies at hand. However, both of their approaches are going in the right direction but also leave to argue if more soil information for kinematic penetrometer tests are needed in order to join the globally recognized classification scheme from Robertson (1990).

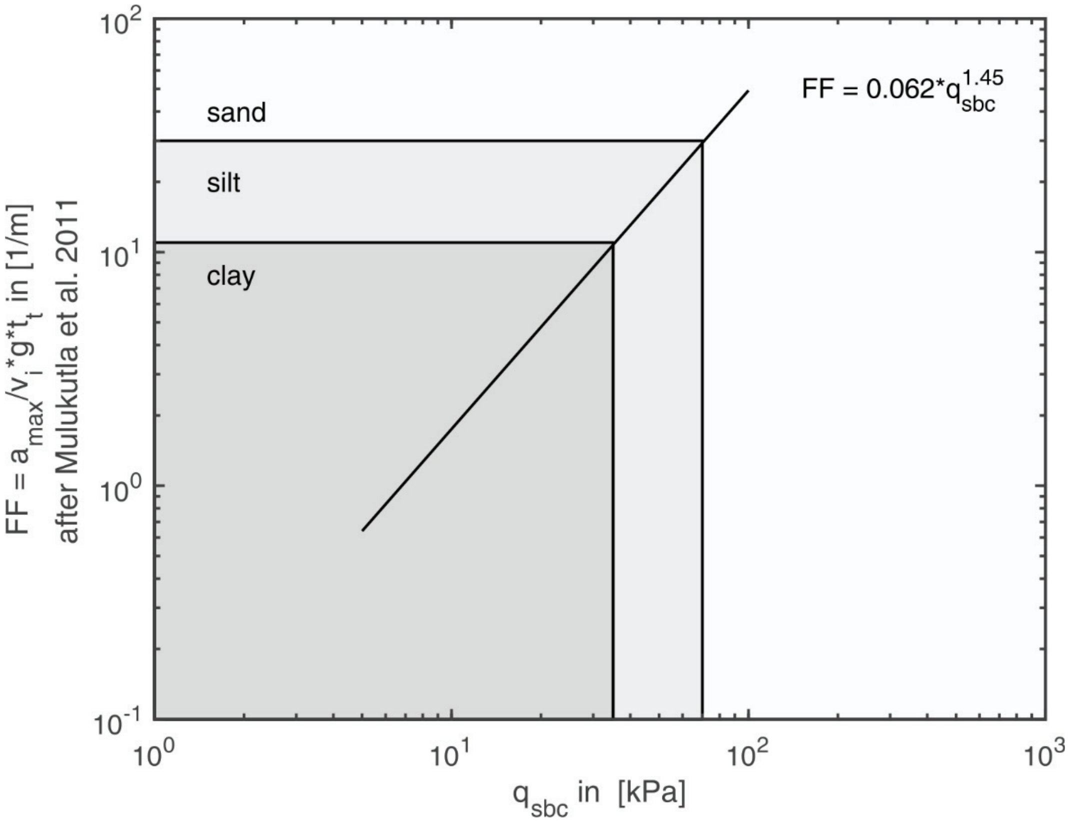

P. Figure 9 Kinematic free fall classification chart after Albatal and Stark (2017). The factor of formnis (FF) is plotted in a double logarithmic plot over the quasi bearing capacity q_{sbc}.

Dissipation tests

During penetration, the cone shifts aside the soil, causing an immediate compaction or dilation. The compaction in cohesive soils increases the pressure on the voids and consequently induces excess pore water pressure in the surrounding sediment (*EQ* 14). Per definition, a *dissipation test* is a pause in penetration to measure the rate at which the induced excesses pore pressure dissipates back to its initial ambient conditions, the equilibrium pore water pressure (Robertson and Cabal, 2010). This dewatering process, which also changes the configuration of the soil matrix, is called a consolidation and it is evaluated via the coefficient of consolidation.

The dissipation rate itself depends on the *coefficient of consolidation,* the *permeability,* the *rigidity* of the soil, the *volume compressibility* and *cone radius* -to only name a few. The rate can already point towards a soil type, because dissipation rates for sand are for example rather short (seconds to minutes), due to its high permeability, while the dissipation time for clays can be up to several hours (Lunne et al., 2002; Robertson and Cabal, 2010; Teh and Houlsby, 1991). In addition to the classification of the soil via its resistance parameters, there is also the *CPTu* dissipation test to help classify not only the soil types and the soil's hydrogeological features.

Complete dissipation tests (with 90% dissipation) provide knowledge about hydrogeological soil characteristics such as the coefficient of permeability (κ), the coefficient of consolidation (c_h), the flow regime, and pore water pressure (pwp) conditions (Neuzil, 1986; Robertson and Cabal, 2010). The dissipation rate itself is an analogy to the correspondence of the void ratio to an increase of the effective stress as observed in *oedometer tests*. Hence, the test can be analysed similarly to an oedometer test by the method of Teh and Houlsby (1991), as advised by Robertson and Cabal (2010). The coefficient of consolidation is then calculated after Teh and Houlsby (1991):

$$c_h = \frac{T^*_{50\%} r^2 \sqrt{I_r}}{t_{50\%}} \qquad 17$$

whereas $T^*_{50\%}$ is the theoretical time-factor, r is the cone radius and I_r is the rigidity index, $t_{50\%}$ the time at which 50% of the excess pore pressure is dissipated in [s]. $t_{50\%}$ is estimated after ISO standards (ISO, 2017). The coefficient of consolidation then yields the permeability via:

$$c_v = \frac{k_v}{m_v \gamma_w} = c_h \left(\frac{k_v}{k_h}\right) \qquad 18$$

where γ_w is the specific unit weight of water in [kN/m^3], m_v the coefficient of volume compressibility the index v refers to vertical and the index h to horizontal axis. P. Figure 10 gives a synthetic data example to simplify the understanding of the dissipation test analysis where excess pore water pressure is plotted over a semi-logarithmic time scale. The panel shows three different phases of the dissipation: 1) the immediate preconsolidation phase, where there the initial compression, 2) the linear part of the dissipation, the primary consolidation phase, and 3) the almost horizontal dissipation phase at the end when the excess pore pressure is close to or at the equilibrium pore pressure, the secondary consolidation phase.

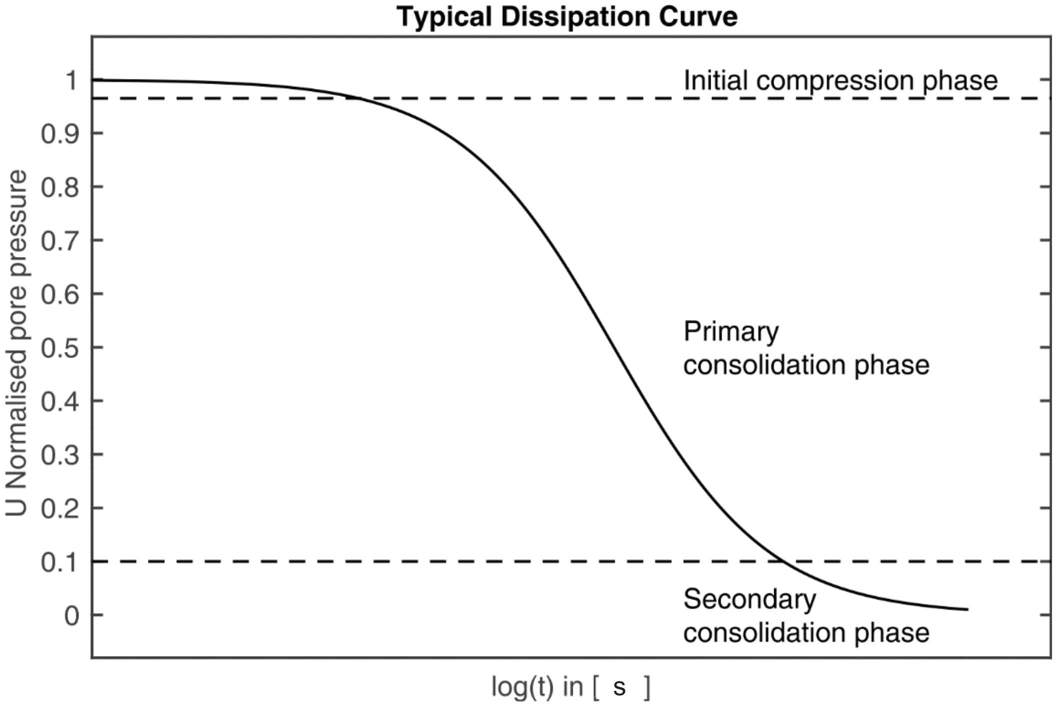

P. Figure 10 Typical pore pressure dissipation curve showing the three phases of the consolidation which are coharent with oedometer tests.

As mentioned before, a full dissipation test (dissipation of 90%) can take up to several hours, thus, data acquisition costs can increase. Especially for free fall campaigns where one penetration is supposed to be seconds to minutes, dissipation tests are rather unusual. Moreover, conducted dissipation tests with former non-standard penetration velocities show more often than standard tests an atypical pore pressure response as reported by several authors (Albatal and Stark, 2017; Chow et al., 2014; Lucking et al., 2017; Paniagua et al., 2016; Roskoden, 2016; Seifert et al., 2008; Stark and Kopf, 2011; Stegmann, 2007).

Atypical responses are described in the literature as: a) a negative excess pore pressure measurements, which dissipate back to equilibrium, or b) as a former rise of the excesses pore pressure before it starts to dissipate back to the equilibrium or c) both (Burns and Mayne, 1998; Burns and Mayne, 2002; Lunne et al., 2002; Robertson et al., 1992). Sully et al. (1999) argues to handle b) and c) by applying the dissipation test analysis not in a semi-logarithmic but time-root plot. They suggest to extrapolate the linear part of the data (just after the maximum) back to the y-intercept.

Other solutions are also researched to understand and shorten dissipation times by establishing pressure decay models, and to predict and extrapolate hydrogeological properties and dissipation data. Burns and Mayne (1998) and Burns and Mayne (2002) use their modelling approaches, for example, to combine the *critical state* and the *cavity expansion* theories. The authors divide the measured pore pressure into normal induced pore pressure, which comes from the cavity expansion theory, and the shear induced pore pressure, which comes from the critical state theory. It is argued that the shearing of the overconsolidated sediment results in dilation, which takes place directly behind the cone shoulders, which in turn creates suction and thus negative pore pressure measurements (Stegmann, 2007). The negative pore pressure is a response to the enhancement of the shear induced pore pressure and is especially found in non-standard penetration velocity campaigns. This also goes along with the findings of Seifert et al. (2008) and Paniagua et al. (2016), who found atypical pore pressure responses in overconsolidated clays and enhanced penetration velocities.

However, there are also other reasons for negative or other non-typical pore pressure data. Seifert et al. (2008) described a rate-related effect, termed '*skin effect*'. The skin is a thin adhesive layer of pore water and sediment suspension at the interface between the probe and the sediment, which moves opposite to the lance penetration, causing suction at the filter, and thus negative excess pressure data. Other reasons for delayed or negative excess pore pressure measurements might be either free gas in the sediment or gas in the filter of the penetration lance (May, 1987; Seifert et al., 2008; Strout and Tjelta, 2005).

Due to the contradictive nature of dissipation tests and dynamic penetration tests, there are not many studies, which include free fall dissipation tests. Expectations are for example: Moernaut et al. (2017) who quantified the fluid escapes in a subaquatic slope in the glacigenic LakeVillarrica in South-Central Chile, and correlated it to reduced sediment strength, and Mumtaz (2018), who studied for example the analysis of free fall atypical dissipation test data. One major result of Mumtaz (2018) is to validate an interpretation technique for dissipation curves to obtain the time value required to estimate consolidation. Furthermore, there are studies of Albatal and Stark (2017) and Lucking et al. (2017), which look at the immediate pore pressure response after penetration, so the initial compaction phase. For this reason, these free fall studies incorporate in their data acquisition miniature dissipation tests to utilise pressure decay rates. The miniature dissipation tests have relative relations to each other, allowing the authors to characterise the sediment in one region. Unfortunately, these measurements are mostly too short for any further hydrogeological investigation. There are, however, dissipation tests models, which are able to extrapolate these pore pressure data, if other soil parameters are known (Burns and Mayne, 2002; Krage et al., 2014). Nevertheless, these models need a dissipation time of at least 30% and well-known soil parameters in order to deliver reliable dissipation data, which can be analysed for the coefficient of consolidation and permeability.

IV. Motivation of this thesis

When regarding the brief history of the cone penetration testing and the current state of the art, it becomes clear that the test serves to analyse not only the state of the soil, but to classify soil types, evaluate soil stability, and correlate *in situ* data to other laboratory parameters with the help of *calibration chamber tests* (Dushi, 2006; Kurup et al., 1994; Salgado et al., 2013). Modular concepts facilitate and encourage the combination of the *CPT* with other measuring techniques to expand the applications of the penetration tests. Besides the mentioned *CPTu* and seismic *CPTs* (*SCPT*) other combinations are feasible. For example: *in situ* soil sampling cones, electrical resistivity penetrometers, vibro *CPTus*, video *CPTs*, and fluorescence detection *CPTs* -to only name a few (Gopinath, 2016; Grey et al., 1993; Jorat, Mörz, et al., 2014b; Raschke and Hryciw, 1997; Robertson, 2009).

Besides these established accomplishments of the standard cone penetration testing, there is a rising scientific and economical need for “amphibious” penetrometer investigations. The climate change and local seal level rise demand feasible solutions to secure coastlines and to map sediment dynamics. Here, however, standard cone penetration tests can often not be applied due to logistical or other issues so that there is an increasing demand for coastal and marine soil investigations using dynamic penetrometers. Especially the kinematic penetration tests are still maturing in their data acquisition, processing, and analysis techniques. Consequently, the kinematic penetrometer lacks the diversity of resistance parameters, which complicates soil classification applicability and sediment mapping performances. Accordingly, the review of the state of the art indicates three separate needs for the dynamic penetration testing:

1. A correction for the strain rate effects on the pore water pressure
2. The possibility to extrapolate short term dissipation data without estimating soil properties beforehand (which can also be applied for standard *CPTu*)
3. The possibility for kinematic light weight penetrometer to join the standard soil classification schemes after Robertson (1990).

These three objectives are the motivation for this doctoral thesis and will be investigated and discussed in the upcoming chapters. To integrate a wider functionality of the kinematic penetrometers this thesis will end in a short outlook, which will describe how to combine these new processing approaches with existing penetration lances and with the earlier mentioned yet to be developed new penetration lance, which would combine the *MARUM* heat probe and the kinematic penetration lance.

V. Description of the manuscripts and the personal contributions

This is a cumulative dissertation, which includes five first authorship manuscripts. The steps needed to achieve the overall goal of this dissertation are covered in the six main chapters of this thesis. Thus, the organisation of the manuscripts reflects mostly the scientific progression rather than the exact chronological order of publication.

Note: Not all manuscripts might be published before the dissertation thesis. Included manuscripts are given in their published or submitted form. Thus, the manuscripts may vary between British and American English, and the citation mode, due to editorial guidelines of each journal. However, the language and citation mode are kept consistent for each manuscript, but may not be uniform over the thesis. References are listed in the literature sections and are given in alphabetical order in each chapter. Tables and figures are counted chapter wise, equations are numbered cumulative through the whole thesis.

Outline Manuscript 1: A laboratory study.

The first chapter was a joined project between the *MARUM* working groups *Geoengineering* and *Marine Geotechnics*. Chapter 1 incorporates the first manuscript, titled:

Analysis of acceleration and excess pore pressure data of laboratory impact penetrometer tests in remolded overconsolidated cohesive soils.

Here we picked up the work of Stephan (2015) and the *IC10_I*. We tried to modify Stephan (2015)'s free fall experiments to recreate *in situ* condition for cohesive soils instead of non-cohesive soils such as sands. The goal of our experiments is to study penetration rate effects under controlled laboratory conditions.

One of the main objectives of this chapter is to introduce a new experimental design to calibrate free fall penetration tests, similar to a *calibration chamber test*. The experimental design was bound to a tight budget. Consequently, the experiments are only considered to be a first step towards the option of a real free fall calibration chamber tests as they could be realised soon.

The main outcome of the chapter, the *geometrical algorithm* to separate the total sediment resistance force into the sediment cone resistance and side friction, was not the striven scientific goal. However, this algorithm has proven itself most valuable, because it shows the influence of the sediment friction on the total sediment resistance for kinematic penetration lances (especially in cohesive soils). Furthermore, it allows two applications:

1) The usage of acceleration data to calculate cone resistance, side friction and all its secondary parameters so that for example standard soil classification charts after Robertson can now be used on acceleration data (for the first time).
2) The potential use of the acceleration data to fill incomplete cone resistance and side friction data sets in case data gaps appear for example due to broken strain gauges or a blocked friction sleeve.

The own work included:

- Literature research
- Scientific outline and objectives
- Project management
- Budget handling
- The design of the experimental container and calculation for its needed dimension (height, diameter, wall thickness to withstand a maximum amount of pressure)
- The design of the containers inside layering
- The search for a cohesive test soil
- The laboratory work to test all considered soils
- The laboratory work to generically change the original soil to fit to the experimental setting
- Experimental structure of the tests per batch and the overall test order, including tests for repeatability
- The homogenous inbuilt of the soil
- Supervision of its three to five days consolidation phase
- Experimental execution for the static and free fall tests
- Data processing
- Calculation of the penetration rate factors to correct the cone resistance
- Mathematical approach to correct the rate effects on pore pressure measurements
- Development of the geometrical algorithm

- Data analysis
- Scientific figures and tables
- Writing of the paper
- Review handling: Corresponding author.

Note: Help was given in the experimental execution by A. Saeed, a student helper. Prof. Dr. A. Kopf, Prof. Dr. T. Mörz and Dr. S. Kreiter have also developed the idea of the first set-up. The technicians T. Fleischmann and C. Zöllner gave technical support. Dr. S. Kreiter, Prof. Dr. T. Moerz, Dr. A. Kopf and Dr. E. Horstman gave content related revisions and insides.

Outline Manuscript 2: A field study in the estuary in the Firth of Thames, New Zealand.

The second chapter is related to past and current *IC*-projects, which worked as well in the Firth of Thames (*IC10_I, IC10_II,* and the *IC* New Zealand project '*The stability of intertidal sediments'* by Hieu Nguyen). Furthermore, it investigates unanswered questions and demands from scientific works of Lovelock et al. (2015), Swales et al. (2015), Swales et al. (2016) and Zhou et al. (2016). Chapter two is a cooperation between the working groups *Coastal Marine Group* (*Waikato University*, New Zealand) and *Marine Geotechnics* (*MARUM*, Germany). Hence, this chapter incorporates the second manuscript, titled:

Rapid transition of sediment consolidation across an expanding mangrove fringe in the Firth of Thames (FoT), New Zealand

The Firth of Thames and its mangrove forest is discussed in literature many times. Its necessity as a natural barrier for marine hazards such as tsunamis, storms and tidal waves is globally acknowledged (Alongi, 2008). Furthermore, mangrove forests are also considered as natural land reclamations and are consequently an important tool for coastal engineering projects in time of local sea level changes induced by the global climate change (Montgomery et al., 2018).

Besides the importance of the mangroves, the sub-tidal forest in the First of Thames was chosen as an area of interest, because it emphasis the need of light weight free fall penetrometer devices such as *NIMROD*. The mangrove forest is a remote area, which is neither easy to access via sea nor land. Standard free fall penetrometer or even standard quasi-static penetrometer would cause many logistical issues and destroy much of the forest itself. Furthermore, urgent needed geotechnical information would most likely be lost from the upper centimetres to meter if standard cone penetration tests would be performed. Thus, the Firth of Thames is considered a perfect study area to ground prove the *geometrical algorithm* developed in chapters before.

We show how *NIMROD* can be facilitated to gather important geotechnical information to investigate the effect of mangrove forests on consolidation processes. Thus, this study helps to assess the forest drowning risk as a consequence of the local sea level change.

The own work included:

- Literature research
- Scientific outline and objectives
- Project management

- Budget handling
- Logistic handling of *NIMROD* (with help from T. Hackmann)
- Construction of a field free fall tower (with help from D. Sandwell)
- Field work planning (two days, including risk management and logistics, with help from D. Sandwell)

  First day data acquisition via boat and wrench, second day via foot and free fall tower
- Instrument handling, data acquisition and sampling (with help from N. Lovett and D. Sandwell)
- Laboratory work (grain size, water content, and oedometer testing (some carried out by I. Schreiber)
- Data processing
- Application of the geometrical algorithm (and its adjustment to *NIMROD*)
- Data analysis and trend evaluation of the consolidation behaviour/interaction between substrate and mangrove forest
- Scientific figures and tables
- Writing of the largest portion of paper (single paragraphs were written by Dr. K. Bryan or Prof. Dr. A. Kopf)
- Review handling: Corresponding author

Note: N. Lovett and D. Sandwell gave field support. D. Sandwell also handled technical support for the realisation of the free fall tower. N. Lovett, I. Schreiber, Prof. Dr. A. Kopf and Dr. K. Bryan gave content related revisions and insides.

Outline Manuscript 3: An extended abstract on the usage of big and meta data in geoscience

In the scope of the *International Geoscientific Student Conference* (*IGSC*) 2019, the technical processing approach for the first study

Analysis of acceleration and excess pore pressure data of laboratory impact penetrometer tests in remolded overconsolidated cohesive soils

is revisited to look at the usage of *big* and *meta data* in the geosciences. The extended extract is entitled:

The usage of incomplete and metadata. Why failing is part of succeeding

This manuscript is to be regarded as a short essay to illuminate how failed experiments and data acquisitions may not result in what we hoped for, but in something different we did not even think about. Hence, failed experiments and data acquisitions are definitely not to be disregarded, because we can evaluate them after the principles of *big data* analysis and widen their significances by looking and comparing their *meta data*.

The own work included:

- Literature research
- Scientific outline and objectives
- Scientific figures and tables
- Writing of the paper

- Review handling: Corresponding author

Outline Manuscript 4: A new dissipation test model, tested with literature and in a field data

Note: Manuscript four and five used to be one manuscript. Due to the immense work to establish and to compare a new dissipation test model to other literature work, the manuscript was split into two to not detract any focus from the different scopes. The two studies are: 1) a new infield dissipation test model and 2) the hydrogeological investigation of the Bramley Drive Slide.

Logically, both studies are a joint venture of the working groups *Earth Science* (*Waikato University*, New Zealand) and *Marine Geotechnics* (*MARUM*, Germany). Hence, these chapters are also a complement to former *IC*-projects: *IC4_II,* and *IC28* (Jorat, Mörz, et al., 2014b; Kluger et al., 2017) which focused on this area of interest. Hence, this chapter incorporates the first of the two spitted manuscript, titled:

Evaluation of dissipation models via literature and new field data from the Bramley Drive, Omokoroa, New Zealand

The advantages of the free fall penetrometers are their easy handling and their rapid data acquisition. Nevertheless, besides the normal penetration test, dissipation tests are needed to gather significant hydrogeological information. Such tests, if cohesive soils are involved, may increase the data acquisition time tenfold. Possible solutions are numerical models, which can extrapolate short-term dissipation data to generate the needed information.

However, most models need soil properties in advance to extrapolate the short-term dissipation data. Such soil properties would need expensive and time intensive laboratory tests. Hence, this chapter's main objective was to develop a numerical dissipation model, which can work in an *ad hoc* mode. Consequently, no assumptions or laboratory tests are needed to run the new developed dissipation model.

The new model was tested on a 30 min long dissipation test, acquired at the Bramley Drive Slide and also compared to literature data and literature models via a performance matrix and a reference dissipation test analysis method after Teh and Houlsby (1991)

The own work included:

- Literature research
- Scientific outline and objectives
- Project management
- Hiring a private *CPTu* company (*CPTit*) for the data acquisition
- Budget handling
- Field work planning (five days, including risk management and logistics, with help from D. Sandwell)
- Data processing
- Programming of three literature dissipation test models to compare to the new model
- Development and programming of a new *ad hoc* numerical dissipation test model
- Data analysis: Performance matrix for the literature and the new *ad hoc model*

- Scientific figures and tables
- Writing of the paper
- Review handling: Corresponding author

Note: The company *CPTit* conducted the data acquisition with their *CPTu* under supervision of Dr. V. Moon and myself. N. Lovett, Prof. Dr. A. Kopf, Dr. M. Kluger, Prof. T. Moerz and Dr. V. Moon gave content related revisions and insides.

Outline Manuscript 5: The application of the new dissipation test model and a hydrogeological investigation of the Bramley Drive Slide, Omokoroa, NZ

The study site, the Omokoroa peninsula, was considered as an area of great interest to test the *ad hoc* model. The site is well investigated and researched by other *IC*-doctoral-candidates, emphasising the interdisciplinary character of *IC* and this thesis.

Besides Omokoroa being a well-researched study site, the still unknown hydrological features of tephras and their dissipation behaviour is viewed as an advantage to test and compare the new developed dissipation model. The obtained long-term dissipation data was used to validate and ground prove the new numerical model.

In addition, we study the hydrogeological effects of different morphologies of the tephra mineral halloysite by interpreting the long-term dissipation data. This study helps to assess the halloysite potential trigger mechanisms of slope failures.

The own work included:

- Literature research
- Scientific outline and objectives
- Project management
- Hiring a private *CPTu* company (*CPTit*) for the data acquisition
- Budget handling
- Field work planning (five days, including risk management and logistics, with help from D. Sandwell)
- Data processing
- Using the new *ad hoc* numerical dissipation test model
- Data analysis: trend evaluation of the coefficient of consolidation for the different morphologies of the tephra mineral halloysite, creation of a comparative and result matrix
- Scientific figures and tables
- Writing of the paper
- Review handling: Corresponding author

Note: The company *CPTit* conducted the data acquisition with their *CPTu* under supervision of Dr. V. Moon and myself. N. Lovett, Prof. Dr. A. Kopf, Dr. M. Kluger, Prof. T. Moerz and Dr. V. Moon gave content related revisions and insides.

References Prefix and Chapter 1

1. Albatal, A., Stark, N., 2017. Rapid Sediment Mapping and in Situ Geotechnical Characterization in Challenging Aquatic Areas. Limnology and Oceanography: Methods, V. 15, No. 8, p. 690-705, doi# doi.org/10.1002/lom3.10192.
2. Alongi, D.M., 2008. Mangrove Forests: Resilience, Protection from Tsunamis, and Responses to Global Climate Change. Estuarine, Coastal and Shelf Science, V. 76, No. 1, p. 1-13, doi# doi.org/10.1016/j.ecss.2007.08.024.
3. Aubeny, C., Shi, H., 2006. Interpretation of Impact Penetration Measurements in Soft Clays. Journal of geotechnical and geoenvironmental engineering, V. 132, No. 6, p. 770-777, doi# doi.org/10.1061/(ASCE)1090-0241(2006)132:6(770).
4. Barentsen, P., 1936. Short Description of a Field Testing Method with Cone-Shaped Sounding Apparatus, Proceedings 1st International Conference on Soil Mechanics and Foundation Engineering, pp. 6-10.
5. Begemann, H., 01 August 2018. The Friction Jacket Cone as an Aid in Determining the Soil Profile, Proceedings of the 6th International Conference on Soil Mechanics and Foundation Engineering, ICSMFE, Montreal, September. Springer, Cham, pp. 8-15.
6. Begemann, H., 1953. Improved Method of Determining Resistance to Adhesion by Sounding through a Loose Sleeve Placed Behind the Cone, Proceedings of the 3rd International Conference on Soil Mechanics and Foundation Engineering, ICSMFE, August, Zurich, pp. 213-217.
7. Biscontin, G., Pestana, J.M., 2001. Influence of Peripheral Velocity on Vane Shear Strength of an Artificial Clay. Geotechnical Testing Journal, V. 24, No. 4, p. 423-429, doi# doi.org/10.1520/GTJ11140J.
8. Burns, S., Mayne, P., 1998. Monotonic and Dilatory Pore-Pressure Decay During Piezocone Tests in Clay. Canadian Geotechnical Journal, V. 35, No. 6, p. 1063-1073, doi# doi.org/10.1139/cgj-35-6-1063.
9. Burns, S.B., Mayne, P.W., 2002. Analytical Cavity Expansion-Critical State Model for Piezocone Dissipation in Fine-Grained Soils. Soils and Foundations, V. 42, No. 2, p. 131-137, doi# doi.org/10.3208/sandf.42.2_131.
10. Casagrande, A., Fadum, R.E., 1940. Notes on Soil Testing for Engineering Purposes, in: Havard Graduate School of Engineering, S.M. (Ed.), Cambridge, Mass., p. 268.
11. Casagrande, A., Wilson, S., 1951. Effect of Rate of Loading on the Strength of Clays and Shales at Constant Water Content. Géotechnique, V. 2, No. 3, p. 251-263, doi# doi.org/10.1680/geot.1951.2.3.251.
12. Chow, S., O'Loughlin, C., Randolph, M., 2014. Soil Strength Estimation and Pore Pressure Dissipation for Free-Fall Piezocone in Soft Clay. Géotechnique, V. 64, No. 10, p. 817-827, doi# doi.org/10.1680/geot.14.P.107.
13. Chow, S., O'Loughlin, C., White, D., Randolph, M., 2017. An Extended Interpretation of the Free-Fall Piezocone Test in Clay. Géotechnique, V. 67, No. 12, p. 1090-1103, doi# doi.org/10.1680/jgeot.16.P.220.
14. Dayal, U., Allen, J.H., 1973. Instrumented Impact Cone Penetrometer. Canadian Geotechnical Journal, V. 10, No. 3, p. 397-409, doi# doi.org/10.1139/t73-034.
15. Dayal, U., Allen, J.H., 1975. The Effect of Penetration Rate on the Strength of Remolded Clay and Sand Samples. Canadian Geotechnical Journal, V. 12, No. 3, p. 336-348, doi# doi.org/10.1139/t75-038.
16. de Ruiter, J., 1971. Electric Penetrometer for Site Investigations. Journal of the Soil Mechanics and Foundations Division, V. 97, No. 2, p. 457-472, doi# -.
17. Dushi, A., 2006. Refurbishment of Louisiana State University Calibration Chamber. Louisiana State University and Agricultural and Mechanical College, p. 122.
18. Eyring, H., 1936. Viscosity, Plasticity, and Diffusion as Examples of Absolute Reaction Rates. The Journal of chemical physics, V. 4, No. 4, p. 283-291, doi# doi.org/10.1063/1.1749836.

19. Gopinath, G., 2016. Application of Electric Cone Penetration Test in Unconsolidated and Consolidated Sediments. Procedia Technology, V. 24, No. -, p. 271-279, doi# doi.org/10.1016/j.protcy.2016.05.036.

20. Grey, C.E., Cooper, S.S., Malone, P.G., 1993. Method and Apparatus for in-Situ Detection and Determination of Soil Contaminants, https://patents.google.com/patent/US5246862A/en#patentCitations US Secretary of Army

21. ISO, 2017. International Organization for Standardization Geotechnical Investigation and Testing - Laboratory Testing of Soil - Part 5: Incremental Loading Oedometer Test (Iso 17892-5:2017); , Geotechnical investigation and testing–Laboratory.

22. Jorat, M., Mörz, T., Schunn, W., Kreiter, S., Moon, V.G., de Lange, W.P., 2014. Geotechnical Offshore Seabed Tool (Gost): Cptu Measurements and Operations in New Zealand, CPT'14. 3rd International Symposium on Cone Penetration Testing, pp. 217-223.

23. Kluger, M., Moon, V., Kreiter, S., Lowe, D., Churchan, G., Hepp, D., Seibel, D., Jorat, M., Moerz, T., 2017. A New Attraction-Detachment Model for Explaining Flow Sliding in Clay-Rich Tephras. Geology, V. 42, No. 2, p. 131-134, doi# doi:10.1130/G38560.1.

24. Kopf, A., Stegmann, S., Krastel, S., Förster, A., Strasser, M., Irving, M., 2007. Marine Deep-Water Free-Fall Cpt Measurements for Landslide Characterisation Off Crete, Greece (Eastern Mediterranean Sea) Part 2: Initial Data from the Western Cretan Sea, Submarine Mass Movements and Their Consequences. Springer, p. 199-208, doi.org/10.1007/978-1-4020-6512-5_21.

25. Krage, C., DeJong, J., Schnaid, F., 2014. Estimation of the Coefficient of Consolidation from Incomplete Cone Penetration Test Dissipation Tests. Journal of geotechnical and geoenvironmental engineering, V. 141, No. 2, p., doi# doi.org/10.1061/(ASCE)GT.1943-5606.0001218.

26. Krastel, S., Braeunig, A., Feldens, P., Georgiopoulou, A., Jaehmlich, H., Lange, M., Lindhorst, K., Llopart, J., Mader, S., Mehringer, L., Merl, M., Muecke, I., Renkl, C., Roskoden, R., Schoenke, M., Schulten, I., Schwarz, J.-P., Stevenson, C., Vallee, M., Wegener, B., Wiesenberg, L., 2016. Geomorphology, Processes and Geohazards of Giant Submarine Landslides and Tsunami Generation Capacity, as Recorded in the Sedimentary Record of the Only Historic Slide of This Kind: The 1929 Grand Banks Landslide of the Canadian Atlantic Continental Margin - Cruise No. Msm47 - September 30 - October 30, 2015 - St. John's (Canada) - Ponta Delgada, Azores (Portugal). MARIA S. MERIAN-Berichte, V. doi.org/10.2312/cr_msm47 No., p. 55, doi# doi.org/10.2312/cr_msm47

27. Kurup, P., Voyiadjis, G., Tumay, M., 1994. Calibration Chamber Studies of Piezocone Test in Cohesive Soils. Journal of Geotechnical Engineering, V. 120, No. 1, p. 81-107, doi# doi.org/10.1061/(ASCE)0733-9410(1994)120:1(81).

28. Leroueil, S., Kabbaj, M., Tavenas, F., Bouchard, R., 1985. Stress–Strain–Strain Rate Relation for the Compressibility of Sensitive Natural Clays. Géotechnique, V. 35, No. 2, p. 159-180, doi# doi.org/10.1680/geot.1985.35.2.159.

29. Lovelock, C.E., Cahoon, D.R., Friess, D.A., Guntenspergen, G.R., Krauss, K.W., Reef, R., Rogers, K., Saunders, M.L., Sidik, F., Swales, A., 2015. The Vulnerability of Indo-Pacific Mangrove Forests to Sea-Level Rise. Nature, V. 526, No. 7574, p. 559, doi# doi.org/10.1038/nature15538

30. Lucking, G., Stark, N., Lippmann, T., Smyth, S., 2017. Variability of in Situ Sediment Strength and Pore Pressure Behavior of Tidal Estuary Surface Sediments. Geo-Marine Letters, V. doi.org/10.1007/s00367-017-0494-6, No. 37, p. pages441–456 doi# doi.org/10.1007/s00367-017-0494-6.

31. Lunne, T., Powell, J.J., Robertson, P.K., 2002. Cone Penetration Testing in Geotechnical Practice. CRC Press.

32. Lunne, T., Powell, J.J.M., Robertson, P.K., 1997. Cone Penetration Testing in Geotechnical Practice. Taylor & Francis.

33. Lunne, T., Robertson, P., Powell, J., 1997. Cone Penetration Testing. Taylor & Francis.

34. Massarsch, K., 2014. Cone Penetration Testing—a Historic Perspective, Proceedings 3rd international symposium on cone penetration testing. , Las Vegas, Nevada, USA, pp. 97-134.

35. May, R.E., 1987. A Study of the Piezocone Penetrometer in Normally Consolidated Clay. University of Oxford, Oxford, p. 264.

36. Mesri, G., Godlewski, P.M., 1977. Time and Stress-Compressibility Interrelationship. ASCE J Geotech Eng Div, V. 103, No. 5, p. 417-430, doi# doi.org/10.1016/0148-9062(77)91005-1.

37. Mitchell, J.K., 1964. Shearing Resistance of Soils as a Rate Process. Journal of Soil Mechanics & Foundations Div, V. 90, No. SM1, p. 29-61, doi# Accession Number: 00264432.

38. Mitchell, J.K., Soga, K., 2005. Fundamentals of Soil Behavior. John Wiley and Sons, Inc, United States of America

39. Moernaut, J., Wiemer, G., Reusch, A., Stark, N., De Batist, M., Urrutia, R., de Guevara, B.L., Kopf, A., Strasser, M., 2017. The Influence of Overpressure and Focused Fluid Flow on Subaquatic Slope Stability in a Formerly Glaciated Basin: Lake Villarrica (South-Central Chile). Marine Geology, V. 383, No., p. 35-54, doi# doi.org/10.1016/j.margeo.2016.11.012.

40. Montgomery, J., Bryan, K., Horstman, E., Mullarney, J., 2018. Attenuation of Tides and Surges by Mangroves: Contrasting Case Studies from New Zealand. Water, V. 10, No. 9, p. 1119, doi# doi.org/10.3390/w10091119.

41. Mulhearn, P., 2002. Influences of Penetrometer Probe Tip Geometry on Bearing Strength Estimates for Mine Burial Prediction. Defence Science and Technology Organisation Canberra (australia), Fishermans Bend, Victoria 3207 Australia p. 27.

42. Mulukutla, G.K., Huff, L.C., Melton, J.S., Baldwin, K.C., Mayer, L.A., 2011. Sediment Identification Using Free Fall Penetrometer Acceleration-Time Histories. Marine Geophysical Research, V. 32, No. 3, p. 397-411, doi# doi.org/10.1007/s11001-011-9116-2.

43. Mumtaz, M.B., 2018. Investigation of Pore Pressures During High-Velocity Impact by a Free Fall Penetrometer. Virginia Tech, p. 73.

44. Neuzil, C., 1986. Groundwater Flow in Low-Permeability Environments. Water Resources Research, V. 22, No. 8, p. 1163-1195, doi# doi.org/10.1029/WR022i008p01163.

45. Nordlund, R., 1963. Bearing Capacity of Piles in Cohesionless Soils. Journal of the Soil Mechanics and Foundations Division, V. 89, No. 3, p. 1-36, doi# -.

46. Paniagua, P., Carroll, R., L'Heureux, J.-S., Nordal, S., 2016. Monotonic and Dilatory Excess Pore Water Dissipations in Silt Following Cptu at Variable Penetration Rate. 5th INTERNATIONAL CONFERENCE ON GEOTECHNICAL AND GEOPHYSICAL SITE CHARACTERISATION (ISC5), V. 5, No. 5, p., doi# hdl.handle.net/11250/2491806.

47. Perlow, M., Richards, A.F., 1977. Influence of Shear Velocity on Vane Shear Strength. Journal of the Geotechnical Engineering Division, V. 103, No. 1, p. 19-32, doi# -.

48. Power, W., Downes, G., McSaveney, M., Beavan, J., Hancox, G., 2005. The Fiordland Earthquake and Tsunami, New Zealand, 21 August 2003, Tsunamis. Springer, p. 31-42, doi.org/10.1007/1-4020-3331-1_2.

49. Ramsey, N., 2002. A Calibrated Model for the Interpretation of Cone Penetration Tests (Cpts) in North Sea Quaternary Soils, Offshore Site Investigation and Geotechnics' Diversity and Sustainability'; Proceedings of an International Conference. Society of Underwater Technology, London, pp. 341-356.

50. Randolph, M., Hope, S., 2004. Effect of Cone Velocity on Cone Resistance and Excess Pore Pressures, Proc., Int. Symp. on Engineering Practice and Performance of Soft Deposits. Yodagawa Kogisha Co., Ltd., Osaka, Japan, pp. 147-152.

51. Raschke, S.A., Hryciw, R.D., 1997. Vision Cone Penetrometer for Direct Subsurface Soil Observation. Journal of geotechnical and geoenvironmental engineering, V. 123, No. 11, p. 1074-1076, doi# doi.org/10.1061/(ASCE)1090-0241(1997)123:11(1074).

52. Rattley, M., Richards, D., Lehane, B., 2008. Uplift Performance of Transmission Tower Foundations Embedded in Clay. Journal of geotechnical and geoenvironmental engineering, V. 134, No. 4, p. 531-540, doi# doi.org/10.1061/(ASCE)1090-0241(2008)134:4(531).

53. Richardson, A.M., Whitman, R.V., 1963. Effect of Strain-Rate Upon Undrained Shear Resistance of a Saturated Remoulded Fat Clay. Géotechnique, V. 13, No. 4, p. 310-324, doi# doi.org/10.1680/geot.1963.13.4.310.

54. Robertson, P., 2009. Interpretation of Cone Penetration Tests—a Unified Approach. Canadian Geotechnical Journal, V. 46, No. 11, p. 1337-1355, doi# doi.org/10.1139/T09-065.

55. Robertson, P., Cabal, K., 2010. Guide to Cone Penetration Testing. Gregg Drilling & Testing Inc, Signal Hill, California 90755.

56. Robertson, P., Sully, J., Woeller, D.J., Lunne, T., Powell, J., Gillespie, D., 1992. Estimating Coefficient of Consolidation from Piezocone Tests. Canadian Geotechnical Journal, V. 29, No. 4, p. 539-550, doi# doi.org/10.1139/t92-061.

57. Robertson, P.K., 1990. Soil Classification Using the Cone Penetration Test. Canadian Geotechnical Journal, V. 27, No. 1, p. 151-158, doi# doi.org/10.1139/t90-014.

58. Robertson, P.K., Campanella, R., Gillespie, D., Greig, J., 1986. Use of Piezometer Cone Data, Use of in situ tests in geotechnical engineering. ASCE, pp. 1263-1280.

59. Roskoden, R., 2016. Cone Penetration Tests the Soil Classification and Analytic Assessments of Dynamic and Static Penetrometer Test Data. Universität Bremen, Master Thesis, 2016, Bremen.

60. Roskoden, R., Kopf, A., Mörz, T., Kreiter, S., 2018. Analysis of Acceleration and Excess Pore Pressure Data of Laboratory Impact Penetrometer Tests in Remolded Overconsolidated Cohesive Soils, Cone Penetration Testing 2018. CRC Press, p. 545-550, -.

61. Salgado, R., Prezzi, M., Kim, K., Lee, W., 2013. Penetration Rate Effects on Cone Resistance Measured in a Calibration Chamber, 4th International Conference on Site Characterization, ISC'4, pp. 1025-1030

62. Sanglerat, G., 1973. The Penetrometer and Soil Exploration. Soil Science, V. 116, No. 2, p. 131, doi# -.

63. Seifert, A., 2011. In Situ Detection and Characterisation of Fluid Mud and Soft Cohesive Sediments by Dynamic Piezocone Penetrometer Testing, Marine Geotechnics. Bremen University Bremen, p. 180.

64. Seifert, A., Stegmann, S., Mörz, T., Lange, M., Wever, T., Kopf, A., 2008. In Situ Pore-Pressure Evolution During Dynamic Cpt Measurements in Soft Sediments of the Western Baltic Sea. Geo-Marine Letters, V. 28, No. 4, p. 213-227, doi# doi.org/10.1007/s00367-008-0102-x.

65. Stark, N., 2011. Geotechnical Investigation of Sediment Remobilization Processes Using Dynamic Penetrometers, Marine Geotechnics. Universität Bremen, Bremen, p. 309.

66. Stark, N., Hay, A.E., Trowse, G., 2014. Cost-Effective Geotechnical and Sedimentological Early Site Assessment for Ocean Renewable Energies, Oceans-St. John's, 2014. IEEE, pp. 1-8.

67. Stark, N., Kopf, A., 2011. Detection and Quantification of Sediment Remobilization Processes Using a Dynamic Penetrometer, OCEANS'11 MTS/IEEE KONA. IEEE, pp. 1-9.

68. Stark, N., Kopf, A., Hanff, H., Stegmann, S., Wilkens, R., 2009. Geotechnical Investigations of Sandy Seafloors Using Dynamic Penetrometers, OCEANS 2009. IEEE, pp. 1-10.

69. Stegmann, S., 2007. Design of a Free-Fall Penetrometer for Geotechnical Characterisation of Saturated Sediments and Its Geological Application, Marine Geotechnics. Universität Bremen, p. 181.

70. Steiner, A., 2013. Sub-Seafloor Characterization and Stability of Submarine Slope Sediments Using Dynamic and Static Piezocone Penetrometers, Marine Geotechnics. Universität Bremen, Bremen, p. 325.

71. Steiner, A., L'Heureux, J.-S., Kopf, A., Vanneste, M., Longva, O., Lange, M., Haflidason, H., 2012. An in-Situ Free-Fall Piezocone Penetrometer for Characterizing Soft and Sensitive Clays at Finneidfjord (Northern Norway), Submarine Mass Movements and Their Consequences. Springer, Dordrecht, p. 99-109, doi.org/10.1007/978-94-007-2162-3_9

72. Stephan, S., 2015. A Rugged Marine Impact Penetrometer for Sea Floor Assessment. Universität Bremen, , Bremen,, p. 268.

73. Stoll, R.D., Akal, T., 1999. Xbp- Tool for Rapid Assessment of Seabed Sediment Properties. Sea technology, V. 40, No. 2, p. 47-52, doi# ISI:000079003400006.

74. Stoll, R.D., Sun, Y.-F., Bitte, I., 2007. Seafloor Properties from Penetrometer Tests. IEEE Journal of Oceanic Engineering, V. 32, No. 1, p. 57-63, doi# doi.org/10.1109/joe.2007.890943.

75. Strout, J.M., Tjelta, T.I., 2005. In Situ Pore Pressures: What Is Their Significance and How Can They Be Reliably Measured? Marine and Petroleum Geology, V. 22, No. 1-2, p. 275-285, doi# doi.org/10.1016/j.marpetgeo.2004.10.024.

76. Sully, J.P., Robertson, P.K., Campanella, R.G., Woeller, D.J., 1999. An Approach to Evaluation of Field Cptu Dissipation Data in Overconsolidated Fine-Grained Soils. Canadian Geotechnical Journal, V. 36, No. 2, p. 369-381, doi# doi.org/10.1139/t98-105.

77. Swales, A., Bentley Sr, S.J., Lovelock, C.E., 2015. Mangrove-Forest Evolution in a Sediment-Rich Estuarine System: Opportunists or Agents of Geomorphic Change? Earth Surface Processes and Landforms, V. 40, No. 12, p. 1672-1687, doi# doi.org/10.1002/esp.3759.

78. Swales, A., Denys, P., Pickett, V.I., Lovelock, C.E., 2016. Evaluating Deep Subsidence in a Rapidly-Accreting Mangrove Forest Using Gps Monitoring of Surface-Elevation Benchmarks and Sedimentary Records. Marine Geology, V. 380, No., p. 205-218, doi# doi.org/10.1016/j.margeo.2016.04.015.

79. Teh, C.I., Houlsby, G.T., 1991. An Analytical Study of the Cone Penetration Test in Clay. Géotechnique, V. 41, No. 1, p. 17-34, doi# doi.org/10.1680/geot.1991.41.1.17.

80. Terzaghi, K., 1943. Theoretical Soil Mechanics. JohnWiley & Sons, New York.

81. Young, A.G., Bernard, B.B., Remmes, B.D., Babb, L., Brooks, J.M., 2011. Cpt Stinger-an Innovative Method to Obtain Cpt Data for Integrated Geoscience Studies, Offshore Technology Conference. Offshore Technology Conference, -, pp. 1-10.

82. Zhou, Z., van der Wegen, M., Jagers, B., Coco, G., 2016. Modelling the Role of Self-Weight Consolidation on the Morphodynamics of Accretional Mudflats. Environmental Modelling & Software, V. 76, No. -, p. 167-181, doi# doi.org/10.1016/j.envsoft.2015.11.002.

Chapter 2:

Manuscript 1

Analysis of acceleration and excess pore pressure data of laboratory impact penetrometer experiments in remolded overconsolidated cohesive soils

first author, published 2018 at the CPT'18, Cone Penetration Testing 2018, pp. 545-550, CRC Press/Balkema, Leiden, NL, ISBN 978-1-138-58449-5

Autors

R. Roskoden[1*],

A. Kopf[2*],

T. Mörz[3*],

S. Kreiter[4*]

*University Bremen, Centre of Marine environmental science (MARUM), Bremen, Germany

([1]rroskode@marum.de (ORCID: https://orcid.org/0000-0003-2170-283X), [2]akopf@marum.de, [3]tmoerz@uni-bremen.de, [4]skreiter@uni-bremen.de)

M.1 Abstract:

Free fall *CPTu* measurements have two data acquisition approaches: direct measurement of sleeve friction (f_s) and tip resistance (q_c) or estimation of these via acceleration data. However, enhanced impact velocities cause strain rate effects on the sediment, which requires to correct q_c, and f_s for these rate effects. The pore pressure (u_2), an important parameter for evaluating soil properties, is not corrected for the penetration rate effects yet. Hence, a laboratory free fall calibration test, with a miniature cone penetration lance, which measures u_2 and acceleration, was designed. The objective was to investigate responses of the acceleration -data to calculate kinematic f_s and q_c. Additionally, we studied dynamic u_2-responses for their penetration rate effect. We also investigated existing penetration rate-corrections for remolded, overconsolidated cohesive soils. In total six experiments were conducted, each of which consisted of four penetrations with impact velocities of 0.02 to 2 m/s. We estimated f_s and q_c from acceleration-data for a remolded, overconsolidated cohesive soil. New rate correction values have been found for this soil, which show a dependency on consolidation histories. Moreover, we identified possible rate effects on u_2-responses as increases in the modulus excess pore pressure. This will help to analyze existing and future u_2-measurements.

M.1.1 Introduction and Objectives

Most Cone Penetration Tests (*CPTu*) are pushed with a constant penetration velocity of 0.02 m/s, termed standard. *CPTu* measures the soil's sleeve friction (f_s), tip resistance (q_c) and pore pressure (u_2). Free fall or dynamic *CPTu* measurements, standardized from the ASTM 1982 for borehole free fall CPT (Riggs, 1982), have two data acquisition approaches: direct measurements of the dynamic q_c and f_s, or estimation of soil strength parameters via acceleration-data (Dayal and Allen, 1973; Stoll et al., 2007b). Dynamic *CPTu* have financial benefits and are more time efficient. However, dynamic *CPTu* measurements systematically overestimate q_c and f_s if compared to standard *CPTu*-data. This is called penetration rate effect (Dayal and Allen, 1973; Dayal and Allen, 1975). Attempts have been made to correct q_c, and f_s for penetration rate effects. For example *EQ* 19:

$$\frac{q_c}{q_{c,\,st}} = \mu \log_{10}\left(\frac{V}{V_{st}}\right) + 1 \qquad 19$$

with $q_{c,st}$ = standard tip resistance, μ = penetration rate factor V = penetration velocity, V_{st}= standard velocity, (Dayal and Allen, 1975). Furthermore, higher penetration velocities might result in increased undrained shear stresses which can cause dilatancy in overconsolidated clays (Burns and Mayne, 1998). This may cause negative u_2 during penetration (Paniagua et al., 2016). Additionally, dynamic u_2-measurements can show exaggerated u_2-responces (Seifert et al., 2008), independent from its sign. Although, u_2 is an important parameter for evaluating soil properties and stability, so far it is not corrected for penetration rate effects. However, Chow et al. (2014) evaluated free fall dissipation tests in centrifuge modelling and concluded that, besides an atypical rise of the pore pressure, the dissipation behavior is identical to standard *CPTu*. Furthermore, Lucking et al. (2017) utilized short term rates of excess pore pressure dissipation to identify sediment types. Nevertheless, the initial atypical u_2-response reduces the engineering applicability for high impact *CPTu*. Soil behavior charts, based on u_2 or f_s, are especially not applicable for kinematic *CPTu* (Robertson, 1990; Roskoden, 2016). Chow et al. (2017) mention a possible back-calculation of the pore pressure ratio, allowing u_2-estimation even without a pressure transducer. However, Lucking et al. (2017) and Albatal and Stark (2017) emphasize the need of free fall calibration chamber tests to investigate u_2-behaviour. Hence, we implemented an experimental setting similar to a calibration chamber test, called 'calibration free fall test'. The objective of the calibration free fall test is to evaluate rate effects and sensor performances for acceleration- and u_2-equipment. The scientific goals are to investigate: (1) kinematic f_s and q_c in remolded overconsolidated cohesive soils. (2) Penetration rate corrections for the given soil. (3) u_2-response for different penetration rates and consolidation pressures and (4) to evaluate polyethylene porous filter stone clogging for pogo-style deployments.

M.1.2 Methodology

The grain size distribution of a natural cohesive soil from the 'Hemelinger Marsch', south of Bremen, Germany, was altered to fit a coefficient of consolidation smaller than 2 x 10^{-7} m/s. Alterations were done via admixing commercially available micro silt (d_{50} = 30 µm) and sand (d_{50} = 0.210 mm) from *Euroquarz GmbH*. Both soils were tested for geotechnical index values such as liquid limit (*LL*), plastic limit (*PL*) and shrinking limit (*SL*), plasticity index (I_p) and shrinking index (I_S) (DIN 18122), coefficient of consolidation (c_v), compression index (C_C), recompression index (C_R) and swelling index (C_S), M.1 Table 1.

M.1 Table 1. Soil classification of original 'Hemelinger Marsch' soil and the synthetically altered soil.

Soil	Hemelinger Marsch	Synthetically altered
Clay	16.8%	8.3%
Silt	73.6%	84.8%
Sand	9.6%	6.9%
LL	60.6%	37.8%
PL	19.0%	13.26%
SL	8.1%	5.9%
I_p	41.6	24.6
I_s	52.5	32.5
c_v [m²/s]	9.5E-7	1,24E-06
C_C	0.4	0.26
C_R	4.3E-2	3.0E-3
C_S	6.52E-2	2.3E-2

The artificially prepared soil was remolded. Its water content was increased to 55% while mixing it constantly until the soil was homogenized to a slurry. The slurry was transferred into a self-designed container. The slurry was then consolidated to an effective normal stress of 64 or 32 kPa. Water content after consolidation was between 35 to 40% (tested at different depths). Vertical homogeneity was visually verified via push cores. Consolidation pressure was removed before testing. The measurements were done via a custom-built miniature cone penetration lance, recording u_2- and acceleration-data. Acceleration was used to calculate the total resistance force (F_T), *EQ* 20:

$$F_T = m\,(g - a) \tag{20}$$

h m = *CPTu* mass in kg, g = gravitational acceleration and a = measured acceleration in m/s², respectively. Six experiments, each with four penetrations with different penetration velocities (0.02 - 2 m/s) per batch, were conducted. For reference purposes, each batch starts with a pushed test (V_{st}). Dynamic tests are guided via a sled (attached to vertical guides, M.1 Figure 1).

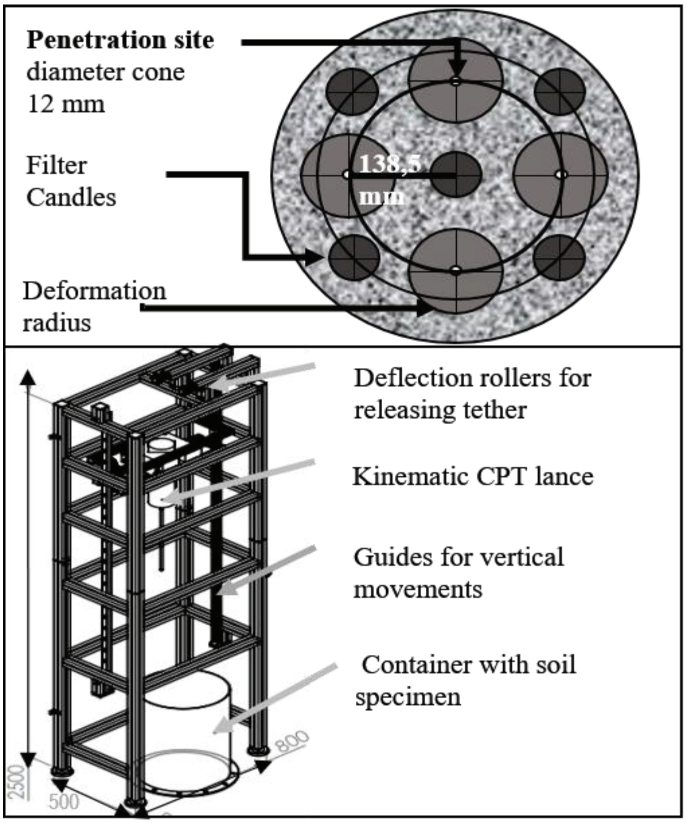

M.1 Figure 1. Upper: Top angle showing plastic defamation radius of penetration sites and drainage/filter-candle sites. Lower: Free fall tower with vertical guidance system and deflection rollers, dimensions in mm (altered after Stephan (2015)).

Repeatability was tested in each batch, by using either impact velocities 1 m/s or 2 m/s twice per batch. Sampling frequency was 500 Hz. Designed container (81 liters, ~0.176 m²) from bottom to top: (1) 10 mm vertical drainage socket. (2) 20 mm gravel layer. (3) Metal grid to separate slurry and gravel. (4) 5 vertical drains (filters candles) ~250 mm long, filled with gravel (to reduce consolidation time). (5) ~465 mm soil (after consolidation). (6) 5 mm polyethylene porous filter plate (porosity ~35%). (7) 100 mm pressure plate (~12 kg). (8) 1 cm water layer to keep current saturation. Schematic design of the experimental setup is shown in M.1 Figure 1.

Note to (4) vertical drains: Similar to an oedometer test, the height of the sample for the consolidation is important to calculate the needed time for the 90% consolidation. Following the example of the DIN

18135:2012-04 (DIN, 2012) the time for the consolidation in the experimental container can be calculated as $t_{90\%} = T_{90\%} * H^2/c_v$, while H is the height of the sample. The vertical drains shorten the drainage paths artificially by which the consolidation time is shorten.

The size of the container was designed to fulfil the boundary conditions for the plastic deformation radius, *EQ* 21 (Lu et al., 2004):

$$R_p = \sqrt[3]{I_r} R_c \tag{21}$$

with R_p = plastic deformation radius, I_r = rigidity index (~50, after Keaveny (1985) solution chart), and R_c = cone radius (6 mm). Hence, no geometric overlap of plastic deformation radius between different penetrations is expected (M.1 Figure 1). Vertical drains are below penetration depth and are not expected to interfere with resistance or u_2-behaviour. For dividing the total resistance into f_s and q_c an additional experiment was carried out. A miniature penetration lance, which can measure q_c and the total resistance force directly, was pushed into the specimen with four different constant velocities (M.1 Table 2, Ex. 0). Before each free fall experiment, the pore pressure assembly (tubing, u_2-sensor and filter stone) was saturated. In-between batches, the filter stone was treated differently to evaluate clogging effects of the filter media. Treatment options were: (1) cleaning by swiping, (2) cleaning by flushing and (3) no cleaning, also called pogo-style (common deployment method for impact penetrometer (Stegmann et al., 2006)). After finishing one experiment the soil was recycled for further experiments and if needed the volume increased by adding more artificial soil-mass. Furthemore, the pore pressure filter stone (same material as the pore pressure plate) was cleaned via pressure washing (initial porosity ~35%).

M.1 Table 2. Experimental setting and cleaning option for each penetration per experiment (Pen I to IV).

Experiment:	*0~*	*3*	*4*	*5*	*6*	*7*
Title	*VE**	*S*	*F*	*F*	*P*	*P*
Cons.[kPa]	*64*	*64*	*32*	*32*	*32*	*32*
Pen I						
static (u2 & FT)	0.02°		0.02	0.02	0.02	
Pen II						
static (u2 & FT)	0.15	x^				
dynamic					1	
pore pressure					x	
acceleration					x	
Pen III						
static (u2 & FT)	0.2					
dynamic		1	1	2	1	1
pore pressure		x	x	x	x	x
acceleration		x		x	x	x
Pen IV						
static (u2 & FT)	0.23					
dynamic		2	1	2	2	2
pore pressure		x	x	x	x	x
acceleration		x		x	x	x

~ Missing numbers in-between experiments-sequence represent failed tests (e.g. data logger failure). VE = Velocity Experiment, S = Swiping, F = Flushing, P = Pogo Style.° Numbers represent impact velocity in m/s.*

^ x = collected data.

M.1.3 Results

M.1.3.1 Estimation of tip resistance and sleeve friction via acceleration data

Due to the homogenization of the soil, and negligible total over burden stress (max 1.2% of total penetration resistance with a max penetration depth of 20 cm) one can assume a constant q_c over depth. Hence, an average q_c-value for experiment 0 is found, which is then subtracted from the total resistance force. This will result in f_s, *EQ* 22

$$F_T = F_q + F_f + F_d + F_b \qquad 22$$

With the force at the tip $F_q = A_c\, q_c$ and the force at the sides $F_f = A_s\, f_s$ (A_c, the q_c-area and A_s, the f_s-area). Albatal and Stark (2017) argue that the force at the sides, F_f, the drag force, F_d, and the buoyancy force, F_b, can be neglected due to limited cone dimensions and penetration depth. However, M.1 Figure 2a shows the total force, normalized to q_c-area, called apparent tip resistance ($q_{c,a}$), and q_c over depth.

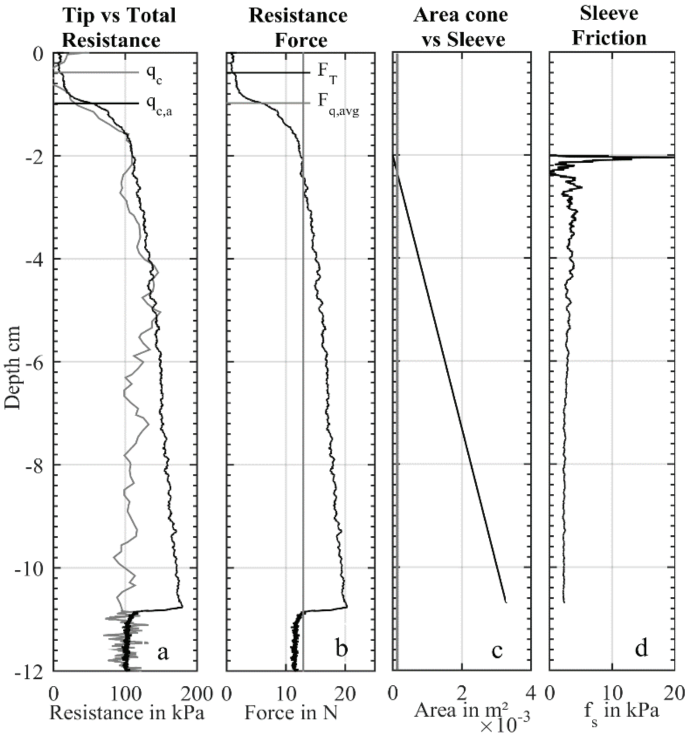

M.1 Figure 2. a: Differences in apparent tip resistance ($q_{c,a}$) and q_c in kPa. b: Resistance force vs average-force at tip. c: Advancing area of the sleeve. d: Deducted sleeve friction in kPa. Execution with standard penetration velocity.

q_c remains around an average of 114 kPa. Whereas, apparent q_c is increasing with depth (~7.33 kPa/cm). Here, the maximum difference between q_c and apparent q_c is 66 kPa, which is 36% of the apparent q_c, but would increase for higher depths. At depth 2 cm (3.3 times cone radius) surficial boarder effects on the q_c and apparent q_c stabilize (Chow et al., 2014). Therefore, this depth was taken as reference depth for the estimation of the dynamic q_c ($q_{c,dy}$). M.1 Figure 2b shows total force in N over depth with an average tip force as reference (~13 N, grey line). The difference of these forces equals the sleeve force. M.1 Figure 2c shows the calculated increasing f_s-area of the advancing lance over depth (black line) vs. the constant q_c-area (~ 0.113x10^{-3} m², grey line). The resulting f_s is shown in M.1 Figure 2d. f_s is constant over depth where the f_s-area is bigger than the q_c-area with a value of ~3 kPa

M.1.3.2 Velocity dependency on tip resistance

M.1 Figure 3 shows all calculated or measured and averaged q_c-data. Estimations of static q_c, where not directly measured, were done via the reference depths 2 cm, where f_s is supposed to equal ~0 and the q_c-area is bigger than the f_s-area. The dynamic tip resistance ($q_{c,dy}$) was calculated via the acceleration-data, EQ 23:

$$q_{c,dy}=\frac{m\,(g-a(s^{*}))}{A_c} \tag{23}$$

with $a(s^*)$ = acceleration data between 2 – 2.5 cm (~3.3 – 4.16 times cone radius), where the q_c-area is bigger than the f_s-area. The correlation of the normalized tip resistance ($Q_c = q_c/q_{c,st}$) vs. the logarithmic normalized penetration velocity gives two regression lines which follow the expression of EQ 19 (M.1

Figure 3). This provides two new penetration rate factors: 0.74 and 0.31 for 32 and 64 kPa effective consolidation stress, respectively.

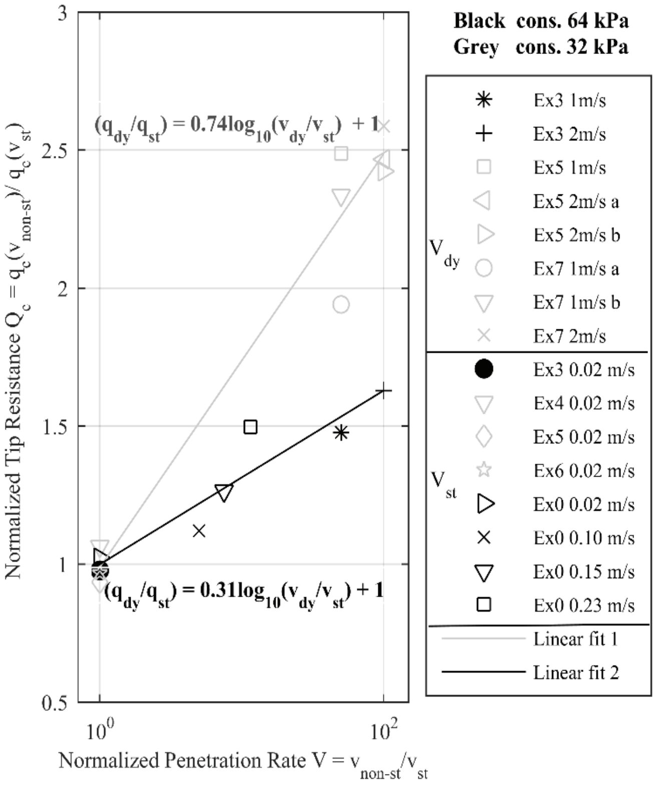

M.1 Figure 3. Dynamic qc normalized to qc for Vst (qc,st) versus the logarithmic V normalized to Vst. Legend is divided into static and dynamic tests. Black symbols represent experiments with a consolidation history of 64 kPa. Grey symbols stand for 32 kPa.

M.1.3.3 Pore pressure data and clogging effect

Measured u_2 over time (t) is shown in M.1 Figure 4*a* displays u_2 for constant velocities (0.02 m/s), while M.1 Figure 4*b* displays dynamic u2-data for falling heights of 5 cm (impact velocity 1 m/s) and M.1 Figure 4*c* for falling heights of 20 cm (impact velocity 2 m/s), respectively. Please note different time scales. Additionally M.1 Figure 4*b* and *c* include free fall time through the air while M.1 Figure 4*a* shows only the penetration time. Hence, M.1 Figure 4*b* and *c* are divided into 3 time sequences: (1) the jerk, the initial 0.02 s of the acceleration, where $\delta a/\delta t \neq 0$ (m/s³), (2) acceleration in the air and (3) acceleration in the sediment. The effectiveness of each cleaning option can be evaluated with M.1 Figure 4. Swiping cleans less than 50% porous filter stones contamination (M.1 Figure 4*b* and *c* experiment 3). Flushing does clean current contamination by ~80 % (M.1 Figure 4*b* and *c*, experiment *4a*, *4b*, 5*a* and 5*b*, respectively). Pogo-deployment hinders u2-acquisition immensely (M.1 Figure 4*b* and *c*, experiment *7* and *6*). Moreover, the effectiveness of the filter stone is reduced by around 35 % per penetration experiment (M.1 Figure 4*a*).

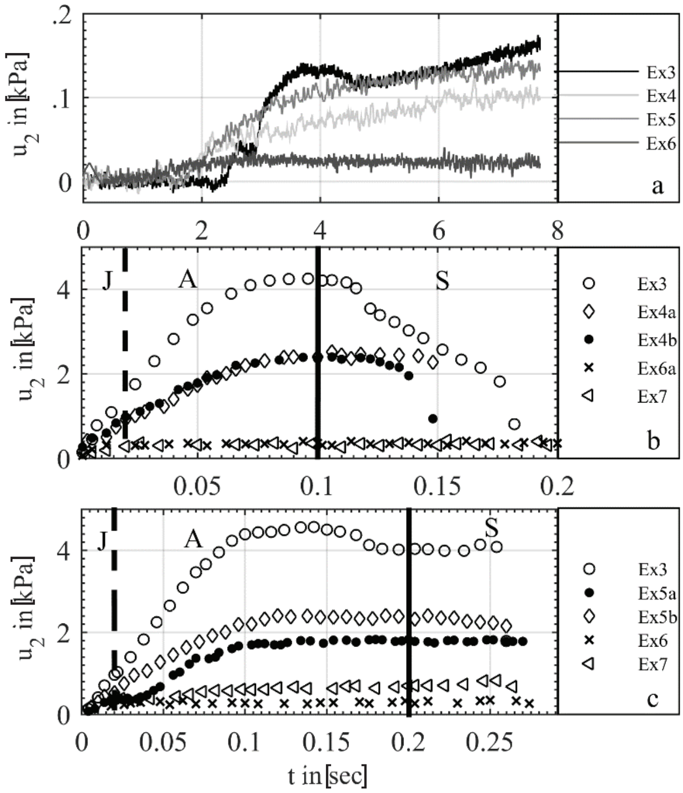

M.1 Figure 4. a: Static u2 over time for experiment 3 to 6. b: Dynamic u2 (falling height = 5 cm, impact velocity = 1 m/s) over time for experiment 3, 4, 6 and 7. 6b is not shown (due to reasons of clarity and comprehensibility) but behaves like 6a. c: Dynamic u2 (falling height = 20 cm, impact velocity = 2 m/s) over time for experiment 3, 5, 6 and 7. Description in text.

M.1.3.4 Qualitative evaluation of dynamic pore pressure data in comparison to static data

M.1 Figure 5 shows a qualitative evaluation of excess pore pressure (δu_2) for experiment 3. The modulus of the dynamic excess pore pressure ($|\delta u_{2,dy}|$) have higher values then the modulus of the static data ($|\delta u_{2,st}|$, M.1 Figure 5a). The trend evaluation indicates a constant or slightly increasing trend after the first 2 cm ($\delta u_{2,dy}/\delta u_{2,st}$ = 3.3, M.1 Figure 5b). A linear fit of static and dynamic excess pore pressure gives a goodness of fit of R^2 = 0.992 (M.1 Figure 5c).

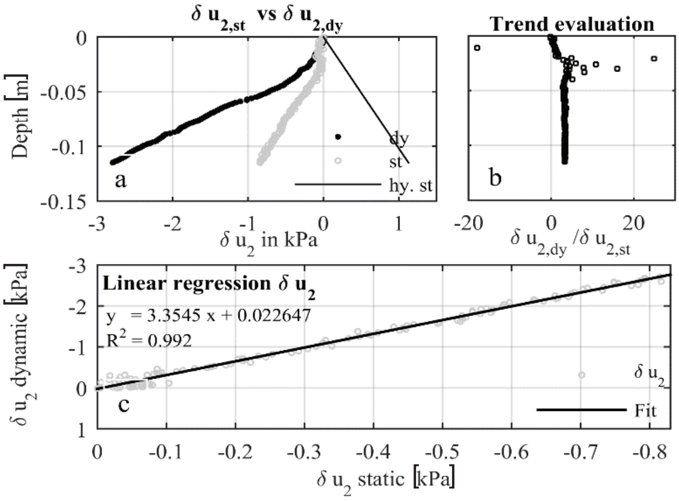

M.1 Figure 5. Excess pore pressure analysis. a: δu_2 static vs. dynamic over depth. b: Ratio of dynamic and static showing trend evolution. c: Linear regression between δu_2 static vs. dynamic.

M.1.4 Discussion

M.1.4.1 Estimation of tip resistance and sleeve friction via acceleration data

In contrast to Stark (2011) and the later publication of Stark (Albatal and Stark, 2017; Lucking et al., 2017), this experiment shows a clear dependency of the total force on sleeve friction (~36%), which increases for greater penetration depth (M.1 Figure 2).

Note: It needs to mentioned that the later publications of Stark (Albatal and Stark, 2017; Lucking et al., 2017), which refer to the *portable FF CPTu Bluedrop*, deal with the friction problem by changing the geometry of the portable device. The tapered geometry only features 8 cm of cylindrical sleeve contact area, which of course reduces the actual influence of the friction for the *Bluedrop* (Albatal and Stark, 2017; Lucking et al., 2017; Stark and Ziotopoulou, 2017). Furthermore, it should also be mentioned that the influence of the side friction does not only depend on the geometry of the instrument (compare *Bluedrop* to *Nimrod* (Stark, 2011)), but also on the soil type. Non-cohesive soils such as sands, which naturally have a lower friction then cohesive soils, might also show negligible friction forces (Stephan, 2015)

However, the estimation of the dragging force and buoyancy force (EQ 22, cumulative effect < 5% of the total force) was found negligible for these free fall calibration tests. M.1 Figure 2 at depth 2 to 2.5 cm shows f_s-instabilities, which is a result of the q_c-area being bigger than the f_s-area. Therefore, we recommend calculating f_s only for depth where the f_s-area is bigger than the q_c-area. Nevertheless, the obtained constant f_s-values after a depth of 2.5 cm indicates success in deducting kinematic f_s via acceleration-data. The derived values of ~3 kPa are in range for cohesive sediments with a clay content of ~8% (Lunne, Powell, et al., 1997).

M.1.4.2 Velocity dependency on tip resistance

Penetration rate factors of this study go well with literature values (Dayal and Allen, 1975; Steiner, 2013). Furthermore, the penetration rate factor for fit one (32 kPa consolidation stress) is almost twice as high as for fit two (64 kPa consolidation test). This suggests the lower the maximum consolidation the higher the penetration rate factor. The consolidation is a reflection of the dissipated pore water in the sediment. Lower stages of consolidation can have a higher pore water volume, which can increase excess pore pressure in cohesive soils, especially with penetration velocities bigger than standard penetration velocity. Hence, the effective stress decreases and q_c increases due to undrained conditions (Salgado et al., 2013).

M.1.4.3 Pore pressure data

M.1 Figure 4a shows a clear decrease in u_2 over all experiments, suggesting a lifespan of the filter stone of 1 to 2 experiments. Static u_2-data for experiment 3 and 4 seem similar, because of the different consolidation stresses. Flushing the filter stone in-between penetrations can enhance the performance of the filter stone (M.1 Figure 4b and c experiment 4a to b and 5a to b). M.1 Figure 4b and c (experiment 3, 6 and 7) show that the options of swiping and pogo-mode are insufficient for laboratory experiments due to lack of ambient pressure which might re-saturate the filter stone (Lucking et al., 2017; Sandven, 2010). Furthermore, the dynamic data indicate a direct influence of the acceleration on the u_2-data, shown in M.1 Figure 4b and c. The jerk and acceleration in the air clearly overprints u_2-data. This can be dealt with if u_2-is set to zero upon impact. Nevertheless, the acceleration-influences on u_2 might suggest that if the acceleration changes abruptly, another jerk might appear, distorting the true soil u_2-signals.

Note: The jerk might especially influence the mass of the u_2-sensor, changing its momentum short and abruptly, overprinting the actual pore pressure signal.

Moreover, there seems to be an artificial bias (visible in M.1 Figure 4c experiment 3, as a sin function), indicating a friction effect from the guiding system and deflection rollers of the free fall tower, on the measurements (M.1 Figure 1). However, no frequency analysis has been done yet.

M.1.4.4 Qualitative evaluation of dynamic pore pressure data in comparison static data

M.1 Figure 5 shows a direct correlation between penetration velocities and modulus excess pore pressure. The relation for mono-layered cases may be estimated via trend evaluations. Layered-systems might not be as simple due to different pore pressure distribution and boundary conditions.

M.1.5 Conclusion

We investigated kinematic *CPTu* parameters on a descriptive basis. No generalisations are made about kinematic testing yet, but we regard our experimental efforts to implement calibration free fall tests as successful. In respect to the goals introduced above, we conclude that: (1) we successfully deployed a method to derive kinematic total force, and divide it into kinematic q_c and f_s for a known geometrical-setup. The deduction of kinematic f_s opens the possibility for further analyzes like the soil classification charts of Robertson (1990) and shall be investigated in a field study in the estuary Firth of Thames, New Zealand, with the impact penetrometer '*Nimrod*' (Stark, 2011). (2) We derived two consolidation-history dependent penetration rate factors for remolded overconsolidated, cohesive soils. (3) Modulus excess pore pressure increases with enhanced penetration velocity if equal experimental conditions are used. (4) Pogo-deployments are insufficient for laboratory tests.

M.1.6 Acknowledgements

We thank the Deutsche Forschungsgemeinschaft (*DFG*) for funding this project through the international graduate school INTERCOAST at MARUM, University of Bremen. Furthermore, we would like to thank C. Zoellner, T. Fleischman and M. Huhndorf for their technical support, A. Saeed for student assistance, J. Titschack for grain size analysis, M. Kluger, A. Roesner, W. Menapace and E. Horstman for helpful comments.

M.1.7 Literature

1. 18122, D., 2000. Din Deutsche Institut Für Normung E. V., Zustandsgrenzen (Konsitenzgrenzen). Beuth, Berlin.
2. Albatal, A., Stark, N., 2017. Rapid Sediment Mapping and in Situ Geotechnical Characterization in Challenging Aquatic Areas. Limnology and Oceanography: Methods, V. 15, No. 8, p. 690-705, doi# doi.org/10.1002/lom3.10192.
3. Burns, S., Mayne, P., 1998. Monotonic and Dilatory Pore-Pressure Decay During Piezocone Tests in Clay. Canadian Geotechnical Journal, V. 35, No. 6, p. 1063-1073, doi# doi.org/10.1139/cgj-35-6-1063.
4. Chow, S., O'Loughlin, C., Randolph, M., 2014. Soil Strength Estimation and Pore Pressure Dissipation for Free-Fall Piezocone in Soft Clay. Géotechnique, V. 64, No. 10, p. 817-827, doi# doi.org/10.1680/geot.14.P.107.
5. Chow, S., O'Loughlin, C., White, D., Randolph, M., 2017. An Extended Interpretation of the Free-Fall Piezocone Test in Clay. Géotechnique, V. 67, No. 12, p. 1090-1103, doi# doi.org/10.1680/jgeot.16.P.220.
6. Dayal, U., Allen, J.H., 1973. Instrumented Impact Cone Penetrometer. Canadian Geotechnical Journal, V. 10, No. 3, p. 397-409, doi# doi.org/10.1139/t73-034.
7. Dayal, U., Allen, J.H., 1975. The Effect of Penetration Rate on the Strength of Remolded Clay and Sand Samples. Canadian Geotechnical Journal, V. 12, No. 3, p. 336-348, doi# doi.org/10.1139/t75-038.
8. DIN, 2012. Din Deutsche Institut Für Normung E. V. Eindimensionaler Kompressionsversuch. Beuth, Berlin.
9. Keaveny, J., 1985. In-Situ Determination of Drained and Undrained. University of California, Berkeley.
10. Lu, Q., Randolph, M., Hu, Y., Bugarski, I., 2004. A Numerical Study of Cone Penetration in Clay. Géotechnique, V. 54, No. 4, p. 257-267, doi# doi.org/10.1680/geot.2004.54.4.257.
11. Lucking, G., Stark, N., Lippmann, T., Smyth, S., 2017. Variability of in Situ Sediment Strength and Pore Pressure Behavior of Tidal Estuary Surface Sediments. Geo-Marine Letters, V. doi.org/10.1007/s00367-017-0494-6, No. 37, p. pages441–456 doi# doi.org/10.1007/s00367-017-0494-6.
12. Lunne, T., Powell, J.J.M., Robertson, P.K., 1997. Cone Penetration Testing in Geotechnical Practice. Taylor & Francis.
13. Paniagua, P., Carroll, R., L'Heureux, J.-S., Nordal, S., 2016. Monotonic and Dilatory Excess Pore Water Dissipations in Silt Following Cptu at Variable Penetration Rate. 5th INTERNATIONAL CONFERENCE ON GEOTECHNICAL AND GEOPHYSICAL SITE CHARACTERISATION (ISC5), V. 5, No. 5, p., doi# hdl.handle.net/11250/2491806.
14. Riggs, C., 1982. A Proposed Standard Test Method for a Free Fall Penetration Test. Geotechnical Testing Journal, V. 5, No. 3/4, p. 89-92, doi# doi.org/10.1520/GTJ10808J
15. Robertson, P.K., 1990. Soil Classification Using the Cone Penetration Test. Canadian Geotechnical Journal, V. 27, No. 1, p. 151-158, doi# doi.org/10.1139/t90-014.

16. Roskoden, R., 2016. Cone Penetration Tests the Soil Classification and Analytic Assessments of Dynamic and Static Penetrometer Test Data. Universität Bremen, Master Thesis, 2016, Bremen.

17. Salgado, R., Prezzi, M., Kim, K., Lee, W., 2013. Penetration Rate Effects on Cone Resistance Measured in a Calibration Chamber, 4th International Conference on Site Characterization, ISC'4, pp. 1025-1030

18. Sandven, R., 2010. Influence of Test Equipment and Procedures on Obtained Accuracy in Cptu, 2nd International Symposium on Cone Penetration Testing.

19. Seifert, A., Stegmann, S., Mörz, T., Lange, M., Wever, T., Kopf, A., 2008. In Situ Pore-Pressure Evolution During Dynamic Cpt Measurements in Soft Sediments of the Western Baltic Sea. Geo-Marine Letters, V. 28, No. 4, p. 213-227, doi# doi.org/10.1007/s00367-008-0102-x.

20. Stark, N., 2011. Geotechnical Investigation of Sediment Remobilization Processes Using Dynamic Penetrometers, Marine Geotechnics. Universität Bremen, Bremen, p. 309.

21. Stark, N., Ziotopoulou, K., 2017. Undrained Shear Strength of Offshore Sediments from Portable Free Fall Penetrometers: Theory, Field Observations and Numerical Simulations, Offshore Site Investigation Geotechnics 8th International Conference Proceeding. Society for Underwater Technology, pp. 391-399.

22. Stegmann, S., Mörz, T., Kopf, A., 2006. Initial Results of a New Free Fall-Cone Penetrometer (Ff-Cpt) for Geotechnical in Situ Characterisation of Soft Marine Sediments. Norwegian Journal of Geology/Norsk Geologisk Forening, V. 86, No. 3, p. 199-208, doi# PANGAEA reference ID: 27196 Serial: RCOM0398.

23. Steiner, A., 2013. Sub-Seafloor Characterization and Stability of Submarine Slope Sediments Using Dynamic and Static Piezocone Penetrometers, Marine Geotechnics. Universität Bremen, Bremen, p. 325.

24. Stephan, S., 2015. A Rugged Marine Impact Penetrometer for Sea Floor Assessment. Universität Bremen, , Bremen,, p. 268.

25. Stoll, R.D., Sun, Y.F., Bitte, I., 2007. Seafloor Properties from Penetrometer Tests. IEEE Journal of Oceanic Engineering, V. 32, No. 1, p. 57-63, doi# 10.1109/Joe.2007.890943.

Chapter 3:

Manuscript 2 - Prefix The geometrical algorithm

P.M.2.1 The influence of friction

The influence of friction for kinematic penetration devices was always neglected or rationalized to be too weak of a force to be recognised in the geotechnical analysis. The argumentations are based on the dimension of the lightweight penetrometers. However, if all the possible forces, which act on a penetrometer lance, are considered, *EQ* 24 is yielded:

$$F_T = F_q + F_f + F_d + F_b \tag{24}$$

with $F_q = A_c\, q_c$, the cone resistance force (A_c, is the area of the cone and q_c is the cone resistance) and $F_f = A_s\, f_s$, the friction force on the sides (A_s is the area of the side, and f_s is the resistance of the sides). The buoyancy force (F_b, *EQ* 25) is

$$F_b = g\rho_s V_s \tag{25}$$

where g is the earth acceleration, ρ density of the soil and V the Volume of the soil displaced, index s for the soil. The drag force (F_d, *EQ* 26)

$$F_d = \frac{1}{2}\rho_s \mathrm{C_D A_c v^2} \tag{26}$$

where C_D is the drag coefficient, and v the penetration velocity.

On the one hand, Albatal and Stark (2017), Stark and Ziotopoulou (2017) and Lucking et al. (2017) argue that the force at the sides, the drag force, and the buoyancy force can be neglected due to the limited cone dimension and low penetration depth. This might be true for the *Bluedrop* and its tapered geometry. However, for the *Nimrod*, which is utilized for the upcoming field study, and its geometry is slightly different. Similar to the *Bluedrop*, the geometry of the Nimrod also allows to neglect the buoyancy and drag force. First of all, these two forces are counter acting, which means here the drag force decreases with penetration because the dynamic velocity decreases with penetration while the buoyancy force increase with penetration and is highest when the penetration device is fully submerged. The cumulative effect of the dragging force and buoyancy force (*EQ* 24) was calculated, e.g. for the free fall calibration tests from the manuscript 1 and was found negligible because it was less than 5% of the total force (Roskoden et al., 2018). Nonetheless, as mentioned in the Manuscript I, not only the geometry of the portable FF CPTu needs to be considered if friction forces are discussed, but also the soil at hand needs to be considered (compare for example Stephan (2015) versus Roskoden et al. (2018)). The latter poses some difficulty, because if no information of the investigated soil is know it will be complicated to decide if the friction force needs to be considered. A possible solution could be to use the current *portable FF CPTu* classification charts to get a first impression about the soil properties (Mulukutla et al., 2011).

In contrast to Stark and Kopf (2011) (Albatal and Stark, 2017; Lucking et al., 2017), the experiment presented by Roskoden et al. (2018) shows a clear dependency of the total force on sleeve friction (~36%), which increases for greater penetration depth but is biggest when the lance is fully submerged.

Note: The maximum influence of the friction force is given when the area of contacted is biggest, assuming homogenous soil conditions.

Depending on the ratio between the rod and cone area, or alternatively the cone radius and penetration depth, (A_c/A_s or $r_c/2d > 1/8$, with d the penetration depth), the influence of the friction cannot be neglected (depending on the geometrical set up of the probe). Hence, EQ 24 can be reduced to EQ 27:

$$F_T = F_q + F_f \tag{27}$$

P.M.2.1.1 Monolayer Case

The monolayer case was greatly discusses in manuscript 1. Hence, only a brief summary is given.

The resistance force at the tip, if the sediment type does not change, will remain constant and is equal to the total resistance force as long as the ratio of cone radius and submerged penetration depth ($r_c/2d$) ≤ 1/8 (Roskoden et al., 2018). Afterwards, the tip force can be used as a constant offset value. Thus, any further enhanced total resistance force during penetration can be added to the friction force if bouncy is neglected as argued before. If these forces are divided by their respective areas (note: mantel area increases with penetration depth), the resulting resistance pressures should remain constant as well. EQ 28 shows the principle

$$F_{T1} = F_{q1} + (F_{T0} - F_{T1}) = F_{q1} + F_{f1} \tag{28}$$

Here, the index 1 at F_{T1} symbolizes that the total resistance during penetration changes (in this case increases). F_{q1}, the cone resistance force stays constant, and all changes in $F_{T1}$are added to the resistance force at the side F_{f1}. Note that F_{f1} will increase constantly but the side friction f_s will remain the same.

Hence, two geotechnical properties, (besides the ultimate bearing capacity) namely the cone resistance and the side friction, are yielded only from the acceleration data, if the other mentioned forces can be neglected. Again this is very much soil dependent and mostly applies to cohesive soils as considered in the *Manuscript I* and *II*.

P.M.2.1.2 Two Layer Case

However, what happens if not a mono but a two layer case is considered. In the geophysical disciplines such as geo-electrics or geo-magnetics very similar problems arise: having one set of measuring parameters but not knowing how many layers need to be considered. The solution here is the backcalculation.

The data analysist assumes a model to fit the predicted data best to the measured data. If the offset between predicted and measured data is too big, the assumed model will be refined until the fitting procedure reaches a defined threshold. The problem at hand is very similar. There is only one measuring parameter, the acceleration, and the amount of layers is unknown before. The problem was very similar described by (Stark and Wever, 2009). In order to create a better understanding a schematic illustration will demonstrate how the geometrical algorithm works, P.M.2 Figure 1.

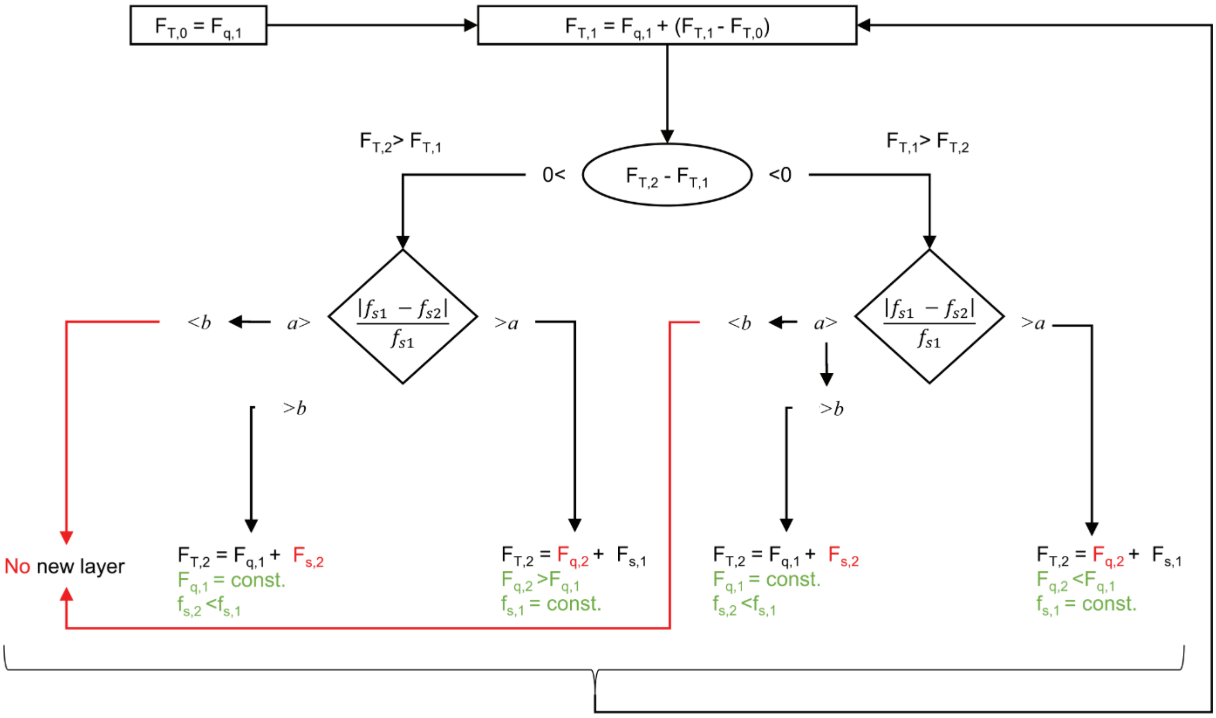

P.M.2 Figure 1 Schematic presentation of the general form of the geometric algorithm. First, the total force will be only attributed to the tip resistance force. While the cone advances the difference between the total and tip resistance force will be ascribed to the side friction force ($F_s = F_T - F_q$).

The first block demonstrates the initial penetration, when $r_c/3d \leq 1/4$. Afterwards, assuming we are still in the same layer, any increase in the total resistance force will be added to the friction force and recalculated into the side friction, as long as the side friction stays stable (in [kPa]). In case the difference of the total resistance is smaller than zero ($F_{T1} - F_{T2} < 0$) and the side friction changes in between the defined default variances a, and b

$$a < \frac{|f_{s1} - f_{s2}|}{f_{s1}} < a \tag{29}$$

then the conclusion is, that a new layer is penetrated. If the change in EQ 29 is smaller than a but bigger than b the change in the total force is too great to assume a constant f_s. Therefore, EQ 28 becomes EQ 30

$$F_{T2} = F_{q1} + (F_{T1} - F_{T2}) = F_{q1} + F_{f2} \tag{30}$$

Note the indexes of F_T are always increasing because F_T always changes. Here also F_f changes its index from 1 to 2 because f_{s1} is out of its default boundaries, so that f_s is not constant anymore. Hence, a new layer is found with the same tip resistance but a smaller side friction.

If the change is greater than the predefined value a, the new layer will have a weaker cone resistance and therefore the value of F_q must be recalculated. Evidently, the recalculation of F_q starts at the depth where f_s was not constant anymore.

If $F_{T1} - F_{T2} > 0$, and $f_s = const.$ then again a new layer is penetrated. So if EQ 29 is bigger than a then that means the penetrometer enters a layer with an increased cone resistance, while if EQ 29 is smaller than a, then this means again f_s is not constant but here the new layer is more cohesive and therefore the sleeve friction increases while the cone resistance stays the same.

The default value a needs to be estimated best by a grainsize analysis which can be correlated for example to the chart of Begemann (01 August 2018) (P. Figure 2).

Note: P.M.2 Figure 1 only describes the general idea of the geometric algorithm. However, the algorithm always needs to be adapted to the local specific parameters: For example dimension of the penetrometer, grain size description etc. Hence, the resolution to detect new layers also depends on the geometry of the penetrometer lance. Smaller lances can detect smaller/ thinner layers more easily.

P.M.2.1.3 Testing of the geometrical algorithm for the two layered case

In the previous manuscript the free fall calibration test is described. However, here only the monolayer cases are presented. Nevertheless, the experiment 8 of the study, which was not discussed yet, was constructed to be a two layered case. The following experimental settings were used to conduct the experiment.

Sample preparation:

First, the same synthetic clay mixture was filled into the experimental container and was consolidated to the total overburden stress of 32 kPa. Then a sand mixture was prepared:

- Sand mixed with gravel (22%) -> 2 kg sand and 0.6 kg gravel
- Water saturated
- Total mass ~ 14 kg
- Layer sickness 5 cm

After implementing the sand layer, the specimen was reconsolidated to 32 kPa. Hence, layering of the specimen was:

- Sand mixture (5 cm)
- Paper (so that during consolidation no sand was moved into the clay mixture)
- Clay
- Grid
- PP Stone Gravel (5cm)

The application of the algorithm and its results can be seen in P.M.2 Figure 2. Here, first the ultimate bearing capacity (q_u) was calculated, to identify the layer boundaries. Second, the total resistance and the difference in total resistance between two measuring points was calculated to identify the changes in the resistance. Third, as mentioned in P.M.2 Figure 1, the tip and side friction are calculated. In this case, almost all the total resistance force for the sand layer was attributed to the tip resistance, because of the boundary effects (area sides was not yet big enough to calculate any friction). However, when the layer changes the difference between q_u and the tip resistance becomes very clear as described in the chapter before (Manuscript I).

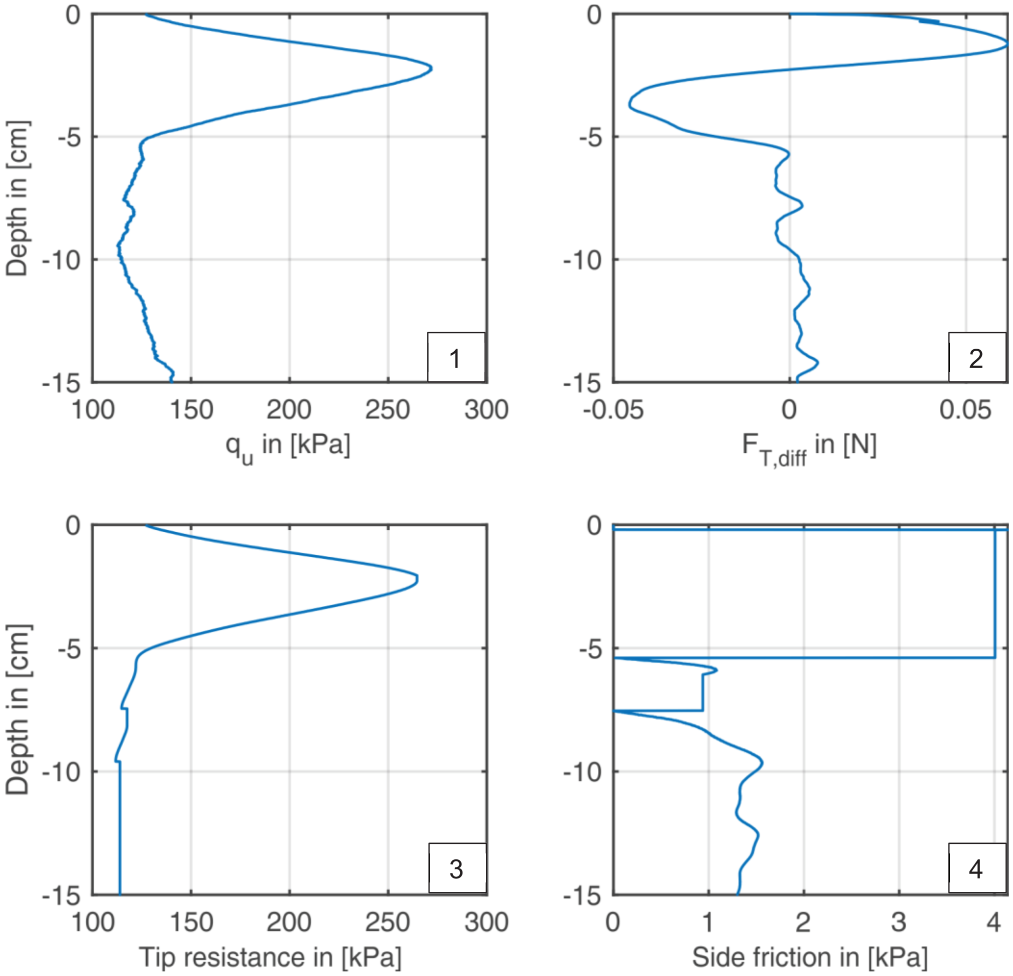

P.M.2 Figure 2 Application of the geometrical algorithm. Panel 1 the total resistance divided by the cone area, so the ultimate bearing capacity [kPa] vs. the depth [cm]. Panel 2 the differences of total resistance [N] vs. the depth [cm] compare P.M.2 Figure 1 at $F_{T,1} - F_{T,2}$. Panel 3 the estimated tip resistance [kPa] vs. the depth [cm]. Panel 4 the estimated side friction [kPA] vs. the depth [cm] Note: The depth of the friction is adapted to the depth of the cone. At ~ 5 cm the friction is zero, because a new layer was penetrated. At ~ 7.5 cm the friction is again zero, which could be either due to local anomaly (e.g. single grain which sank down), which makes it seem like a new layer is penetrated again

An infield application and ground proofing of the geometrical algorithm can be seen in the Manuscript II, which was published in the peer reviewed Cone Penetration Test conference *CPT'18*.

P.M.2.2 References

1. Albatal, A., Stark, N., 2017. Rapid Sediment Mapping and in Situ Geotechnical Characterization in Challenging Aquatic Areas. Limnology and Oceanography: Methods, V. 15, No. 8, p. 690-705, doi# doi.org/10.1002/lom3.10192.

2. Begemann, H., 01 August 2018. The Friction Jacket Cone as an Aid in Determining the Soil Profile, Proceedings of the 6th International Conference on Soil Mechanics and Foundation Engineering, ICSMFE, Montreal, September. Springer, Cham, pp. 8-15.
3. Lucking, G., Stark, N., Lippmann, T., Smyth, S., 2017. Variability of in Situ Sediment Strength and Pore Pressure Behavior of Tidal Estuary Surface Sediments. Geo-Marine Letters, V. doi.org/10.1007/s00367-017-0494-6, No. 37, p. pages441–456 doi# doi.org/10.1007/s00367-017-0494-6.
4. Mulukutla, G.K., Huff, L.C., Melton, J.S., Baldwin, K.C., Mayer, L.A., 2011. Sediment Identification Using Free Fall Penetrometer Acceleration-Time Histories. Marine Geophysical Research, V. 32, No. 3, p. 397-411, doi# doi.org/10.1007/s11001-011-9116-2.
5. Roskoden, R., Kopf, A., Mörz, T., Kreiter, S., 2018. Analysis of Acceleration and Excess Pore Pressure Data of Laboratory Impact Penetrometer Tests in Remolded Overconsolidated Cohesive Soils, Cone Penetration Testing 2018. CRC Press, p. 545-550, -.
6. Stark, N., Kopf, A., 2011. Detection and Quantification of Sediment Remobilization Processes Using a Dynamic Penetrometer, OCEANS'11 MTS/IEEE KONA. IEEE, pp. 1-9.
7. Stark, N., Wever, T.F., 2009. Unraveling Subtle Details of Expendable Bottom Penetrometer (Xbp) Deceleration Profiles. Geo-Marine Letters, V. 29, No. 1, p. 39-45, doi# doi.org/10.1007/s00367-008-0119-1.
8. Stark, N., Ziotopoulou, K., 2017. Undrained Shear Strength of Offshore Sediments from Portable Free Fall Penetrometers: Theory, Field Observations and Numerical Simulations, Offshore Site Investigation Geotechnics 8th International Conference Proceeding. Society for Underwater Technology, pp. 391-399.
9. Stephan, S., 2015. A Rugged Marine Impact Penetrometer for Sea Floor Assessment. Universität Bremen, , Bremen,, p. 268.

Manuscript 2

Rapid transition of sediment consolidation across an expanding mangrove fringe in the Firth of Thames New Zealand.

first author, published at the Geo-Marine Letters, 2019, DOI:10.1007/s00367-019-00589-9

Authors

Robert R Roskoden*,[1]

Achim Kopf*,[3]

Isabel Schreiber*,[2]

Karin R Bryan#

*MARUM–Center for Marine Environmental Sciences, University of Bremen,
Leobener Straße, 28359 Bremen, Germany

([1]rroskode@marum.de (ORCID: https://orcid.org/0000-0003-2170-283X),
[2]akopf@marum.de, [3]ischreib@uni-bremen.de)

#School of Science, University of Waikato, Private Bag 3105, Hamilton 3240, New Zealand
(karin.bryan@waikato.ac.nz)

M.2 Abstract

Mangrove habitats are complex systems, which are subjected to both natural and human external forces such as tidal variations, sediment supply, deforestation and climate change, which in many locations are causing mangroves to decline and even disappear. Global measurements of surface elevations have been conducted at many locations to understand if sedimentation rates in mangrove areas will keep pace with sea-level rise. However, extending results to other areas requires a detailed understanding of subsidence processes in mangrove areas. Here, we provide a detailed geotechnical investigation (sediment cone resistance and friction, coefficient of consolidation, grain size, normalised tip resistance and friction ratio etc.), critical for understanding surficial sediment dynamics and vertical sediment accretion rates, of the mangrove forest edge and its surrounding mud flat in the Firth of Thames, New Zealand. Eight *in situ* samples were collected and tested in oedometer experiments to evaluate the coefficient of consolidation. Furthermore, a kinematic penetrometer, NIMROD, was used to estimate the resistance forces of the mud flat and mangrove forest, from which soil properties were evaluated. Our results show that mangroves are able to change soil properties to enhance sediment resistance towards erosion. An increase of sediment strength correlated with an increase of mangrove tree density as well as a decrease in the coefficient of consolidation. Hence, the increase of tree density to a decrease of the coefficient of consolidation correlates as well. In this study our results suggest that the Firth of Thames mangroves are able to accrete enough sediment to keep up with local sea level rises if sediment supplies remain similar in the future. The correlation of tree density to the coefficient of consolidation can be used to assess future mangrove-soil interaction and mud flat progression. Finally, the applicability of literature soil classifications for the kinematic penetrometer was realized for the first time and applied to mangrove and mud flat areas.

M.2.1 Introduction:

M.2.1.1 Mangrove forests

Mangroves occur in tropical and subtropical low-lying estuaries, river deltas and muddy coasts and occupy 1,465,000 ha of coastline globally (Alongi, 2008). Large mangrove forests in estuaries can be found, for example, in South Africa, Australia and New Zealand (Swales et al., 2015). These coastal forests develop in mesotidal and macrotidal areas and provide a valuable habitat for flora and fauna (Alongi, 2008; Lovelock et al., 2015; Montgomery et al., 2018; Morrisey et al., 2010; Swales et al., 2015; Zhou et al., 2016). Their economic value is estimated to be around 194,000 – 900,000 USD per ha (Alongi, 2008; Lovelock et al., 2015). Due to their specific intertidal habitat, mangroves forests are often subjected to natural hazards such as storms surges, tidal bores, cyclones, hurricanes and tsunamis, and can play an important role in protecting low-lying coastal land (Alongi, 2008; Dahdouh-Guebas et al., 2005; Kathiresan and Rajendran, 2005). In addition, the reduction of hydrodynamic forces by mangrove forests promotes sedimentation and therefore land reclamation (Zhou et al., 2016).

Mangroves have been shown to keep pace with sea level rise over geologic timescales (Sasmito et al., 2016). Many studies exist investigating the modern-day mangrove sedimentation-potential relative to the local sea level rise using surface elevation tables (SET) (Lovelock et al., 2015; Swales et al., 2015; Swales et al., 2016). Unfortunately, especially in areas where subsidence processes are important SETs-techniques can be difficult to use (Alongi, 2008). Shallow subsidence processes include consolidation and compaction due to the self-weight of the sediment. Consolidation is a geotechnical process in which a load (either external or self-weight) acts on the water in the pore space in between the granular soil structure, and causes the sediment to reduce its volume by dewatering. The coefficient of consolidation (c_v) describes the rate at which soil undergoes consolidation if subjected to loading. When consolidation is complete, compaction reduces its volume even further, in which case the load acts on the granular structure itself. Due to the subsidence effects, recent modelling studies show that the effect of consolidation cannot be neglected and can lead to inaccurate time estimations (up to ten years) for wetland restoration projects (Zhou et al., 2016) and so Zhou et al. (2016) emphasize the need for *in situ* measurements to validate model predictions.

Detailed geotechnical information is a critical part of evaluating surficial sediment dynamics and their influence on vertical accretion rates to plan coastal engineering actions. Consolidation can be measured using a laboratory oedometer test, in which samples are subjected to a known loading. Grain size can also be measured in the laboratory but can be difficult to sample in remote areas. More efficient data sampling can be achieved with *in situ* cone penetration testing (*CPTu*). Consequently, to reduce the amount of sampling further needed geotechnical parameters such as sediment strength are commonly conducted with an *in situ* cone penetration piezometer and later correlated to few gathered samples. However, *CPTus* have many disadvantages, such as self-weight, which complicates the logistics and is exceedingly problematic for mud flat and mangrove studies, where the intertidal nature, the soft sediments and dense branching/root networks make boat or land access extremely difficult. Even more importantly, the self-weight often destroys the soil properties in the upper meters of the sediment (Steiner, 2013).

Here, a unique kinematic free fall penetrometer called 'NIMROD' (Stark, 2011) was chosen to investigate the geotechnical properties of a mangrove forest edge and surrounding mud flat in the Firth of Thames, New Zealand. In addition, eight *in situ* samples were taken and tested in oedometer experiments to evaluate the coefficient of consolidation and the grain size distribution. In our study, we explore the following scientific questions:

1. Is the coefficient of consolidation dependent on mangrove density?
2. Does the influence of mangroves distort the interpretation of the cone resistance forces for the geotechnical classification of soils?
3. Can the penetrometer resistance forces be correlated to the regional coefficients of consolidation?
4. Can this correlation shed light on how mangroves influence the consolidation process?

The answer to these research questions may help further modelling approaches for bed formation dynamics and give a clear understanding of the interaction between mangroves and the soil. Furthermore, it helps to improve future interpretation of dynamic and kinematic cone penetration investigations.

M.2.1.2 Study area Firth of Thames

The Firth of Thames, located in New Zealand's north island (37.25°S, 175.4°E), is characterised as a ~800 km² mesotidal estuary (M.2 Figure 1). The mangrove forest occupies an area between 1 and1.89 m above MSL (Montgomery et al., 2018). Mean annual precipitation is ~1,211 mm (Swales et al., 2015). Two rivers (Waihou and Piako) supply the Firth with 190,000 t sediment per year (Swales et al., 2015). The supplied sediment is terrigenous rhyolitic glasses, which transform into smectite muds after deposition in the Firth. The forest sits on a convex mud–ramp with a gradient of approximate 0.4° to horizontal mean sea level (down-sloping seaward, Swales et al. (2015)). The mangrove area is restricted to around 11 km² in the southern part of the Firth (Swales et al., 2015).

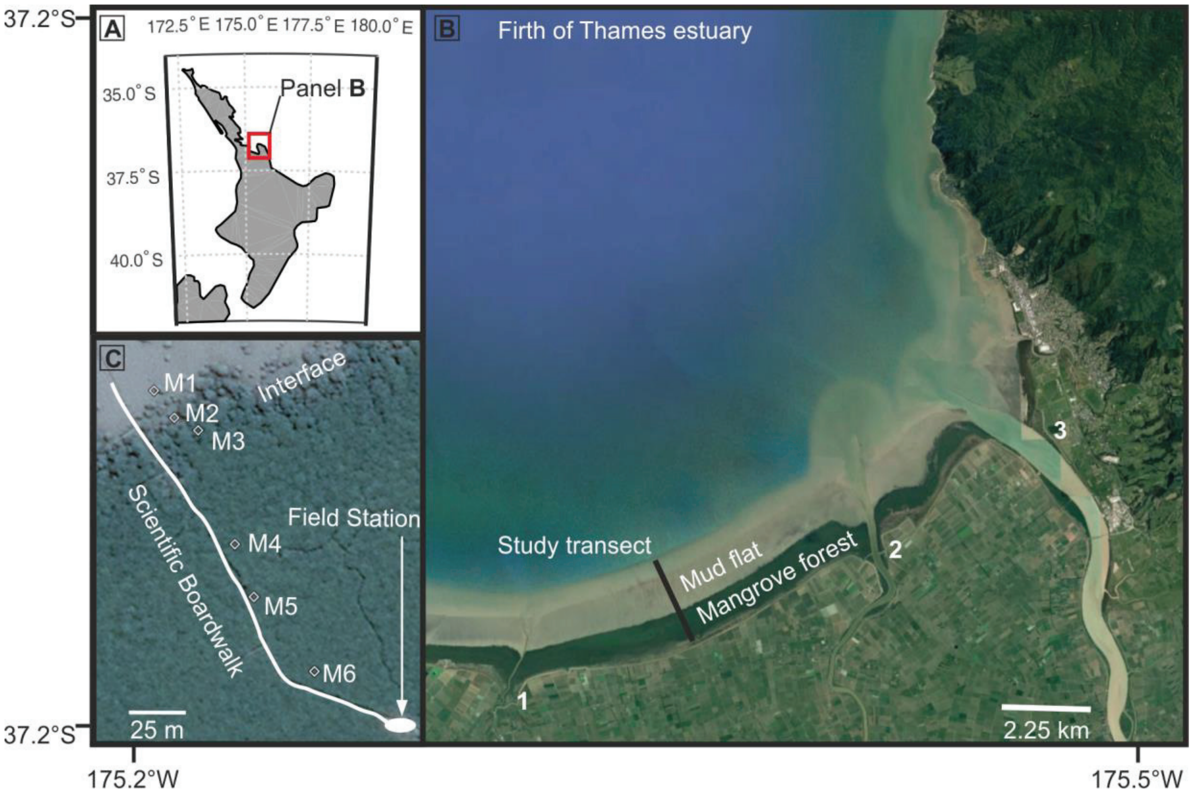

M.2 Figure 1 ***A****: Matlab (version R2015a) map of the North Island of New Zealand showing the Firth of Thames in a red rectangle.* ***B****: Modified Google Earth map 2018 (version 7.1.8.3036), Firth of Thames, New Zealand (37.25°S, 175.4°E), 21.09.2018. Marked as reference are from left to right 1 Waitakaruru River, 2 Piako River and 3 Waihou River. The study transect* (orientated perpendicular to the shoreline) is~3.6 km east of the 1 Waitakaruru River and ~5 km west from the 2 Piako River. ***C****: The study transect in the mangrove section displaying the measurement locations M1 (at the interface of 'mud flat-mangrove forest'), M2 (behind the interface) and M3 to M6 (increasing density of mangroves). M1 to M5 also represent the sampling location for the oedometer tests. M7 to M9 (not shown in panel C) are ~ 800 m south of the interface 'mud flat -mangrove forest' and ~ 600 m south of M6.*

M.2.2 Methods

M.2.2.1 Laboratory work

Five locations (M1 to M5) were identified for push-core sampling, representing areas of differing mangrove density (M.2 Table 1). The samples were tested for their grainsize distribution (for ground truthing purposes) and coefficient of consolidation. In order to test for repeatability, locations M3 to M5 (in the mangrove forest) were sampled twice with a spatial separation between replicates of up to 10 m. The first two samples were collected at the forest fringe and subsequent samples into the forest towards higher mangrove densities. Samples were taken using 25 cm long push cores. To ensure no more disturbance than necessary, samples were transported upright, keeping the *in situ* top/bottom position constant.

Grain size distribution was measured using the 'Malvern Mastersizer 3000 laser diffraction particle size analyzer'. Grain size samples were taken from the middle of each core (~ 10 cm). The test procedure followed the pre-programmed template for marine sediment at the University Waikato. The refraction index was 1.5, particle density 1, absorption index 0.2, refractive index 1.33 and 30% ultrasound for the pre-measurement Organic matter was not dissolved beforehand.

A one-dimensional compression test, called the oedometer test, measures the compaction of a soil due to vertical loading, which results in dewatering. The specimen is loaded incrementally, with the normal load (i.e. vertical stress) being doubled every 24 h while vertical deformation is measured over time. The test can characterise the following soil properties: Coefficient of consolidation (c_v), compression index (C_C), recompression index (C_R) and swelling index (C_S). The test was done with the 'Wykeham Farrance (Model 26 - WF0302)'-apparatus, following ISO (2017).

Since samples were taken near the surface, we assume no real vertical, *in situ*, total overburden effective stress on the samples. Hence, oedometer loading was sustained for 24 h at 250, 500, 1000 and 2000 g (~ 3 - 24 kPa). The log(t)-method after Casagrande and Fadum (1940) was chosen for the evaluation of the coefficient of consolidation. By identifying the initial, primary and secondary consolidation, which determines the time of 50 % consolidation, the coefficient of consolidation (c_v) was calculated as

$$c_v = 0.197 * \frac{\frac{(h)^2}{4}}{t_{50\%}} = \frac{k}{m_v \gamma_w} \tag{31}$$

with h, the height of the sample at 50 % consolidation, $t_{50\%}$ time of 50 % consolidation, k, the hydraulic conductivity, m_v, the coefficient of volume compressibility and γ_w, the specific unit weight of water.

The compression index (C_c), is the slope of the differences of the void ratio the differences of the effective stress

$$C_C = \frac{\Delta e}{\Delta \log \sigma'_{v0}} \tag{32}$$

with e, the void ratio, and σ'_{v0}, the effective vertical stress.

M.2.2.2 Kinematic Free Fall penetration tests

In contrast to free fall piezocone tests (*FFCPTu*) like those with the MARUM SUE (Stegmann et al., 2006), STING (Mulhearn, 2002), or even standard *CPTus* (Lunne et al., 2002), kinematic free fall penetrometers do not measure cone resistance (q_c) and side friction (f_s) directly but calculate them from acceleration data (Stark, 2011; Stephan, 2015). NIMROD was combined with the geometrical analysis approach of Roskoden et al. (2018) to estimate the resistance forces of the mud flat and mangrove forest. The kinematic free fall penetrometer NIMROD (M.2 Figure 2) , records pressure continuously as well as a wide range of high accuracy acceleration data (Stark (2011). The vertical accelerometer sensors are in the ranges of +/-1.7g, +/-18g, +/-35g, +/-70g and +/-250g. In addition, a dual axis accelerometer is used to determine tilt. Logger sampling rate is at 1 kHz. The pressure transducer is used to measure pore water and hydrostatic pressure up to 200 m water depth. NIMROD's weight is approximately 13.5 kg, measuring 81 cm in total length and consists of a 25 cm tail, 46 cm pressure housing and 10 cm long cone. Cone diameter is 11 cm, the resulting cone area is 95 cm².

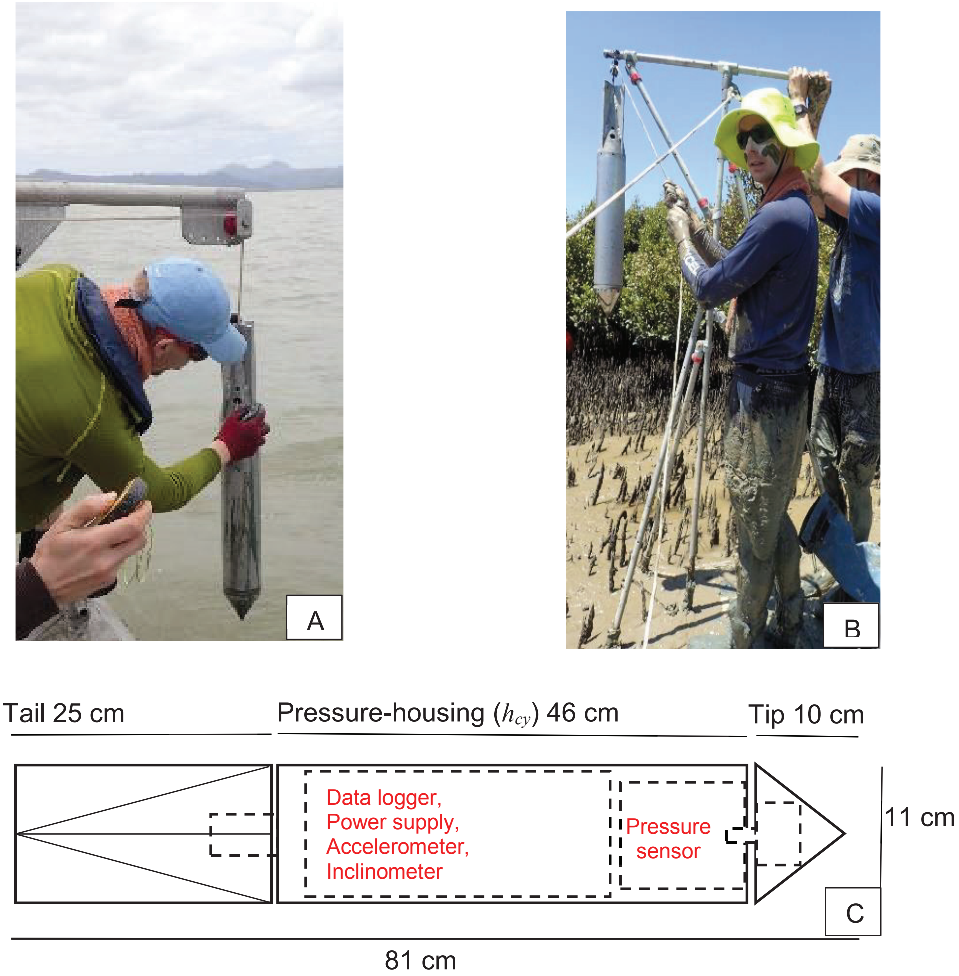

M.2 Figure 2 Panel A: NIMROD deployed at high tide using a winch on the boat transect; Panel B: NIMROD deployed using a purpose-built mobile free fall tower, height of the tower 2 m; Panel C: Design print of NIMROD and its dimensions.

NIMROD was deployed along a transect of ~2.25 km length (see M.2 Figure 1, black line marked *C*). The transect was located at the centre of the forest (and was orientated perpendicular to the shoreline), ~3.6 km east of the Waitakaruru River and ~5 km west from the Piako River. The transect was divided into two sections:

1. An outer section, which was sampled from a boat (called boat section), extending from the fringe seaward (location names B1 to B25)
2. An inner section (called mangrove section), which was sampled by foot (location names M1 to M9). This section also starts at the fringe but extends landward into the mangrove forest. Deployment was done with a purpose-built free fall tower (M.2 Figure 2 B)

For the boat section, NIMROD was deployed using a winch to ensure a consistent height above sea level (Figure 2). Along the forest transect, NIMROD was deployed using a purpose-built free fall tower, also ensuring a consistent falling height of ~120 cm (measured from the tip to ground level, Figure 2).

A free fall lance penetrates the soil using gravitational acceleration only. Upon impact, the penetrometer decelerates until the external forces such as friction and resistance at the tip exceed the instrument's kinetic energy.

Penetration depth is governed by falling height and sediment properties; therefore, penetration velocity and soil resistance can be used to determine sediment types (Dayal and Allen, 1973; Stark, 2011; Stoll et al., 2007b). Mulukutla et al. (2011) proposed the following factor of firmness (FF) as a measure of sediment type:

$$FF = \frac{a_{max}}{v_i * t_p * g} \tag{33}$$

where a_{max}, is the maximum acceleration of the instrument, v_i, is the impact velocity and t_p, the total penetration time and g, the gravitational constant 9.81 m/s². The factor of firmness decreases with an increase of grain size and decreases with the embedded instrument depth.

Further modifications to *Equation* 31 were made to connect deceleration records to geotechnical soil characteristics like undrained shear strength (Dayal and Allen, 1973; Dayal and Allen, 1975; Stark, 2011; Steiner, 2013; Stoll et al., 2007a). For the NIMROD measurements reported here, the original approach from Stark (2011) is to used calculate the quasi-static bearing capacity. The approach was expanded using geometrical considerations to determine quasi-static tip resistance and side friction (Roskoden et al., 2018). In this study, the deceleration and estimated quasi-static bearing capacity, cone resistance and side friction, were utilized to classify the soil and to detect changes between mangrove and non-mangrove areas. Soil samples are used to verify the measurements from NIMROD and correlate geotechnical properties to the penetration data.

Using Newton's second law of motion, the total resistance force (F_t) needed to decelerate NIMROD is:

$$F_t = m * dec \tag{34}$$

with m, the mass of NIMROD and dec, the deceleration. Considering all the possible forces, the total force can be apportioned into

$$F_t = F_q + F_f + F_d + F_b \tag{35}$$

where the force at the tip is $F_q = A_c\, q_c$ (A_c, is the area of the cone and q_c is the cone resistance) and the force at the sides (side resistance) is $F_f = A_s\, f_s$ (A_s is the area of the side, and f_s is the resistance of the sides). Albatal and Stark (2017) argue that the force at the sides, F_f, the drag force, F_d, and the buoyancy force, F_b, can be neglected due to the limited cone dimension and penetration depth. Hence, Albatal and Stark (2017) do not calculate the cone resistance but the total resistance, which they called the ultimate dynamic bearing capacity

$$q_{ud} = F_t / A_c \tag{36}$$

Roskoden et al. (2018) showed that, especially for cohesive soils, the side friction should not be neglected. Depending on the ratio between the rod and cone area, the influence can make up to ~40% of the total force (all depending on the geometrical set up of the kinematic free fall probe). Hence, following the argument of Roskoden et al. (2018) *Equation* 35 can be reduced to:

$$F_t = F_q + F_f \tag{37}$$

Following Albatal and Stark (2017), we neglect any side friction as long as the height of the submerged cylindrical pressure housing is smaller than 1/3 of the total pressure housing length. After that, side friction cannot be ignored anymore and the total force is divided into tip and side friction resistance forces (F_q and F_f, respectively). The tip force, if the sediment type does not change, should remain constant and can be calculated for a penetration depth smaller then 1/3 of the pressure housing. Afterwards, the tip force can be used as a constant offset value. Thus, any further enhanced total resistance force during penetration can be added to the friction force. If these forces are divided by their respected areas (note: pressure-housing area increases with penetration depth, while cone area stays constant) the resulting resistance pressures should remain constant. The resulting dynamic cone resistance is

$$q_{cd} = F_q / A_c \tag{38}$$

and the dynamic side friction follows

$$f_{sd} = F_f / A_s \tag{39}$$

with the indexes d indicating dynamic values.

For soil characterization purposes, we also introduce the normalized cone resistance Q_t

$$Q_t = q_n / \sigma'_{v0} \tag{40}$$

with q_n ($= q_t - \sigma_{v0}$) being the net cone resistance and q_t ($= q_c + u(1\text{-}a)$) being the pore pressure (u, as measured with NIMROD) -corrected cone resistance, σ_{v0} being the total overburden stress and σ'_{v0} being the vertical effective overburden stress. The normalized friction ratio F_R is

$$F_R = f_s / q_n \tag{41}$$

Possible stratigraphic changes may result for example in an increase of the total resistance force, which will simultaneously cause an enhancement of the frictional resistance. An iterative algorithm can be used to analyze the penetrometer records where these changes are detected and the current tip force is reassessed every time a new layer is identified. A new layer is therefore identified by an atypical change of the side friction pressure (s. M.2 Figure 3).

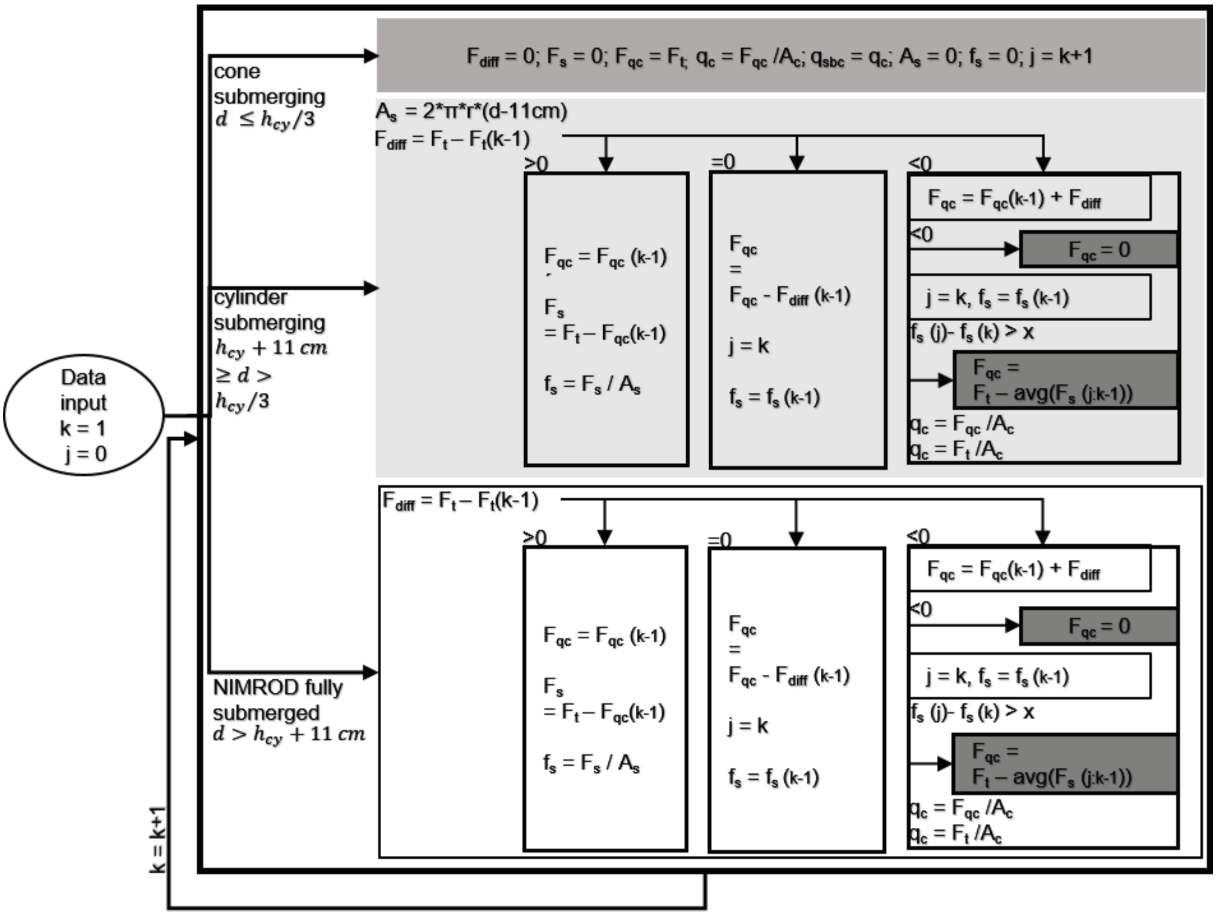

*M.2 Figure 3: Schematic of the algorithm implemented to split the total resistance force into the cone resistance and side friction. Glossary k and j, are counters for record number, and record number within new layer. d, depth, h_{cy}, cylinder height of NIMROD's shaft, F, the resistance force, A, area index: $diff$ = difference, t = total, s = side q_c = cone resistance q_{sbc}, quasi static baring capacity x, regional threshold (here: 1.5*side friction, can be estimated either using meta data or chosen arbitrary by the analyst). NOTE: specifically, the index number of the variables in the for-loop is always k.*

Dynamic penetration measurements systematically overestimate tip and side resistance forces if compared to standard *CPTu* measurements (Roskoden et al., 2018). This is called the penetration rate effect (Dayal and Allen, 1973; Dayal and Allen, 1975). Attempts have been made to correct for penetration rate effects. For example, *Equation* 42 calculates the penetration rate factor (PRF) to correct rate effects on cone resistance:

$$PRF = \frac{\mathrm{q_{cd}}}{\mathrm{q_{cst}}} = \mu \log_{10}\left(\frac{\mathrm{v}}{\mathrm{v_{st}}}\right) + 1 \qquad 42$$

with q_{cst} = standard tip resistance, μ = penetration rate factor (different for each considered parameter (Steiner, 2013)) v = velocity during penetration, v_{st}= standard velocity (2 cm/s) (Dayal and Allen, 1975; Steiner, 2013). Using this correction, the ultimate dynamic bearing capacity can be converted into a quasi-static bearing capacity

$$q_{sbc} = q_{ud}/PRF_{ud} \tag{43}$$

whereas the dynamic tip resistance and side friction result in the quasi-static resistance pressures,

$$q_{cst} = q_{cd}/PRF_{cd} \tag{44}$$

and quasi static sleeve friction

$$f_{sst} = f_{sd}/PRF_{sd} \tag{45}$$

where the index st refers to quasi-static parameters.

Penetration velocities and depths (d) are acquired by integrating the deceleration data over time

$$v(t) = \int dec(t)\,\partial t \tag{46}$$

and

$$d(t) = \iint dec(t)\,\partial t \tag{47}$$

with t, the time during penetration.

M.2.3 Results

M.2.3.1 Laboratory work

M.2.3.1.1 Grain size distribution

The results for all eight samples are plotted as an average normal and cumulative distribution plot (see M.2 Figure 4). Dx(10) is about 0.8 µm which translates to clay, Dx(50) is around 4.3 µm, which translates to fine silt and Dx(90) is around 43.9 µm which is fine to coarse silt. In summary, the soil can be interpreted as a *clayey medium to coarse silt*.

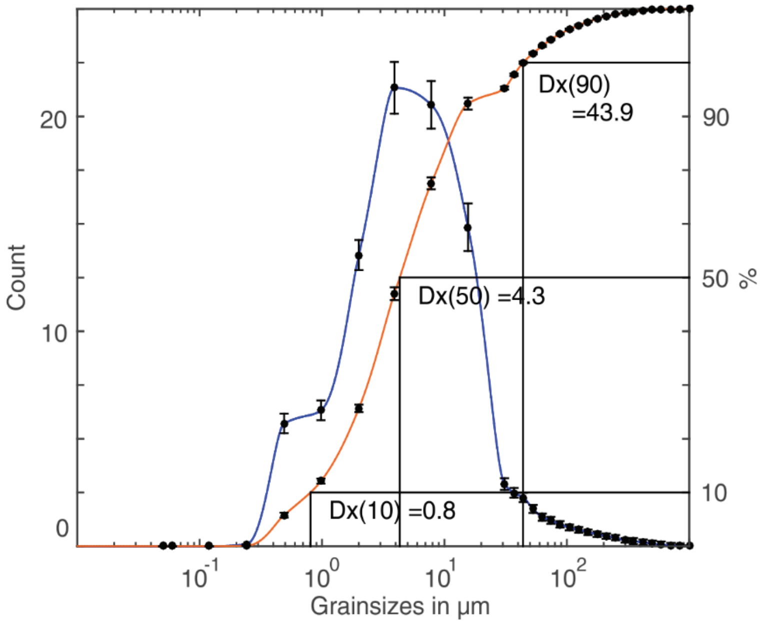

M.2 Figure 4: Grainsize analysis of the samples FoT1 to FoT2 at location M1 to M4. Singular grainsize analysis do not differ in curve form, therefore, an average grainsize was calculated and the single grainsizes were used to calculate standard deviations, which were used to calculate the error bars.

M.2. 3.1.2 Oedometer testing

Oedometer testing is accomplished by subjecting the sample to known loads (incrementally increased in stages), and measuring the temporal change in vertical deformation after each loading increment. An arbitrary example of the analysis of an oedometer test for the loading stage 250 g or ~ 3 kPa (sample FoT2) is shown in M.2 Figure 5. The deformation is measured using ISO (2017) and then plotted as a semi-logarithmic time plot. A tangent is drawn to the linear part of the curve for the primary and secondary consolidation phase. The cross point (red star) marks the end of the primary consolidation time. t50% is determined as the midpoint of initial consolidation and end of primary consolidation. With t50%, the coefficient of consolidation is calculated using *Equation* 31. The sample heights and diameters were 1.9 and 6.2 cm for each test. M.2 Table 1 shows the calculated water and moisture content, dry and bulk density in kg/m³, volume of solids and voids in m³, the resulting void ratio, the porosity, the averaged coefficient of consolidation in cm²/s for each sample and the compression index.

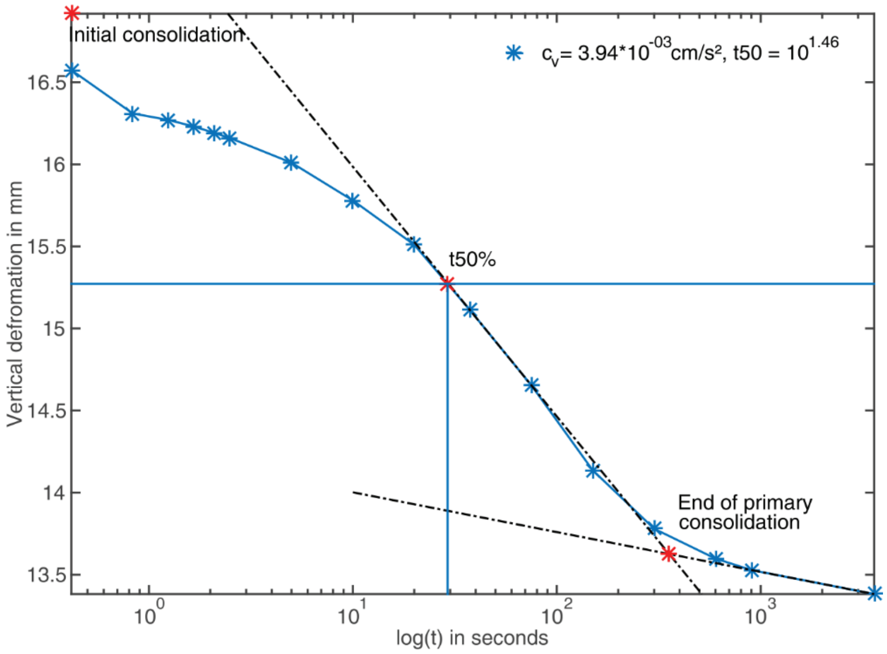

M.2 Figure 5 Display of the oedometer FoT2 stage 250 g or ~ 3 kPa . Vertical deformation is plotted against the log(t). Red values are estimated using the Casagrande method to determine the initial consolidation, which marks the beginning of the primary consolidation and the end of the primary consolidation. Start and end point of the primary consolidation phase are utilised to estimate t50%. We used sample FoT2 for this example.

Note: Even if the vertical load changes, the ratio of hydraulic conductivity and coefficient of volume change, from *Equation* 31, does not change (Terzaghi et al., 1996). Therefore, the coefficient of consolidation can be averaged for all loading steps (s. M.2 Table 1).

M.2 Table 1: Calculated coefficient of consolidation per loading step and averaged per load and side. The table shows a gradient in coefficient of consolidations decreasing towards higher mangrove density.

Location	*M1*	*M2*	*M3*		*M4*		*M5*			
Sample	*FoT1*	*FoT2*	*FoT3*	*FoT4*	*FoT5*	*FoT6*	*FoT7*	*FoT8*	*AVG*	*STD*
water content										
before	72%	63%	64%	64%	59%	59%	61%	60%	63%	4%
after	53%	52%	50%	54%	49%	49%	50%	51%	51%	2%
ρd[kg/m^3]	3.9E+02	5.2E+02	4.9E+02	5.4E+02	5.9E+02	6.7E+02	5.5E+02	5.3E+02	5.3E+02	7.5E+01
ρw[kg/m^3]	1.4E+03	1.4E+03	1.3E+03	1.5E+03	1.4E+03	1.6E+03	1.4E+03	1.3E+03	1.4E+03	8.8E+01
Void ratio e intial	6.36	4.47	4.84	4.27	3.86	3.27	4.18	4.39	4.5E+00	8.4E-01
Porosity	86%	82%	83%	81%	79%	77%	81%	81%	81%	3%
AVG Load [cm^2/s]	1.7E-02	2.7E-03	4.2E-03	3.9E-03	3.4E-03	2.8E-03	2.3E-03	2.3E-03	4.9E-03	4.8E-03
AVG Site [cm^2/s]	1.7E-02	2.7E-03	4.1E-03		3.1E-03		2.3E-03		5.9E-03	5.7E-03
Compression index	1.5	1.6	1.3	8.4E-01	1.1E	1.1	1.2	9.7E-01	1.2	0.2

The averaged coefficients of consolidation at each site (M1 – M5) show a decreasing gradient from the mud flat to the middle of the forest. A similar gradient can be seen in the compression index. The typical range of the compression index is 0.1 to 10. The higher the compression index, the more compressible the soil. Hence, the compression index follows a linear trend (slope ~-0.0227) from sample FoT1 to FoT8, showing a reduction in the compression values.

M.2. 3.2. Analysis of acceleration data

The maximum theoretical free fall velocity is predicted to occur at 5 m water depth. Hence, the variations for the impact velocities for the boat section are relatively high due to water depths of less than 5 m. However, the constant falling height used in the measurements along the mangrove section (controlled by the free fall tower) assures similar impact velocities. M.2 Figure 6 shows the soil classification for both transect sections after Mulukutla et al. (2011) (compared to the model by the same authors, represented as a red line). The Mulukutla et al. (2011) classification scheme is based on correlation of the factor of firmness to the embedded normalised depth. The model classifies grain sizes by characterizing their different resistance properties. The classifications by Mulukutla et al. (2011) range from '*Coarse Silt or softer sediments'* to '*Medium, Fine or Very Fine Sand*'. The Firth of Thames data plot slightly above the model line. The data shows a transition from '*Coarse Silt or other soft Sediments*' to '*Very Coarse Silt*' from the boat transect section to the mangroves section. In both sections there is a slope showing an increase in the factor of firmness and decrease in embedded normalised depth. The factor of firmness increases with enhancing mangrove density.

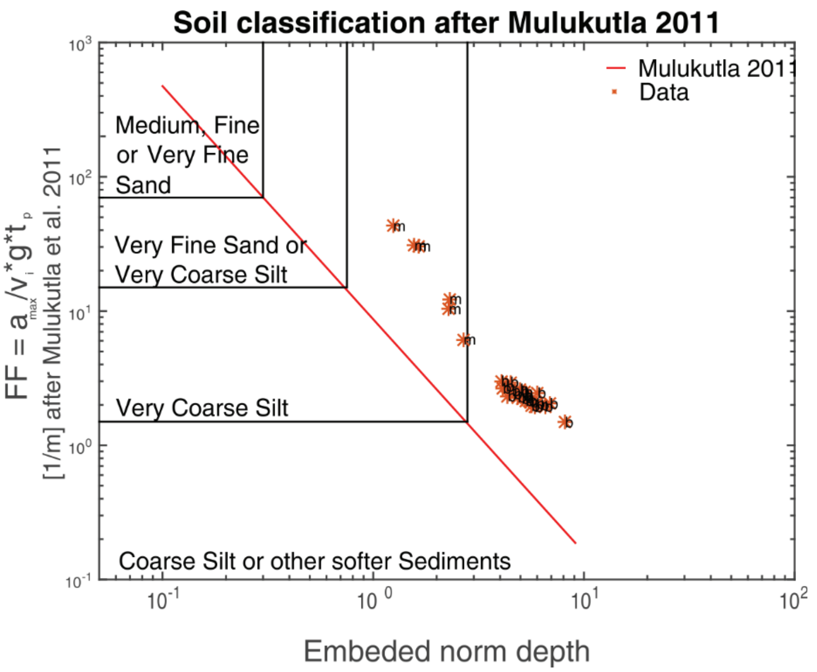

*M.2 Figure 6 Classification after Mulukutla et al. 2011. The two different sections of the transect are classified by two different fields. Data are assigned indicative letters **m** for mangrove and **b** for boat transect. Both sections show an increase in FF and a decrease in the embedded depth with a dependency on the mangrove density.*

After the geometrical-algorithm (M.2 Figure 3) was applied to the acceleration data, the tip resistance and sleeve friction could be plotted for the mud plane and mangrove forest (M.2 Figure 7). Displayed are the rate-corrected variations of quasi-static bearing capacity (also called total resistance pressure) and cone resistance (M.2 Figure 7A and C) with depth.

Note: Correction values for EQ 42 have been μ = 0.13 (cone resistance, Steiner et al. (2012)), and μ = 0.45 (sleeve friction, Young et al. (2011)) after P. Table 3.

In case of the mangrove data, there is almost no difference between the tip resistance and the quasi-static bearing capacity (M.2 Figure 7 A). In case of the mud flat data, a clear difference is visible between the quasi-static bearing capacity and the cone resistance (M.2 Figure 7 C). While the quasi-static bearing capacity increases with depth up to 150 kPa, the tip resistance stays constant at ~80 kPa. The change in the quasi-static bearing capacity is due to the enlargement of the submerging pressure housing area. The tip resistance can change either due to changes in the sediment type, an increase in consolidation, or a change of sediment transport processes, so in other words a change in sedimentation.

Note: A further discussion about these changes will be given later on.

In comparison to the mangrove data, the tip resistance of the mud flat data is 2.5 times less dominant (M.2 Figure 7A and C). The rate-corrected side friction increases at first in the upper 2 cm (M.2 Figure 7 B and C), but fluctuates between 0.5 – 1.5 kPa in the case of the mangrove data (panel B). In the case of the mud flat, the side friction increases slightly with depth and levels around 5 kPa and the side friction (M.2 Figure 7 D) is around 5 times higher than with the mangrove data (M.2 Figure 7 B).

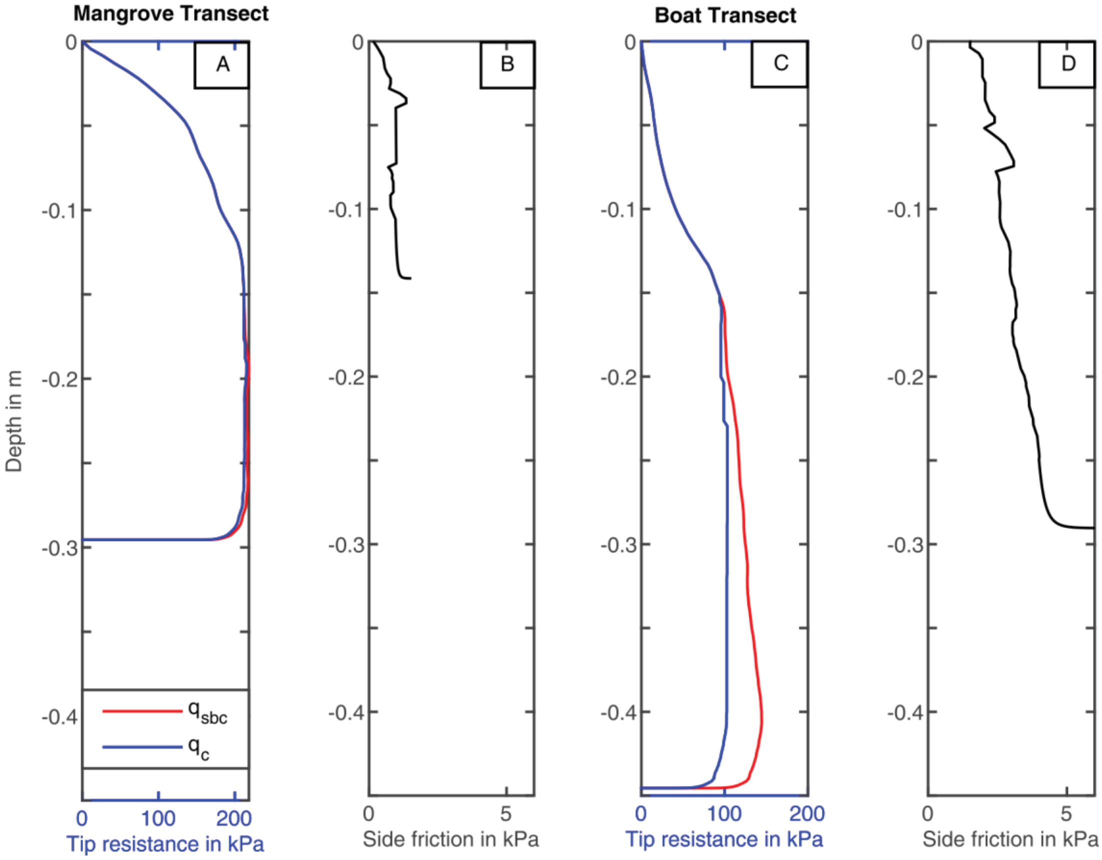

M.2 Figure 7: Comparing mangrove (M4, 80 m away from the mangrove-mud flat interface) to mud flat data (B2, ~72 m away from the interface). Penetration depth in the mud flat is much higher and the side friction is 5 times more dominant. As a consequence, the difference between the tip resistance and the quasi-static bearing capacity (or total resistance) do not differ much. However, the quasi-static bearing capacity is two times higher at a comparable penetration depth (30 cm).

Note: The increasing side friction at the end of the penetration, seen in M.2 Figure 8, panel B and D, are artefacts due to the penetration rate correction via the log-formula.

The global soil classification chart from Robertson et al. (1992) can be used to determine the general geotechnical soil type. The classification is not based on grain size but rather on behaviour types. Therefore, the chart illustrates where a given sediment plots in comparison to the background data of the classification scheme. The sediment types are described in M.2 Table 2.

M.2 Table 2 Soil behaviour types after Robertson et al. (1992). Column one describes the zones in M.2 Figure 9. Column two the soil behaviour types and column three the classification index.

Zone	*Soil Behaviour Type*	*Classification index (Ic)*
1	Sensitive, fine grained	N/A
2	Organic soils – peats	> 3.60
3	Clays – silty clay to clay	2.95 – 3.60
4	Silt mixtures – clayey silt to silty clay	2.60 – 2.95
5	Sand mixtures – silty sand to sandy silt	2.05 – 2.60
6	Sands - clean sand to silty sand	1.31 – 2.05
7	Gravelly sand to dense sand	< 1.31
8	Very stiff sand to clayey sand*	N/A
9	Very stiff, fine grained*	N/A

*Heavily over-consolidated or cemented

Normally, kinematic penetration data cannot be used for these classification schemes due to the lack of friction information. However, after applying the geometrical algorithms after Roskoden et al. (2018) (s. M.2 Figure 3) to divide the total resistance values in to tip and side resistance forces, an application of Roberson et al (1992) can be attempted for the first time. For each NIMROD deployment, an average geotechnical soil type is calculated using the tip resistance and side friction. The data are plotted in their normalised form in Robertson et al. (1992)'s classification chart (M.2 Figure 9A). The colour scheme in M.2 Figure 9 represents the distance to the most landward data point (M9) in the mangrove section measurements. Panel A in M.2 Figure 9 shows the classification chart itself while panel B shows the same data as in the classification. The sediments collected along the boat section were identified as 68% soil behaviour type 3 (*Clays -silty clay and clay*) and 32% as type 4 (*Silt mixtures, clayey silt to silty clay*). 88% of soil type 4 are within 100 m distance to the mangroves-mud flat interface.

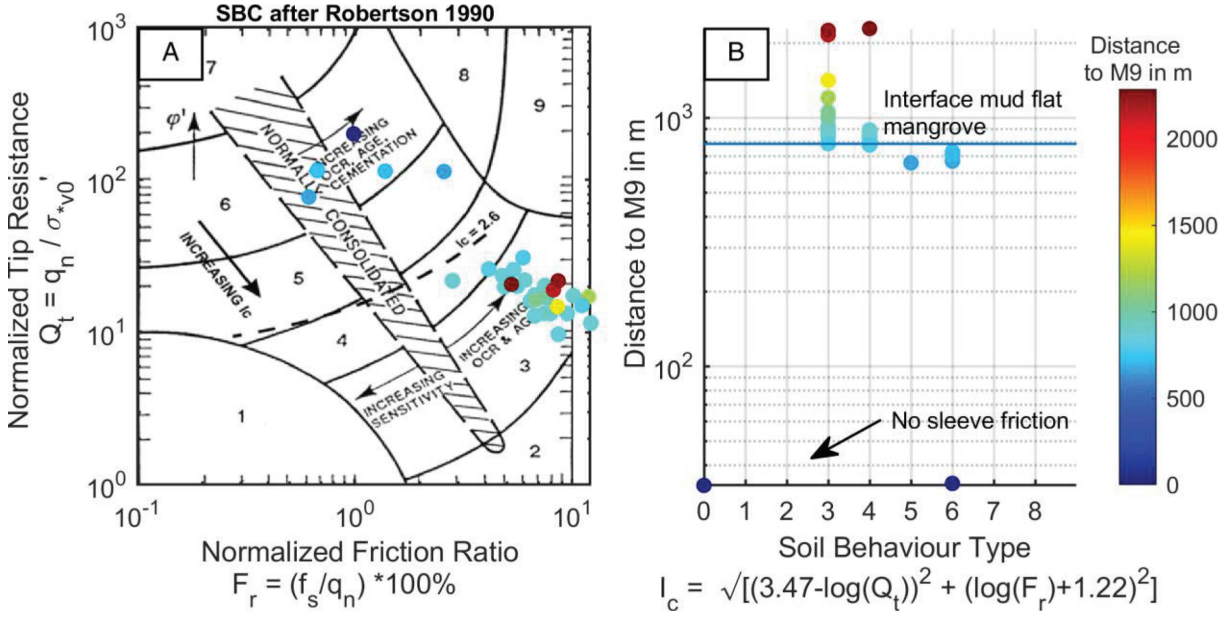

M.2 Figure 9: Soil behaviour chart after Robertson (1990). A: Soil behaviour fields plotted as a function of the normalised friction ratio and tip resistance. B: Soil behaviour types (SBT) calculated via the I_c value (formula in figure) on the x-axis plotted versus the distance (M9, ~800 m south of the interface of the mud flat and mangrove forest marked with an arrow, 'No sleeve friction' is closest to the land. Its distance is set to 0, hence, distance increases seaward). Colour in data points (panel B) represent distance and follow the same colour coding as in panel A.

The sediments on the mangrove section are characterised as 11% of soil type 3, 4 and 5 (*silty sand to sandy silt*), respectively. However, 55% of the data are identified as soil type 6 (clean sand to silty sandy silt). The last 11% do not plot on the chart, because the penetration depth was not deep enough to produce the side friction data. Nevertheless, a direct correlation between mangrove density and soil behaviour type is evident for both transects. Note that the sediment grain size did not change substantially over the study transect indicating that all changes in the soil behaviour type are due to the presence of mangroves.

In order to identify the influence of the mangroves on the soil, we compared the quasi-static bearing capacity in the mangrove forest with the coefficient of consolidation from the eight samples (s. M.2 Figure 10C). Note that information on vegetation characteristics (taken from Montgomery et al., 2018) was not available for all sampling sites and was interpolated for M.2 Figure 10 panel B.

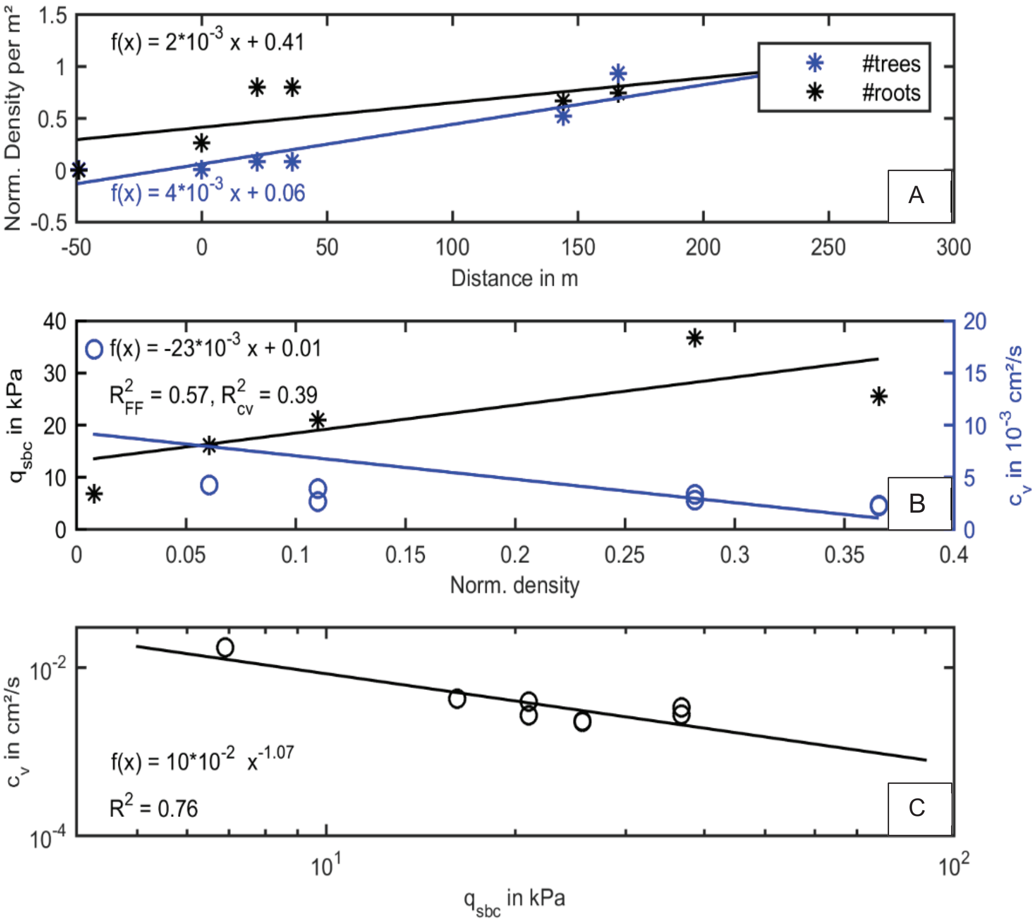

M.2 Figure 10: Correlation plots. A: Linear correlation of the normalised number of trees/ aerial roots per m² and position, data from Montgomery et al. (2018). B: Correlation of the quasi-static bearing capacity and coefficient of consolidation to the normalised tree density (density calculated using the correlation of panel A). C: The double logarithmic plot of the coefficient of consolidation to the quasi-static bearing capacity showing a power law correlation with R² = 0.76. Note: M3, and M5 have each one q_{sbc} and two c_v values (because M3 – M5 have each two samples).

Note: The hypothesis was that there is a functional relationship between the geotechnical soil properties: coefficient of consolidation and normalised tree density. Following the principle of the simplest model, the first approximation is to look for linear relationships, because they are easy to understand, interpret and do not need non-physical modelling parameters. Obviously, M.2 Figure 9B shows a rather weak linear correlation between these two aforementioned variables, because it only explains 39% of the variability in the coefficient of consolidation ($R^2 = 0.39$, $R = 0.62$). However, the moderate correlation between the resistance and normalised tree density ($R^2 = 0.57$, $R = 0.75$) and the strong correlation between the coefficient of consolidation and the resistance ($R^2 = 0.76$, $R = 0.87$) indicates an indirect physical and mathematical relation between the two variables. Real statistical relevance proven by statistical tests (for example t-tests) is hard to archive in local field studies, especially if study areas are as remote and logistically challenging as the Firth of Thames, because they require a higher data volume to make real statistical evaluations about the relation between the given physical entities. Therefore, we regard the found linear relationships with caution but we do believe to have identified a first indirect approximation of the physical relationship between the normalised tree density and coefficient of consolidation.

M.2 Figure 9A displays the normalised density of mangrove trees and pneumatophores (aerial roots) per m², correlated with the distance to the mangrove-mud flat interface (interface at distance 0 m, negative distance values refer to distances outside the mangrove forest seaward). The linear correlation is used to calculate the normalised density to the locations where data points are collected in this study. The normalised tree density is then correlated to the quasi-static bearing capacity and the coefficient of consolidation (M.2 Fig. 9B). The tree density data only explains 39% of the variability in the coefficient of consolidation, whereas the tree density explains 57% of the quasi-static bearing capacity variability. M2. Figure 9C shows the correlation between the coefficient of consolidation (y-axis) and the quasi-bearing capacity (x-axis) in a double logarithmic plot. With an increase of quasi-static bearing capacity, the coefficient of consolidation decreases. The relationship is best characterised by a power law relationship, which explains 75% of the variability. A decrease in the coefficient of consolidation indicates a decrease in the rate at which the soil undergoes consolidation. Softer and more saturated soils have a high coefficient of consolidation while firmer and less saturated soils, have a lower coefficient of consolidation. The change in magnitude for the coefficient of consolidation at normalised tree densities of 5% is clearly shown (compare panel B and C). This indicates that the threshold, which changes the coefficient of consolidation, is 5% of mangrove tree population per m² (normalised). In other words, a mangrove cover of 500 cm^2 per m^2 is necessary to change consolidation properties of the soil from soft and highly saturated (so soil behaviour type 3 and 4 after Robertson's classification chart (1992)) to firm and low saturation.

Note: Pore pressure measurements were not utilised for this field investigation since the filter stone was clogged after the first measurements. For further investigation in any mangrove forest during low tide, we suggest to use silicon oil for filter saturation instead of water. Furthermore, a portable high-pressure cleaner would be of use.

M.2.6 Discussion

Eight *in situ* samples were processed for grain size and subjected to oedometer tests, which evaluated the consolidation properties and trends along a transect of measurements that covers mangrove and mudflat areas. The trend analysis emphasises differences in the consolidation behaviour from the mud flat compared to the mangrove forest. In addition, different soil classification schemes were applied to the acceleration data from the Firth of Thames. The technique of Roskoden et al. (2018) was used to differentiate between total resistance, tip resistance and side friction. This allowed the first application of the Robertson (1990) soil classification chart for a dynamic free fall penetrometer. Grain size analysis from sediment samples was used to ground-truth the penetrometer data.

M.2.6.1. Consolidation due to mangroves roots

A change in the coefficient of consolidation normally depends on the grain size distribution, if sediment types with the same consolidation history are compared. Since no change in the sediment properties was confirmed by the grain size analyses, we can directly link the alteration of the coefficient of consolidation to the density of the mangrove trees. Mangroves reduce the coefficient of consolidation and, by doing so, create a more consolidated soil. We believe that the main mechanisms behind this consolidation are the dewatering of the sediment by mangrove roots (from here on called ‘osmotic-consolidation’), which is governed by the depth level of the roots (as a function of tree height), the root density and types of roots, and the physical structures of the roots themselves, which provide an additional resistance on the penetrometer. Several studies have shown that soils in un-impacted mangrove sites have greater shear strength than sites where the roots and trees have been damaged (e.g. by hurricanes or clear-cutting, reviewed in McIvor et al. (2013)), which they attribute to the binding of surface soil by root structures. Mangrove soils are also known to shrink and expand in response to osmotic pressure caused by the mangrove roots (Cahoon et al. (2011), Gilman et al. (2008)). In addition to these two mechanisms, the weight of the mangrove trees themselves would cause an increase in the overburden weight, which would consolidate the sediments within the forest. Finally, mangroves also occur over a defined range of inundation regimes, and so an increase in mangrove abundance is also associated with an increase in the average duration of exposure to air, which in turn causes an increase in evaporation and consolidation in sediments (Fiot and Gratiot, 2006).

Our observations of the effect of mangroves on consolidation are also confirmed by a decreasing compression index trend. The higher level of consolidation reduces the erosion risk of tidal currents and wind waves but also reduces future consolidation potential. The estimated low coefficient of hydraulic conductivity of ~ 1 cm/a (Swales et al., 2015) in conjunction with the coefficient of consolidation results presented here, suggests a low compressibility soil around the mangroves. The sediment input measured at the study site is 25 to 31 mm/a (Swales et al., 2016). The bulk density is 400 to 590 kg/m^3 (Swales et al., 2016). These aforementioned facts cause a stress increase of up to 1.0 to 2.36 kg/a per m^2. This stress increase per year roughly equals the first loading step of the oedometer tests. Hence, we can use the final deformation values of the oedometer test (for 3 kPa) to estimate the vertical deformation due to the extra loading of the annual sediment inputs. The vertical deformation due to consolidation is, 5.6 mm (mud flat, M1) to 2.4 mm (at the middle of the mangrove forest, M5). With an averaged relative sea level rise extracted from satellite data (1993 – 2015) of 4.3 mm/a (Swales et al., 2016) added to the consolidation, the vertical change in height could be 6.7 to 9.9 mm/a. This suggests that mangrove induced consolidation reduces the elevation of a sediment deposit by up to 42 % in the Firth of Thames, therefore, playing a significant role in surface elevation change prediction. From a geotechnical point of view, this change in consolidation is due to the mangroves and, considering the high sedimentation rate, this study site is still accreting at a greater rate than SLR. Furthermore, the soil, consolidated by the mangroves, is more resistant to other vertical changes induced by erosion and further self-weight consolidation processes as aforementioned.

Our work shows that mangrove forests are highly influenced by consolidation processes. Hence, SET-measurements need to account for consolidation processes to capture the real sediment surface evaluation.

M.2.6.2. Analysis of acceleration data and soil classification

Soil classification charts normally identify sediment deposits without the consideration of embedded rocks and/or roots. Evidently, any classification applied to sediment collected in the mangrove transect section may not identify the “real” (i.e. undisturbed) soil strata. Evidence of that are the grain size analysis of the eight samples, which do not show any changes in the sediment type. As a consequence, all sediment should plot in the same SBT field in Robertson's chart (M.2 Figure 9), but this was not observed. Given that the "warmer" blue colours in M.2 Figure 9 represent proximity to mangroves (i.e. large root density), this means that roots shift the SBT from 3 to 6 despite the similarity in sediment composition.

The classification scheme based on Mulukutla et al. (2011) is easily programmed and the data analysed quickly. The unique technique to incorporate metadata such as penetration time, acceleration, velocity and depth is a clear advantage. The analysis should be included in every free fall penetrometer investigation even if tip resistance and side friction are measured directly. However, this approach only provides a bulk estimate for each penetrometer drop, providing no information on the variation of structure with depth, in which case the soil classification reduces to a 2D problem. Depending on the scientific question, this might complicate geotechnical investigations. Therefore, the Mulukutla et al. (2011) soil classification scheme, which is based on the acceleration data alone, cannot be applied on the mangrove transects to identify a change in sediment deposits, because it is not possible to control for the effect of the mangroves. However, the classification can still be used in the mud flat area.

An application of the Robertson-chart for kinematic penetrometers has rarely been done before. Therefore, the separation algorithm of Roskoden et al. (2018) is an inimitable approach, which allows further geotechnical analysis for deployments of such dynamic penetrometers. In general, the Robertson (1990) soil classification results provided classes such as '*Clays-Silty Clay And Clay'*, '*Silt Mixtures Clayey Silt to Silty Clay'* (for the boat section) to '*Sands –Clean Sand To Silty Sand'* (for the mangrove section), which is similar to the classifications after Mulukutla et al. (2011); see Figs. 6 and 8 above.

Note: On the one hand, one needs to consider that the tip resistance or more in general the resistance forces and the factor of firmness can vary either due to changes in the sediment type, consolidation, and sedimentation or flow regime (to only name a few). On the other hand, no extraordinary events such as storms or spring tides, which could change the sedimentation process and therefore change the measured resistance forces, could be seen in the mudflat penetration data. Furthermore, with a penetration depth between 30 to 60 cm in an inter-tidal area with a constant but moderate sediment supply (Swales et al., 2016), and no visible changes in resistance data, we assume no changes of the consolidation due to depth or other reasons but the mangroves. Nevertheless, there is no single conclusion on why the resistance forces may change, which is why it is even more important in this study to shift the analysis away from changes in sediment types, and towards the interpretation of soil behavior types after Robertson (1990).

Robertson (1990) argues that his behaviour types do not directly identify grain sizes such as clay, silt and sand and suggests that his defined behaviour types indicate a certain soil behaviour. Therefore, if a data point plots into the field '*Sands –Clean Sand to Silty Sand'*, this particular soil behaves like a sand. However, it could also be an over-consolidated and cemented silt or a clast-, shell detritus- or root-bearing clay/silt, or a change in sedimentation which is observed. Therefore, certain geotechnical properties such as: the normalised cone resistance, normalised friction ratio, degree of cementation (precipitation of crystalline structures affecting the effective porosity and permeability), sensitivity (ratio of sediment undrained shear strength undisturbed vs. remoulded), age (secondary consolidation processes) and over consolidation ratio (ratio of current total overburden effective stress to former total overburden effective stress) have also been evaluated in Robertson's chart. Thus, separating the total resistance force/quasi-static bearing capacity of the dynamic penetrometer into cone resistance and side friction, gives us the advantage of identifying how the mangrove soil behaves with respect to a global database.

Note: The utilised geometrical algorithm is not yet a perfect solution for the issues of the kinematic penetration lance. It is a method, which strongly depends on the data processor. The processors interpretation is determined on the chosen default values for the upper and lower limit for the change in side friction. Furthermore, there are the issues of local sedimentation anomalies such as roots or shells, which may distort the interpretation of the soil behaviour types. Such issues can only be resolved if more penetration data can be accumulated at the same locations. For the mudflat area the volume of data seems reasonable to argue that the identified soil behaviour types are representing the actual geotechnical properties of the mudflat. However, on the one hand, in the mangrove area the penetration data density is relatively low compared to the change in the normalised tree density. On the other hand, our interpretation of the soil behaviour types in the mangrove area depends on the inclusion of roots and others sedimental objects. Furthermore, we do see an incensement of the resistance forces with an enhancement of the normalised tree density, which we interpret in this case study as an argument for our hypothesis: that the mangroves change the soil behaviour. However, we are aware, that the change in the normalised tree density, bioturbation and other sedimental issues might just mimic certain soil behaviour types, which taken into consideration in our analysis as aforementioned.

Since we correlated the mangrove density to the location in the forest relative to the fringe and the location to the soil behaviour types, we can see that the soil behaviour type changes with mangrove density. The higher the mangrove density in the soil the higher the sediment behaviour type number. A change from soil behaviour type 3, 4 to 5, 6 suggests a much firmer soil behaviour.

Note: We rather suspected the soil type 1 (sensitive, fine grained) or 2 (organic soil/peat) for the mudflat area due to the possibility of organic matter being sedimented. Possible reasons could be systematic errors such as: 1) wrong penetration rate factor, the utilised rate factors are from the literature (P. Table 3) and may not be suitable for mudflat areas, 2) another possibility could be that the expected soil composition was different than expected due to a more coarse silt portion (M.2 Figure 4).

Higher cementations (due to roots and/or precipitation of organic matter and/or crystalline structure) and/or higher consolidation ratios (which would represent here, a ratio of the yield stress and the present effective overburden stress) could be possible interpretations here, but have not been issued in our laboratory analysis.

M.2.7 Conclusion

An estimation of soil resistance forces in and around mangroves was derived from deceleration data using a portable kinematic free fall penetrometer (quasi bearing capacity, factor of firmness, cone resistance and side friction). The data was related to grain size (for the mud flat) and to geotechnical properties such as the coefficient of consolidation (mud flat and mangrove forest). The correlations are shown to follow a power-function relationship. Mangrove were shown to have a strong influence on the soils consolidation behaviour, binding the sediments at place.

Concerning our four scientific objectives, we conclude that:

1. A linear trend between the coefficient of consolidation and the mangrove density was found presenting higher consolidated sediments within the mangrove forest interior (M.2 Figure 10A).
2. NIMROD estimated the resistance forces (factor of firmness, total resistance, tip resistance and side friction) of the mud flat and mangrove forest. The technique developed in the laboratory by Roskoden et al. (2018) to extract tip resistance and side friction from the acceleration data was tested in the field. The extraction was considered successful for the study at hand (M.2 Figure 6 to M.2 Figure 9 M.2 Figure 10).

   Note: No generalization are given for the applicability of the geometrical algorithm for other field investigations. Further laboratory and field tests with known soil behaviour, and sediment types are needed.

   The application of a global soil classification chart for kinematic free fall penetrometer (s. M.2 Figure 9), allowed us here the identification of geotechnical soil behaviour types 3, 4 and 5, 6 for the mud flat and the mangrove forest.

   Note: We make no generalisation if other soil behaviour types, especially the soil behaviour types 1, 8, and 9, can be reproduced/ correctly identified by the geometrical algorithm. Here, again, further research needs to be done.

   The availability of mangroves changed or at least mimicked a change in geotechnical bulk properties such as cementation and or a higher consolidation ratio.
3. The resistance forces can be correlated with the regional coefficients of consolidation. The correlation is a power-function in a double logarithmic plot with a $R^2 = 0.76$ (s. M.2 Figure 10C).
4. The trend is used to predict a reduction in the consolidation process due to mangrove density. The cut-off value appeared to be a normalised tree density of 5%. This changes the soil behaviour from soft with high consolidation potential (M1: compression index 1.55, coefficient of consolidation $1.7 \cdot 10^{-2}$ cm²/s) to firm with reduced consolidation potential (M5: compression index 0.99 coefficient of consolidation 1.7, coefficient of consolidation $2.3 \cdot 10^{-3}$ cm²/s). If the final deformation values are compared, the consolidation (vertical deformation due to dewatering) is reduced by 45%.

Overall, the approach allowed us to map the geotechnical properties of intertidal sediments in the upper Firth of Thames quickly in two days. More data were collected than expected during both transects. A direct connection between the stiffness of the soil and the mangrove tree-density was detected and confirms that sediments that have been consolidated due to mangrove presence tend not to consolidate much further, reducing the vertical deformation potential of mangrove forests with increasing forest density. We highly recommend the usage of portable kinematic penetrometers for remote areas like mangrove forests, because they allow a quick, easy and economically feasible data acquisition.

M.2.8 Acknowledgements:

Dean Sandwell, Nicola Lovett, Erik Horstman for excellent field help. Marsden contract 14-UOW-011 to fund Karin R. Bryan’s time. Andrew Swales for access to the boardwalk. Vicki Moon for laboratory usage. The DFG programme “Intercoast” for funding the research stay and PhD project of Robert R. Roskoden.

M.2.9 Literature

1. Albatal, A., Stark, N., 2017. Rapid Sediment Mapping and in Situ Geotechnical Characterization in Challenging Aquatic Areas. Limnology and Oceanography: Methods, V. 15, No. 8, p. 690-705, doi# doi.org/10.1002/lom3.10192.
2. Alongi, D.M., 2008. Mangrove Forests: Resilience, Protection from Tsunamis, and Responses to Global Climate Change. Estuarine, Coastal and Shelf Science, V. 76, No. 1, p. 1-13, doi# doi.org/10.1016/j.ecss.2007.08.024.
3. Cahoon, D.R., Perez, B.C., Segura, B.D., Lynch, J.C., 2011. Elevation Trends and Shrink–Swell Response of Wetland Soils to Flooding and Drying. Estuarine, Coastal and Shelf Science, V. 91, No. 4, p. 463-474, doi# doi.org/10.1016/j.ecss.2010.03.022.
4. Casagrande, A., Fadum, R.E., 1940. Notes on Soil Testing for Engineering Purposes, in: Havard Graduate School of Engineering, S.M. (Ed.), Cambridge, Mass., p. 268.
5. Dahdouh-Guebas, F., Jayatissa, L.P., Di Nitto, D., Bosire, J.O., Seen, D.L., Koedam, N., 2005. How Effective Were Mangroves as a Defence against the Recent Tsunami? Current biology, V. 15, No. 12, p. R443-R447, doi# doi.org/10.1016/j.cub.2005.06.008.
6. Dayal, U., Allen, J.H., 1973. Instrumented Impact Cone Penetrometer. Canadian Geotechnical Journal, V. 10, No. 3, p. 397-409, doi# doi.org/10.1139/t73-034.
7. Dayal, U., Allen, J.H., 1975. The Effect of Penetration Rate on the Strength of Remolded Clay and Sand Samples. Canadian Geotechnical Journal, V. 12, No. 3, p. 336-348, doi# doi.org/10.1139/t75-038.
8. Fiot, J., Gratiot, N., 2006. Structural Effects of Tidal Exposures on Mudflats Along the French Guiana Coast. Marine Geology, V. 228, No. 1-4, p. 25-37, doi# doi.org/10.1016/j.margeo.2005.12.009.
9. Gilman, E.L., Ellison, J., Duke, N.C., Field, C., 2008. Threats to Mangroves from Climate Change and Adaptation Options: A Review. Aquatic botany, V. 89, No. 2, p. 237-250, doi# doi.org/10.1016/j.aquabot.2007.12.009.
10. ISO, 2017. International Organization for Standardization Geotechnical Investigation and Testing - Laboratory Testing of Soil - Part 5: Incremental Loading Oedometer Test (Iso 17892-5:2017); , Geotechnical investigation and testing–Laboratory.
11. Kathiresan, K., Rajendran, N., 2005. Coastal Mangrove Forests Mitigated Tsunami. Estuarine, Coastal and Shelf Science, V. 65, No. 3, p. 601-606, doi# doi.org/10.1016/j.ecss.2005.06.022.
12. Lovelock, C.E., Cahoon, D.R., Friess, D.A., Guntenspergen, G.R., Krauss, K.W., Reef, R., Rogers, K., Saunders, M.L., Sidik, F., Swales, A., 2015. The Vulnerability of Indo-Pacific Mangrove Forests to Sea-Level Rise. Nature, V. 526, No. 7574, p. 559, doi# doi.org/10.1038/nature15538
13. Lunne, T., Powell, J.J., Robertson, P.K., 2002. Cone Penetration Testing in Geotechnical Practice. CRC Press.
14. McIvor, A., Spencer, T., Möller, I., Spalding, M., 2013. The Response of Mangrove Soil Surface Elevation to Sea Level Rise, Natural Coastal Protection Series: Report 3. Cambridge Coastal Research Unit Working Paper 42. .
15. Montgomery, J., Bryan, K., Horstman, E., Mullarney, J., 2018. Attenuation of Tides and Surges by Mangroves: Contrasting Case Studies from New Zealand. Water, V. 10, No. 9, p. 1119, doi# doi.org/10.3390/w10091119.

16. Morrisey, D.J., Swales, A., Dittmann, S., Morrison, M.A., Lovelock, C.E., Beard, C.M., 2010. The Ecology and Management of Temperate Mangroves. Oceanography and marine biology, V. 48, No., p. 43-160, doi# doi.org/10.1201/EBK1439821169-c2.

17. Mulhearn, P., 2002. Influences of Penetrometer Probe Tip Geometry on Bearing Strength Estimates for Mine Burial Prediction. Defence Science and Technology Organisation Canberra (australia), Fishermans Bend, Victoria 3207 Australia p. 27.

18. Mulukutla, G.K., Huff, L.C., Melton, J.S., Baldwin, K.C., Mayer, L.A., 2011. Sediment Identification Using Free Fall Penetrometer Acceleration-Time Histories. Marine Geophysical Research, V. 32, No. 3, p. 397-411, doi# doi.org/10.1007/s11001-011-9116-2.

19. Robertson, P., Sully, J., Woeller, D.J., Lunne, T., Powell, J., Gillespie, D., 1992. Estimating Coefficient of Consolidation from Piezocone Tests. Canadian Geotechnical Journal, V. 29, No. 4, p. 539-550, doi# doi.org/10.1139/t92-061.

20. Robertson, P.K., 1990. Soil Classification Using the Cone Penetration Test. Canadian Geotechnical Journal, V. 27, No. 1, p. 151-158, doi# doi.org/10.1139/t90-014.

21. Roskoden, R., Kopf, A., Mörz, T., Kreiter, S., 2018. Analysis of Acceleration and Excess Pore Pressure Data of Laboratory Impact Penetrometer Tests in Remolded Overconsolidated Cohesive Soils, Cone Penetration Testing 2018. CRC Press, p. 545-550, -.

22. Stark, N., 2011. Geotechnical Investigation of Sediment Remobilization Processes Using Dynamic Penetrometers, Marine Geotechnics. Universität Bremen, Bremen, p. 309.

23. Stegmann, S., Mörz, T., Kopf, A., 2006. Initial Results of a New Free Fall-Cone Penetrometer (Ff-Cpt) for Geotechnical in Situ Characterisation of Soft Marine Sediments. Norwegian Journal of Geology/Norsk Geologisk Forening, V. 86, No. 3, p. 199-208, doi# PANGAEA reference ID: 27196 Serial: RCOM0398.

24. Steiner, A., 2013. Sub-Seafloor Characterization and Stability of Submarine Slope Sediments Using Dynamic and Static Piezocone Penetrometers, Marine Geotechnics. Universität Bremen, Bremen, p. 325.

25. Steiner, A., L'Heureux, J.-S., Kopf, A., Vanneste, M., Longva, O., Lange, M., Haflidason, H., 2012. An in-Situ Free-Fall Piezocone Penetrometer for Characterizing Soft and Sensitive Clays at Finneidfjord (Northern Norway), Submarine Mass Movements and Their Consequences. Springer, Dordrecht, p. 99-109, doi.org/10.1007/978-94-007-2162-3_9

26. Stephan, S., 2015. A Rugged Marine Impact Penetrometer for Sea Floor Assessment. Universität Bremen, , Bremen,, p. 268.

27. Stoll, R.D., Sun, Y.-F., Bitte, I., 2007a. Seafloor Properties from Penetrometer Tests. IEEE Journal of Oceanic Engineering, V. 32, No. 1, p. 57-63, doi# doi.org/10.1109/joe.2007.890943.

28. Stoll, R.D., Sun, Y.F., Bitte, I., 2007b. Seafloor Properties from Penetrometer Tests. IEEE Journal of Oceanic Engineering, V. 32, No. 1, p. 57-63, doi# 10.1109/Joe.2007.890943.

29. Swales, A., Bentley Sr, S.J., Lovelock, C.E., 2015. Mangrove-Forest Evolution in a Sediment-Rich Estuarine System: Opportunists or Agents of Geomorphic Change? Earth Surface Processes and Landforms, V. 40, No. 12, p. 1672-1687, doi# doi.org/10.1002/esp.3759.

30. Swales, A., Denys, P., Pickett, V.I., Lovelock, C.E., 2016. Evaluating Deep Subsidence in a Rapidly-Accreting Mangrove Forest Using Gps Monitoring of Surface-Elevation Benchmarks and Sedimentary Records. Marine Geology, V. 380, No., p. 205-218, doi# doi.org/10.1016/j.margeo.2016.04.015.

31. Terzaghi, K., Peck, R.B., Mesri, G., 1996. Soil Mechanics in Engineering Practice. John Wiley & Sons, United States of America

32. Young, A.G., Bernard, B.B., Remmes, B.D., Babb, L., Brooks, J.M., 2011. Cpt Stinger-an Innovative Method to Obtain Cpt Data for Integrated Geoscience Studies, Offshore Technology Conference. Offshore Technology Conference, -, pp. 1-10.

33. Zhou, Z., van der Wegen, M., Jagers, B., Coco, G., 2016. Modelling the Role of Self-Weight Consolidation on the Morphodynamics of Accretional Mudflats. Environmental Modelling & Software, V. 76, No. -, p. 167-181, doi# doi.org/10.1016/j.envsoft.2015.11.002.

Chapter 4 Manuscript 3 - Prefix

In the previous chapters, the free fall calibration test, its resulting geometrical algorithm, and its infield ground proving in the Firth of Thames, NZ, have been discussed. The following chapter (*Manuscript 3*) takes an honest look at the free fall calibration test, and its results. Here, the original scientific goals and objectives are discussed. Consequently, *Chapter 3* illustrates how and why these goals changed over time.

Chronically speaking, *Manuscript 3* emerged last of all the manuscripts, but is placed in the middle of this doctoral thesis, because it is also meant to be a link between the two different scientific frames, which are joint here. On the one hand, the first part of this dissertation was primarily about kinematic free fall penetrometers, their history, advantages and improvements. On the other hand, the upcoming chapters will cover hydrogeological analyses via standard *CPTu* devices in Omokoroa, NZ.

However, as mentioned in the *Prefix* of this dissertation, the scientific goals of this thesis are twofold by default. Firstly, this thesis strives to improve dynamic free fall tests and their processing/ analysis techniques, secondly, we try to ground prove the new developed techniques in the field by contributing to global scientific issues on a local scale. Consequently, the geometrical algorithm was developed in the laboratory of Prof. Dr. Achim Kopf at the research institute *MARUM*, Bremen, Germany, but was tested together with Prof. Dr. Karin Bryn at the Waikato University, in the Firth of Thames, New Zealand.

Here, we tackled the issue of local sea level rises due to global warming, and assessed the interaction between a mangrove forest and its habitual soil. The overall scientific question here was and still is, whether the mangrove forest will survive the local sea level rise, or drown. *Manuscript II* has not solved the issue, but looked at the problem from a different angle providing one important clue, which has not been considered in the past.

Manuscript 3 was written for the *International Geoscientific Student Conference* 2019 (*IGSC*), after I had been asked to participate by the *Student Geoscientific Society e.V. Berlin & Potsdam* (*SGS*). Thinking about what I could contribute to the student conference, which may also be in line with my own thesis I thought about how the geometrical algorithm came to place. Originally, we wanted to tackle the problem of the strain rate effects on the pore pressure data. However, with many technical issues, we could only come up with a very specific solution for the strain rate effect on the pore pressure. Hereby, I mean that the solution shown in the *Manuscript I* is only valid for the particular case presented in that chapter. Nevertheless, as the following manuscript will show, even though we failed to yield a universal strain rate correction for the pore pressure, we came up with something unexpected, the geometrical algorithm. The algorithm definitely assisted us in the mangrove issue, mentioned earlier, a universal stain rate correction would not have done that. Therefore, *Manuscript 3* is named:

The usage of incomplete and metadata. Why failing is part of succeeding.

Herein, I want to discuss the issue of data science, big data, and meta data analysis in the geo-sector. I consider this manuscript the link between the two parts of my dissertation, because in both parts I resolve my scientific issues by not only looking at the primary, but also at the meta data.

This manuscript has also some personal relevance to it, because it is supposed to show that even if our predefined scientific goals are not matched with the research done yet, giving up is not an option, because failing is part of succeeding. Hence, even so, *Manuscript 3* is officially an extended abstract; I would prefer to consider it as an essay on how to deal with failed experiments and how to reuse the data of these experiments as I think this is an important issue for young scientists. Lastly, I would like to point out the relevance of this issue by mentioning that this abstract received an award for best oral presentation, because, as I believe, it is written with a personal note and connection rather than with an only objective and scientific perspective.

Manuscript 3

The usage of incomplete and metadata. Why failing is part of succeeding

first author, In Proceedings of the 8th International Geoscience Student Conference, Uppsala, Sweden, 2019. (forthcoming), diva2:1383507, DOI: 10.33063/diva-401520

Author

Robert R Roskoden

Centre of Marine Environmental Science (Marum)
([1]rroskode@marum.de (ORCID: https://orcid.org/0000-0003-2170-283X)

M.3.1 Motivation

In science, it is uncommon to find publications stating the failure of a project. An example is Eileen Parkers, PhD. Parkes (2019) states in the journal nature: '*Failure is something that all scientists experience — but it's hard to tell, looking at our shiny conferences, polished presentations and glossy journals.*' Quite often, the answer to failed experiments, tests and field data acquisitions is to repeat the failed studies as many times as possible to get it right. Nevertheless, what do we do if repetition is not an option? This paper is an example of how to revaluate and recycle data to find something unexpected.

M.3.2 Introduction

In soil mechanics, soil information are important for scientific investigations and geo-engineering objectives as for example hazard assessments, building of pipelines, or laying cables (Stegmann, 2007). The Tilted Tower of Pisa illustrates the importance of soil information. The tilting is due to the consolidation of the soil. However, the consolidation could have been quantified before the tower was built. Therefore, soil properties need to be examined before the initiation of civil projects. The examination can either be *ex situ* (laboratory testing) or *in situ*. *Cone Penetration Tests* (*CPTu*) are the most feasible means to *in situ* soil investigations (Steiner, 2013). The *CPTu* measures the soils sleeve friction (f_s), cone resistance (q_c) and pore pressure (u_2). The sediment friction and cone resistance introduce the sediment friction ratio (f_s/q_c), which in turn classifies the soil at hand by identifying the '*soil behaviour type*' (Robertson, 1990). In marine field studies, there are two possible ways to acquire *CPTu* data: The aforementioned standard approach, or the '*free fall cone penetration test*'. The latter, which penetrates the ground by its own momentum, has the advantages of faster data acquisitions, and higher sensitivity towards thinner sediment layers (Seifert, 2011; Stark, 2011; Stegmann, 2007; Steiner, 2013). Nevertheless, free fall acquisitions are often prone to data anomalies, due to their high penetration rate. One of these anomalies are the *penetration rate effects* (Stark, 2011; Steiner, 2013). Rate effects increase the actual soil resistance properties (q_c, f_s, and u_2), making the data less useful for the typical analytical investigations like the aforementioned *soil behaviour type* classification (Roskoden, 2016). Corrections for q_c, and f_s exist. However, many corrections are based on the correlation of laboratory shearing tests with different shearing velocities instead of real laboratory free fall tests (Biscontin and Pestana, 2001; Steiner, 2013). Therefore, we found the need to establish a free fall calibration test, an experiment, which simulates scaled-down in field conditions to test for *penetration rate effects*. We were especially motivated to find a solution for *penetration rate effects* on *pore pressure data*. Therefore, we created a laboratory free fall calibration test (M.1 Figure 1). Here we penetrate a synthetically altered natural soil from the Hemelinger Marsch in seven free fall experiments M.1 Table 1 and M.1 Table 2). One experiment consisted of four penetration: i) a static penetration for reference reasons and ii) three free fall penetrations. However, striven by high scientific goals we failed, because of unsuspected pore pressure filter clogging. Nevertheless, we archived something unexpected in the end. In this paper, we will discuss how to change the perspectives on failed experiments and how to revalidate scientific data. I hypothesize that by the concepts of scientific *translation* and *adaptation* we change the perspective on failed studies and learn how to reuse unwanted outcomes to establish publishable scientific results. Thus, the scientific objectives are: a) the *translation* of the daily life principle zero waste to *Zero (data) waste*, and b) the *adaptation* to geoscientific foreign analysis methods such as *Data science: Meta, big, and* *smart - mining your own data* will be explained. Examples will be given by literature reviews of Lucking et al. (2017) and Roskoden et al. (2018). Note: Aforementioned methods are no scientific methods, but rather ideas or principles on how to handle unsuccessful data acquisitions and or data correlations.

M.3.3 Methods:

M.3.3.a) Zero (data) waste

There is no (data) waste in science. Scientists are specialists in deducting even the smallest evidences -even if it is just circumstantial- out of incomplete data sets. One of the best examples to look at is the paper of Lucking et al. (2017). In their investigation of the tidal estuary in New Hampshire (USA) with the free fall penetrometer '*BlueDrop*', Lucking et al. (2017) acquired the following data: acceleration, tilt and pore pressure. As mentioned before, one of the biggest advantages of a free fall penetrometer is its fast data acquisitions due to its fast penetration technique. However, one specific task of the cone penetration test is the dissipation tests, which is a pause in penetration to measure the rate of pore pressure dissipation. The dissipation tests is a valued experiment, which gives great sub-soil information - essential to evaluate e.g. the coefficient of consolidation. However, the nature of the tests are counterproductive to the advantages of the free fall penetration tests. The free fall test is favoured for its fast data acquisition, whereas dissipation tests can take up hours of acquisition time. Therefore, by disembarking the *BlueDrop* from the soil shortly after penetration, Lucking et al. (2017) has incomplete dissipation data. However, *translating* the approach of *zero waste* to *zero (data) waste* Lucking et al. (2017), unlike other scientist (Krastel et al., 2016; Steiner, 2013; Stephan, 2015), analysed their short-term dissipation data in relation to one another. Hence, Lucking et al. (2017) were maybe not able to detect the coefficient of consolidation, but created for their study a unique soil property, the short-term dissipation, which was included in their scientific task to map the study area. Thus, the method or principle here is not to waste incomplete data, but to reuse these data-sets by putting them in relative relation to one another. One first approach might be to plot all data, even if regarded as failure, next to each other to see relative rather than global changes, correlations, or to identify relative data classes or data clusters specific to the study at hand.

M.3.3b) Data science: Meta, big, and smart - mining your own data.

The present term '*big data'* was defined in the 1990s by John Mashey (Lohr, 2013). Unfortunately, *big data* and their analyses have so far not often been subject to geological sciences. However, *big data* can be considered to originate from the geosciences. Already early seismic surveys from the 1960s produced tremendous amounts of data fulfilling the nowadays-defined attributes of *big data* – *volume, veracity, velocity, value* and *variety* (Greenberg, 2017). Especially the latter, the *variety*, is the most hindering attribute to really carry out the *big data* analyses. Nevertheless, if we looked at the *metadata* the *variety* of geological data increases and *big data* analyses analogies can be *adopted* by the soil sciences. *Metadata* – grossly defined as data about data- gives information about the data format, type etc. Moreover, *metadata* also refers to auto statistical information about the primary collected or secondary derived data sets. Such *metadata* is also called *process data*. Often experiments are regarded as unsuccessful, if there is not a visible correlation in the primary data. However, if we look at the *process data*, new correlations or even causations can be found, which either explain why the experiment failed or actually show the expected correlations in a different domain. One example, which illustrates this point are the aforementioned *soil behaviour types* defined by Robertson (1990). Soil types were the attempt to correlate *CPTu* measurements to grain sizes. Yet, quite often this direct correlation only works for local studies where cores are used to confirm *CPTu* resistances signatures as done by Ramsey (2002). Robertson (1990)'s approach, to define *soil behaviour types*, allowed him (1990) to assign specific *CPTu* signatures to certain global soil behaviours rather than actual grain sizes. Consequently, his study is based on globally collected *CPTu* data sets (so actual *big data*), instead of high qualitative specified laboratory experiments, which attempt to correlate the mean grain size of one sediment layer to the *CPTu* resistance signatures. Therefore, the approach here is to strength the *variety* of the collected data by using the auto statistical information, so the *process data*, about the collected data. One first approach might be to look at the *variance, covariance,* and *standard deviation* of the data. Furthermore, the data can often be normalised to see relative trends within the data.

M.3.4 Results

M.3.4a) Zero (data) waste

In the beginning of our studies, we collected trail data via standard (static) laboratory *CPTu* measurements to test our equipment (M.1 Figure 1, Roskoden et al. (2018)). Here, labelled as experiment 0, the idea was to recreate the same penetration velocities as in the planed free fall experiments, but with constant pushes to understand the differences between the free fall and the static penetrations. However, the equipment was not able to reach the needed 0.5, 1, and 2 m/s high static penetration-velocities (M.1 Table 2, Roskoden et al. (2018)). Instead, experiment 0' highest velocity was ~ 23 cm/s (standard velocity: 2cm/s). The experiment was regarded as failed. Nevertheless, the experiment clearly shows, that the influence of the side friction cannot be neglected for lightweight free fall penetrometers, as suggest by Stark (2011) and Stephan (2015). Furthermore, we reused the data by following the approach of Dayal and Allen (1975). The data was normalised and plotted in relation to one another, revealing a log-relationship for sediment resistance and penetration rate (M.1 Figure 3). The log-correlations were no initial objective of the study since the log-relationship is not a new revelation. However, the resulting correlation factors of 0.74 and 0.31 (also called soil factors or soil proxies) and their consolidation dependency (pre consolidation 32 and 64 kPa) are new scientific outcomes. Additionally, in reference to the primary objective to find a strain rate pore pressure correction, we followed the maxim of zero (data) waste. The pore pressure data was plotted in relation to each other. The result is shown in M.1 Figure 4a and shows clearly the strain rate effect, which by itself is a result. Furthermore, we identified a linear relation between the dynamic and static pore pressure measurements (M.1 Figure 5b).

M.4.b) Data science: Meta, big, and smart - mining your own data.

After establishing the influence of the side friction on the total resistance for lightweight penetrometers (M.1 Figure 2), we started to follow the general approach of the data science to look at the basic statistics of the data (Roskoden et al., 2019). Programmatic loops and feedback algorithms auto-analysed the *process data*. Therefore, we changed the *variety* of the primary acceleration data. The *process data* was used to identify sediment changes. Here, we utilised the *variance, covariance* and *standard deviation* of the primary and secondary derived data to identify internal changes in the different data sets. By mining our own *process data* and combining the *process* and *primary data* with each other a *smart data* set, which can identify changes in the sediment layers or average the penetration information create main site characterisation for trend analyses. The prove of concept was done in a field study in the Firth of Thames in New Zealand (Roskoden et al., 2019). Here, each penetration was assigned a total resistance, a cone resistance and a side friction value. The newly yielded parameters could be normalised and plotted against the global data sets of Robertson (1990). The results of the classification charts were then verified with sediment samples. Evidently, we incorporated the geometrical set-up and dimensions of the penetrometer, which are by its definition also *metadata*, into the algorithm as well.

M.3.5 Discussion

Two principles of reusing data have been introduced and explained by referring to literature examples: a) *zero (data) waste,* and b) *Data science: Meta, big, and smart - mining your own data*.

M.3.5a) Zero (data) waste

Experiment 0 was no success if evaluated for its original purpose: to create a pore pressure strain-rate correction. However, via experiment 0, we created a valuable data set. In contrast to Stark (2011) and others, who argue to disregard the side friction due the lightweight penetrometer dimensions, we have actual evidence, that such argumentation is error prone (M.1 Figure 2, Roskoden et al. (2018)). In hindsight experiment 0 was the backbone of the second upcoming paper (Roskoden et al., 2019).

While we have not fulfilled the objective to identify the pore pressure strain-rate correction, we helped to identify the pore pressure problem more. Furthermore, we created a pore pressure strain rate correction unique to our specific case, which may lay the foundation for future pore pressure strain rate correction experiments similar to the experiment 0, which lay the backbone to the geometrical algorithm for the upcoming paper of Roskoden et al. (2019).

M.3.5b) Data science: Meta, big and smart - mining your own data.

Experiment 0 only emphasizes the need to identify the differences between total, tip and side resistance, because it is contradicting the assumptions of Stark (2011) and Stephan (2015). However, only the use of *process data* revealed the possible infield differentiation of the resistance forces via a geometrical algorithm. Therefore the utilisation of *process data* allows lightweight penetrometers data to join the *soil behaviour type* classifications after Robertson (1990). Even though, this was not an expected outcome this might increases the value of any lightweight penetrometer investigation as shown by Roskoden et al. (2019).

M.3.6 Conclusion

We all know that failure is part of science. However, scientist rarely talk about their failures or even publish them. Most failed experiments, field data acquisitions, and tests can be revaluated and data can be recycled by *translating* daily maxims to scientific approaches and by *adapting* to alternative methods from geoscientific foreign sciences. Therefore, in conclusion, the *adaption* of other scientific methods (e.g. data sciences) and the *translation* of daily maxims will help scientist to revaluate and recycle unsuccessful data acquisitions and incomplete data sets.

M.3.7 Literature

1. Biscontin, G., Pestana, J.M., 2001. Influence of Peripheral Velocity on Vane Shear Strength of an Artificial Clay. Geotechnical Testing Journal, V. 24, No. 4, p. 423-429, doi# doi.org/10.1520/GTJ11140J.
2. Dayal, U., Allen, J.H., 1975. The Effect of Penetration Rate on the Strength of Remolded Clay and Sand Samples. Canadian Geotechnical Journal, V. 12, No. 3, p. 336-348, doi# doi.org/10.1139/t75-038.
3. Greenberg, J., 2017. Big Metadata, Smart Metadata, and Metadata Capital: Toward Greater Synergy between Data Science and Metadata. Journal of Data and Information Science, V. 2, No. 3, p. 19, doi# doi.org/10.1515/jdis-2017-0012.
4. Krastel, S., Braeunig, A., Feldens, P., Georgiopoulou, A., Jaehmlich, H., Lange, M., Lindhorst, K., Llopart, J., Mader, S., Mehringer, L., Merl, M., Muecke, I., Renkl, C., Roskoden, R., Schoenke, M., Schulten, I., Schwarz, J.-P., Stevenson, C., Vallee, M., Wegener, B., Wiesenberg, L., 2016. Geomorphology, Processes and Geohazards of Giant Submarine Landslides and Tsunami Generation Capacity, as Recorded in the Sedimentary Record of the Only Historic Slide of This Kind: The 1929 Grand Banks Landslide of the Canadian Atlantic Continental Margin - Cruise No. Msm47 - September 30 - October 30, 2015 - St. John's (Canada) - Ponta Delgada, Azores (Portugal). MARIA S. MERIAN-Berichte, V. doi.org/10.2312/cr_msm47 No., p. 55, doi# doi.org/10.2312/cr_msm47
5. Lohr, S., 2013. The Origins of ‘Big Data': An Etymological Detective Story, The New York Times. Arthur Ochs Sulzberger.
6. Lucking, G., Stark, N., Lippmann, T., Smyth, S., 2017. Variability of in Situ Sediment Strength and Pore Pressure Behavior of Tidal Estuary Surface Sediments. Geo-Marine Letters, V. doi.org/10.1007/s00367-017-0494-6, No. 37, p. pages441–456 doi# doi.org/10.1007/s00367-017-0494-6.
7. Parkes, E., 2019. Scientific Progress Is Built on Failure. nature https://www.nature.com/articles/d41586-019-00107-y.
8. Ramsey, N., 2002. A Calibrated Model for the Interpretation of Cone Penetration Tests (Cpts) in North Sea Quaternary Soils, Offshore Site Investigation and Geotechnics' Diversity and Sustainability'; Proceedings of an International Conference. Society of Underwater Technology, London, pp. 341-356.
9. Robertson, P.K., 1990. Soil Classification Using the Cone Penetration Test. Canadian Geotechnical Journal, V. 27, No. 1, p. 151-158, doi# doi.org/10.1139/t90-014.
10. Roskoden, R., 2016. Cone Penetration Tests the Soil Classification and Analytic Assessments of Dynamic and Static Penetrometer Test Data. Universität Bremen, Master Thesis, 2016, Bremen.
11. Roskoden, R., Kopf, A., Mörz, T., Kreiter, S., 2018. Analysis of Acceleration and Excess Pore Pressure Data of Laboratory Impact Penetrometer Tests in Remolded Overconsolidated Cohesive Soils, Cone Penetration Testing 2018. CRC Press, p. 545-550, -.
12. Roskoden, R.R., Bryan, K.R., Schreiber, I., Kopf, A., 2019. Rapid Transition of Sediment Consolidation across an Expanding Mangrove Fringe in the Firth of Thames, New Zealand. V. -, No. 40, p. 295-308, doi# doi.org/10.1007/s00367-019-00589-9.
13. Seifert, A., 2011. In Situ Detection and Characterisation of Fluid Mud and Soft Cohesive Sediments by Dynamic Piezocone Penetrometer Testing, Marine Geotechnics. Bremen University Bremen, p. 180.
14. Stark, N., 2011. Geotechnical Investigation of Sediment Remobilization Processes Using Dynamic Penetrometers, Marine Geotechnics. Universität Bremen, Bremen, p. 309.
15. Stegmann, S., 2007. Design of a Free-Fall Penetrometer for Geotechnical Characterisation of Saturated Sediments and Its Geological Application, Marine Geotechnics. Universität Bremen, p. 181.

16. Steiner, A., 2013. Sub-Seafloor Characterization and Stability of Submarine Slope Sediments Using Dynamic and Static Piezocone Penetrometers, Marine Geotechnics. Universität Bremen, Bremen, p. 325.

17. Stephan, S., 2015. A Rugged Marine Impact Penetrometer for Sea Floor Assessment. Universität Bremen, , Bremen,, p. 268.

Chapter 5 Manuscript 4 - Prefix

With the *Manuscript IV* the content of this thesis will seem to change from dynamic free fall penetrometer tests to hydrogeological analyses via standard *CPTu*s. However, let it be known that this upcoming manuscript was inspired by the work of Albatal and Stark (2017). The authors' kinematic penetrometer, *Bluedrop*, was operated as a method to quickly characterise the sub-surface of Yakutat Bay, Alaska, United States. However, similar to the description in the manuscript before, the authors utilised not only their primary measured data such as the ultimate bearing capacity, and the pressure sensor data, but also evaluated incomplete dissipation test data. Here, the dissipation tests have only been eight to twelve seconds each, but still the authors managed to use the incomplete data to detect relative differences to strengthen their classification arguments.

This recapture indicates quite well that dynamic penetrometer tests are not intended to pause their penetration to monitor the pressure decay behaviour of sub-surface sediments. The fact is even more stressed if the concluded data logging system is considered. The concluded system emphasises, especially for kinematic devices, the objective of the instruments, which is data quantity, the ability to map an area as quickly as possible with as many acquisition locations as possible.

Consequently, our scientific goal is to create a tool, which can extrapolate short and incomplete dissipation tests to not only analyse the relative differences in the pressure data. Moreover, we strive to investigate the hydrogeological properties with this aforementioned extrapolation tool. Admittedly, such tools already exist. However, as the literature research suggests, these extrapolation models need soil classifying input parameters (such as the rigidity index) prior to data extrapolation. Either such inputs need to be estimated or experimentally yielded, rendering the aforementioned intend of the kinematic penetrometer useless. Subsequently, the goal of *Manuscript IV* extends to design a dissipation test model, which is able to extrapolate the measured data without any parameter estimation. Thus, the data fitting and extrapolation is supposed to function in an *ad hoc* mode so that more dynamic free fall data can also be analysed regarding their dissipation test behaviour.

Following the suggestions from the manuscript before we use not only the primary data to fit the model to the dissipation test, but also include meta data analysis such as logarithmic gradient calculations and equalised data sampling. Our own model is tested against three literature established models and evaluated by the reference method of Teh and Houlsby (1991) as suggested by Robertson and Cabal (2010).

To achieve our scientific objective, we have been in the need of long-term dissipation test data (dissipation time is at least 90% of the equilibrium pore pressure), which can be used to verify our model. Therefore, the investigation site Bramley Drive, Omokoroa, New Zealand, was chosen, because it is already part of the *Intercoast* research interests. In addition, former acquired data from other investigations lead to the believe that the tephra soil and its halloysite clay mineral at hand form loosely packed soil micro-structures with high micro-porosity, and low permeability. Furthermore, it is assumed that these altered tephras therefore increased therefore the probability of slope failure, because the halloysite micro-structures low permeability layers can generate high excess pore water pressure in overlying sediments, which may eventually trigger slope failures. Hence, the current research implies an urgent need for a hydrogeological investigation of the Bramley Drive slide.

Therefore, we believe that the Bramley Drive slide is the perfect target site, because it fulfils the need of *Intercoasts* interdisciplinary work (because we are contributing to other *IC*-projects), and we can verify our own dissipation test model in the field for an unknown soil. Thus, a geotechnical company (*CPTit*) from New Zealand was hired to acquire five CPTu profiles on a predefined transect, which include four dissipation tests in four different depth. For Manuscript IV, the dissipation test at 22 m was utilised to test the different models against each other. Furthermore, the literature data from the three different models was recalculated by the different models and by the reference method to evaluate their applicability for unknown soils.

As a very important note, I like to emphasise here that *Manuscript IV* and *V* used to be one single manuscript. However, due to the intense dissipation modelling evaluation, we chose to separate the two foci: a) introduction of a new dissipation test model, which is independent from any prior estimated input data, and b) the hydrogeological investigation of the Bramley Drive slide. Therefore, only one out of four dissipation tests was chosen to evaluate the new model. However, all dissipation tests were utilised in *Manuscript V* to investigate the physical interaction between the sub-surface and its pore water. Nevertheless, due to the split there might be some overlaps or similarities between the two manuscripts. Such similarities are for example the usage of the same figure for the study area. The *Manuscript IV* is already reviewed by its co-authors and is submitted to the Canadian Geotechnical Journal in January 2020.

P.M.4 References

1. Albatal, A., Stark, N., 2017. Rapid Sediment Mapping and in Situ Geotechnical Characterization in Challenging Aquatic Areas. Limnology and Oceanography: Methods, V. 15, No. 8, p. 690-705, doi# doi.org/10.1002/lom3.10192.
2. Robertson, P., Cabal, K., 2010. Guide to Cone Penetration Testing. Gregg Drilling & Testing Inc, Signal Hill, California 90755.
3. Teh, C.I., Houlsby, G.T., 1991. An Analytical Study of the Cone Penetration Test in Clay. Géotechnique, V. 41, No. 1, p. 17-34, doi# doi.org/10.1680/geot.1991.41.1.17.

Manuscript 4

Evaluation of a new dissipation test model with field data from a slide prone coastal area, New Zealand

first author, submitted 02.01.2020 at Canadian Geotechnical Journal, Manuscript ID cgj-2020-0004

Authors:

Robert R. Roskoden[§,1]

Achim Kopf[§,2]

Tobias Moerz[§,3]

Vicki Moon°

Max O. Kluger[§,4]

[§]MARUM – Center for Marine Environmental Sciences, University of Bremen, Bremen, Germany ([1]rroskode@marum.de (ORCID: https://orcid.org/0000-0003-2170-283X), [2]akopf@marum.de, [3]tmoerz@uni-bremen.de, [4] mkluger@marum.de (ORCID: https://orcid.org/0000-0001-9130-8948)

°School of Science, University of Waikato, Hamilton, New Zealand (vgmoon@waikato.ac.nz)

M.4 Abstract

The physical interaction between the subsoil and its groundwater is important for any engineering geological sector, which is concerned with ground stability. Hence, the knowledge of hydrogeological soil characteristics such as permeability (κ), the coefficient of consolidation (c_h), and pore water pressure (pwp) conditions, are necessary to understand the stability of the subsoil. The cone penetration test ($CPTu$) is an inexpensive and convenient *in situ* method, which can log, among others, the dissipation of induced pore water pressure with time. From this measurement, it is possible to estimate relevant *in situ* hydrogeological properties, such as the coefficient of consolidation. However, when performing dissipation tests in low-permeability soils the dissipation of induced pore pressure can be time consuming. Thus, numerous scientists try to model dissipation test data to fit or extrapolate incomplete data to decrease dissipation time and therefore, research costs.

In this paper, a new dissipation model (*ad-hoc model* hereafter) was developed by combining two established dissipation models. The ad-hoc model was compared with existing dissipation models by fitting and extrapolating the models to dissipation data obtained from a slide prone coastal area in New Zealand, which is mainly composed of volcanic ash (tephra) soils. Our results give reasons to question the applicability of standard literature models for dissipation predictions in tephra soils.

M.4 1 Introduction

M.4 1.1 Dissipation tests

The physical interaction between subsoil and groundwater is a very important aspect for any engineering geologist working with installations, such as anchors and foundations. Many examples exist where physical soil properties have not been considered properly and the interplay between soil, groundwater, and the extra load of the installation resulted in a mass wasting event (Hampton et al., 1996; Koizumi et al., 2010). The knowledge of hydrogeological soil characteristics such as effective porosity, its resulting permeability (κ), and the coefficient of consolidation (c_h) is necessary to understand subsoil interactions and processes (Neuzil, 1986; Robertson and Cabal, 2010). For instance, low permeability layers can generate high excess pore water pressure by hampering the water dissipation in overlying sediments, which may eventually trigger slope failure (Tsaparas et al., 2002).

The coefficient of consolidation and other hydrogeological related factors can be indirectly measured by an inexpensive *in situ* method, the cone penetration test ($CPTu$). A $CPTu$ can log the dissipation of induced pore water pressure and can therefore, be used indirectly to estimate the *in situ* permeability (Lunne, Powell, et al., 1997; Robertson, 1990). While penetrating, the localised soil displacement at the $CPTu$-cone, induces excess pore water pressure in the surrounding sediment. After the penetration is stopped, the induced pore water pressure dissipates back towards the initial ambient pore pressure conditions, also called the equilibrium pore water pressure (Robertson and Cabal, 2010). Dissipation tests can be analysed similarly to an oedometer test, in which the void ratio changes with an effective stress increase. Both dissipation and oedometer tests provide vital information for soil stability analyses, such as coefficient of consolidation, volume compressibility, and permeability. Moreover, a $CPTu$ directly measures the cone resistance (q_c) and sleeve friction (f_s), from which the normalised cone resistance (Q_n), friction ratio (F_R), undrained shear strength (s_u) can be derived (Robertson, 1990). M.4 Figure 1 presents a schematic *CPTu* cone that penetrates the ground. Also illustrated are the cavity theory with its failure wedges, as well as the skin-effect, which can form around the cone and the rod creating hydrodynamic friction and drag forces (Stark et al., 2014).

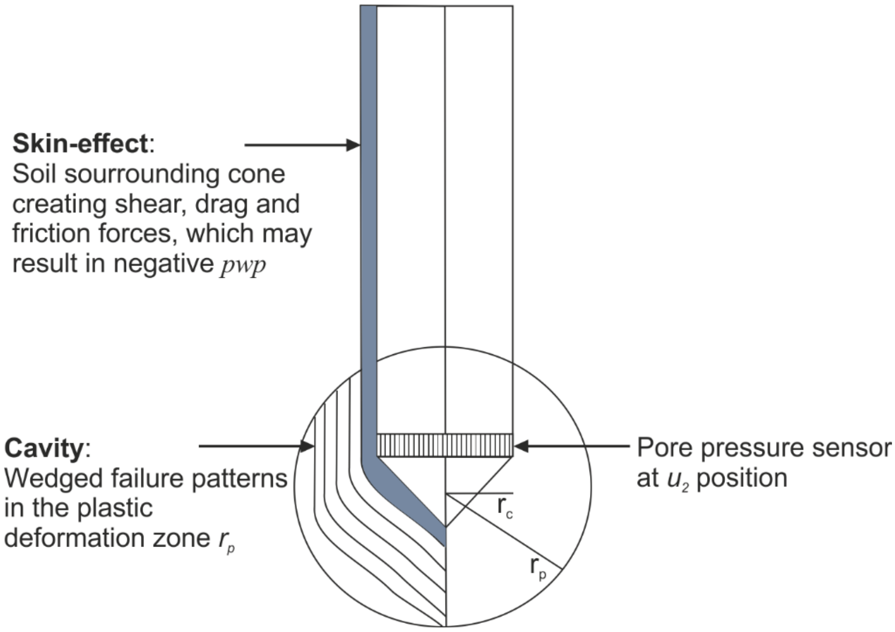

M.4 Figure 1 Schematic presentation of a CPTu *(modified from Burns and Mayne (2002)).* r_c: *cone radius;* r_p: *radius of the plastic deformation zone; pwp: pore water pressure measured at position* u_2*. Further explanations concerning the cavity patterns can be found in Burns and Mayne (2002). Please consider the work of Seifert et al. (2008) for further explanations of the skin-effect .*

M.4 1.2 Dissipation test modelling and Data Extrapolation

Performing dissipation tests in low-permeability soils can be time consuming. For example, a low permeability may lead to dissipation times longer than 24 hours. In addition to that, and depending on the study area, a dissipation test longer than 24 hours may be influenced by the tides, and therefore, the determined dissipation parameters can be erroneous. In order to decrease time and costs for low permeability soils, numerous scientists have been trying to model dissipation test data since the beginning of the last third of the 20th century (Lunne, Powell, et al., 1997; Torstensson, 1977). Hence, dissipation models are useful to fit or extrapolate the collected data. The temporal extrapolation of incomplete dissipation data not only allows the assessment of hydrogeological properties (Krage et al., 2014) but also ensures the evaluation of the coefficient of consolidation at the time of 50% pressure decay ($t_{50\%}$).

The biggest issue of the dissipation test modelling is the non-linear data correlation. Even in a double or semi logarithmic display, the time and pore pressure decay do not correlate linearly to each other. Therefore, no linear regression tools such as the least square method or linear goodness of fits (R^2), such as roots mean square, can be applied if pore pressure versus time are modelled. Hence, non-linear solutions such as hyperbolic fitting functions or numerical power series approximations for differential equations must be utilised. The evaluation of such fitting functions can often only be done via the minimisation of the least square error (SSR) of the residuals or the standard error of regression (SER). In contrast to the linear R^2-method, SSR and SER depend on the amount of measured vs. predicted data points. The greater the data volume, the bigger SSR and SER, whereas R^2 is always in between 0 to 1. The same becomes clear, when looking at the SI units. R^2 is unit free whereas SSR and SER have the same unit as the evaluated data. Hence, it is not possible to compare SSR and SER either to each other, or among each other for different models. The use of these evaluators is only restricted to the model itself to choose the best fit out of all the predicted curves. However, such a methodical evaluation of semi logarithmic functions often results in an over fitting of the dissipation data, because of the unequal data distribution in the different logarithmic sections. Therefore, SSR and SER need to be regarded with care if one is to make sure to choose the best probable soil solution and not the best numerical fit. As a result, many dissipation test models already include evaluation techniques to choose the best fit out of all predicted curves. Consequently, it is important to emphasise that a model is not only the methodical approximation of a data fit, but also, and maybe more importantly, the mean on how to evaluate the model predictions.

As a result, each model and its strategy to evaluate the best fit, determines the dissipation rate, so the slope of the linear part of the dissipation curve, the $t_{50\%}$ value and therefore, by proxy, the coefficient of consolidation.

In addition to fit and the extrapolation of the measured pore water pressure dissipation curves, dissipation modelling enables multivariable analysis of geological parameters such as the rigidity index (I_r), over-consolidation ratio (OCR), and total overburden stress (σ_{v0}) (Burns and Mayne, 2002). Thus, it can be used to verify laboratory and field data by means of simulation of dissipation curves.

M.4 1.3 Literature Dissipation Test Models

Current and acknowledged dissipation test models are, for example, the models after: Burns and Mayne (2002), Krage et al. (2014), and Jang et al. (2015), which all are based on different soil theories or fitting concepts. The model after Burns and Mayne (2002) combines the critical state and spherical cavity expansion theory, which was formulated on the *Modified Cam Clay* (MCC) model. The models after Krage et al. (2014), and Jang et al. (2015) utilise the dissipation test analysis after Teh and Houlsby (1991), which is based on the combination strain path theory and finite element analysis.

The theoretical background of both models might be the same, but their modelling concepts are not. Krage et al. (2014) establishes the usage of a hyperbolical fitting function and combines it with the approach of Teh and Houlsby (1991) to estimate the coefficient of consolidation. Jang et al. (2015) propose an indirect fitting technique, which enables plotting the dissipation data as a linear scatter plot. Hence, a linear regression of the data is possible. The coefficient of consolidation is then calculated via a modified hyperbolic formula, which depends on the linear regression parameters: the slope and the y-intersect.

All mentioned literature dissipation test models have been tested in their corresponding studies on different soil. The example soils of each study and their soil properties are listed in M.4 Table 1 and will be utilised in this study.

M.4 Table 1 Literature dissipation test soils as found in the corresponding papers. If indicated values are yielded or estimated

	Burns and Mayne (2002)	Jang et al. (2015)	Krage et al. (2014)
Location	*Onsoy, Norway*	*Nakdong River, Korea*	*Onsoy, Norway*
Soil	*normally consolidated soft marine clay*	*normally consolidated soft silty clay*	*normally consolidated silty clay, CH (fat clay)*
Clay percentage		~ 35	
Dissipation depth [m]	18.5	29	10
Groundwater depth [m]	2.25	1.5	-
Ir [-]	123.8	200	100
OCR [-]	1.4	1. 1 - 1.2	1.4**
Water content [-]	0.60	0.49	-
Liquid Limit	75	50	-
Plastic Limit	39*	30	-
Plasticity index	36	20	
overburden stress [kPa]	273.9	490*	123.6*
effective overburden stress [kPa]	114.5	200	25.5*
effective stress friction angle	34	-	-
s_u ***[kPa]***	49	50	49**
ρ_t ***[Mg/m³]***	1.33**	1.75	1.26**
Shear Modulus G	6066.2*	10000*	4900*
Salinity [g/L]	-	6	-
cone area [cm²]	15	15	10
u_0 ***[kPa]***	159.4	290*	98.1*
u_i ***[kPa]***	498	435 + 290	350
excess u_i ***[kPa]***	338.6*	435*	251.9*
$t_{50\%}$	3500	619	2766

* calculated

** estimated

M.4 1.4 Scientific Objectives

Three established literature dissipation test models are presented and evaluated regarding a low-permeability soil of a slide prone coastal area in New Zealand. The models are: Burns and Mayne (2002), Krage et al. (2014), and Jang et al. (2015). Furthermore, a combination of the models of Krage et al. (2014) and Jang et al. (2015) will be presented as an alternative dissipation model for instantaneous use in the field, termed here '*ad hoc model*'. Its advantage lies in the reduced amount of *in situ* input parameters, and its modified curve-evaluation approach. All dissipation test models will be investigated in this study for their: a) performance by the concept of cross-processing and b) capability to handle reduced dissipation data sets.

The evaluation of a) and b) is done via a comparison of the predicted coefficients of consolidation with those coefficients calculated by the established method of Teh and Houlsby (1991). Additionally, we will introduce a dissipation test of a weathered tephra soil as a special case, which will be analysed by all four introduced dissipation models. Consequently, the focus of the research in this paper lies on answering the following questions:

i. How can we introduce a dissipation test model, which is only dependant on the dissipation data itself and not on estimated soil properties?
ii. Which of the four dissipation models (including the newly introduced *ad hoc model*) provides the most accurate predictions of the literature dissipation curves?
iii. Which model is the most adequate to investigate an unknown soil such as the tephra soil from New Zealand?
iv. Which model can extrapolate the dissipation test from New Zealand best?

This study also aims to better understand the dissipation modelling procedures, by reviewing current literature models. It will help to reduce assumptions made for dissipation analysis, reduce the required dissipation time itself for soils with low permeability and, hence, reduce research costs, especially for tephra-bearing soils.

M.4 1.5 Study Area

Our study area is located at Omokoroa, which is a highly populated peninsula in a suburb of Tauranga Harbour, on the east coast of the North Island of New Zealand (M.4 Figure 2). The local deposits consist mainly of tephra, pyroclastic deposits, and their altered products (Moon et al., 2013). As an area with active tectonic and volcanic zones and common rainfall events, Omokoroa is prone to slope failure and associated landslides and slumps, which have been reported previously (Kluger, Jorat, et al., 2019; Moon et al., 2013). In early April 2017, storm and rainfall events triggered several new landslides on the peninsula of Omokoroa, marking the region as a high-interest investigation site for rainfall-induced slope failures. Moon et al. (2013) and Kluger, Jorat, et al. (2019) ascribed the occurrence of landslides to the landslide history of Omokoroa and related specific rainfall events.

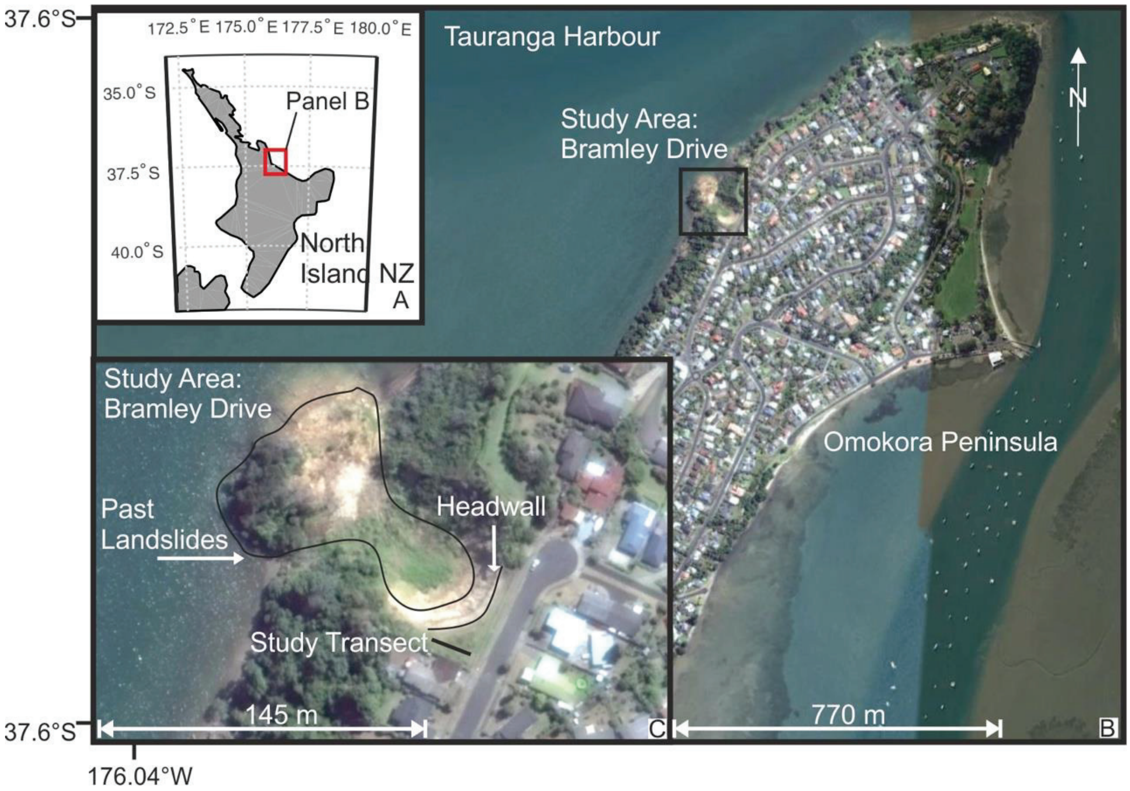

M.4 Figure 2 Study Area: Panel A: Overview map showing the north island of New Zealand. Red rectangle indicates the zoomed in area (Tauranga Harbour with the Peninsula Omokoroa) displayed in B. Panel B: Peninsula Omokoroa in the Tauranga Harbour area, encircled is the study area, Bramley Drive. Panel C: Study area Bramley Drive, indicated are the past landslide deposits the headwall of 1979 Bramley Drive landslide and the study transect. Source: 'Omokoroa', 37,630242° S, 176.046106 W Google Earth 2018, 07.01.2019.

The aforementioned slides and slumps commonly failed in altered clay-rich tephra (Kluger et al., 2017; Kluger, Jorat, et al., 2019). Smalley et al. (1980) found out that the clay-rich tephra at the Bramley Drive study site are highly enriched with the clay mineral halloysite. Halloysite is a phyllosilicate of the kaolin subgroup (Joussein et al., 2005) and forms loosely packed soil micro-structures with a high degree of micro-porosity, low permeability, with a low plasticity index and a high liquid index. It is assumed that these clay-rich tephra increased the propensity for slope failure (Moon et al., 2013; Moon, Lowe, et al., 2015). The alteration of the tephra by weathering classifies the soil as a cohesive soil. A typical Robertson soil classification defines the soil at 22 to 23 m as a *clayey silty clay*. Therefore, this study area is regarded as a good example to test dissipation modelling techniques.

M.4 2. Methods

M.4 2.1 Dissipation Tests

The wealth of work by Robertson defines the dissipation test as "a test when the decay of the pore pressure is monitored during a pause in penetration" (Robertson and Cabal, 2010). The rate of the pressure decay depends on the coefficient of consolidation, which itself depends on the compressibility of the surrounding soil, its effective porosity and its permeability. The difference to the laboratory oedometer test is the orientation of the aforementioned soil properties. These are measured *in situ* in the horizontal direction, whereas the laboratory oedometer test provides information about the uniaxial shortening in vertical direction and associated changes in soil properties. Nevertheless, The vertical and horizontal soil properties can be derived from one another (Terzaghi (1943), *EQ* 48):

$$c_v = \frac{k_v}{m_v \gamma_w} = c_h \left(\frac{k_v}{k_h}\right) \qquad 48$$

where c is the coefficient of consolidation, k the coefficient of permeability and γ_w is the specific unit weight of water. The index v refers to vertical, and the index h to the horizontal axis.

Complete dissipation tests, in which the pore water pressure dissipated by at least 90 %, can be easily interpreted with the widely used method of Teh and Houlsby (1991), which was chosen as reference method in this study, as suggest by Robertson and Cabal (2010). Similar to an oedometer test, the duration where the excess pore water pressure dissipated by 50% ($t_{50\%}$) is estimated after standards of ISO (2017). The coefficient of consolidation is then calculated after Teh and Houlsby (1991) *EQ* 49:

$$c_h = \frac{T^*_{50\%} r^2 \sqrt{I_r}}{t_{50\%}} \qquad 49$$

where T^* is the modified theoretical time-factor, r is the cone radius, I_r is the rigidity index and t the time, and the index *50%* indicates 50% pressure decay.

M.4 2.2 Literature Dissipation Test Modelling

CPTu is considered an inexpensive *in situ* method. However, when a dissipation test is conducted in a low-permeability soil, the costs can easily exceed the costs of laboratory tests, even if the specimens need to be excavated by means of sediment core sampling. Consequently, geotechnical engineers and other scientists use modelling solutions, with the capability to extrapolate incomplete dissipation data to calculate the *in situ* coefficient of consolidation and other soil properties.

Before we present the review of the three literature models it is important to differentiate important terms for this study: *Parameter*, a term in the model, which defines the model's properties such as curvature etc. A parameter is either held constant or is systematically changed. If a parameter is associated with soil specific attributes, it is called a *soil parameter*. If this soil parameter has a real physical establishment such as the rigidity index or the coefficient of consolidation, the soil parameter can be called *soil property*. If no soil associations for a parameter are evident, the parameter is termed *modelling parameter* and is consequently not measurable in the field or laboratory. *Variables* are entities, which are changed in order to find the best fit. Therefore, a non-constant parameter can be considered a variable. Input-parameters are parameters, which are entered in the beginning of the modelling processes. Input-parameters may change during iteration phases of the modelling process.

M.4 2.2.1 Cross-processing

Cross-processing describes how we evaluated the capabilities of the different models, presented in this study. In the cross-processing procedure, the dissipation data set from one literature model is used as an input for all the other models, which, as a result, predict the coefficient of consolidation. Hence, all three-literature dissipation data sets plus the dissipation data set from this study are processed by all presented dissipation test models. Furthermore, all data sets are also evaluated by the aforementioned reference method of Teh and Houlsby (1991). Hence, all predicted coefficients of consolidation are evaluated by the reference method and the average deviation is calculated as a proxy to define which model makes the closest prediction to the reference method of Teh and Houlsby (1991) *EQ* 50:

$$\frac{1}{\mathrm{n}}\sum_{1}^{\mathrm{n}}\left|\left(\frac{\left(\mathrm{c}_{\mathrm{h(pre)}}\right)}{\left(\mathrm{c}_{\mathrm{h(ref)}}\right)}\right)-1\right| \tag{50}$$

n, is the numbers of data sets tested by one model, *ref*, stands for reference calculated via *EQ* 49, and *pre,* for predicted from the different models

M.4 2.2.2 Model after Burns and Mayne (2002)

The model of Burns and Mayne (2002) is based on the cavity expansion theory and the critical-state theory of soil mechanics. The cavity expansion theory was first noticed by Bishop et al. (1945). Vesic (1972) gave the general solution to the cavity expansion problem in an elastic-perfectly plastic material with a non-associated Mohr-Coulomb yield surface (Cudmani and Osinov, 2001). The theory deals with the axiom that the soil-mass under load develops wedged failure patterns, called cavities (M.4 Figure 1). It is believed that the formation of the cavity itself is responsible for the failure in the end. Thus, the cavity expansion theory deals with expansion of these failure patterns or cavities in a soil which fulfils given properties (Pandit et al., 1985). These properties are:

1. the cavity shape is either spherical or cylindrical;
2. the soil is assumed to be homogenous and linear elastic to linear plastic; and
3. loading conditions for the cavity are either static, dynamic or with variable penetration velocities or have a variable cone diameter (note: all aforementioned different loading conditions change the applied pressure conditions on the soil cavity).

The critical state of a soil is reached when additional shearing does not further affect the shear resistance of the soil. In this state the volumetric strain of the soil is constant (Schofield and Wroth, 1968). For their model, Burns and Mayne (2002) divide the measured pore water pressure (u_m) into three parts, *EQ* 51:

$$u_m = u_0 + \Delta u_{oct} + \Delta u_{sh} = u_0 + 4s_u \ln\left(\frac{r_c\sqrt[3]{I_r}}{r}\right) + \sigma'_{vo}\left[1 - \frac{OCR}{2}\right]^{\Lambda} \tag{51}$$

where u is the pore pressure. The indexes *m, 0, oct, and sh* refer to measured, hydrostatic, octahedral, and shear induced pore water pressure, respectively. Octahedral represents the induced pore water pressure from the cavity expansion, whereas shear induced pore pressure results from the critical state. s_u, is the undrained shear strength and r_c is the cone radius (Note: the plastic deformation radius is $r_p = r_c(\sqrt[3]{I_r})$). σ'_{v0}, is the effective vertical overburden stress; OCR is the over-consolidation ratio, and Λ is the plastic volumetric strain. Burns and Mayne (2002) assume a cylindrical cavity expansion for defining the dissipation of the pore water pressure over time and distance as a differential equation of the second order, *EQ* 52:

$$\frac{\partial u}{\partial t} = c_h\frac{\partial^2 u}{\partial r^2} + \frac{c_h}{r}\frac{\partial u}{\partial r} \tag{52}$$

where t is the time and r is the radius around the cavity (Note: $r_c < r < r_p$). An analytical solution to this problem yields the following exponential equation (Randolph and Wroth, 1979) , EQ 53:

$$\boldsymbol{u} = \boldsymbol{v} e^{-c_h \alpha^2 t} \tag{53}$$

where α is a modelling parameter (in the range 1 to 10^3) for the numerical approximation of the power series without any soil relation. Here v is a function of r. The insertion of EQ 51 into EQ 52 yields a Bessel function (a numerical approximation of a differential equation) of the order zero. The general form of v is therefore, given in EQ 54:

$$\begin{aligned} v(r) = {} & A\,J_o(\alpha r) + BY_o(\alpha r) \\ & = J_o(\alpha r)Y_0(\alpha r_p) - J_o(\alpha r_p)Y_0(\alpha r) \ \ for\ the\ octahedral\ induced\ pwp \\ or\ v(r) = {} & J_o(\beta r)Y_0(\beta r_{sh}) - J_o(\beta r_{sh})Y_0(\beta r)\ for\ the\ shear\ induced\ pwp \end{aligned} \tag{54}$$

where J_0 and Y_0 are the Bessel function of the first and second kind of the order zero. Note that index refers to the order; the second part of EQ 54 is only true if $r = r_p$ where $u = 0$, from here on called $v(r_{p,0})$.

The constants B and A represent the octahedral and shear induced pore water pressure and are obtained from the first 50 roots of EQ 54 as shown in the graphical representation in M.4 Figure 3. The predicted pore water pressure is then calculated as the total sum of all roots from the three pore pressure components and is then inserted in EQ 51, resulting in EQ 55:

$$u_m = u_0 + \Delta u_{oct} + \Delta u_{sh} = u_0 + \sum_{n=1}^{50} B_n v(r_{p,0}) e^{-c_h \alpha^2 t} + \sum_{n=1}^{50} A_n v(r_{sh,0}) e^{-c_h \beta^2 t} \tag{55}$$

where n is a running index for each α and β (Note: β is a modelling parameter similar to α) found for each root of EQ 54. EQ 55 represents the analytical solution for the radial dewatering process during consolidation of the pore space.

The best coefficient of consolidation is chosen by the evaluation of the standard error of the regression (SER), EQ 56:

$$SER = \sqrt{\frac{1}{n} \sum_{1}^{n} (u_{pre} - u_{mea})^2} \tag{56}$$

where n is the number of predicted data points and the indexes pre and mea refer to predicted and measured. However, the influence of I_r and OCR are evaluated manually by the means of a visual comparison of predicted and measured data to choose the model curve, which best fits the soil and not which best fits the numerical approximation.

In order to create a better understanding of how to calculate the predicted pore water pressure after Burns and Mayne (2002), a schematic representation is shown in M.4 Figure 3. The red dashed lines depict iterative loops, while black solid lines depict the insertion of input parameters. The schematic overview consists of seven steps. Step 1: Here, the input parameters OCR, Λ, γw, γs, *water table (wt) depth*, σ'_{v0}, σ_{v0}, s_u, r_c, r_s, α,and β are defined. Step 2: A start value (for example 50) for the rigidity index is chosen and entered to calculate the plastic deformation radius, which is then entered at step 3a. Step 3 (here only explained for the octahedral part): a) r_p is passed to $v(r)$ while at step 3b α or β (given for the range 1 to 10^3) are inserted. The first 50 roots of the derivative of $v(r)$ are then calculated (*EQ* 54). At step 4a the first 50 roots of $v(r)$ are inserted in the formulas shown in M.4 Figure 3 (step 4a). After inserting Λ, σ'_{v0}, OCR, I_r, s_u, r_c, r_s, the parameters B and A are yielded at step 4b. Step 5: a) The coefficient of consolidation is changed iteratively, while at the same time in step 5b B and A are inserted in the pore water pressure formula (*EQ* 55). At step 6, every result for each coefficient of consolidation is compared to the measured dissipation data and the best fit is chosen via *EQ* 56 and saved. At the final step 7, the rigidity index is changed and the process starts from the beginning. In the end, the best fit for the combination of OCR and I_r is determined visually by plotting all modelled dissipation curves next to each other.

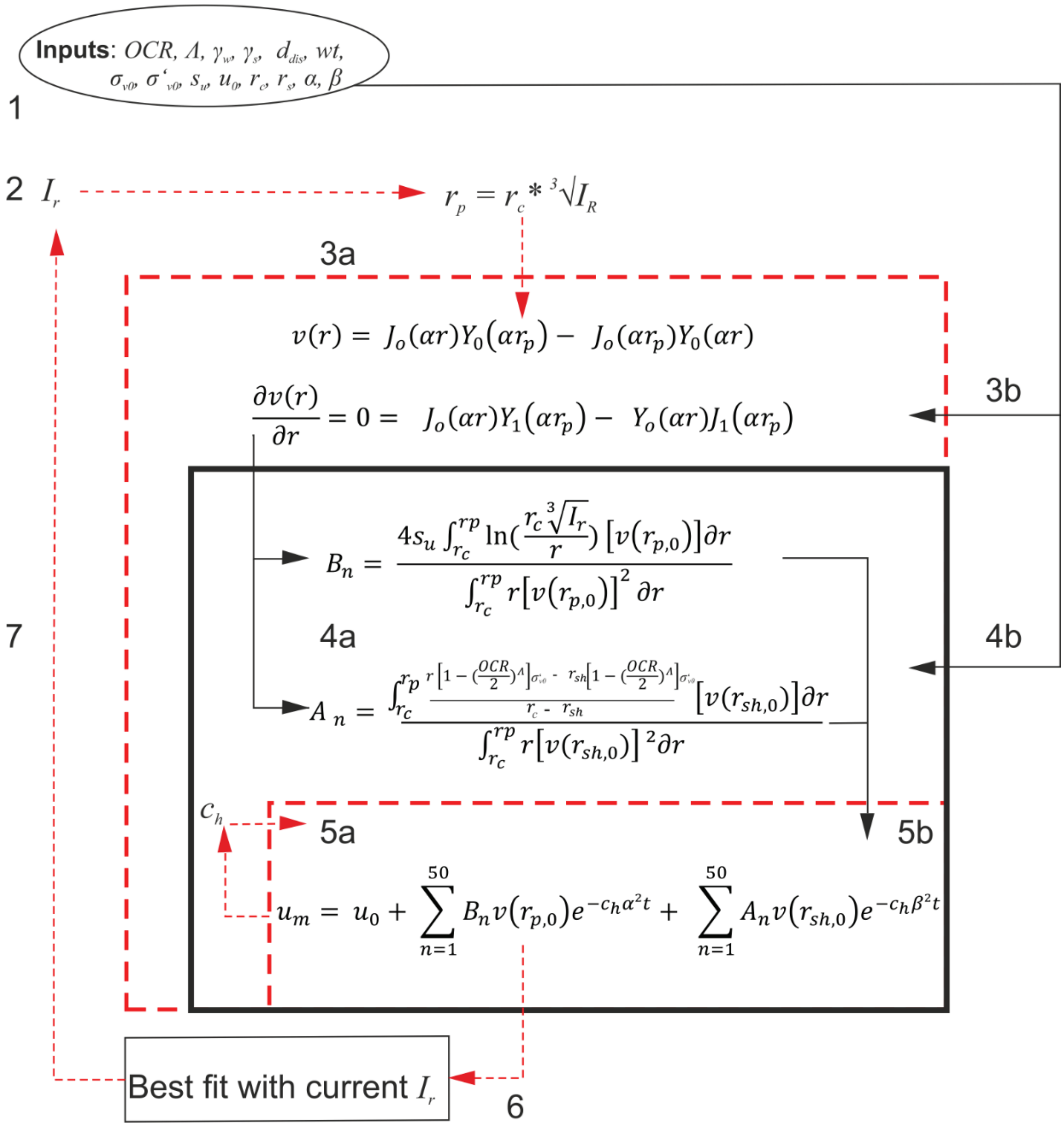

M.4 Figure 3 Schematic overview of the dissipation model after Burns and Mayne (2002) as described above.

M.4 2.2.3 Model after Krage et al. (2014)

The model by Krage et al. (2014) is based on the combination of the numerical theory of Teh and Houlsby (1991) for the coefficient of consolidation and the hyperbolic fitting function of DeJong and Randolph (2012) (*EQ* 57):

$$t = T^*_{50\%} \sqrt[b]{\left({}^{1}/_{U} - 1\right)} \frac{r^2\sqrt{I_R}}{c_h} \tag{57}$$

where $T^*_{50\%}$ is the modified theoretical time-factor (= 0.245) from Teh and Houlsby (1991), b (being in the range 0.1 to 1.5) is a modelling parameter and U is the normalised pore water pressure (being between 0 to 1) *EQ* 58:

$$U = \frac{u - u_0}{u_i - u_0} = \frac{\Delta u}{u_i - u_0} \tag{58}$$

where u_i, is the initial pore water pressure and Δu, the excess pore water pressure. A schematic display of the dissipation model after Krage et al. (2014) can be seen in M.4 Figure 4.

Red arrows depict an iterative loop. Krage et al. (2014) suggested an estimation/measurement of the rigidity index beforehand so that the problem reduces to a two-variable issue. Thus, the cone radius and rigidity index are inserted as input parameters.

The parameter b controls the slope of the linear part of the logarithmic fitting curve while the rigidity index moves the curve along the time axis determining the actual $t_{50\%}$-value in combination with the found coefficient of consolidation. In an iterative approach the modelling parameter b and the ratio of $\sqrt{(I_r)}/c_h$ are altered until a best fit is determined. Krage et al. (2014) evaluate the estimation level via a minimization of the sum of squares of the residuals of all measuring points (M.4 Figure 4, *EQ* 59).

$$SSR = \sum_i log\left[\frac{U_{i,pre}}{U_{i,mes}}\right]^2 \tag{59}$$

With SSR being the sum of squares of the residuals; i, pre and mes are the running indices for each measured and predicted data point, respectively.

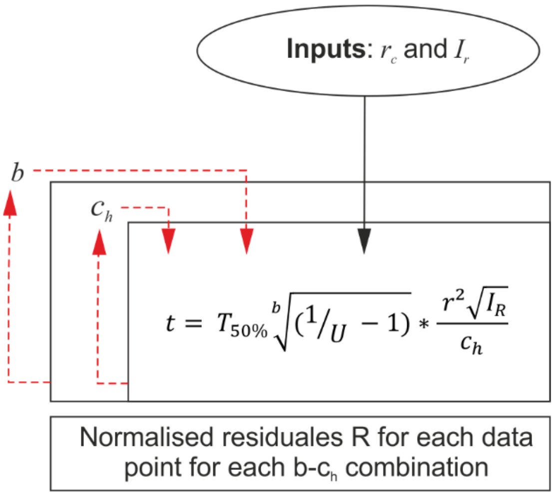

M.4 Figure 4 Schematic overview of the dissipation model after Krage et al. (2014), for description see text above.

M.4 2.2.4 Model after Jang et al. 2015

Both aforementioned modelling approaches (Burns and Mayne, 2002; Krage et al., 2014) work with direct fitting methods, calculating theoretical pore water pressure data and comparing it to the measured data. Chung et al. (2013) propose an indirect fitting method. Hence, not the pore water pressure itself is fitted to the measured data, but the ratio of the time to an alternative definition of the excess pore water pressure (U_d), *EQ* 60:

$$U_d = \frac{u_i - u}{u_i - u_0} = \frac{u_d}{u_i - u_0} \qquad 60$$

U_d being the alternative normalised excess pore water pressure and u_d the alternative excess pore water pressure. Jang et al. (2015) presented an advanced method of the indirect fit, here, the *time pore water pressure ratio* (t/U_d^k) is expressed as a linear function of the time itself (*EQ* 61):

$$\frac{t}{{U_d}^{\kappa}} = \alpha_J + \varepsilon t \qquad 61$$

where κ is a modelling parameter ($\kappa>0$), α_j is the y-intercept, and ε is the slope. The same function can be derived for the normal definition of the normalised pore pressure (U) either with t or the (normal) theoretical time factor T (Note: $T \neq T^*$, *EQ* 62):

$$\frac{T}{U^{\lambda}} = D + NT \qquad 62$$

where λ is the modelling parameter, D is the y-intercept, and N is the slope. Note: *EQ* 62 uses U not U_d.

Using *EQs* 61 and 62 the coefficient of consolidation can be calculated after Teh and Houlsby (1991) with the normal time factor T (*EQ* 63):

$$c_h = \frac{T}{t} r^2 = \left(\frac{D}{((1/U^{\lambda}) - 1)} \, \frac{((1/{U_d}^{\kappa}) - 1)}{\alpha_J} \right) r^2 \qquad 63$$

For *EQ* 62, many soil-dependent literature solutions exist and have been presented by Jang et al. (2015). Therefore, λ and D only need to be looked up in the literature as presented by Jang et al. (2015). Nevertheless, it is important to make sure to choose the right theoretical solution with the current problems at hand. If no information about the soil are known, the authors suggest calculating the coefficient of consolidation with all four theoretical solutions as a mean. Table 1 gives a small summary of common literature values, which were also used in this study (Jang et al., 2015):

M.4 Table 2 Solution for the modelling parameter λ and D found for theoretical time factor and normalised pwp (U) issue after common literature data calculated by Jang et al. (2015).

Theoretical solutions via:	***Soil***	***λ***	***D***
Torstensson (1977)	Clay which fulfils the cavity expansion theory conditions	2.1632	6.2692
Teh and Houlsby (1991)	Idealised homogenous elastic perfectly plastic clay	1.8099	0.6872
Randolph and Wroth (1979)	Homogenous elastic plastic soft clay	2.1774	7.7985
Baligh and Levadoux (1986)	Boston blue clay, lean marine illitic with medium sensitivity (~7)	2.1867	15.4334

By putting the normalised pore pressure and time into a linear relation (EQ 61 and 62) the usage of linear regression tools such as the least square method are possible. Consequently, the goodness of the fit can be evaluated, for example, via R². M.4 Figure 5 shows a systematic overview of how to program the dissipation model after Jang et al. (2015). Again, red arrows depict iterative loops, whereas black arrows depict the insertion of input parameters. Time, the pore water pressure data itself, the cone radius, and the literature values for λ and D are used as input parameters. The alternative normalized pore water pressure is calculated and plotted linearly over time. The model parameter κ is then iteratively changed until the best fit is found.

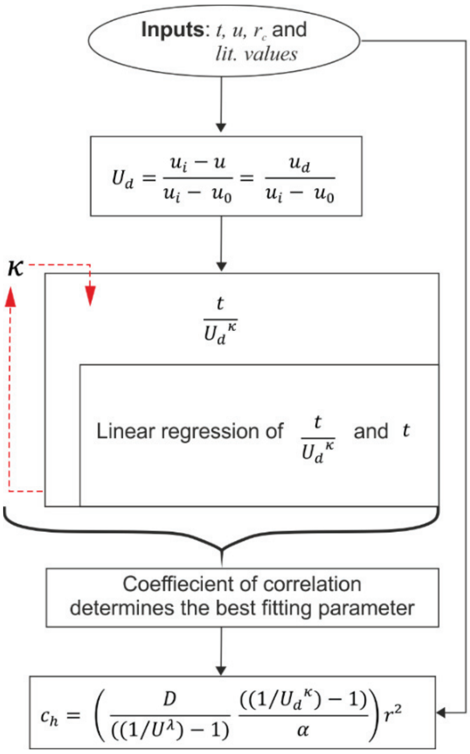

M.4 Figure 5 Schematic overview of the dissipation model after (Jang et al., 2015), for description see text above.

M.4 2.3 Ad hoc model: A combination of Krage et al. (2014) and Jang et al. (2015)

In this paper, we review three existing and differing dissipation models. Moreover, we want to improve current practises and modelling techniques. On the one hand, the model after Burns and Mayne (2002) is quite complex and cannot be used for immediate data modelling in the field, because the runtime is long and too many unknown input variables are needed. On the other hand, when the pros and cons from Krage et al. (2014) and Jang et al. (2015) are directly compared (M.4 Table 3) we still see the need for a model combining the best parts of both model approaches.

M.4 Table 3 Direct comparison of the advantages and disadvantages of the dissipation models after Krage et al. (2014) and Jang et al. (2015).

	Pro	*Con*
Krage et al. (2014)	• Data can be extrapolated • Curves are very well simulated	• Needs input parameter extracted from laboratory work
Jang et al. (2015)	• No need for input data • Compares already measured data to literature data by the modelling parameters λ and D	• Cannot extrapolate data

Driven by the desire to generate a model that only depends on the dissipation data and not on protracted laboratory–derived soil properties (e.g., rigidity index), a new approach is suggested, based on a feedback loop, as shown in M.4 Figure 6.

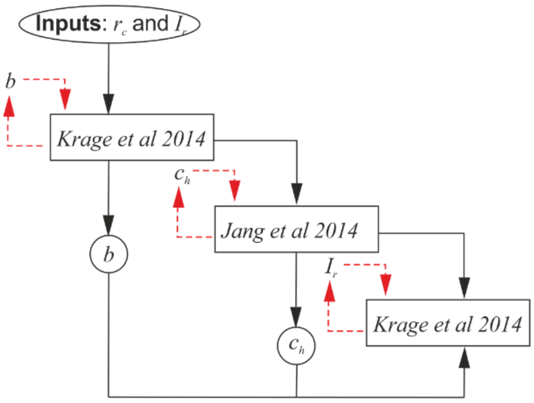

M.4 Figure 6 Schematic overview of the combination of the dissipation model after Krage et al. (2014) and Jang et al. (2015) in a 3 level feedback loop always modelling for one variable and using the new output as an input for the next loop-level.

In the first level of M.4 Figure 6, the model after Krage et al. (2014) is utilised to predict the best fit for any inserted rigidity index by fitting the ratio $\sqrt{(I_r)}/c_h$ and the modelling parameter b to the measured data. However, only the parameter b is saved. In contrast to the approach of Krage et al. (2014), the best b is determined via an error estimation of the slopes of the linear part of the logarithmic curve and not via minimization of the SSR of all measuring points (EQ 64).

$$e_s = \left| \frac{\Delta U_m}{\Delta \log(t_m)} - \frac{\Delta U_p}{\Delta \log(t_p)} \right| \qquad 64$$

The generated best fit is sampled at equally distributed points over the logarithmic time intervals. The samples are then forwarded to the second level of the $ad\ hoc\ model$. Here, the model after Jang et al. (2015) calculates the best fit between the syntactic/down sampled, and equally distributed data as mentioned in the chapter before. Determination of the best fit follows the standard of a linear regression, calculating the coefficient of consolidation via EQ 63 and M.4 Table 2. Afterwards, in the third level of M.4 Figure 6, the data is returned into Krage et al. (2014) so that the parameter b and the coefficient of consolidation are used as inputs from the former two levels. This allows the model after Krage et al. (2014) to calculate a best fit based on the rigidity index as a variable. Evaluation of that fit is determined firstly via a comparison of the slopes of the linear part of the logarithmic curve and secondly via a sum of errors for each single data point of the linear part of the logarithmic curve (EQ 65).

$$e_U = \sum_{U=0.8}^{U=0.1} \left| t_{p,U} - t_{m,U} \right| \qquad 65$$

M.4 2.4 Dissipation Test Extrapolation

An extrapolation is an estimation beyond the range of observations, which links two variables to each other via a mathematical relation. In this paper we are looking at three different mathematical relations, which are supposed to link the pore pressure to the measured time. Their relations are: a) a numerical power-series solution, b) a hyperbolical and c) a linear function. The extrapolation potential, so how good the different literature approaches can extrapolate the measured data, is also evaluated in the paper. Here, we are utilising the dissipation data of this study by truncating it from 0-20, 0-50, and 0 – 80%. The truncated data sets are used to estimate $c_{h,50\%}$. The extrapolated model curve and the yielded $c_{h,50\%}$ are compared to the calculated reference $c_{h,50\%}$ value (EQ 49) and the original data set.

M.4 3. Results and Discussion

M.4 3.1 Dissipation Test evaluation Omokoroa

The dissipation test from the Bramley Drive landslide (22 to 23 m, this study) can be seen in M.4 Figure 7. The test presented here, can be described as a standard dissipation test with the initial pore pressure being the maximum measured pore pressure. Here, the *excess pore pressure* (Δu) is plotted over the logarithmic time, and the pressure decay at 50% ($t_{50\%}$ ≈ 65 s) is emphasised by a red line. The initial pore pressure (u) is ~1320 kPa; the equilibrium pore pressure is ~94.3 kPa. Hence, the initial excess pore pressure is ~1186 kPa.

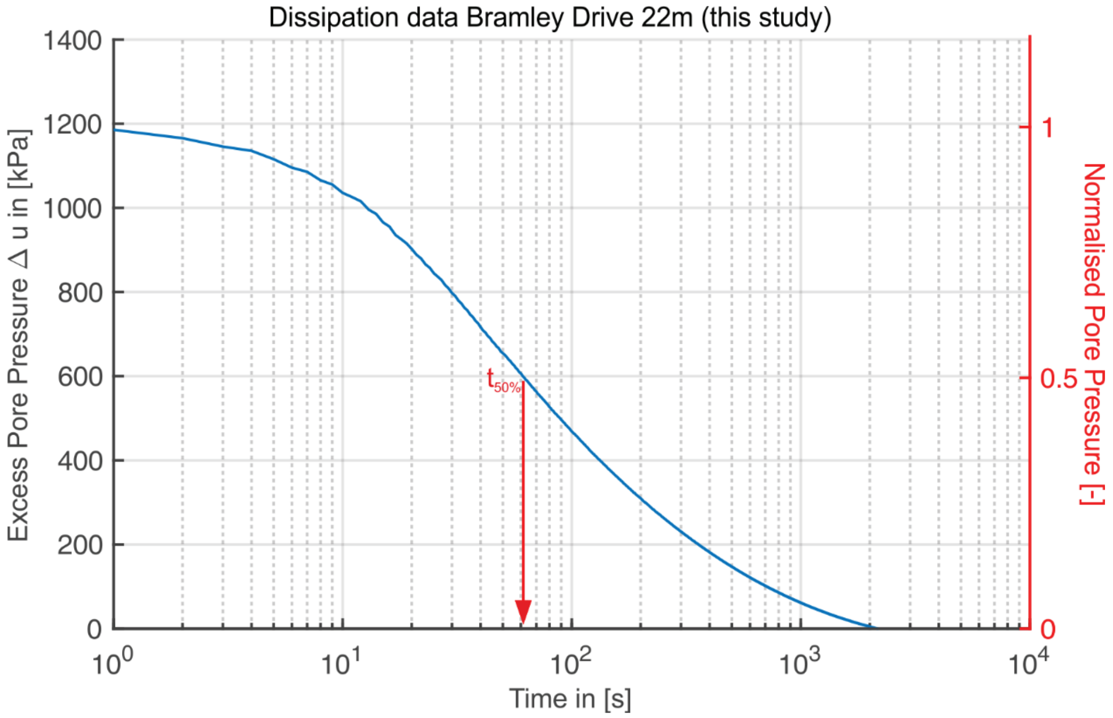

M.4 Figure 7 Excess pore pressure in [kPa] (left, black axis) plotted over time t in [s] and the normalised pore pressure [-] (right, red axis) plotted over the same t in [s]. The time is displayed logarithmically. Indicated by a red line is the time at 50% dissipation.

Moon et al. (2013) investigated the soil structure of the study area and described the dominant halloysite clay mineral as loosely packed and with a high micro-porosity (51 to 77%). Hence, Moon et al. (2013) concluded a very low permeability. Therefore, the $t_{50\%}$ of 65 s was unexpected. Comparable dissipation tests in halloysite clay-rich tephra have been acquired by Jorat, Kreiter, et al. (2014) at Pyes Pa (37.774299° S 176.118527° E), ~15 km away from the study site. Here, non-standard dissipation test with $t_{50\%}$ ≈ 1949 to 5155 s have been described. Similar to Moon et al. (2013), Jorat, Kreiter, et al. (2014) described very low coefficients of hydraulic conductivities down to 9.23*10^{-10} while Kluger, Kreiter, et al. (2019) also described similar low coefficients of *vertical* hydraulic conductivity at Bramley Drive

(Omokoroa) at the same study site ($4.7*10^{-10}$), which lead to the conclusion that similar $t_{50\%}$ values are to be expected. The *horizontal* coefficients of hydraulic conductivity determined here, is $4.9*10^{-6}$ and therefore, about 4 powers bigger than the estimated permeability by Kluger, Kreiter, et al. (2019) and Jorat, Kreiter, et al. (2014) (M.4 Table 4). This high coefficient of hydraulic conductivity corresponds to an intermediate drainage and is comparable to a saturated silt. Here, we interpret the differences in the vertical and horizontal coefficients of hydraulic conductivity as an anisotropic effective porosity.

M.4 Table 4 Calculation of the permeability in Omokoroa at 22.13 m depth.

Depth [m]	ρ [kg/m³]	$\alpha_m = Q_{tn}$ [-]	q_t [kPa]	σ_{v0} [kPa]	M [kPa]	c_h via EQ 48	k_h [m/s]
measured	from Kluger, Kreiter, et al. (2019)	(Robertson and Cabal, 2010)	measured	$\rho g h$	$\alpha_m(q_t - \sigma_{v0})$	(Teh and Houlsby, 1991)	$(c_h \gamma_w)/M$
22.13	1550	3.81	1856	347	5752.8	2.8E-05	4.9E-06

M.4 3.2 Literature dissipation test modelling

M.4 3.2.1 Cross-processing evaluating model prediction accuracy

The coefficients of consolidation from the literature data have been recalculated by the reference method from Teh and Houlsby (1991) (*EQ* 48, M.4 Table 5). Also included in this table is the coefficient of consolidation form the study area at Bramley Drive.

M.4 Table 5 Recalculation of the coefficient of consolidation from the literature via the reference method of Teh and Houlsby (1991) (EQ 48, last row of the table)

	Burns and Mayne (2002) ***Soft marine clay at Onsoy, Norway***	**Krage et al. (2014)** ***Terrestrial silty clay at Onsoy, Norway***	**Jang et al. (2015)** ***Soft silty clay at Nakdong River***	***Ad hoc model Omokoroa coast Weathered tephras (clayey silty clay)***
$c_h = \dfrac{T^*_{50\%} r^2 \sqrt{I_r}}{t_{50\%}}$	3.7E-07	2.8E-07	2.7E-06	2.8E-05

The estimated coefficient of consolidation for the study area was yielded by the assumption of a rigidity index of 250 ($I_r = G/s_u$, with G the shear modulus). This value was chosen due to former triaxial testing of Kluger, Kreiter, et al. (2019), which determined the shear modulus, and the undrained shear strength. In the study of Jorat, Kreiter, et al. (2014), the rigidity index was calculated with the shear wave velocity and was around 50 for all investigated depths. The yielded coefficient of consolidation in Jorat, Kreiter, et al. (2014)'s study ($1 – 3*10^{-6}$) were one power smaller than the value calculated here (M.4 Table 5, *EQ* 50). As shown by *EQ* 50 the influence of the rigidity index on the coefficient of consolidation is small. Therefore, the differences in the yielded coefficients of consolidation are related to the different $t_{50\%}$ values, described earlier.

To compare the different models to each other, the different datasets of Burns and Mayne (2002); Jang et al. (2015); Krage et al. (2014) and the dissipation test from the Bramley Drive (this study) were processed with each model as presented above ("cross-processing" hereafter). Afterwards, all predicted coefficient of consolidation have been evaluated by the results of M.4 Table 5 (EQ 50, M.4 Table 6). The average of the deviation (last row M.4 Table 6) indicates how much the calculated coefficients differ from the reference coefficients of consolidation calculated by EQ 50. This showed that the lower the average deviation, the higher is the potential of the model to evaluate an unknown soil for its dissipation behaviour via the coefficient of consolidation (M.4 Table 6). In M.4 Table 6, the three literature models show an average deviation from the reference method of 64, 26, and 32%, respectively. The deviation of Krage et al. (2014) and Jang et al. (2015) are very similar and are regarded to be in a good agreement with the reference method of Teh and Houlsby (1991). The 64% deviation of the model from Burns and Mayne (2002) is roughly the double of Krage et al. (2014) and Jang et al. (2015), which was expected as suggested by the literature (Paniagua et al., 2016). The *ad hoc model* gives the smallest average deviation of 11%. Not only is the average deviation the smallest but the *ad hoc model* found almost in every single data set the most-accurate coefficient of consolidation compared to the reference method of Teh and Houlsby (1991).

M.4 Table 6 Result matrix comparing the potential of the different models to recreate the coefficient of consolidation from one another. Displayed are the ratios |ch(pre) - ch(ref)|/ch(ref) and the average deviation from the predicted to the original data (recalculated via Teh and Houlsby (1991)).

	Burns and Mayne (2002)	Jang et al. (2015)	Krage et al. (2014)	***Ad hoc model***
	$\lvert c_{h(pre)} - c_{h(ref)}\rvert / c_{h(ref)}$			
Burns and Mayne (2002) ***Soft marine clay at Onsoy, Norway***	78%	21%	57%	17%
Jang et al. (2015) ***Soft silty clay at Nakdong River***	63%	18%	38%	6%
Krage et al. (2014) ***Terrestrial silty clay at Onsoy, Norway***	29%	15%	6%	8%
This study Omokoroa coast ***Weathered tephras (clayey silty clay)***	86%	49%	24%	11%
Average Deviation from *Teh and Houlsby (1991)* $\frac{1}{4}\sum\left\lvert\left(\frac{(c_{h(pre)})}{(c_{h(ref)})}\right)-1\right\rvert$	64%	26%	32%	11%

M.4 Table 6 signifies a striking dependency of the established literature models, on their environment. There is a clear trend for the models of Burns and Mayne (2002) Jang et al. (2015), and Krage et al. (2014) on how good the coefficient of consolidation can be yielded, compared with the results of EQ 50 in M.4 Table 6. Here, M.4 Table 6 indicates that aquatic dissipation tests are harder to analyse. When the literature dissipation tests are directly compared with each other, it is possible to link the environmental trend (marine, river, terrestrial) to the dissipation behaviour itself. Independent of the $t_{50\%}$ values (M.4 Table 1), the slopes (Soft marine clay at Onsoy, Norway = 0.25, Soft silty clay at Nakdong River = 0.42, and Terrestrial silty clay at Onsoy, Norway 1.5) of the linear part of the dissipation tests decrease when the environment becomes more aquatic/marine. The slope of the dissipation curves directly links to the data distribution in a dissipation test, which highly influences the best-fit model evaluations. On the contrary to these arguments, stands the dissipation test at the Omokoroa study side. Here, the depositional environment is a coastal area, which should be in between the results of the terrestrial and river data (M.4 Table 6). However, besides the environmental factor, the coefficient of consolidation also depends strongly on the age of the deposits and the hereby linked diageneses processes (Hamilton, 1964). All literature described soils have been deposited in last Holocene, whereas the Omokoroa tephras have been deposited around the late Pleistocene (Jorat, Kreiter, et al., 2014), making Omokoroa to be the oldest depositional environment. This may explain why the literature models have a higher deviation from the reference method than the *ad hoc model*. In contrast to the other models, the *ad hoc model* does not show any dependency on the dissipation slope. The independency is likely a result of its improved best-fit algorithm (*EQs* 64and 65), which already incorporates the evaluation of dissipation test slope.

M.4 3.3 Model application on the study area Omokoroa

All calculated coefficients of consolidation for the study area Bramley Drive are presented in M.4 Table 7 for comparison. Due to the high deviations between the dissipation models and the reference method of Teh and Houlsby (1991) (24 to 86%), M.4 Table 6 and M.4 Table 7 give reason to question the applicability of standard literature models for predictions in tephra soils, making the study area a perfect target to evaluate the new *ad hoc model*.

M.4 Table 7 showing all calculated coefficient of consolidation for the study area Bramley Drive; all numbers in m²/s.

	Teh and Houlsby (1991)	**Burns and Mayne (2002)**	**Jang et al. (2015)**	**Krage et al. (2014)**	***Ad hoc model***
Estimated($^{\#}$) or yielded soil properties(°)	c_h *via* T^* I_r 250$^{\#}$	*OCR* 2.9 I_r 200°	-	I_r 250$^{\#}$	I_r 175°
c_h in [m²/s]	2.8E-05	4.00E-06	1.4E-5	2.2E-05	2.5E-05

$^{\#}$estimated value

°predicted/calculated

M.4 3.3.1 Burns and Mayne (2002)

M.4 Figure 8 plots the measured pore pressure over the logarithmic displayed time. Here, it becomes clear that the model after Burns and Mayne (2002) combines real physical entities to the model's coefficient of consolidation predictions. M.4 Figure 8 shows eight different best-fit model curves. The curves represent different rigidity indices ($50 \leq \mathrm{I_r} \leq 500$ in 50-interval steps), their corresponding coefficients of consolidation, and the calculated *SERs*. In M.4 Figure 8, the curve with smallest *SER* slightly underestimates the measured data, but the shape and magnitude provide a reasonable fit. The modelled coefficients of consolidation are mostly one order of magnitude smaller than the interpretation of Teh and Houlsby (1991). The curve with the smallest SER deviates from reference result by ~86% (M.4 Table 7). Nevertheless, the model, as seen in M.4 Figure 8, was able to extrapolate the data in both time directions. Hence, speculation about the immediate settling or dissipation behaviour are possible via the model of Burns and Mayne (2002).

For the Bramley Drive data, the curve, which best predicts the pore pressure dissipation has an OCR of 2.9 with an I_r of 200 (compared to M.4 Figure 8, SER 0.9). The I_r 200 was selected due to the smallest SER and seems reasonable, since the assumed index for the reference calculation was 250. Given that the model here used a 50-interval step, the predicted rigidity index is found to be in good agreement with the reference method. The OCR 2.9 was selected manually. The selection was done by comparing different plots with different OCR. Additionally, the selection of the best OCR was done under inclusion of the SER, and the comparison of coefficient of consolidation acquired with EQ 50. Prediction with lower $OCRs$ could not reach the initial pore pressure conditions and were therefore, disregarded. The OCR of 2.9 seems unrealistically high for any area, which has not experienced mechanical compression (Kluger, Kreiter, et al., 2019). Kluger, Kreiter, et al. (2019) however, did find an OCR of 2.3 for the same study area, which Kluger, Kreiter, et al. (2019) argues to be a result of the weathering processes of the clay mineral halloysite. Consequently, the term *apparent over-consolidation ratio* was used. The difference of the over-consolidation ratios between these two studies is around 26%. The difference can be seen as minor if considering the different *ex* und *in situ* measuring techniques.

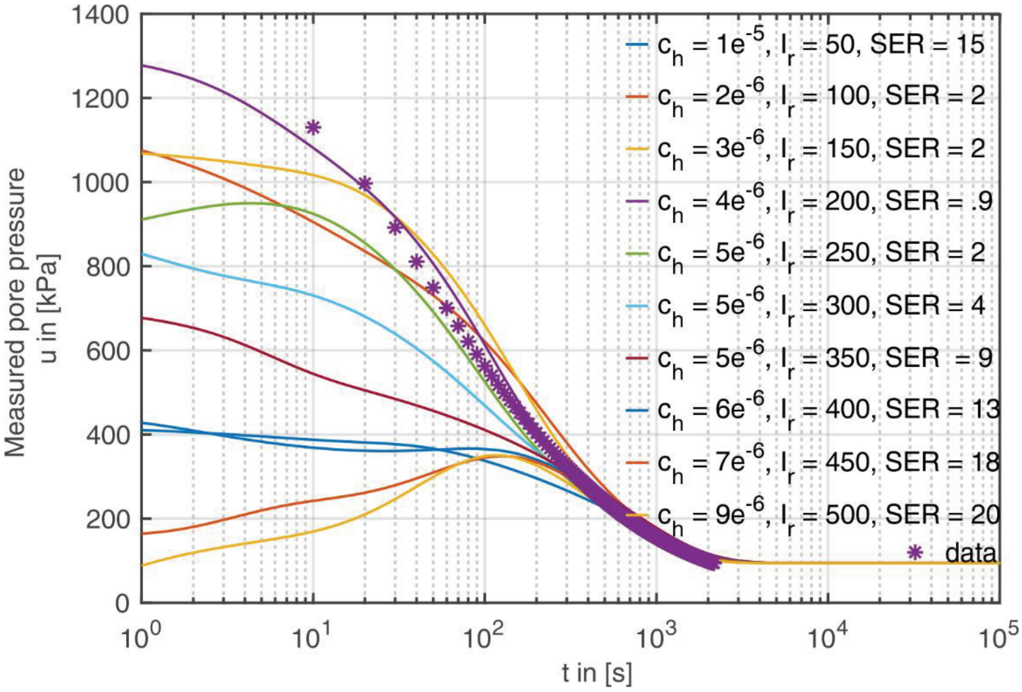

M.4 Figure 8 Dissipation test model after Burns and Mayne (2002) for depth 22.13 m, OCR is 2.9, best fit (here with I_r 200) is derived visually. Plotted is the pore pressure in [kPa] over the logarithmic time in [s].

M.4 3.3.2 Krage et al. (2014)

The model after Krage et al. (2014) needs an initial estimation of I_r, which was ~250. This value was chosen due to former triaxial testing of Kluger, Kreiter, et al. (2019). I_r 250 was found to work well with the reference method of Teh and Houlsby (1991) (*EQ* 48 and M.4 Table 7). The shape and deviation of the model curve relative to the original data creates a good fit, but mostly aligns with latest part of the data. The actual $t_{50\%}$ is not really matched (Figure 8). The best fit is yielded here via a minimization of the sum of squares of the residuals of all measuring points (*EQ* 59, M.4 Figure 4). Hence, the smaller the *SSR* the better the fit. However, the more data points there are, the bigger *SSR* automatically gets, therefore, the model always needs be evaluated in comparison to all possible fits and with different I_r. The predicted coefficient of consolidation is 2.2*10^{-5} and is ~24% smaller than the reference coefficient (M.4 Table 7). In comparison to the other models, ~24% is that the second smallest deviation to the reference method.

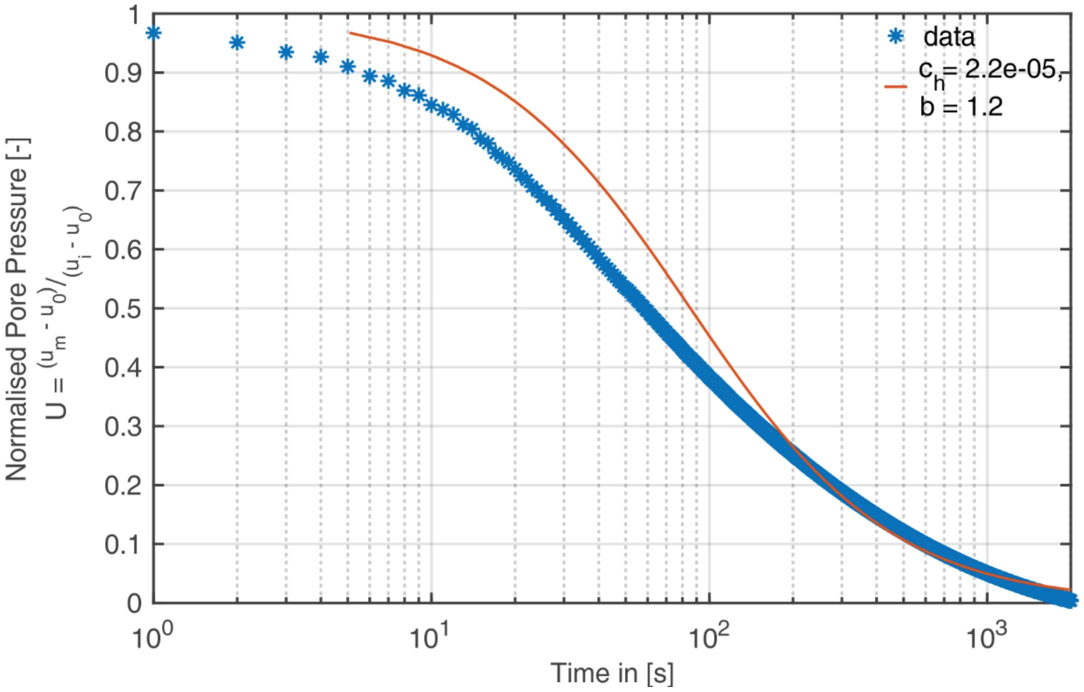

M.4 Figure 9 Model after Krage et al. (2014), description in the text above. Plotted is the normalised pore water pressure [-] from EQ 58 over the logarithmic time in [s], for the dissipation depth 22.13 m.

M.4 3.3.3 Jang et al. (2015)

The results from the model after Jang et al. (2015) fit well to the original data (M.4 Figure 10) due to the linearization of the normalised pore pressure and time (*EQs* 61 and 62, M.4 Figure 5). In M.4 Figure 10 panel A, the *alternative normalised pore water pressure* (U_d, *EQ* 60) is plotted over the time. Panel B plots the *time-alternative normalised pore water pressure ratio* (t/U_d^k, *EQ* 61), linearly over the time. Also shown in the same panel is the linear regression and its regression parameters such as slope ($\beta = 0.94$), y-intersect ($\alpha = 130.5$) and the determined modelling parameter k (= 1.5, orange line). Panel C plots the measured and predicted U_d over time next to each other. Panel D shows the coefficient of consolidation (*EQ* 63) for the normalised pore water pressure (1 to 100%) for the different reference-modelling parameters from M.4 Table 2. Being interested in the coefficient of consolidation at 50% pressure dissipation, the coefficients are derived by matching the coefficient at $U_{50\%}$ as indicated by the legend (M.4 Figure 10 panel D). For the case at hand, the coefficient of consolidation, as shown by M.4 Table 7, is yielded from averaging the four shown coefficients of consolidation in the legend of M.4 Figure 10 panel D. As suggested by Jang et al. (2015) the average of the four yielded coefficients of consolidation is used for the analysis of unknown soils from Omokoroa. Hence, the predicted coefficient of consolidation here is $1.44*10^{-5} m^2/s$, which has the second biggest deviation (~50%) to the reference method of Teh and Houlsby (1991) (*EQ* 48 and M.4 Table 7). The model evaluation is done here via the R^2. Best fits are usually found with R^2 close to one, which indicates very good fit.

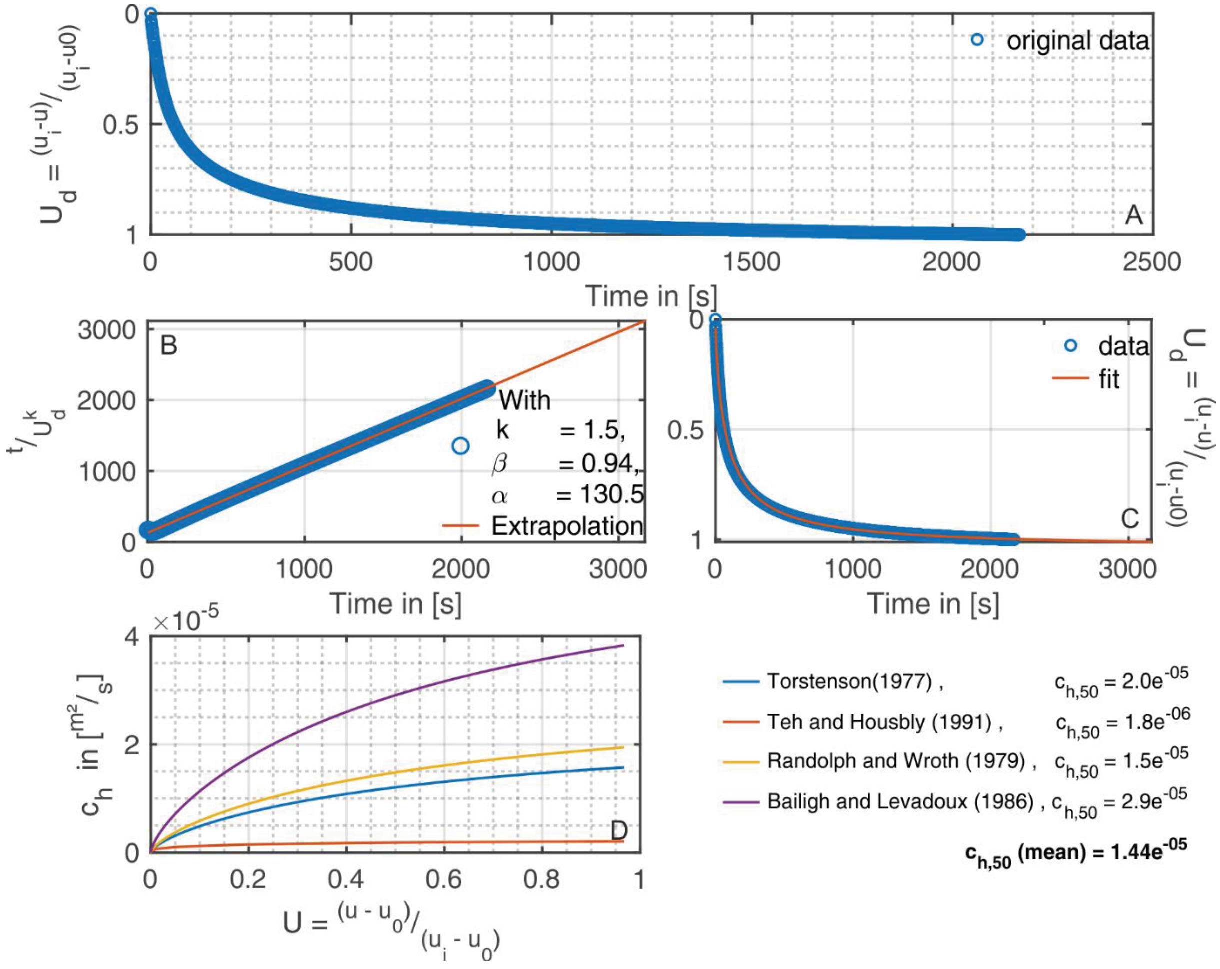

M.4 Figure 10 Dissipation model after Jang et al. (2015) for the dissipation depth 22.13 m. Panel A: Alternative normalised pore pressure over time. Panel B: Time normalised via the normalised pore pressure U_d linear plotted over the time in [s] with the y-intercept α and the slope β. Panel C: Alternative normalised pore pressure over time, comparing measured and predicted data. Panel D: Coefficient of consolidation plotted over the normalised pore pressure U_d calculated via EQ 63 with the reference values from M.4 Table 2. The mean coefficient of consolidation is given below the legend for Panel D.

The model of Jang et al. (2015) strongly relies on the soil parameters from M.4 Table 2. This parameter table can be expanded by following the instructions of Jang et al. (2015). If more information is known about the current investigated soils, the results can improved beyond those of the averaged coefficient of consolidation.

M.4 2.3 Ad hoc model: A combination of Krage et al. (2014) and Jang et al. (2015)

M.4 Figure 11 consists of three different panels. Panel A shows the step after the measured dissipation data, which was simulated by the model of Krage et al. (2014) (M.4 Figure 6), but evaluated by *EQ* 64. Here, only the modelling parameter b and a down-sampled data set were saved. Hence, panel A shows an equal and down-sampled syntactic data set, which was passed to and simulated by the model of Jang et al. (2015). The best fit and therefore, the best coefficient of consolidation was found as described by Jang et al. (2015). Afterwards, the modelling parameter b, the down-sampled data, and the found coefficient of consolidation were passed back to the model of Krage et al. (2014) (M.4 Figure 6). Hence, in the model of Krage et al. (2014) only I_r is left as a variable and is therefore, iteratively changed (M.4 Figure 11, Panel B) until the best fit is found and evaluated with *EQ* 65 (M.4 Figure 11, Panel C).

The visual evaluation of the *ad hoc model* (M.4 Figure 11) shows a better result than the model of Krage et al. (2014) (Figure 8). However, there is a certain similarity, which is not surprising, because the *ad hoc model* uses the approach of Krage et al. (2014) to predict the dissipation data, but uses a different approach to fit the predicted, to the original data (*EQ* 64 and 65). However, the differences are in the evaluation of the modelling parameter, the estimation of rigidity index and the resulting coefficient of consolidation. As a result, the *ad hoc model* predicts the coefficients of consolidation ($2.5*10^{-5}$) closest (~11%, M.4 Table 6 and M.4 Table 7) to the calculation after Teh and Houlsby (1991). Furthermore, the new model also predicts the rigidity index without any pre-existing or additional measurement information as shown by M.4 Figure 11.

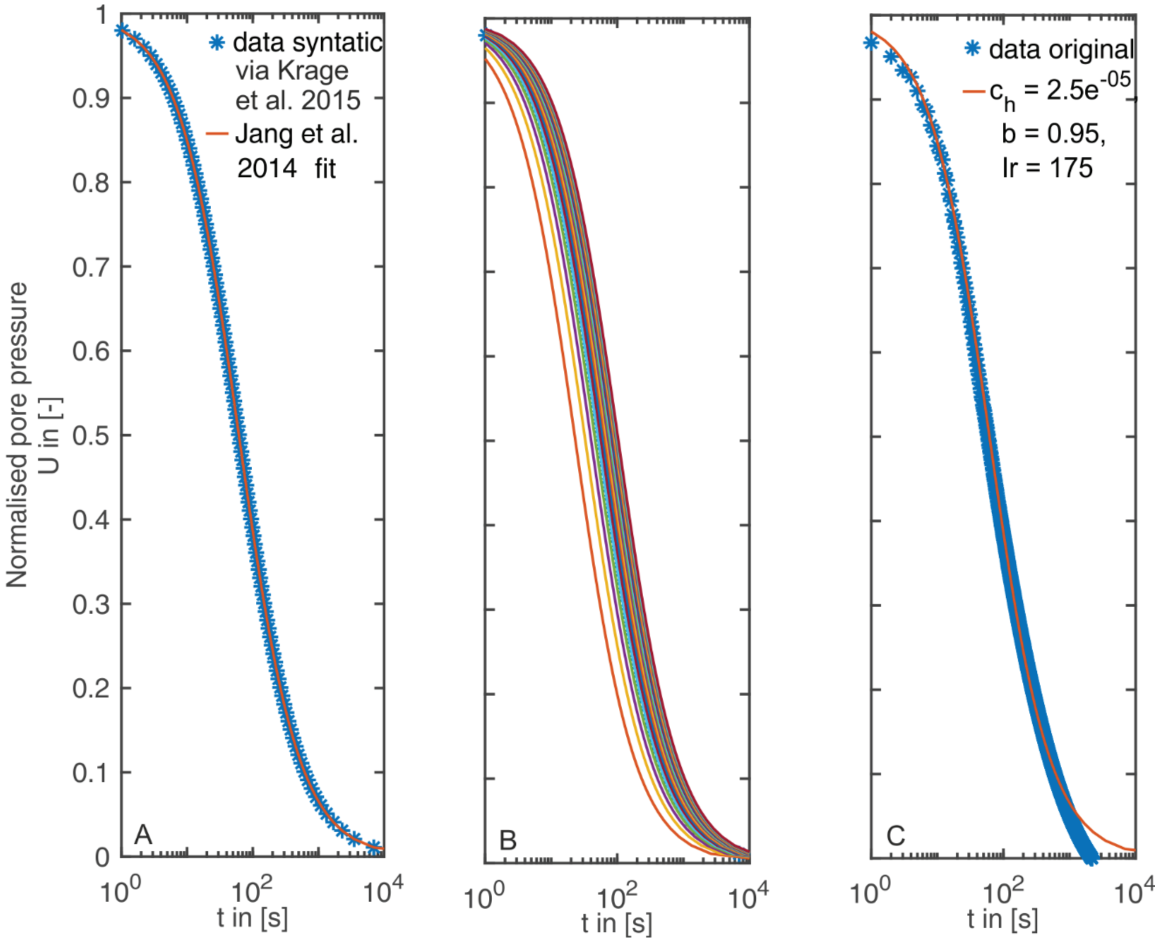

M.4 Figure 11 New modelling approach: A combination of Krage et al. (2014) and Jang et al. (2015). Plotted are the normalised pore water pressure [-] from EQ 58 over the logarithmic time in [s] for the dissipation depth 22.13 m. Panel A the step after the measured dissipation data was simulated by the model of Krage et al. (2014) forwarded to and simulated by Jang et al. (2015). Panel B: The forwarded data from Jang et al. (2015) are modelled after Krage et al. (2014), but here ch and b are used as input parameters, which makes I_r the only variable. Hence, I_r iteratively changes until the best fit is found (Panel C).

M.4 3.4 Dissipation Test Extrapolation

One of the most important trademarks of dissipation test models is their potential to extrapolate short-term dissipation data. The extrapolation of the pore pressure data, or its normalised version, has three main properties, which characterise the goodness of the extrapolation: a) the data fit's visual performance, b) the standard deviation from coefficients of consolidation (form the truncated data to the non-truncated data), and c) average deviation from the truncated data to the reference method of Teh and Houlsby (1991). To estimate a), b), and c) we utilised the Bramley Drive dissipation data in order to test each model for its extrapolation potential. Hence, M.4 Figure 12 consists of 4 panels. Each panel represents one of the introduced dissipation tests models (indicated by their headlines) and shows three extrapolation curves (except panel A), which is compared in the plots directly with the original data. The Omokoroa data set truncated by 20, 50 and 80%. Evidently, 80% data reduction corresponds to a residual data set of 20%. As an example, M.4 Figure 12 panel C, the violet curve with legend-name 0.2 corresponds to the data reduction of 80%. The only exception is the panel A, the model extrapolation of

Burns and Mayne (2002). Due to the multivariable analysis of Burns and Mayne (2002) it is not possible to plot all data extrapolation sets in one plot. Therefore, only the data extrapolation for 50% is shown in panel A. The different curves in panel A correspond to the different utilised rigidity indices. The other extrapolation plots of Burns and Mayne (2002) can be seen in the appendix.

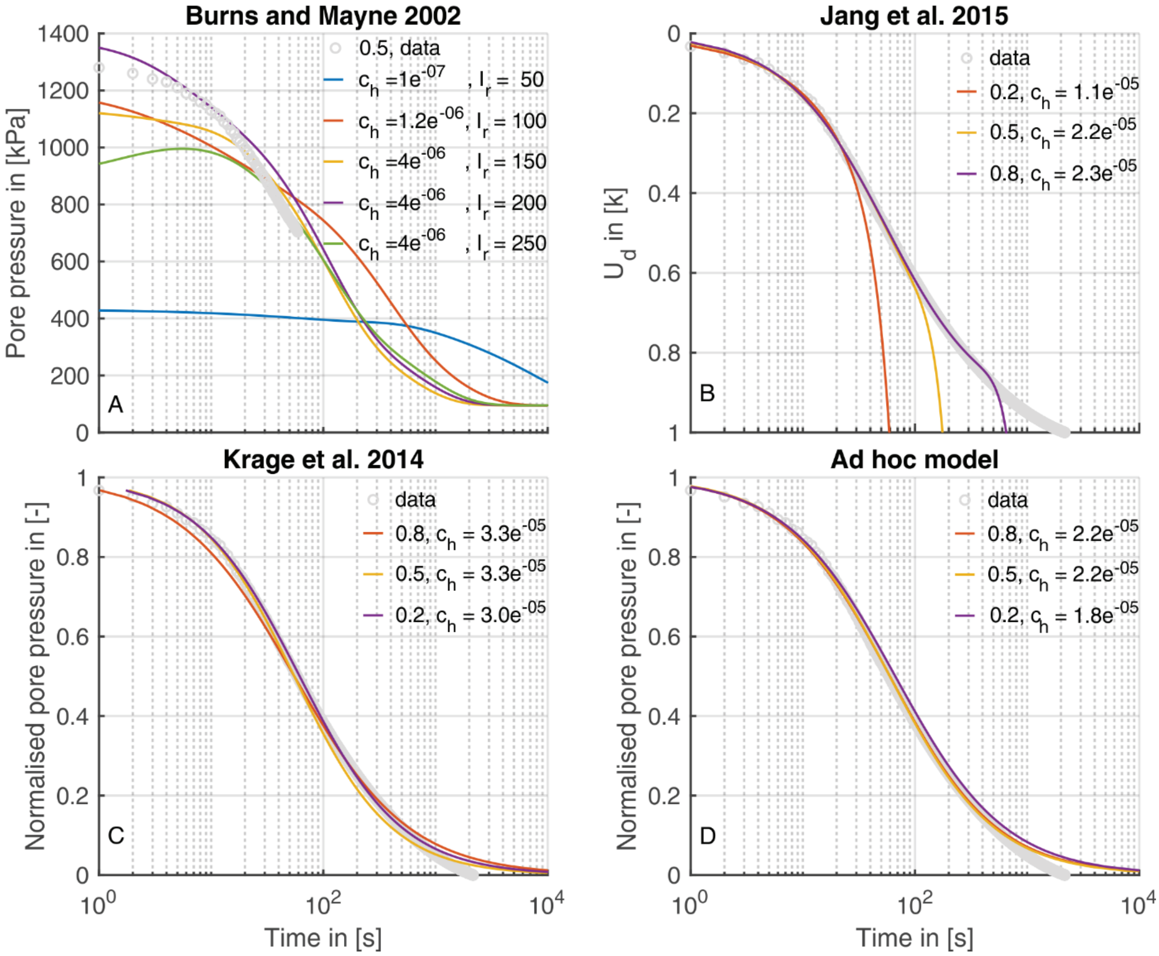

M.4 Figure 12 Evaluation of the extrapolation potential of the different models for different level of dissipation data reductions (input data was reduced by 20, 50 and 80%). Panel A: Burns and Mayne (2002). Here, due to clarity reasons only the data reduction of 50% is shown. Panel A plots the absolute pore pressure over time, Panel B: Jang et al. (2015), plotted are the alternative normalised pore pressure over time. Panel C: Krage et al. (2014), plotted is the normalised pore pressure over time. Panel D: The ad hoc model, plotted is the normalised pore pressure over time.

The analysis of the extrapolation performance (a to c) is done in M.4 Table 8. Note that row a) is based on a subjective interpretation of M.4 Figure 12. Nevertheless, M.4 Table 8 clearly states that the amount of data subjected to the model influences the model performance and its interpretation of the coefficient of consolidation. For example, the models from Burns and Mayne (2002) and Jang et al. (2015) have a bad visual performance as shown by M.4 Figure 12 and M.4 Table 8 (row a). The models of Krage et al. (2014) and the *ad hoc model* on the other hand fit the predicted normalised pore pressure well to the measured data. However, if looked at the variance of the yielded coefficients of consolidation the model performance of Jang et al. (2015) and Krage et al. (2014) is not consistent with the solutions in M.4 Table 7 (row b). On the contrary, the analysis of the coefficient of consolidation seems to improve with the truncated data sets. Hence, it is not surprising that the average deviation of the coefficient of consolidation to the reference method of Teh and Houlsby (1991) for the truncated data decreases for Krage et al. (2014) and Jang et al. (2015) (row b). The increased performance derives for the model of Krage et al. (2014) due to the truncation of the data, which equalizes the data distribution in the logarithmic display, allowing a data fit not to the late part of the dissipation test but to the initial or middle part of the dissipation (row c). In case of the improved coefficient of consolidation by the model of Jang et al. (2015), it is only logical that the reduced data input changes the yielded regression properties such as slope and y-intercept and therefore, changes the outcomes for the model. The less influenced interpretation of the coefficient of consolidation is given by the model of Burns and Mayne (2002). Even so, the rigidity index the coefficient of consolidation stays constant throughout the whole truncations. The *ad hoc model* on the other hand satisfies in all three extrapolation domains. Furthermore, the yielded rigidity indices are ~ 150 and therefore, still in good agreement with the index in M.4 Table 7. Admittedly, the interpretation of the coefficient of consolidation worsens by ten percent points (compare M.4 Table 7 to M.4 Table 8, row c), while the models of Jang et al. (2015) and Krage et al. (2014) improved, but it is still better than the results of the models presented in M.4 Table 7.

M.4 Table 8 Analysis of the extrapolation performance of the dissipation tests models.

	Burns and Mayne (2002)	**Jang et al. (2015)**	**Krage et al. (2014)**	***Ad hoc model***
a) Visual performance from 50% reduction *	4	5	1-2	1
b) Deviation c_h from 0% reduction	0%	45%	49%	18%
c) Deviation from Teh and Houlsby (1991) from 50% reduction	86%	18%	18%	21%

**1 (= very good) to 6 (= very bad)*

M.4 5. Conclusion

Comparing all dissipation models to each other is difficult because they all use very different approaches to predict the dissipation behaviour of the measured data but also have different evaluation approaches (visual estimation, *SSR* and R^2). However, as seen in the results and the discussion, we used the outputs and compared them directly to the standard reference method after Teh and Houlsby (1991). The discussion shows that all literature models need some kind of initial estimation of input parameters in order to work. Therefore, concerning our scientific questions, we conclude that:

i. By combining the model approach of Krage et al. (2014) and Jang et al. (2015) we found a way to develop a model, which is capable of predicting the coefficient of consolidation without any estimated or measured input parameters (M.4 Figure 11).
ii. The newly developed *ad hoc model* provides the best predictions for the known literature curves and shows no soil dependency (M.4 Table 6 and M.4 Table 7).

Note: We suggest the use of the model in cases where typical dissipation curves are expected and where there are time and/or financial restrictions. Other models, for example the model after Burns and Mayne (2002), would give a broader analysis of the soil and could actually deal with atypical dissipation test analysis, because they incorporate shear induced pore pressures.

iii. Following the conclusions of (i) and (ii), the *ad hoc model* is the most adequate model to investigate an unknown soil, where typical dissipation test behaviour is expected. The *ad hoc model* provides very good predictions for the known literature curves (M.4 Table 6), but it also has very low deviations in the calculation of the coefficient of consolidation for the study area (M.4 Table 7).

iv. To evaluate the extrapolation potential is not easy. Following the analysis shown in M.4 Table 8, the conclusion is that the ad hoc model shows the best extrapolation capabilities. However, laying extra emphasis on the results in M.4 Table 8 row c, it is clear that the model after Krage et al. (2014) predicted c_h with the truncated data slightly better than the ad hoc model.

Furthermore, the *ad hoc* model is the only model able to be applied in the field in an instantaneous manner, because it does not require any pre-existing input parameters, and only utilizes the collected dissipation data. Its potential to extrapolate the data after 20% dissipation, comes as a result of the inclusion of the model of Krage et al. (2014) and will help to reduce acquisition time and research coasts.

Note: The development of the ad hoc model, even though done via standard cone penetration tests, adds to the overall goal of this thesis to improve free fall cone penetration tests analysis. The extrapolation potential and the self-estimation of the rigidity index facilitates the dissipation data acquisition, because short term dissipation data sets (as often found in free fall penetration campaigns) can be utilised for further analysis. Hence, the *ad hoc model* can be applied on short term data to predict $c_{h,50\%}$ without knowing the I_r and therefore the *ad hoc model* fits the purpose of the free fall penetration testing.

M.4 6 Acknowledgments

We thank the *DFG* graduate school program for funding this research as part of the "*Intercoast*" project. We also want to thank the Waikato University for its financial and non-financial support as well as the geotechnical operating company *CPTit*. Finally yet importantly, we thank Nicola Lovett for her insightful remarks on an earlier version of this study.

M.4 7. Literature

1. Baligh, M.M., Levadoux, J.-N., 1986. Consolidation after Undrained Piezocone Penetration. Ii: Interpretation. Journal of Geotechnical Engineering, V. 112, No. 7, p. 727-745, doi# doi.org/10.1061/(ASCE)0733-9410(1986)112:7(727).
2. Bishop, R., Hill, R., Mott, N., 1945. The Theory of Indentation and Hardness Tests. Proceedings of the Physical Society, V. 57, No. 3, p. 147, doi# doi.org/10.1088/0959-5309/57/3/301.

3. Burns, S.B., Mayne, P.W., 2002. Analytical Cavity Expansion-Critical State Model for Piezocone Dissipation in Fine-Grained Soils. Soils and Foundations, V. 42, No. 2, p. 131-137, doi# doi.org/10.3208/sandf.42.2_131.

4. Chung, S., Kweon, H., Jang, W., 2013. Hyperbolic Fit Method for Interpretation of Piezocone Dissipation Tests. Journal of geotechnical and geoenvironmental engineering, V. 140, No. 1, p. 251-254, doi# doi.org/10.1061/(ASCE)GT.1943-5606.0000967.

5. Cudmani, R., Osinov, V., 2001. The Cavity Expansion Problem for the Interpretation of Cone Penetration and Pressuremeter Tests. Canadian Geotechnical Journal, V. 38, No. 3, p. 622-638, doi# doi.org/10.1139/t00-124.

6. DeJong, J.T., Randolph, M., 2012. Influence of Partial Consolidation During Cone Penetration on Estimated Soil Behavior Type and Pore Pressure Dissipation Measurements. Journal of geotechnical and geoenvironmental engineering, V. 138, No. 7, p. 777-788, doi# doi.org/10.1061/(ASCE)GT.1943-5606.0000646.

7. Hamilton, E.L., 1964. Consolidation Characteristics and Related Properties of Sediments from Experimental Mohole (Guadalupe Site). Journal of Geophysical Research, V. 69, No. 20, p. 4257-4269, doi# doi.org/10.1029/JZ069i020p04257.

8. Hampton, M.A., Lee, H.J., Locat, J., 1996. Submarine Landslides. Reviews of Geophysics, V. 34, No. 1, p. 33-59, doi# doi.org/10.1029/95rg03287.

9. ISO, 2017. International Organization for Standardization Geotechnical Investigation and Testing - Laboratory Testing of Soil - Part 5: Incremental Loading Oedometer Test (Iso 17892-5:2017); , Geotechnical investigation and testing–Laboratory.

10. Jang, W., Chung, S., Kweon, H., 2015. Estimation of Coefficients of Consolidation and Permeability Via Piezocone Dissipation Tests. KSCE Journal of Civil Engineering, V. 19, No. 3, p. 621-630, doi# doi.org/10.1007/s12205-013-1418-2.

11. Jorat, M., Kreiter, S., Mörz, T., Moon, V., De Lange, W., 2014. Utilizing Cone Penetration Tests for Landslide Evaluation, Submarine Mass Movements and Their Consequences. Springer, Cham, p. 55-71, doi.org/10.1007/978-3-319-00972-8_6.

12. Kluger, M., Kreiter, S., Moon, V., Orense, R., Mills, P., Mörz, T., 2019. Undrained Cyclic Shear Behaviour of Weathered Tephra. Géotechnique, V. 69, No. 6, p. 489-500, doi# doi.org/10.1680/jgeot.17.P.083.

13. Kluger, M., Moon, V., Kreiter, S., Lowe, D., Churchan, G., Hepp, D., Seibel, D., Jorat, M., Moerz, T., 2017. A New Attraction-Detachment Model for Explaining Flow Sliding in Clay-Rich Tephras. Geology, V. 42, No. 2, p. 131-134, doi# doi:10.1130/G38560.1.

14. Kluger, M.O., Jorat, M.E., Moon, V.G., Kreiter , S., de Lange, W., Mörz, T., Robertson, T., Lowe, D.J., 2019. Rainfall Threshold for Initiating Effective Stress Decrease and Failure in Weathered Tephra Slopes. Landslides, V. doi:10.1007/s10346-019-01289-2, No., p. 1-15, doi# doi:10.1007/s10346-019-01289-2.

15. Koizumi, Y., Lee, J., Yokota, Y., Yamamoto, T., Fujisawa, K., 2010. Numerical Analysis of Landslide Behavior Induced by Tunnel Excavation, ISRM International Symposium-EUROCK 2010. International Society for Rock Mechanics and Rock Engineering, Lausanne, Switzerland.

16. Krage, C., DeJong, J., Schnaid, F., 2014. Estimation of the Coefficient of Consolidation from Incomplete Cone Penetration Test Dissipation Tests. Journal of geotechnical and geoenvironmental engineering, V. 141, No. 2, p., doi# doi.org/10.1061/(ASCE)GT.1943-5606.0001218.

17. Lunne, T., Powell, J.J.M., Robertson, P.K., 1997. Cone Penetration Testing in Geotechnical Practice. Taylor & Francis.

18. Moon, V.G., Cunningham, M.J., Wyatt, J.B., Lowe, D.J., Morz, T., Jorat, M., 2013. Landslides in Sensitive Soils, Tauranga, New Zealand. Proc. 19th NZGS Geotechnical Symposium, V. 19, No. -, p., doi# -.

19. Moon, V.G., Lowe, D.J., Cunningham, M.J., Wyatt, J., Churchman, G., de Lange, W., Mörz, T., Kreiter, S., Kluger, M.O., Jorat, M.E., 2015. Sensitive Pyroclastic-Derived Halloysitic Soils

in Northern New Zealand: Interplay of Microstructure, Minerals, and Geomechanics. Volcanic Rocks and Soils., V. 10.1201/b18897-3, No., p. 3-21, doi# 10.1201/b18897-3.

20. Neuzil, C., 1986. Groundwater Flow in Low-Permeability Environments. Water Resources Research, V. 22, No. 8, p. 1163-1195, doi# doi.org/10.1029/WR022i008p01163.

21. Pandit, N.S., Chaney, R.C., Fang, H.-Y., 1985. Review of Cavity Expansion Models in Soil and Its Applications. Current Practice in Geo. Engng, International Book Traders, Delhi, V. -, No., p. 35-53, doi# -.

22. Paniagua, P., Carroll, R., L'Heureux, J.-S., Nordal, S., 2016. Monotonic and Dilatory Excess Pore Water Dissipations in Silt Following Cptu at Variable Penetration Rate. 5th INTERNATIONAL CONFERENCE ON GEOTECHNICAL AND GEOPHYSICAL SITE CHARACTERISATION (ISC5), V. 5, No. 5, p., doi# hdl.handle.net/11250/2491806.

23. Randolph, M.F., Wroth, C., 1979. An Analytical Solution for the Consolidation around a Driven Pile. International Journal for Numerical and Analytical Methods in Geomechanics, V. 3, No. 3, p. 217-229, doi# doi.org/10.1002/nag.1610030302.

24. Robertson, P., Cabal, K., 2010. Guide to Cone Penetration Testing. Gregg Drilling & Testing Inc, Signal Hill, California 90755.

25. Robertson, P.K., 1990. Soil Classification Using the Cone Penetration Test. Canadian Geotechnical Journal, V. 27, No. 1, p. 151-158, doi# doi.org/10.1139/t90-014.

26. Schofield, A., Wroth, P., 1968. Critical State Soil Mechanics. McGraw-Hill London.

27. Seifert, A., Stegmann, S., Mörz, T., Lange, M., Wever, T., Kopf, A., 2008. In Situ Pore-Pressure Evolution During Dynamic Cpt Measurements in Soft Sediments of the Western Baltic Sea. Geo-Marine Letters, V. 28, No. 4, p. 213-227, doi# doi.org/10.1007/s00367-008-0102-x.

28. Smalley, I., Ross, C.W., Whitton, J., 1980. Clays from New Zealand Support the Inactive Particle Theory of Soil Sensitivity. Nature, V. -, No. -, p. 576–577, doi# doi.org/10.1038/288576a0.

29. Stark, N., Hay, A.E., Trowse, G., 2014. Cost-Effective Geotechnical and Sedimentological Early Site Assessment for Ocean Renewable Energies, Oceans-St. John's, 2014. IEEE, pp. 1-8.

30. Teh, C.I., Houlsby, G.T., 1991. An Analytical Study of the Cone Penetration Test in Clay. Géotechnique, V. 41, No. 1, p. 17-34, doi# doi.org/10.1680/geot.1991.41.1.17.

31. Terzaghi, K., 1943. Theoretical Soil Mechanics. JohnWiley & Sons, New York.

32. Torstensson, B.-A., 1977. The Pore Pressure Probe. Nordiske Geotekniske M* te, V., No., p. 1-15, doi#.

33. Tsaparas, I., Rahardjo, H., Toll, D.G., Leong, E.C., 2002. Controlling Parameters for Rainfall-Induced Landslides. Computers and geotechnics, V. 29, No. 1, p. 1-27, doi# doi.org/10.1016/S0266-352X(01)00019-2.

34. Vesic, A.S., 1972. Expansion of Cavities in Infinite Soil Mass. Journal of Soil Mechanics & Foundations Div, V. 98, No. 3, p. 265-290, doi# Accession Number: 00236349.

Chapter 6 Manuscript 5 - Prefix

As mentioned one chapter before, *Manuscript IV* and *V* used to be one and have been split up into two manuscripts. The necessity of that split emerges when looking at the scientific objectives. With the introduction of the new dissipation test model and hydrogeological investigation of the Bramley Drive slide, the two major topics together would be too overwhelming. Hence, similar to the *Manuscript I* and II we consider *Manuscript V* to be an application of the results of *Manuscript IV*. Therefore, *Manuscript V* is meant to ground prove the developed dissipation test model.

Here, we investigated the interaction between the sub-surface, and its ground water with four different dissipation tests at four different depths (~19, ~22, ~23, and ~26 m, acquired by the hired geotechnical company *CPTit*), which are believed to resemble three different halloysite morphologies (the dissipation data at depth 22 m was already discussed in the *Manuscript IV*). One of the scopes is to study the different excess pore pressure responses of the different morphologies to deduct whether the different micro-structures of the halloysite have an impact on the excess pore pressure decay. The result of this study will help to understand the ongoing landslides and slumps on the highly populated Omokoroa peninsula.

Besides using only our own model to investigate the hydrogeological properties of the study area, we also utilised the model after Burns and Mayne (2002) for its multivariable analysis technique. Even if the model of Burns and Mayne (2002) is not the best model to investigate a tephra, halloysite soil, as shown by the manuscript before, it will indicate relative changes for the four different depths investigated.

The results of this study confirm not only the hypotheses made about the different micro-structures, but also give surprising conclusions about the ground water interplay pore pressure conditions.

However, even with the split not all data from the standard cone penetration investigation could yet be analysed. As a result, a third Omokoroa paper is under consideration to install a 3D underground model of the Bramley Drive slide. *Manuscript V* is only a first draft and is yet still in the co-authors review process

P.M.5 References

1. Burns, S.B., Mayne, P.W., 2002. Analytical Cavity Expansion-Critical State Model for Piezocone Dissipation in Fine-Grained Soils. Soils and Foundations, V. 42, No. 2, p. 131-137, doi# doi.org/10.3208/sandf.42.2_131.

Manuscript 5

Evaluating the hydrogeological properties of the Bramley Drive slide, New Zealand

first author, in co-author review process

Authors:

Robert R. Roskoden[§,1]

Achim Kopf[§,2]

Tobias Moerz[§,3]

Vicki Moon°

Max O. Kluger[§,4]

[§]MARUM – Center for Marine Environmental Sciences, University of Bremen, Bremen, Germany ([1]rroskode@marum.de (ORCID: https://orcid.org/0000-0003-2170-283X), [2]akopf@marum.de, [3]tmoerz@uni-bremen.de, [4] mkluger@marum.de (ORCID: https://orcid.org/0000-0001-9130-8948)

°School of Science, University of Waikato, Hamilton, New Zealand (vgmoon@waikato.ac.nz)

M.5 Abstract

We investigate a recent landslide on the Omokoroa peninsula, New Zealand, using *in situ* Cone Penetration Testing ($CPTu$) with pore pressure dissipation. The peninsula lies within an area comprising active tectonic and volcanic zones and common rainfall events, and is prone to slope failure. Five $CPTu$ measurements and four dissipation tests have been conducted. The dissipation tests have been done at penetration depth of ~19, ~22, ~23, and ~26 m. These four depth intervals represent three different dominating halloysite morphologies (tubular, spheroidal and polyhedrons/plates). They were chosen in order to study the influence of the halloysite morphology on the hydrogeological behaviour. With the help of the dissipation test data the anisotropic conditions of the aquifers, the flow regime and the aquifer's state have been determined. Two dissipation test models have been utilise to carry out a multivariable analyses of the geological parameters: rigidity index (I_r), the overconsolidation ratio (OCR), the total overburden stress, and the coefficient of consolidation. The *in situ* estimations of coefficients of consolidation have been verified by *ex situ* oedometer testing. $CPTu$ location 1, 2 and 4 have been utilised to monitor the underground water table by installing perforated plastic tubes into the push holes. Dip meter readings have been done over 48 h. Clearly visible in the data is an increasing trend of the consolidation potential, a change in the flow regime, pore pressure conditions and anisotropy with depth, which are connected to the changes in the microstructure of the halloysite morphologies.

M.5.1 Introduction

M.5.1.1 Study Area

The study region of our $CPTu$ project is the Omokoroa peninsula, a suburb of Tauranga at the coast of the North Island of New Zealand (M.4 Figure 2). The peninsula lies within an area comprising active tectonic and volcanic zones and common rainfall events, and is hence prone to slope failure and associated landslides and slumps (as reported by Moon et al. (2013) and Kluger, Jorat, et al. (2019)). Landslide risk is particularly large because the local deposits consist mainly of tephra, pyroclastic deposits, and their altered products (Moon et al., 2013). In early April 2017, storms and precipitation events triggered several new landslides on the peninsula of Omokoroa. At the Bramley Drive site (M.4 Figure 2), the coastal bluffs at the site are 33 m above high tide. The scarp is approximately 60 m wide with slope angles ranging from 50° to 60°. The steepest slope angle (~ 70°) is at southern part. The scarp flattens out at approximately 25 m below the edge of the cliff. The debris runs from here roughly 100 m to the intertidal flats. The volume of the debris is estimated ~ 3500 m^3 and is assigned to two main events from 1979 and 2014. The local stratigraphy can be summarised, from top to bottom, as: Hamilton Ashes (down to 10 m below the surface), upper Pahoia Tephra (10 to 21 m), lower Pahoia Tephra (21 to 26 m), and the Te Puna Ignimbrite underneath (Moon et al., 2013; Moon, Lowe, et al., 2015). A more detailed description can be found in Moon et al. (2013) whereas Moon, Lowe, et al. (2015) documented the degradation of the landslide scar.

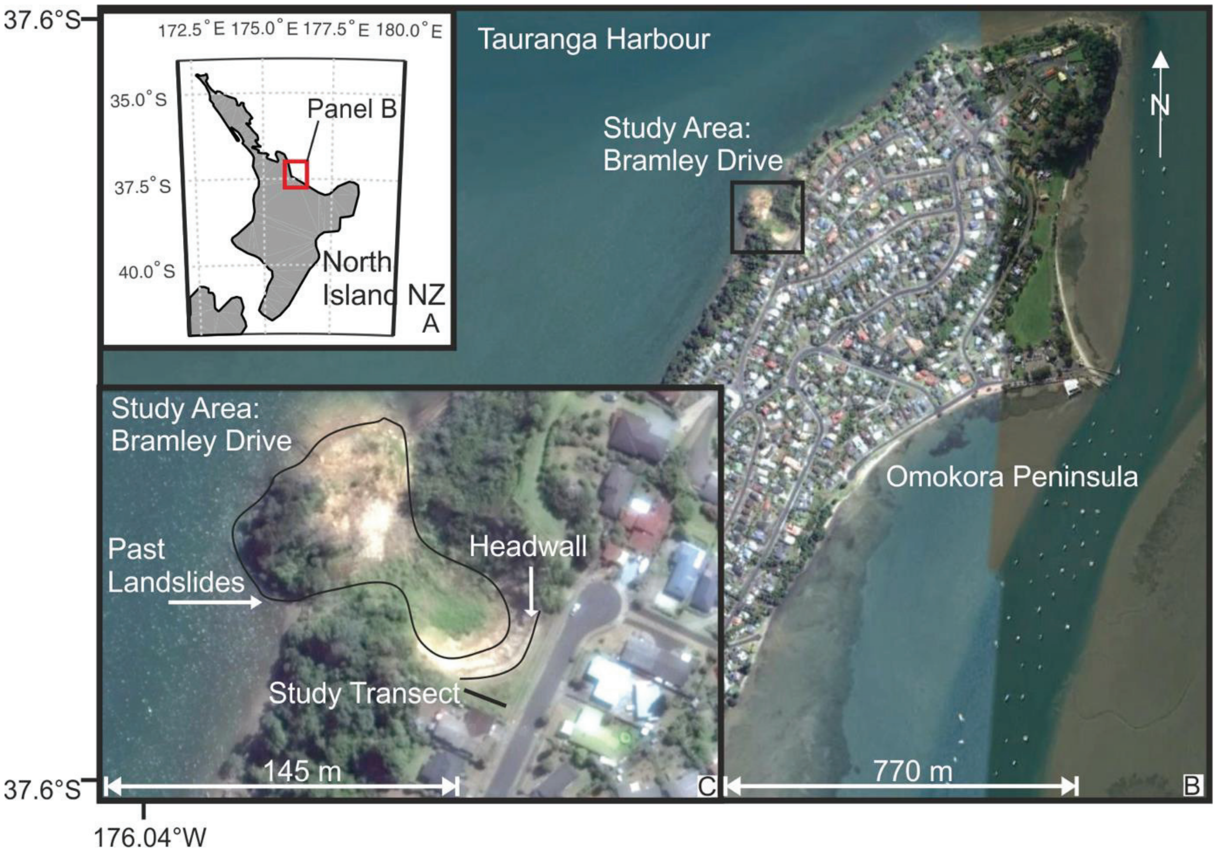

M.5 Figure 1 North Island New Zealand. Study Area: Panel A, overview map showing the North Island of New Zealand. Red rectangle indicates the zoom in area (Tauranga Harbour with the Peninsula Omokoroa) displayed in B; Panel B, Omokoroa Peninsula in the Tauranga Harbour area encircled is the study area Bramley Drive; Panel C, study area Bramley Drive, indicated are the past landslide deposits the headwall of 1979 Bramley Drive landslide and the study transect. Source: 'Omokoroa', 37,630242° S, 176.046106 W Google Earth 2018, 07.01.2019.(Roskoden et al., unpublished).

Moon et al. (2013) and Kluger, Jorat, et al. (2019) have described the landslide history of Omokoroa and related specific rainfall events to the occurrence of landslides. Previous slides and slumps commonly have been interpreted to originate in altered clay-rich layers in the lower Pahoia Tephra sequence (Kluger et al., 2017; Kluger, Jorat, et al., 2019). At the Bramley Drive study site, Smalley et al. (1980) found that the altered tephra is enriched with the clay mineral halloysite. Halloysite is a kaolin subgroup phyllosilicate (Joussein et al., 2005) and forms loosely packed soil microstructures with high, but mostly micro and ineffective, porosity, low permeability, a low plasticity index and a high liquid index. It is assumed that these altered tephra increased the propensity for slope failure although borehole logging could not determine a propagating shear surface of the Bramley Drive landslide. In essence, Moon, Lowe, et al. (2015) postulated a correlation of deformation patterns and the importance of earth tides from inclinometer data, with the sensitive layer increasing the tidal effect.

When searching for a link to the regional hydrogeology, recent investigations identified two discrete aquifers. The first aquifer includes the upper Pahoia Tephra and is open to the atmospheric pressure. The second one goes from the lower Pahoia sequence to the Te Puna Ignimbrite (Moon, Lowe, et al., 2015). The investigations also show an increased excess pore water pressure within a halloysite-enriched layer at around 22 to 23 m depth (so in the lower Pahoia Tephra sequence (Kluger, Jorat, et al., 2019)), hereafter called '*failure-prone layer*'. However, the hydrogeological properties (the coefficient of consolidation, permeability, aquifer pressure conditions and the flow regime) are not yet investigated for the tephra. Due to the many studies in the area we have a unique opportunity to investigate a possible correlation of hydrogeological properties to the mineralogical features of tephra (Christophers, 2015; Jorat, Mörz, et al., 2014a; Kluger et al., 2017; Mills and Moon, 2016; Moon, 2016; Moon et al., 2013; Moon, Lowe, et al., 2015). Grain size, porosity, void interconnectivity, anisotropic conditions and clay morphology, among other parameters affect the permeability and flowing regime and may vary with depositional and weathering history (Bennett et al., 1996; Chilingar, 1964; Kantorowicz, 1990; Neuzil, 1986; Pallatt et al., 1984; Shepherd, 1989). Thus, the permeability and its connected coefficient of consolidation seem to be among the main keys to understand the hydrogeological system of the Bramley Drive landslide.

M.5.1.2 Dissipation and Oedometer tests

As a working hypothesis for Bramley Drive slide, it is assumed that a low permeability layer generated a high excess pore water pressure in the overlying sediments, which overcame the total overburden stress and triggered a slope failure (Tsaparas et al., 2002). The key factors governing slope failure are hydrogeological properties such as permeability and its connected coefficient of consolidation. An *ex situ* testing approach is the oedometer test (ISO, 2017). In an oedometer test, the change in void ratio is continuously measured with time. Unfortunately, the sampling procedure can be distorting for the soil and therefore alter the outcomes for the measured hydrogeological properties. Nevertheless, the oedometer analysis of the pressure decay over time can be applied to an *in situ* method: the cone penetration test (*CPTu*) (Robertson et al., 1992).

The *CPTu* is an inexpensive method, which measures primarily the cone resistance (q_c), sleeve friction (f_s), and pore pressure (u_2). Moreover, a *CPTu* can be used to estimate the *in situ* permeability of the soil (Lunne, Powell, et al., 1997; Robertson, 1990). The localised soil displacement at the *CPTu* tip induces excess pore water pressure in the surrounding sediment. When the *CPTu* is stopped, the induced pressure dissipates back to the equilibrium pore water pressure (Robertson and Cabal, 2010). The method to measure the pressure decay is termed: *dissipation test*. The rate of the pressure dissipation is an analogy to the change in void ratio with effective stress increase as observed in oedometer tests. The difference to the oedometer test is the orientation of the aforementioned soil properties. These are measured *in situ* in the horizontal direction, while the laboratory oedometer test gives information about the vertical direction. Radial complexity arises in both tests especially if anisotropic conditions are present, which can be identified by the oedometer test. Here, two different samples, which need to be from the same location, are installed into the oedometer with two different orientations (vertical versus horizontal in references to the *in situ* conditions). The ratio of the vertical and horizontal tests identifies the anisotropic conditions. Monitoring these conditions allows the user to identify changes in sediment macro and micro fabric.

Besides the anisotropic conditions of the aquifers, the flow regime and the aquifer's state can be determined with a dissipation test. The regime depends highly on the sediment structure and its effective porosity and therefore permeability (and its anisotropy). The flow regime is either hydrostatic (no vertical flow), or shows artesian (upward flow) or downward/horizontal flow (signalled with an equilibrium pore water pressure lower than the assumed hydrostatic pore water pressure).

M.5.1.3 Dissipation test modelling

Penetration tests are an inexpensive mean to collect important geotechnical information. However, if hydrogeological investigations are included in the geotechnical data acquisition, penetration test can be prolonged. Dissipation testing can delay the data acquisition by several hours when low permeability layers such as weathered tephra are tested. Hence, the biggest advantage of any dissipation model ought to be to extrapolate the acquired short-term dissipation data. Due to the extrapolation hydrogeological properties such as the coefficient of consolidation and the permeability can still be properly assessed (Krage et al., 2014). Consequently, dissipation test modelling results in temporal and therefore financial benefits. Additional advantages are the multivariable analyses of geological parameters such as the rigidity index (I_r), the overconsolidation ratio (OCR), and the total overburden stress (Burns and Mayne, 2002). Hence, we will utilise the multi-variable analyses of the model from Burns and Mayne (2002) to widen the outputs of our data collection for the study area. Moreover, the dissipation *ad hoc model* from Roskoden et al. (under review), which was designed to perform hydrogeological investigations in unknown low permeability soils, will be applied to the long-term dissipation tests of this study. The models will help interpret the hydrogeological features and will allow us to answer our research questions for the Bramley Drive landslide.

M.5.1.4 Scientific Objectives

The focus of this research lays upon answering the following questions:

i. Do we see trends in dissipation tests taken at different depths?
ii. Do we see trends in the two dissipation models for the soil variable-analysis?
iii. Can we make conclusions about the an/isotropic conditions and the flow regime?
iv. Do any found trends or changes correlate with the halloysite morphology changes?

By answering these questions for the Bramley Drive landslide, this study will give insights about the hydrogeological behaviour of altered tephra and will contribute a key variable to understand the ongoing landslide hazards in the study area Omokoroa, New Zealand.

M.5.2 Methods

M.5.2.1 Oedometer testing

For the oedometer testing we followed the standards of DIN 18135:2012-04 (DIN, 2012). The consolidation behaviour was determined via Terzaghi‘s law (Terzaghi et al., 1996) and is connected to coefficient of permeability (k_v) via:

$$c_v = 0.197 * \frac{\frac{(h)^2}{4}}{t_{50\%}} = \frac{k_v}{m_v \gamma_w} \qquad 66$$

with m_v, the vertical volume compressibility; γ_w, the specific unit weight of water; h, the height of the sample and $t_{50\%}$, the time at 50% dissipation. The oedometer tests were conducted similar to Kluger, Jorat, et al. (2019). First, specimens were built into the oedometer undisturbed to keep the *in situ* soil structure intact. Afterwards, the same samples were saturated to the liquid limit, remoulded, and then built into the oedometer again to test for the remoulded coefficient of consolidation.

M.5.2.2 Dissipation tests and water table measurements

In this study, there have been five $CPTu$ measurements. Two tests on the outskirts of the research profile to identify the different dissipation depths. The inner three $CPTu$ locations include three long- (> 20 h) and one shorter (ca. 30 min) dissipation test. Each of the dissipation tests has been performed in one out four depths. These four depth intervals represent three different dominating halloysite morphologies (tubular, spheroidal and polyhedrons/plates) (Kluger et al., 2017). The tests have been done at penetration depth of ~19, ~22 (~30 min dissipation test, already analysed in Roskoden et al. (under review)), ~23 and ~26 m to study the influence of the halloysite morphology on the hydrogeological behaviour. Hence, all tests have been acquired in the second aquifer in the lower Pahoia sequence or in the Te Puna Ignimbrite. The long-term dissipation test at ~23 m has been acquired after the dissipation test at ~22 m by prolonging the $CPTu$ push. Hence, the dissipation test at 22 and 23 m are exactly at the same geographical location. $CPTu$ location 1, 2 and 4 have been utilised to monitor the underground water table by installing perforated plastic tubes into the push holes. These have been monitored via a dip-meter over 50 h (expect location 4). Furthermore, the dissipation tests are verified by oedometer tests.

Complete dissipation tests, in which the pore water pressure dissipates by at least 90 % of its excess value (i.e. 90% of the artificial value induced by penetration of the probe have been lost towards ambient pressure values), can be easily interpreted via the commonly accepted method of Teh and Houlsby (1991), as suggest by Robertson and Cabal (2010). Similar to an oedometer test, $t_{50\%}$ is estimated after standards of ISO (2017). The coefficient of consolidation is then calculated after Teh and Houlsby (1991):

$$c_h = \frac{T^*_{50\%} r^2 \sqrt{I_r}}{t_{50\%}} \qquad 67$$

whereas $T^*_{50\%}$ is the theoretical time-factor, r is the cone radius and I_r is the rigidity index.

The rate of the pressure decay depends on the coefficient of consolidation, which itself depends on the compressibility of the surrounding soil and its effective porosity and hence its permeability (EQ.66). In the anisotropic cases, the vertical and horizontal soil properties can be derived from one another (EQ. 18):

$$c_v = \frac{k_v}{m_v \gamma_w} = c_h \left(\frac{k_v}{k_h}\right) \qquad 68$$

where the index v refers to vertical and the index h to horizontal axis.

M.5.2.3 Dissipation modelling

M.5.2.3.1 Burns and Mayne (2002): Dissipation test modelling

The model of Burns and Mayne (2002) combines the cavity expansion and critical state theory (M.5 Figure 2). In the dissipation test model the measured pore water pressure (u_m) is divided into three parts, EQ 69:

$$u_m = u_0 + 4s_u \ln(\frac{r_c \sqrt[3]{I_r}}{r}) + \sigma'_{vo}\left[1 - \frac{OCR}{2}\right]^{\Lambda} \qquad 69$$

where u is the pore pressure. The indexes $m, 0, oct, and\ sh$ refer to measured, hydrostatic, octahedral, and shear induced pore water pressure, respectively. σ'_{v0}, is the effective vertical overburden stress; OCR is the over-consolidation ratio, and Λ is the plastic volumetric strain. Burns and Mayne (2002) identify the dissipation of the pore water pressure over time and distance as a differential equation of the second order, EQ 70:

$$u_m = u_0 + \sum_{n=1}^{50} B_n v(r_{p,0}) e^{-c_h \alpha^2 t} + \sum_{n=1}^{50} A_n v(r_{sh,0}) e^{-c_h \beta^2 t} \qquad 70$$

v is a function of r and is numerically approximated by a Bessel function of the first and second kind of the order zero. The constants B and A represent the octahedral and shear induced pore water pressure and are obtained from the first 50 roots of v. α is a modelling parameter (in the range 1 to 10^3) for the numerical approximation of the power series without any soil relation (for further details Roskoden et al. (under review) and Burns and Mayne (2002)). EQ 69 is utilised to estimate the octahedral and shear induced pore water pressure, and then entered in EQ 70. Here the coefficient of consolidation is systematically changed until the results of EQ 69 are met.

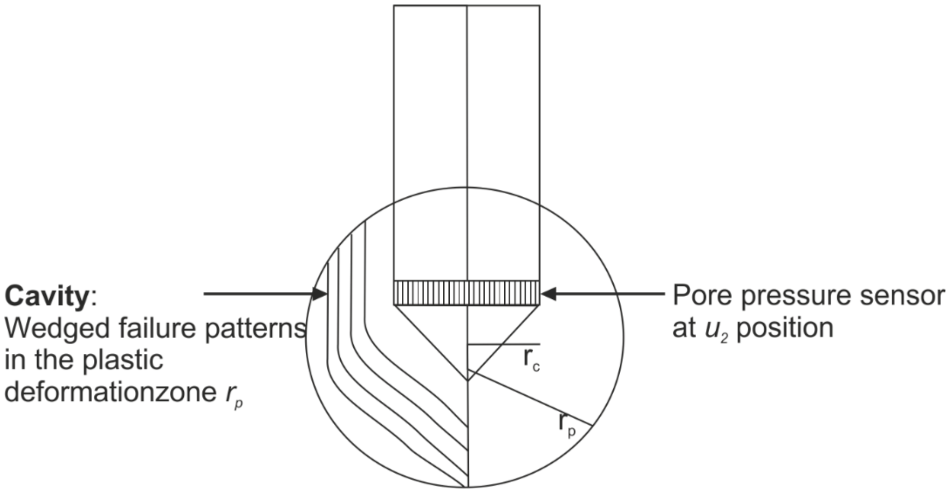

M.5 Figure 2 Schematic overview of a cone while penetrating developing cavities in the deformation zone.

M.5.2.3.2 The ad hoc model: A combination of Krage et al. (2014) and Jang et al. (2015)

The *ad hoc model* was developed by Roskoden et al. (under review) in 2018 for the infield dissipation test at the Bramley Drive. Here, two former literature models after Krage et al. (2014) and Jang et al. (2015), which depend on soil properties as input parameters have been combined to be independent of former property estimation. The model of Krage et al. (2014) is described by equation 71:

$$t = T_{50\%} \sqrt[b]{\left({}^{1}/_{U} - 1\right)} * \frac{r^2\sqrt{I_r}}{c_h} \tag{71}$$

whereas $T_{50\%}$ is the theoretical time-factor (= 0.245) from Teh and Houlsby (1991), b (in the range 0.1 to 1) a modelling parameter; r, the cone radius; I_r, the rigidity index; and U the normalised pore water pressure (0 to 1). Here, any rigidity index is used as an input parameter. Therefore, the coefficient of consolidation and b are fitted to the dissipation data. However, only b is saved and an equally distributed amount of sampling points per log-decade are passed on to the model of Jang et al. (2015) (which by itself is not able to extrapolate short term dissipation data (Roskoden et al., under review)). The model after Jang et al. (2015) redefines the definition of the normalised pore pressure (U), so that U is increasing with time. The redefined pore pressure is termed U_d and defined by *EQ* 72:

$$U_d = \frac{u_i - u}{u_i - u_0} = \frac{u_d}{u_i - u_0} \tag{72}$$

whereas u, is the pore pressure, index i stands for initial, 0 for equilibrium and Δu, the excess pore water pressure. The ratio time over U_d is plotted in a normalised linear time plot via *EQ* 73:

$$\frac{t}{U_d{}^{\kappa}} = \alpha_j + \varepsilon t \tag{73}$$

with κ a modelling parameter ($\kappa > 0$) α the y-intercept, and ε the slope. The coefficient of consolidation can be calculated after Teh and Houlsby (1991) with the normal time factor T (*EQ* 74):

$$c_h = \frac{T}{t} r^2 = \left(\frac{D}{((1/U^{\lambda}) - 1)} \, \frac{((1/U_d{}^{\kappa}) - 1)}{\alpha_J} \right) r^2 \tag{74}$$

For *EQ* 63, many soil-dependent literature solutions exist and have been presented by Jang et al. (2015). Therefore, λ and D only need to be looked up in the literature as presented by Jang et al. (2015). The determined coefficient of consolidation is than saved again and the predicted data, the determined coefficient of consolidation and the modelling parameter b are again passed to the model after Krage et al. (2014). Now the model fits the data with the rigidity index as its only variable as illustrated in M.4 Figure 6.

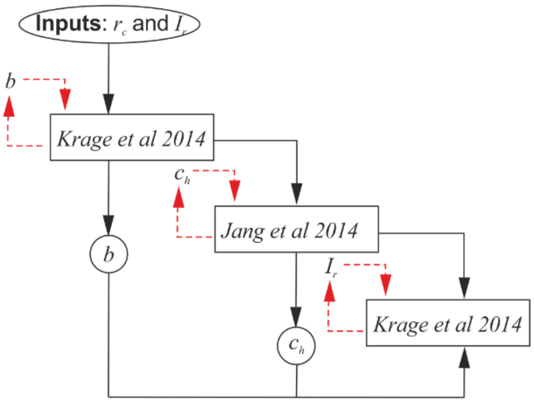

M.5 Figure 3 Schematic overview of how to combine the dissipation model after Krage et al. (2014) and (Jang et al., 2015) in a 3 level feedback loop always modelling for one variable and using the new output as in input for the next loop-level.

M.5.Results

All calculated coefficients of consolidation are presented in M.5 Table 1 for comparison.

M.5.3.1 Oedometer testing

The coefficient of consolidation is calculated using *EQ* 66. M.5 Table 1 shows the coefficient of consolidation from this and other studies for the Bramley Drive landslide for four different core and *CPTu* depths. The Bramley Drive dissipation tests are evaluated after Teh and Houlsby (1991). For *equation* 67 we assumed a rigidity index of 250. The estimation was done via the undrained shear strength ($Ir = G/s_u$, with G the shear modulus and s_u the undrain shear strength) from the work of Kluger, Kreiter, et al. (2019). The rigidity index is trusted not to change greatly over depth, because neither the shear modulus nor the undrained shear strength, change greatly over depth in the study of Kluger, Kreiter, et al. (2019). Furthermore, predicted rigidity indexes (from the *ad hoc model*) have also been utilised to calculate the coefficient of consolidation after Teh and Houlsby (1991) (M.5 Table 1). No real difference could be found between the coefficient of consolidation calculated with the estimated (from the work of Kluger et al. (2017)) or predicted rigidity index (predicted from the *ad hoc model*). Clearly visible in the oedometer tests as well as in the dissipation data (M.5 Table 1) is an increasing trend of the consolidation potential with depth. However, at ~22.7 m the coefficient of consolidation suddenly decreases, which corresponds with a change in halloysite morphology from tubular to spheroidal structures. The remoulded samples show comparable coefficient of consolidation independent on depth or halloysite morphology. Their values are on average (the smallest ~10^{-7} m²/s) smaller than compared to the other oedometer or dissipation tests. The undisturbed but rotated oedometer samples show a clear change from 10^{-7} m²/s to 10^{-5} m²/s between 22 and 23 m. Again, here, the supposed halloysite changes its dominant morphology from tubular structures to spheroids. Furthermore, there is a difference of one magnitude between the non-rotated samples and the rotated samples, suggesting an anisotropy of the soil.

M.5 Table 1 showing all calculated and rounded coefficient of consolidation from either laboratory data, measured dissipation data and modelled dissipation data all in m²/s

Depth		***Oedometer***				***Teh and Houlsby (1991)***		***Burns and Mayne (2002)***	***Ad hoc model***
Core	*CPTu*	c_v	c_h * rotated§	c_h re-moulded§	$c_{h,rotat.}/c_{h,re\text{-}mould.}$ *ratio*	c_h *via* T^* I_r 250 $t_{50\%}$ *300 70 140 40*	c_h *via* T^* I_r 275; 175; 150; 250	*OCR* 2,9 I_r 150, *OCR* 2,9 I_r 200, *OCR* 2,6 I_r 200, *OCR* 3.3 I_r 150	I_r 275; 175; 150; 250
19,0	19,0	1E-06#	1E-07	1E-07	1	4.9E-06	5.1E-06	1.4E-05	6.2E-06
22,2	22,1		1E-07	1E-07	1	2.8E-05	2.4E-05	4.0E-06	2.5E-05
23,0	22,7		1E-05	1E-07	1E-2	1.3E-05	1.0E-05	2.2E-05	1.2E-05
27,6	26,5		1E-05	1E-06	1E-1	6.2E-05	6.2E-05	1.1E-04	4.5E-05
Average deviation from Teh and Houlsby (1991)							10,9%	104,0%	19,9%

*by 90° rotated before built in

#from Kluger, Kreiter, et al. (2019)

§this study

M.5.3.2 Dissipation test and water table measurements

M.5 Figure 4 shows all three long-term dissipation tests. Each test represents a different weathering stage of the halloysite, which in term represents different morphologies of the halloysite. Clearly visible is that the initial excesses pore water pressure increases with depth from ~900 kPa to ~1500 kPa. Counterintuitively, the $t_{50\%}$ decreases from 300 to 40 seconds with depth. However, keeping in mind that at depth 26 m there is the Ignimbrite, one would expect a short $t_{50\%}$ value. The failure prone layer does not show an enhanced $t_{50\%}$ value compared to the test above and is actually two times smaller than for the test above (100 vs. 300 seconds). However, the slope of the tangent for $t_{50\%}$ is smallest at 23 m. Hence, only the pre-primary-consolidation phase at 19 m is longer. The primary decay until $t_{90\%}$ is actually 90 seconds longer at 23 m than it is at 19 m. This trend can also be seen if the coefficients of consolidation are compared to each other (M.5 Table 1).

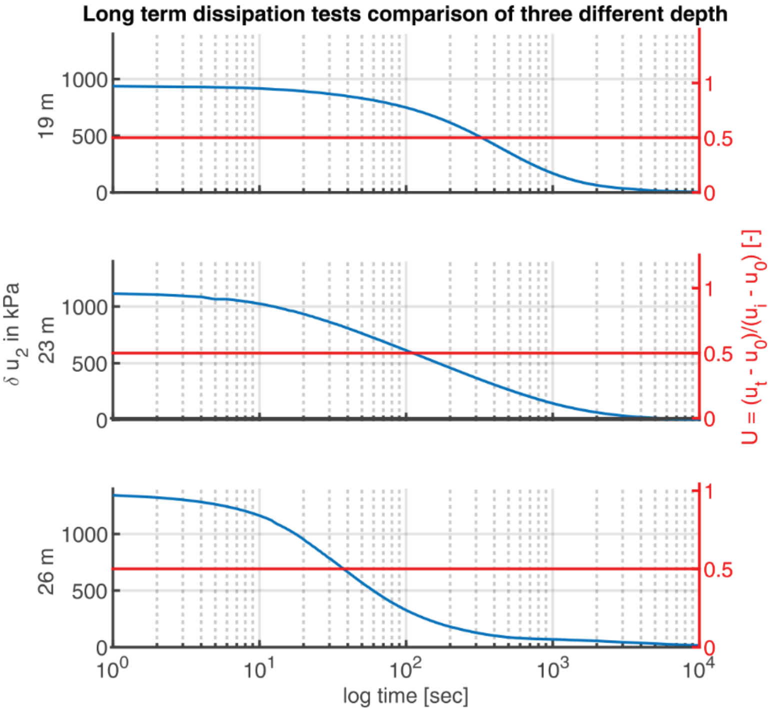

M.5 Figure 4 All three dissipation tests at 19, 22 and 26 m. The reduction of $t_{50\%}$, and the increase of u_i with depth is clearly shown.

M.5 Figure 4 lists all *CPTu* pushes, their corresponding measured water tables and if available all corresponding dissipation meta data such as initial pore water pressure, equilibrium pore water pressure and the supposed hydrostatic pore water pressure (water table depth - equilibrium pore water pressure times 9.81 m/s²). Following the instruction after the guide of Robertson and Cabal (2010) the last column of M.5 Table 2 indicates the predicted flow regime for each layer

M.5 Table 2 Water table information to evaluate the flowing regime after Robertson and Cabal (2010). Calculated values are rounded.

CPTu Pushes	*Water Table Depth in [m]*	*Dissipation Depth in [m]*	*Initial PWP in [kPa]*	*Equilibrium PWP in [kPa]*	*Hydrostatic Pressure in [kPa]*	*Hydrostatic – Equilibrium*	*Flowing Regime*
5	16,6^	19	973	33	24,0	-9,0	No Flow or Slightly Artesian
4	16,6^	22,1	1315	95	54,4	-40,6	Artesian
4	16,6^	22,7	1166	32	60,3	28,3	H/D Flow
3	16,6^	26,5	1392	107	97,6	-9,4	No Flow or Slightly Artesian
2	17,5**	-	-	-	-	-	-
1	15,6**	-	-	-	-	-	-

*H/D = horizontal/ downward , ** measured WT depth after 24h (M.5 Figure 5), ^averaged value from *CPTu* pushes 1 and 2 (because push 1 and 2 are the end member of the *CPTu* transect)

The most striking observation here is the presence of three different flow regimes in a single aquifer. There is a hydrostatic or nearly hydrostatic regime at 19 m just above the failure prone layer, artesian conditions in the failure prone layers, and a horizontal or downward flow just below the failure prone layer flow. The Ignimbrite has the same flow regime as found at 19 m. The water table depth were monitored over time for three $CPTu$ push-locations for over 48 h via a dip-meter (1, 2 [outskirts of the profile] and 4 [middle of the profile]). All water tables started around the same depths (~22 to 24 m). The initial measured water tables (~22 to 24 m) is below the actual dissipation depths -besides at 19 and 26 m (pushes $CPTu$ 3 and 5), which are assumed to have had collapsed push holes after retrieving the penetrometer. The water tables in the non-collapsed wholes levelled out after 24 h at 15.6 and 17.5 m (M.5 Table 2, M.5 Figure 5). Because the push wholes did not fill with the groundwater immediately we classify the weathered tephras here as cohesive soils.

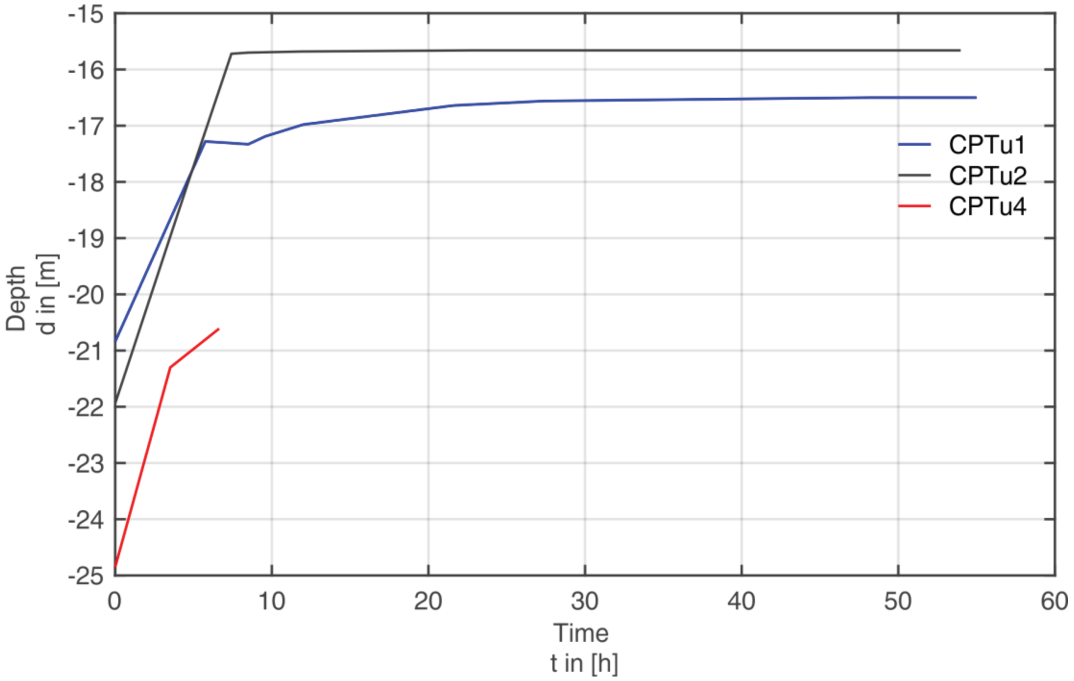

M.5 Figure 5 CPTu water tables monitored over time via a dip-meter. CPTu 1 and 2 are monitored for three days form 15.12.2017 -17.12.2017, while CPTu was only monitored on the 17.12.2017. It seems that the water tables find their equilibrium after 10 h at 15 m CPTu-whole depth.

M.5.3.3. Dissipation modelling

M.5.3.3.1 Burns and Mayne (2002): Variable analysis

The results of the modelling after Burns and Mayne (2002) are shown representatively in M.4 Figure 8 for depth 22.7 m. M.4 Figure 8 shows the best-fitted coefficient of consolidations for combinations of the over consolidation ratios (OCR) to the rigidity index ($50 \leq I_r \leq 500$ in 50 interval steps). The best coefficient in combination with the rigidity index is chosen via an estimation of the standard error of regression (Roskoden et al., under review). For the example data, the curve, which best predicts the pore water pressure has an OCR of 2.6 with and I_r of 200. In general, the predicted curve slightly overestimates the measured data. The initial pore water pressure of the data starts at ~1060 kPa, where as the model predicts a slightly higher initial pore water pressure. The equilibrium pore water pressure is at ~32 kPa. The form and magnitude of the best fit seems reasonable. In the literature, the rigidity ranges from 50 to 500 for different soils (Lunne et al., 2002). The rigidity index describes the stiffness or the resistance of a soil to deformation. For the soil at hand, I_r ranges from 150 to 200 with an average of 175. The modelled $OCRs$ range from 2.6 to 3.3 and seem to increase generally with depth. The smallest OCR is at ~23 m (M.5 Table 1, M.4 Figure 8).

The modelled coefficients of consolidation differ on average ~104% from standard interpretation of Teh and Houlsby (1991) (M.5 Table 1). The general trend follows the calculated trend of Teh and Houlsby (1991). However, clear changes in between the different tested layers are not as visible as calculated via Teh and Houlsby (1991) (M.5 Table 1). Nevertheless, the model, as seen in M.4 Figure 8, was able to extrapolate the data in both time directions. Hence, speculation about the immediate settling or dissipation behaviour are possible via the model of Burns and Mayne (2002).

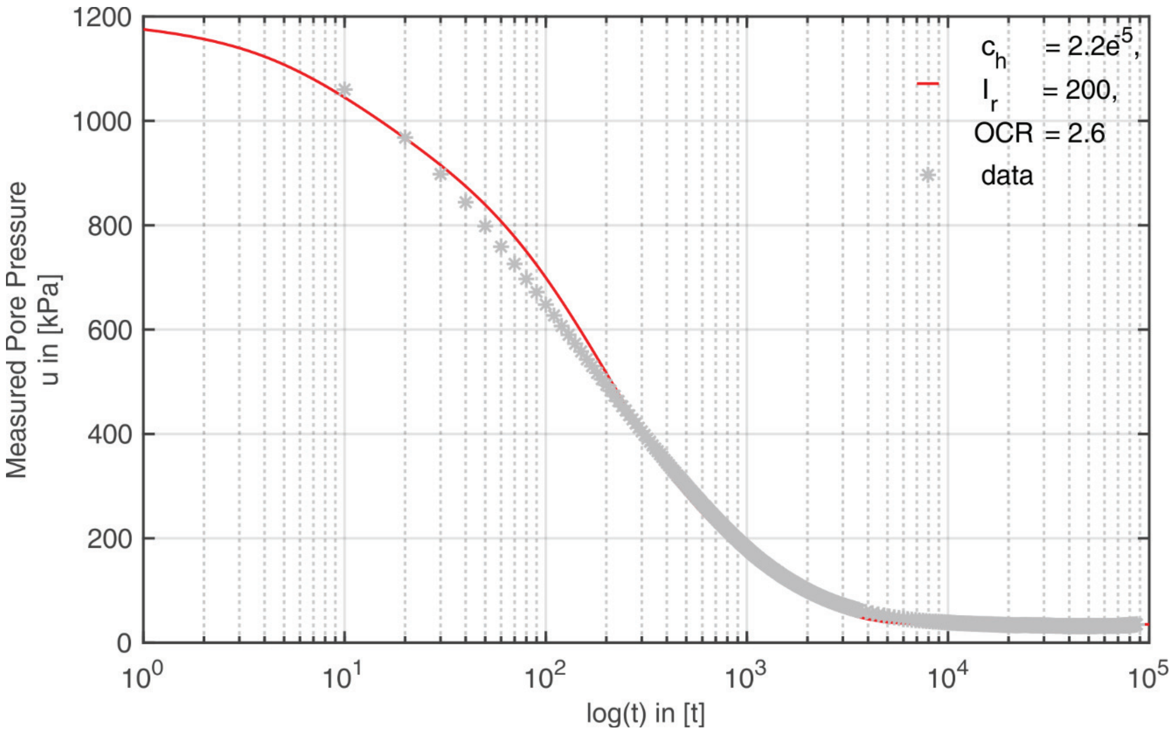

M.5 Figure 6 Dissipation test modelling after Burns and Mayne (2002) for depth 22.7 m, OCR is 2.6, best fit (here with I_r 200) is derived visually. Predicted coefficient of consolidation is 2.2e^{-5}.

M.5.3.3.The ad hoc model: A combination of Krage et al. (2014) and Jang et al. (2015)

The visual evaluation of the predicted curve fits well the measured data as shown by Figure 7, but predicts coefficient of consolidation closer to the standard calculation after Teh and Houlsby (1991). Furthermore, the *ad hoc model* also predicts the rigidity index without any pre-existing information. The predicted rigidity index ranges from 150 to 275 with an average of 212.5. Again, no real trend for the rigidity index can be seen over depth. Nevertheless, an increasing trend in the coefficient of consolidation is clearly visible with depth.

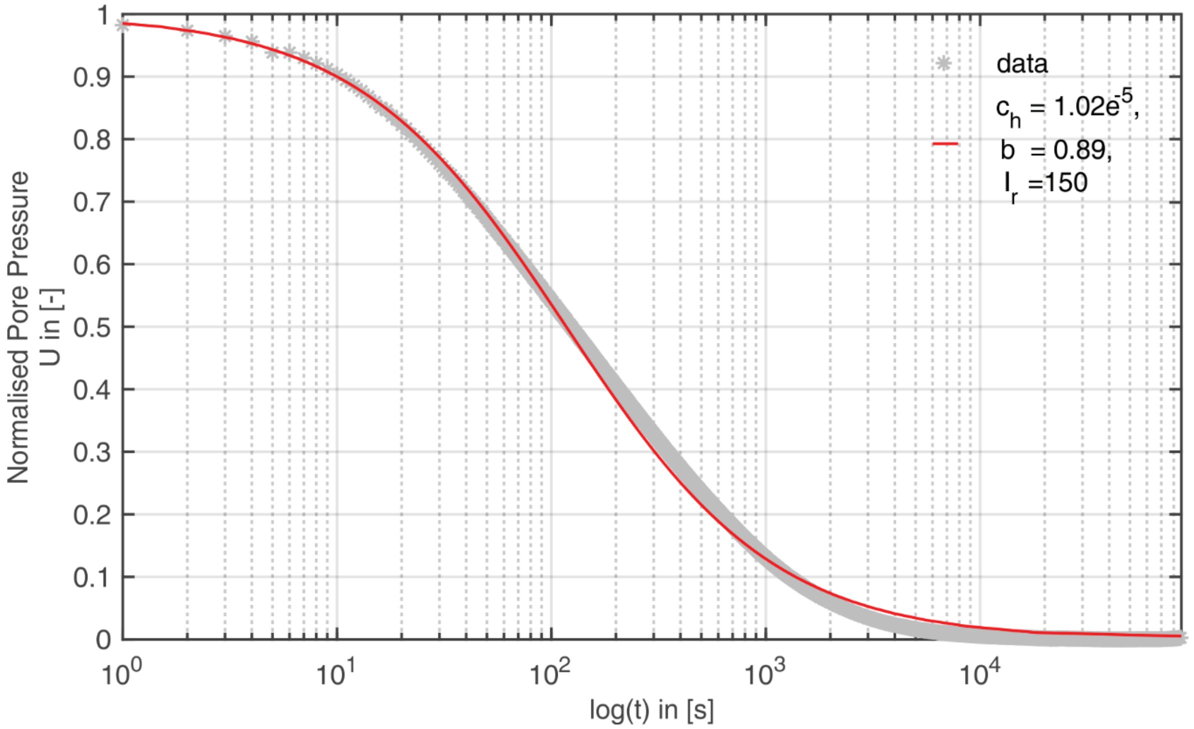

M.5 Figure 7 New modelling approach: A combination of Krage et al. (2014) and Jang et al. (2015) which formed the ad hoc model from Roskoden et al. (under review) for depth 22.7 m.

M.5.4 Discussion

M.5.4.1 Dissipation tests and water tables

The results in M.5 Table 1 and M.5 Figure 4 state clear differences for example in the initial pore water pressure. These differences (1 – [19m/26m - 900 kPa /1500 kPa] ~87%) mainly represent the increase in the total overburden stress. The other 13% differences for the initial pore pressure cannot be explained due to the differences in depth (and therefore the differences in the total overburden stress) but are believed to represent differences in the lithology or halloysite morphologies.

Furthermore, we see that the first aquifer was not fully saturated during the investigation, because the water levels have all been measured in the lower Pahoia Tephra sequence. Nevertheless, the penetration of the two discrete aquifers creates a bypass creating an equilibrium water table level at ~ 16.5 m, which was mostly filled by the second aquifer. This water table depth is in great agreement with the findings of Kluger, Kreiter, et al. (2019). However, M.5 Table 2 raises the question if there really only two independent aquifers. The first two aquifers are as described by Moon et al. (2015): aquifer one from 0-18 m in the upper Pahoi Tephra sequence, aquifer two in the lower Pahoi Tephra sequence, and a hypothetical third aquifer in the Ignimbrite underneath. If there is indeed a third aquifer, then aquifer two and three are separated by the potential detachment layer of the Bramley Drive slide between 22 and 23 m, which would make this layer an aquitard- a separating layer with low permeability. This line argumentation is supported by the dissipation rates, which decrease at the failure probe layer.

M.5.4.2 Dissipation test modelling

M.5.4.2.1 Burns and Mayne (2002)

The coefficients of consolidation for the Bramley Drive (M.5 Table 1), show a ~104% average deviation from the reference method after Teh and Houlsby (1991). Considering, that we handle a non-linear relation a deviation of ~104% can still be considered as reasonable (Jang et al., 2015). The model deviates the most from the reference method at depth 22m (single deviation ~188%, M.5 Table 1) showing a decreased coefficient of consolidation. Unlike the reference method, the model cannot see a trend in the coefficients of consolidation. Even though I_r does not show a trend either, it is noticed that the dissipation tests between 22 to 23 m have the same and the highest I_r –values in this model. After the model of Burns and Mayne (2002) the predicted average rigidity index for the Bramley Drive slide is 175. It is lower than the assumed rigidity index of 250 after Kluger, Kreiter, et al. (2019). However, due to the rigidity index-interval steps of 50, the difference of 75 is here regarded as minor. Therefore, we find no real difference between the assumed and predicted I_r. Nevertheless, the fits/ predicted coefficients of consolidation (M.5 Table 1) can only be predicted if a high over consolidation ratio (2.6 – 3.3) is entered as an input parameter. Literature OCR -values range from 1 to 10 (Lunne, Powell, et al., 1997). Hence, a difference of 12% with increasing depth seems reasonable. Conversely, there is no reason why there should be an increased OCR at all, since, the study area did not experience mechanically compression (Kluger, Kreiter, et al., 2019). Kluger, Kreiter, et al. (2019) also found an increased OCR (2.3) for the Bramley Drive slide, which has a difference to the here found OCR of up to 30%. Kluger, Kreiter, et al. (2019) argue that an increased OCR might occur due to the weathering of the tephra. The differences in the OCR might occur due to different measuring techniques (laboratory vs. *in situ* testing), or due to small horizontal local changes. On the other hand, the fact that at 23 m there is smaller OCR than above may indicate that the predicted OCR-values after Burns and Mayne (2002) should be evaluated with care as reported also by Paniagua et al. (2016). On the other hand, the value at 23 m may support the argumentation of Kluger, Kreiter, et al. (2019) and the increased OCR due to weathering processes, again emphasising a soil property change at the failure prone layer. Furthermore, the enhanced OCR at 23 vs. 22 m mirrors the artesian conditions described before in these depths (M.5 Table 2). Hence, all variables indicate changes at the depth around the failure prone layer at 22 to 23 m.

M.5.4.2.2 The ad hoc model

The *ad hoc model* shows a smaller average deviation from the reference method after Teh and Houlsby (1991) (~20 %, M.5 Table 1). The biggest differences to the Teh and Houlsby (1991) method exist at 19 and 26.5 m (~27.5 %, M.5 Table 1.). The average predicted rigidity index is 212.5. In contrast to the Burns and Mayne (2002)'s model, the lowest rigidity indices are at 22 and 23 m. A lower index suggest a smaller stiffness of the soil along the failure-prone layer. If the *ad hoc-model* predicted rigidity indices are entered in the reference method by Teh and Houlsby (1991), the newly calculated coefficients of consolidation show an average difference of ~11% to the calculated values with the rigidity index of 250. Thus, similar to the argumentation from above in regard of the model after Burns and Mayne (2002) the differences in the rigidity index (212.5 vs. 250) are considered as minor. Furthermore, we argue that the stiffness at the failure-prone layer must be weaker rather than stronger due to the better modelling results from the *ad hoc model* to the reference method. Moreover, a higher rigidity index is to be expected in stiffer sediment; therefore, the rigidity index should be higher for the Ignimbrite and not for the lower Pahoia Tephra sequence.

When comparing the two models, they display a change in the coefficient of consolidation at 19 vs. 22 m (M.5 Table 1). The *ad hoc model* indicates an increase in coefficient, whereas the model after Burns and Mayne (2002) shows a decrease in coefficient of consolidation (M.5 Table 1). An increasing trend can also be seen in the rotated oedometer tests and in the reference processing method after Teh and Houlsby (1991), although the enhancement is first noticeable at 23 m (M.5 Table 1). Taking into account that the laboratory data has a lateral offset to the dissipation sites, one can argue that the noticed changes between 22 and 23 m refer to the same change of layers for both testing methods. Therefore, we argue that the general trend of the *ex situ* and *in situ* tests with a sudden increase at a depth of 22-23 m coincides with the position of the assumed failure-prone layer.

M.5.4.3 The anisotropic conditions and the flowing regime

When comparing the remoulded, rotated and non-rotated oedometer data, there is at least one order of magnitude of difference in the coefficients of consolidation between them. The permeability is directly proportional to the coefficient of consolidation (*EQ.* 68, if the coefficient of volume compressibility ~ const. over depth, here on average $1.7*10^{-4} \mp 4.0*10^{-5}$) so that a relative change deducted from the consolidation data can be directly linked to relative changes in permeability or its coefficient hydraulic conductivity. The ratio of the different oedometer data suggests a 10-fold increase in the vertical coefficient of consolidation at 19 m. The increase also translates to the permeability (k_v = ~10^{-6} to $k_{rotated}$ ~10^{-7}). The same argumentation also holds when the ratios of $c_{remoulded}/c_h$ and $c_{remoulded}/c_v$ are compared. At 23 m the horizontal consolidation increases by 2 orders of magnitude compared to the value at 19 m, suggesting a profound change hydrogeological soil properties, supporting the argumentation of a change in the anisotropic conditions.

This still circumstantial evidence can be supported by the following line of arguments: The horizontal permeability increases from ~19 to ~22m at the failure prone layer (k_h = $8.7*10^{-7}$ increases to $4,9*10^{-6}$ compare c_h in M.5 Table 1, *EQ.* 68) but so does the pore pressure increase as well (nearly hydrostatic to artesian M.5 Table 2). This argument implies that the vertical permeability must be reduced at the failure-prone layer in order to generate artesian conditions. A similar effect can be seen if looked at the *CPTu* data from Moon et al. (2013). Here, a 10 times increased pore pressure (compared to hydrostatic conditions) was describe for the first time at the failure prone layer between 22 to 23 m. Furthermore, Moon, Lowe, et al. (2015) and Moon, de Lange, et al. (2015) describe extreme low permeabilities (10^{-7} to 10^{-9}) for the study area. Such permeabilities are even lower than reported in the literature. Wesley (1977) for example described the permeability of a soil from Indonesia (with halloysite as its main clay mineral) around 10^{-7} to 10^{-6} similar to current study. Moreover, Moon, de Lange, et al. (2015) show an even greater excess pore pressure (at 22 to 23 m) measured with a new *CPTu* technique, called *vibro CPT*. The *vibro CPT* is more sensible to the effects of low permeability. The vertically vibrating cone matches the natural frequency of water. Consequently, the vibration enhances the built up of excesses pore water pressures and amplifies low permeability layers. Due to the reason mentioned above, we imply that the flow direction changes at the failure prone layer, supporting the line of argumentation for the change in the anisotropic relationships within the lithological column at the failure prone layer.

M.5.5 Conclusion

Concerning our initial scientific questions (points i through iv in section 1.4 above), we conclude that:

i. There are clear differences in the dissipation tests at the different depths, which are described in M.5 Figure 4 and M.5 Table 2.
ii. There are trends in the soil variable analysis of the dissipation test models: decreased rigidity indexes at the failure prone layer, an increased *OCR*s and increasing horizontal coefficient of consolidation and therefore an increasing permeability as presented in M.4 Figure 8, 7, and M.5 Table 1.
iii. The anisotropic conditions and the flowing regime change at the same depth where the soil properties change (mentioned in ii) and where halloysite morphology changes as well (M.5 Table 1 and M.5 Table 2).
iv. We can correlate these trends for the soil properties (I_R, *OCR* and c_h) as well as the changes in the anisotropy and flowing regime to the changes in the tephra halloysite morphology from tube-like to spherical microstructures.

Last, the line of arguments implies the following: The change of the consolidation and ergo the permeability (M.5 Table 1, *EQ.* 69), the variations in flow regime as well as pressure conditions (M.5 Table 2), and the deducted change in the anisotropy as well as a reduction of the soil stiffness between 22 and 23 m (M.5 Table 1) justify that the deposits in the presumed detachment zone respond to high rainfall events with high excess pore pressure, which can exceed the overburden pressure, triggering a slope failure.

M.5.6 Acknowledgments

We thank the *DFG* (German Science Foundation) for funding this research via the international Graduate School “*Intercoast*”. We also want to thank the University of Waikato for its financial and non-financial support as well as the geotechnical operating company *CPTit* for help with the dissipation tests. Finally yet importantly, we thank Nicola Lovett for her insightful advice.

M.5.7 Literature

1. Bennett, R.H., Hulbert, M.H., Meyer, M.M., Lavoie, D.M., Briggs, K.B., Lavoie, D.L., Baerwald, R.J., Chiou, W.A., 1996. Fundamental Response of Pore-Water Pressure to Microfabric and Permeability Characteristics: Eckernförde Bay. Geo-Marine Letters, V. 16, No. 3, p. 182-188, doi# 10.1007/bf01204507.
2. Burns, S.B., Mayne, P.W., 2002. Analytical Cavity Expansion-Critical State Model for Piezocone Dissipation in Fine-Grained Soils. Soils and Foundations, V. 42, No. 2, p. 131-137, doi# doi.org/10.3208/sandf.42.2_131.
3. Chilingar, G.V., 1964. Relationship between Porosity, Permeability, and Grain-Size Distribution of Sands and Sandstones, Developments in Sedimentology. Elsevier, p. 71-75, doi.org/10.1016/S0070-4571(08)70469-2.

4. Christophers, A.J., 2015. Paleogeographic Reconstruction of the Omokoroa Domain, Bay of Plenty, New Zealand. University of Waikato, p. 194.

5. DIN, 2012. Din Deutsche Institut Für Normung E. V. Eindimensionaler Kompressionsversuch. Beuth, Berlin.

6. ISO, 2017. International Organization for Standardization Geotechnical Investigation and Testing - Laboratory Testing of Soil - Part 5: Incremental Loading Oedometer Test (Iso 17892-5:2017); , Geotechnical investigation and testing–Laboratory.

7. Jang, W., Chung, S., Kweon, H., 2015. Estimation of Coefficients of Consolidation and Permeability Via Piezocone Dissipation Tests. KSCE Journal of Civil Engineering, V. 19, No. 3, p. 621-630, doi# doi.org/10.1007/s12205-013-1418-2.

8. Jorat, M., Mörz, T., Schunn, W., Kreiter, S., Moon, V., de Lange, W., 2014. Geotechnical Off-Shore Seabed Tool (Gost): Cptu Measurements and Operations in New Zealand CPT'14, V. -, No. -, p. 217-223, doi# -.

9. Joussein, E., Petit, S., Churchman, J., Theng, B., Righi, D., Delvaux, B., 2005. Halloysite Clay Minerals–a Review. Clay minerals, V. 40, No. 4, p., doi# doi.org/10.1180/0009855054040180.

10. Kantorowicz, J., 1990. The Influence of Variations in Illite Morphology on the Permeability of Middle Jurassic Brent Group Sandstones, Cormorant Field, Uk North Sea. Marine and Petroleum Geology, V. 7, No. 1, p. 66-74, doi# doi.org/10.1016/0264-8172(90)90057-N.

11. Kluger, M., Kreiter, S., Moon, V., Orense, R., Mills, P., Mörz, T., 2019. Undrained Cyclic Shear Behaviour of Weathered Tephra. Géotechnique, V. 69, No. 6, p. 489-500, doi# doi.org/10.1680/jgeot.17.P.083.

12. Kluger, M., Moon, V., Kreiter, S., Lowe, D., Churchan, G., Hepp, D., Seibel, D., Jorat, M., Moerz, T., 2017. A New Attraction-Detachment Model for Explaining Flow Sliding in Clay-Rich Tephras. Geology, V. 42, No. 2, p. 131-134, doi# doi:10.1130/G38560.1.

13. Kluger, M.O., Jorat, M.E., Moon, V.G., Kreiter , S., de Lange, W., Mörz, T., Robertson, T., Lowe, D.J., 2019. Rainfall Threshold for Initiating Effective Stress Decrease and Failure in Weathered Tephra Slopes. Landslides, V. doi:10.1007/s10346-019-01289-2, No., p. 1-15, doi# doi:10.1007/s10346-019-01289-2.

14. Krage, C., DeJong, J., Schnaid, F., 2014. Estimation of the Coefficient of Consolidation from Incomplete Cone Penetration Test Dissipation Tests. Journal of geotechnical and geoenvironmental engineering, V. 141, No. 2, p., doi# doi.org/10.1061/(ASCE)GT.1943-5606.0001218.

15. Lunne, T., Powell, J.J., Robertson, P.K., 2002. Cone Penetration Testing in Geotechnical Practice. CRC Press.

16. Lunne, T., Powell, J.J.M., Robertson, P.K., 1997. Cone Penetration Testing in Geotechnical Practice. Taylor & Francis.

17. Mills, P., Moon, V., 2016. Static Failure Mechanisms in Sensitive Volcanic Soils in the Tauranga Region, New Zealand, 11th Australia and New Zealand Young Geotechnical Professionals Conference, Queenstown, New Zealand.

18. Moon, V., 2016. Halloysite Behaving Badly: Geomechanics and Slope Behaviour of Halloysite-Rich Soils. Clay minerals, V. 51, No. 3, p. 517-528, doi# doi.org/10.1180/claymin.2016.051.3.09.

19. Moon, V.G., Cunningham, M.J., Wyatt, J.B., Lowe, D.J., Morz, T., Jorat, M., 2013. Landslides in Sensitive Soils, Tauranga, New Zealand. Proc. 19th NZGS Geotechnical Symposium, V. 19, No. -, p., doi# -.

20. Moon, V.G., de Lange, W.P., Garae, C., Morz, T., Jorat, M., Kreiter, S., 2015. Monitoring the Landslide at Bramley Drive, Tauranga, Nz, 12th Australia New Zealand Conference on Geomechanics: ANZ 2015 Changing the Face of the Earth-Geomechanics and Human Influence, Wellington, New Zealand.

21. Moon, V.G., Lowe, D.J., Cunningham, M.J., Wyatt, J., Churchman, G., de Lange, W., Mörz, T., Kreiter, S., Kluger, M.O., Jorat, M.E., 2015. Sensitive Pyroclastic-Derived Halloysitic Soils in Northern New Zealand: Interplay of Microstructure, Minerals, and Geomechanics. Volcanic Rocks and Soils., V. 10.1201/b18897-3, No., p. 3-21, doi# 10.1201/b18897-3.

22. Neuzil, C., 1986. Groundwater Flow in Low-Permeability Environments. Water Resources Research, V. 22, No. 8, p. 1163-1195, doi# doi.org/10.1029/WR022i008p01163.

23. Pallatt, N., Wilson, J., McHardy, B., 1984. The Relationship between Permeability and the Morphology of Diagenetic Illite in Reservoir Rocks. Journal of Petroleum Technology, V. 36, No. 12, p. 2,225-222,227, doi# doi.org/10.2118/12798-PA.

24. Paniagua, P., Carroll, R., L'Heureux, J.-S., Nordal, S., 2016. Monotonic and Dilatory Excess Pore Water Dissipations in Silt Following Cptu at Variable Penetration Rate. 5th INTERNATIONAL CONFERENCE ON GEOTECHNICAL AND GEOPHYSICAL SITE CHARACTERISATION (ISC5), V. 5, No. 5, p., doi# hdl.handle.net/11250/2491806.

25. Robertson, P., Cabal, K., 2010. Guide to Cone Penetration Testing. Gregg Drilling & Testing Inc, Signal Hill, California 90755.

26. Robertson, P., Sully, J., Woeller, D.J., Lunne, T., Powell, J., Gillespie, D., 1992. Estimating Coefficient of Consolidation from Piezocone Tests. Canadian Geotechnical Journal, V. 29, No. 4, p. 539-550, doi# doi.org/10.1139/t92-061.

27. Robertson, P.K., 1990. Soil Classification Using the Cone Penetration Test. Canadian Geotechnical Journal, V. 27, No. 1, p. 151-158, doi# doi.org/10.1139/t90-014.

28. Roskoden, R., Kopf, A., Moon, V., Moerz, T., Kluger, M., unpublished. Evaluation of a New Dissipation Test Model with Field Data from a Slide Prone Coastal Area.

29. Roskoden, R., Moerz, T., Kluger, M., Moon, V., Kopf, A., under review. Evaluation of a New Dissipation Test and Model with Field Data from the Bramley Drive Landslide Area, Omokoroa, New Zealand.

30. Shepherd, R.G., 1989. Correlations of Permeability and Grain Size. Groundwater, V. 27, No. 5, p. 633-638, doi# doi.org/10.1111/j.1745-6584.1989.tb00476.x.

31. Smalley, I., Ross, C.W., Whitton, J., 1980. Clays from New Zealand Support the Inactive Particle Theory of Soil Sensitivity. Nature, V. -, No. -, p. 576–577, doi# doi.org/10.1038/288576a0.

32. Teh, C.I., Houlsby, G.T., 1991. An Analytical Study of the Cone Penetration Test in Clay. Géotechnique, V. 41, No. 1, p. 17-34, doi# doi.org/10.1680/geot.1991.41.1.17.

33. Terzaghi, K., Peck, R.B., Mesri, G., 1996. Soil Mechanics in Engineering Practice. John Wiley & Sons, United States of America

34. Tsaparas, I., Rahardjo, H., Toll, D.G., Leong, E.C., 2002. Controlling Parameters for Rainfall-Induced Landslides. Computers and geotechnics, V. 29, No. 1, p. 1-27, doi# doi.org/10.1016/S0266-352X(01)00019-2.

35. Wesley, L., 1977. Shear Strength Properties of Halloysite and Allophane Clays in Java, Indonesia. Géotechnique, V. 27, No. 2, p. 125-136, doi# doi.org/10.1680/geot.1977.27.2.125.

Chapter 7

Conclusions and Outlook

This doctoral thesis is multidisciplinary in nature and had the following overall scientific objectives: a) Improvement of common praxis and application of dynamic and kinematic free fall cone penetration tests, b) The assessment of global sediment (re-) mobilisation processes on a local scale in NZ, and the link to the coefficient of consolidation. For this purpose, new theoretical processing and analysis techniques have been developed, which facilitate the correlation of kinematic penetration data (e.g. ultimate bearing capacity, cone resistance etc.) to other soil properties, which are connected to sediment mobilisation processes. The implementation of these techniques has been achieved on the one hand by designing a free fall calibration test, which continues the work of Stark (2011) and Stephan (2015). The resulting geometrical processing algorithm was tested in the field in the Firth of Thames, New Zealand, by quantifying the interaction between mangroves and their soils via the coefficient of consolidation.

On the other hand, the hydrodynamic soil-pore fluid interaction has been theoretically and practically addressed by studying and simulating three literature dissipation test models. The acquired knowledge was translated to design a new dissipation test model, termed *ad hoc model*. The *ad hoc model's* performance was tested and compared with the other literature dissipation test models at the Bramley Drive landslide to assess the hydrogeological mechanism of weathered tephras.

Following the summary sections of the individual thesis chapters above, the conclusions of this doctoral thesis are divided into the two categories:

a) Conclusions for the improvement of the common praxis and application of dynamic and kinematic free fall cone penetration tests

The implementation of the free fall calibration test continues the work of Stark (2011) and Stephan (2015). Here, restrictions in the soil assessment have been reported, because not the cone resistance but the ultimate bearing capacity was calculated and analysed. For non-cohesive or low friction/adhesion sediments, Stephan (2015) and Dayal and Allen (1973) argue that, the ultimate bearing capacity is equal to the sediments cone resistance, which is then utilised for further geotechnical analyses. However, especially for cohesive soils, but also for non-cohesive soils, this assumption is error-prone. To broaden the application of the kinematic penetrometer devices and to combine them with common cone penetration test analysis techniques, the free fall calibration tests were designed to evaluate the total resistance force anew.

Thus, from this doctoral thesis, the following conclusion can be drawn

- A new and successful solution has been found to process acceleration data to calculate the total resistance force and to separate the acting forces on the kinematic penetration lance into cone resistance and side friction for a known geometrical-setup. This solution is termed *the geometrical algorithm* (Manuscript 1).

- *The geometrical algorithm* was derived by a self-designed free fall calibration test and shows a good repeatability potential (Manuscript 1, M.1 Figure 3).
- We also conclude from the free fall calibration tests a dependency of the soil specific rate coefficients (*SSRC*) on the consolidation history. Here, the *SSRCs* correlate inversely proportional to the consolidation pressure (*cp*): *cp* (64kPa) yielded a *SSRC* of ~0.31 and *cp* (32kPa) yielded a *SSRC* of ~0.74 (Manuscript 1).
- For the Firth of Thames, New Zealand, we successfully designed an infield acquisition method: the mobile free fall penetration tower to mimic laboratory settings such as consistent and known penetration heights, and consequently penetration velocities (Manuscript 2).
- Due to the mobile free fall penetration tower, repeatability tests could successfully be deployed (Manuscript 2).
- Additionally, because of the known geometrical set-up of the mobile free fall penetration tower, the application of the geometrical algorithm was facilitated and cone resistance, side friction, the ultimate bearing capacity and the factor of firmness could easily be extracted from the acceleration data (Manuscript 2).
- Due to the implementation of the geometrical algorithm, the application of a global soil classification chart for kinematic free fall penetrometer was possible for the first time and allowed an identification of geotechnical soil behaviour types for the mud flat and the mangrove forest in the Firth of Thames, New Zealand (Manuscript 2).

As a result of the conclusion from above, we highly recommend the usage of portable kinematic penetrometers for remote areas like mangrove forests, because they allow a quick, easy, economically feasible data acquisition with a now integrated soil classification after Robertson (1990) (Manuscript 2).

Besides the geometrical algorithm, the free fall calibration test was originally designed to assess dynamic excesses pore pressure behavior and to find an excesses pore pressure penetration rate correction. However, the current design of the calibration test, does not allow a quantification of the kinematic pore pressure data (Manuscript 1). Therefore, only occasional qualitative conclusions can be drawn:

- The open design of the free fall calibration test, so the non-constant consolidation pressure and the non-existing water column, favored the clogging of the pore pressure filter stone (Manuscript 1).
- The clogging of the pore pressure filter stone mostly prevented the quantification of the pore pressure data (Manuscript 1). The same problematic could also be seen in the field in the Firth of Thames. Here, the pore pressure data could not be utilized at all, because after the first penetration at low tide at the mangrove forest, the missing water column and the cohesive sediment clogged the pore pressure filter of NIMROD (Manuscript 2).
- The absolute excesses pore pressure increases with enhanced penetration velocities if equal experimental conditions for mono-layered cases are met (for instance same consolidation settings, Manuscript 1).

- In mono-layered cases a linear relationship between the penetration velocity and the absolute excesses pressure could be found, which allows a correction of the kinematic pore pressure data (again: if equal experimental conditions for mono-layered cases are met, Manuscript 1).
- The mentioned pore pressure correction is only considered as an initial approach to correct dynamic pore pressure data and cannot yet be regarded as a universal solution (Manuscript 1).

In addition to the correction of the dynamic excesses pore pressure, the hydrodynamic soil-pore-fluid interaction was studied to derive a dissipation test model, which fits the requirements of the free fall penetration test lances: a facilitated, enhanced, and accelerated assessment of the excesses pore pressure dissipation behaviour. Therefore, a dissipation test model was needed to extrapolate short-term dissipation test data without any predefined input parameters (Manuscript 4). The here designed *ad hoc model* allows the following conclusion:

- By combining the current model approaches of Krage et al. (2014) and Jang et al. (2015) a model was developed, which is capable of predicting the coefficient of consolidation without any estimated or measured soil properties (Manuscript 4).
- On the contrast, the newly designed model is able to predict not only the coefficient of consolidations but also the rigidity index (Manuscript 4).
- The *ad hoc models* potential to extrapolate the data after 20 to 30 % dissipation time, comes as a result of the inclusion of the model of Krage et al. (2014) and will help to reduce acquisition time and research coasts. However, the model after Krage et al. (2014) predicts the extrapolated coefficient of consolidation slightly better than the *ad hoc model*. Nevertheless, and most importantly, the *ad hoc model* shows the best extrapolation capabilities compared to current literature models if model consistency, data fitting, and predications of the coefficient of consolidations are considered all together (Manuscript 4).
- Following the conclusion from above, the *ad hoc model* is the only model (in comparison with the introduced literature models) able to be applied in the field in an instantaneous manner, because it does not require any pre-existing input parameters, only utilizes the collected dissipation data, and extrapolates incomplete dissipation data (Manuscript 4).
- Furthermore, the *ad hoc model* was found to be the most adequate model to investigate an unknown soil (Manuscript 4).

b) Conclusions for the assessment of global sediment (re-)mobilisation processes on a local scale in New Zealand, and the link to the coefficient of consolidation

Two very different studies areas have been investigated for their potential of sediment (re-) mobilisation. On the one hand, there is the Firth of Thames, an estuary with an integrated bio-habitat, the mangrove forest. Here, two special cases are combined in one: 1) the increased remobilisation/erosional potential due to the periodical tidal changes in the subtidal zone and 2) the interaction between the mangrove forest and the estuary soil (which was here marked as a special interest, Manuscript 2). Note that the erosional potential is investigated by another Intercoast related PhD project (New Zealand PhD candidate Hiue Nguyen).

On the other hand, there is the Bramley Drive, in Omokoroa, a highly populated peninsula prone to sediment mass movements, such as sediment flows and landslides, induced by rainfall events. Here, the interplay between the change in the clay mineralogy and the hydrogeological properties is marked as a special interest (Manuscripts 4 and 5).

Even though, both study areas are very different in their geological setting, the sediment (re-) mobilisation mechanism, and in their marks of interest, both areas have been investigate for their hydrogeological characteristics, especially for their consolidation potential. In both cases, the coefficient of consolidation was used as a proxy to either estimate the interaction, mangrove trees and sediment consolidation, or clay mineral micro-structure and sediment consolidation. The differences lay in the drawn conclusions for each study area. For the Firth of Thames the coefficient of consolidation was utilised to estimate a cut-off value at which the sediment immobilises instead of (re-) mobilises due to the influence of the mangrove on the consolidation potential (Manuscript 2). Whereas in Omokoroa the coefficient of consolidation was investigated to clarify how the change in the microstructure creates a failure prone zone in the sediment column (Manuscript 4 and 5). Consequently, following conclusions about the sediment (re-) mobilisation and its link to the coefficient of consolidation can be made:

- The availability of mangroves changes or at least mimics a change in geotechnical bulk properties such as cementation and or a higher consolidation rates. A linear trend between the coefficient of consolidation and the mangrove density was found (Manuscript 2).
- The mangrove coverage cut-off value appears to be a normalised tree density of five percent. Five percent coverage change the soil behaviour from soft with high consolidation potential (M1: compression index 1.55, coefficient of consolidation $1.7*10^{-2}$ cm²/s) to firm with reduced consolidation potential (M5: compression index 0.99, coefficient of consolidation $2.3*10^{-3}$ cm²/s). Thus, mangroves have a strong influence on the soils consolidation behaviour, binding the sediments at place by reducing the final vertical deformation (for example due to new external loads such as new sediment inputs) by up to ~45%. Consequently, the higher the mangrove coverage the smaller the chances for the sediment to (re-) mobilise (Manuscript 2).
- Furthermore, the resistance forces can be correlated with the regional coefficients of consolidation. The correlation is a power-function in a double logarithmic plot with a $R^2 = 0.76$ (Manuscript 2).

Overall, the approach allowed us to conclude a direct connection between the stiffness of the soil and the mangrove tree-density. The findings confirm our assumptions that sediments, which have already been consolidated due to mangrove presence, tend to not consolidate much further due to external loading (Manuscript 4).

In case of the Bramley Drive study, there are clear differences in the dissipation tests (thus coefficient of consolidation) at the different depth, which correspond to different clay mineral microstructures. Therefore, we conclude that:

- The trends in the soil variable analysis of the dissipation test models of Burns and Mayne (2002) and the *ad hoc model* (decreased rigidity indexes, increased *OCRs*, and increasing coefficient of consolidation and therefore an increasing permeability) correspond to the changes in the clay microstructure (Manuscript 5).

- The anisotropic conditions and the flow regime change at the same depth where the soil properties (mentioned above), and halloysite morphology change. Consequently, these coincided changes lead to the conclusion that the alteration of the clay mineral microstructure correlates to the found trends in I_r, OCR, and c_h, as well as the change in the anisotropy and flow regime. Thus, we conclude that the change in the tephra halloysite morphology from tube-like to the spherical microstructure is responsible for the high sediment (re-) mobilisation risk at the study area Bramley Drive (Manuscript 5).
- Especially, the deducted change in the anisotropy as well as a reduction of the soil stiffness between 22 and 23 m justify that the deposits in the presumed detachment zone respond to high rainfall events with high excess pore pressure, which can exceed the overburden pressure, triggering slope failures and therefore sediment mass movement events (Manuscript 5).

In summary, the conclusions from above indicate a direct link between the (re-)mobilisation processes and the coefficient of consolidation. In both studies did the coefficients of consolidation change due to external forces such as: mangrove coverage or clay mineral microstructure. However, both studies show the same tendency: A decrease in the coefficient of consolidation (10^{-2} to 10^{-3} [Manuscript 2]) signifies a decrease in the sediment (re-)mobilisation potential, whereas an increase in the coefficient of consolidation (10^{-6} to 10^{-5} [Manuscripts 4 and 5]) signifies destabilisation processes and increased sediment (re-) mobilisation potential.

Finally yet importantly, I would like to end this part of the doctoral thesis by citing the conclusion of the Manuscript 3.

‘We all know that failure is part of science. However, scientist rarely talk about their failures or even publish them. Most failed experiments, field data acquisitions, and tests can be revaluated and data can be recycled by *translating* daily maxims to scientific approaches and by *adapting* to alternative methods from geoscientific foreign sciences. Therefore, in conclusion, the *adaption* of other scientific methods (e.g. data sciences) and the *translation* of daily maxims will help scientist to revaluate and recycle unsuccessful data acquisitions and incomplete data sets.

Outlook

The main thrust of research carried out in this study, 1) the estimation of cone penetration resistance forces from the acceleration data, and 2) the design of the new dissipation test model may find multiple applications in the common praxis in the near future.

1) The geometrical algorithm

The geometrical algorithm cannot only be used for kinematic penetration lances, but also dynamic and standard penetrometer may favour from the new data processing technique. Penetrometer investigations in cohesive sediments may be influenced by the skin-effect (Manuscript 4), which can complicate the friction sleeve measurements. Here, the geometrical algorithm can be used (expressly if the cone resistance is measured directly) to substitute or to support the friction sleeve measurements.

Evidently, the same argument can be made the other way around in case there are data gaps in the cone resistance force. A failure in the data acquisition of the resistance forces may generally appear if strain gauges of the cone or sleeve are damaged for example due to too high resistance forces (especially for free fall campaigns). Nevertheless, most free fall lances incorporate their accelerometers internally, well protected from the actual soil/penetrometer confrontational surfaces (cone and sleeve). Hence, even if there are data gaps in the resistance forces it will be most likely that the acceleration data will be complete and therefore can be utilised for the geometrical algorithm.

Less common, but not impossible are suspensions in the accelerometer data. Here, one can use the geometrical algorithm to back calculate the cone resistance and sleeve friction into accelerometer data, which is practically important for the depth analysis of the free fall penetration lances.

2) The dissipation test ad hoc model

The ad hoc dissipation test model was tested in the field with a standard cone penetrometer. Besides the obvious application in the field to analyse dissipation data, the model can also be used to predict $t_{50\%}$ values by the means of extrapolation and therefore, by extend, to estimate the coefficient of consolidation, hereby saving a lot of time and research money.

Again I would like to relate to the work of Stephan (2015) who used the kinematic approach of Stark (2011) to investigate geotechnical properties along the acquisition of heat probe measurements. Stephan (2015) employed accelerometer sensors for the heat probe lances to broaden the data outcome of heat probe measurements by integrating sediment resistance analysis. According to conclusion of the thesis, it is only logical to address the next evolutional step: a profiling piezometer-heat probe lance capable of measuring temperature, acceleration and pore pressure data. Such an instrument has the potential to estimate cone resistance and side friction via the geometrical algorithm to analyse the interplay between the soil and power water, and to extrapolate and thus evaluate short-term dissipation test data in real-time via the *ad hoc model*. Potentially, it may be possible to adopt the *ad hoc model* to also extrapolate temperature decay curves, since they follow the same dissipation pattern as shown by Pfender and Villinger (2002). O. Figure 1 was chosen from the work of Pfender and Villinger (2002), to emphasis the similarities to a dissipation test where often the normalised pore pressure is plotted over the time instead of the normalised temperature over time.

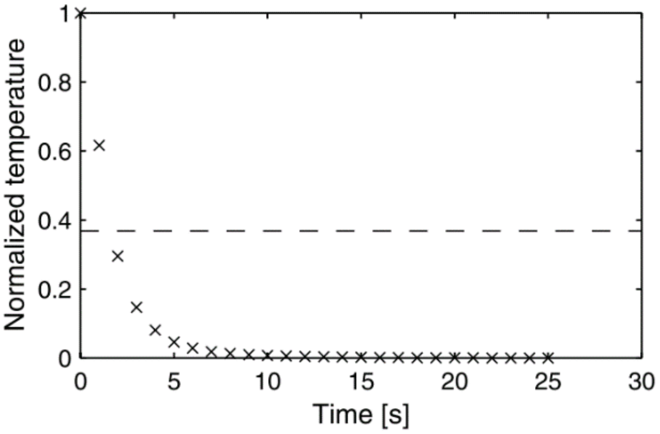

O. Figure 1 Shows the normalized temperature versus the time in [s] from Pfender and Villinger (2002)

Last, as a final outlook, drawn from my own data and programming experience, I encourage the interdisciplinary field of the geotechnics to adopt to the tools of machine learning and big and meta data analysis. In the course of big and meta data analysis as well as machine learning, many laboratory experiments and processing steps (as undrained shear tests, oedometer tests, triaxle tests, free fall cone penetration processing, and expressly the included free fall penetration test depth analysis, to only name a few) have the potential to be automated, reducing user processing errors to a minimum. Admittedly, these changes already initiated partly in the geoscience around one and a half decades ago. However, those changes were mostly integrated in the disciplines of geo- and climate informatics, and geophysics (to name only the most common fields) (Bergen et al., 2019; Karpatne et al., 2018; Lary et al., 2016).

References - Conclusions

1. Bergen, K.J., Johnson, P.A., Maarten, V., Beroza, G.C., 2019. Machine Learning for Data-Driven Discovery in Solid Earth Geoscience. Science, V. 363, No. 6433, p., doi# doi.org/10.1126/science.aau0323
2. Burns, S.B., Mayne, P.W., 2002. Analytical Cavity Expansion-Critical State Model for Piezocone Dissipation in Fine-Grained Soils. Soils and Foundations, V. 42, No. 2, p. 131-137, doi# doi.org/10.3208/sandf.42.2_131.
3. Dayal, U., Allen, J.H., 1973. Instrumented Impact Cone Penetrometer. Canadian Geotechnical Journal, V. 10, No. 3, p. 397-409, doi# doi.org/10.1139/t73-034.
4. Jang, W., Chung, S., Kweon, H., 2015. Estimation of Coefficients of Consolidation and Permeability Via Piezocone Dissipation Tests. KSCE Journal of Civil Engineering, V. 19, No. 3, p. 621-630, doi# doi.org/10.1007/s12205-013-1418-2.
5. Karpatne, A., Ebert-Uphoff, I., Ravela, S., Babaie, H.A., Kumar, V., 2018. Machine Learning for the Geosciences: Challenges and Opportunities. IEEE Transactions on Knowledge and Data Engineering, V. 31, No. 8, p. 1544 - 1554 doi# doi.org/10.1109/TKDE.2018.2861006.
6. Krage, C., DeJong, J., Schnaid, F., 2014. Estimation of the Coefficient of Consolidation from Incomplete Cone Penetration Test Dissipation Tests. Journal of geotechnical and geoenvironmental engineering, V. 141, No. 2, p., doi# doi.org/10.1061/(ASCE)GT.1943-5606.0001218.
7. Lary, D.J., Alavi, A.H., Gandomi, A.H., Walker, A.L., 2016. Machine Learning in Geosciences and Remote Sensing. Geoscience Frontiers, V. 7, No. 1, p. 3-10, doi# doi.org/10.1016/j.gsf.2015.07.003.
8. Pfender, M., Villinger, H., 2002. Miniaturized Data Loggers for Deep Sea Sediment Temperature Gradient Measurements. Marine Geology, V. 186, No. 3-4, p. 557-570, doi# doi.org/10.1016/S0025-3227(02)00213-X.
9. Robertson, P.K., 1990. Soil Classification Using the Cone Penetration Test. Canadian Geotechnical Journal, V. 27, No. 1, p. 151-158, doi# doi.org/10.1139/t90-014.
10. Stark, N., 2011. Geotechnical Investigation of Sediment Remobilization Processes Using Dynamic Penetrometers, Marine Geotechnics. Universität Bremen, Bremen, p. 309.
11. Stephan, S., 2015. A Rugged Marine Impact Penetrometer for Sea Floor Assessment. Universität Bremen, , Bremen,, p. 268.

Acknowledgment

To whom this may concern,

I rather make it short than long, because everyone I am naming should know what he or she have done to be deeply appreciated by me in the doctoral thesis (without any order):

Timo Fleischmann, Christian Zöllner, Dean Sandwell, Walter Menapace, Alexander Rösner, Petra Renken, Andre Hüpers, Sylvia Stegmann, Max Kluger, Dina Al-Sammarrie, Woflgang Schunn, Florian Stähler, Marc Huhndorf, Kathrin Huhn, Fiona Rachholz, Sam Walker, Nicola Lovett, Erik Horstman.

Special thanks are reserved to my supervisors:

Achim Kopf, Vicki Moon, Karin Bryan and Tobias Mörz as well as my second external referee Nina Stark. Nina's former work often inspired and actually enabled me to start my own dissertation, because Nina developed the kinematic penetration lance NIMROD. So thank you for that Nina.

Here, I am emphasising my appreciation for my doctor father Achim Kopf for not giving up on me in my darkest moments. Achim, you gave me the time and space to fall, and to learn how to get back on track, thank you for that.

Besides appreciating all the people who had any influence on this doctoral thesis I would be nothing without my best friends picking me up or kicking me in the ass whenever I needed it. Thank you:

Karsten Sonnenberg, Vivien Nobles (and my wannabe nephew Emmanuel Nobles), Max Haupt, René Benckendorf, Frederike Körting, and Gregory Schröder you are the family I chose and I could not have done a better job (even if it took some years to find you all).

Last but not least, I am thanking my two dads: Wolfgang Roskoden and Lutz Dreilling. Being a dad is not easy especially with a pig-headed son.

And in case who is wondering why I did not list my mom Kirsten Dreiling yet:

Mom finding words to appreciate what you have done is not easy. I would need another dissertation to make sure I can even begin to understand my gratitude for you. You gave me life not once but twice, you helped me survive broken hearts, and even death itself in form of cancer. There is nothing I can say or do, which will ever show how much I acknowledge what you have done. There is only this one small thing, which may give you an idea of how much I love you.

I would like to dedicate this dissertational thesis to:

Kirsten Dreiling

My Mother, My Protector, My Friend!

Appendix

Affirmation

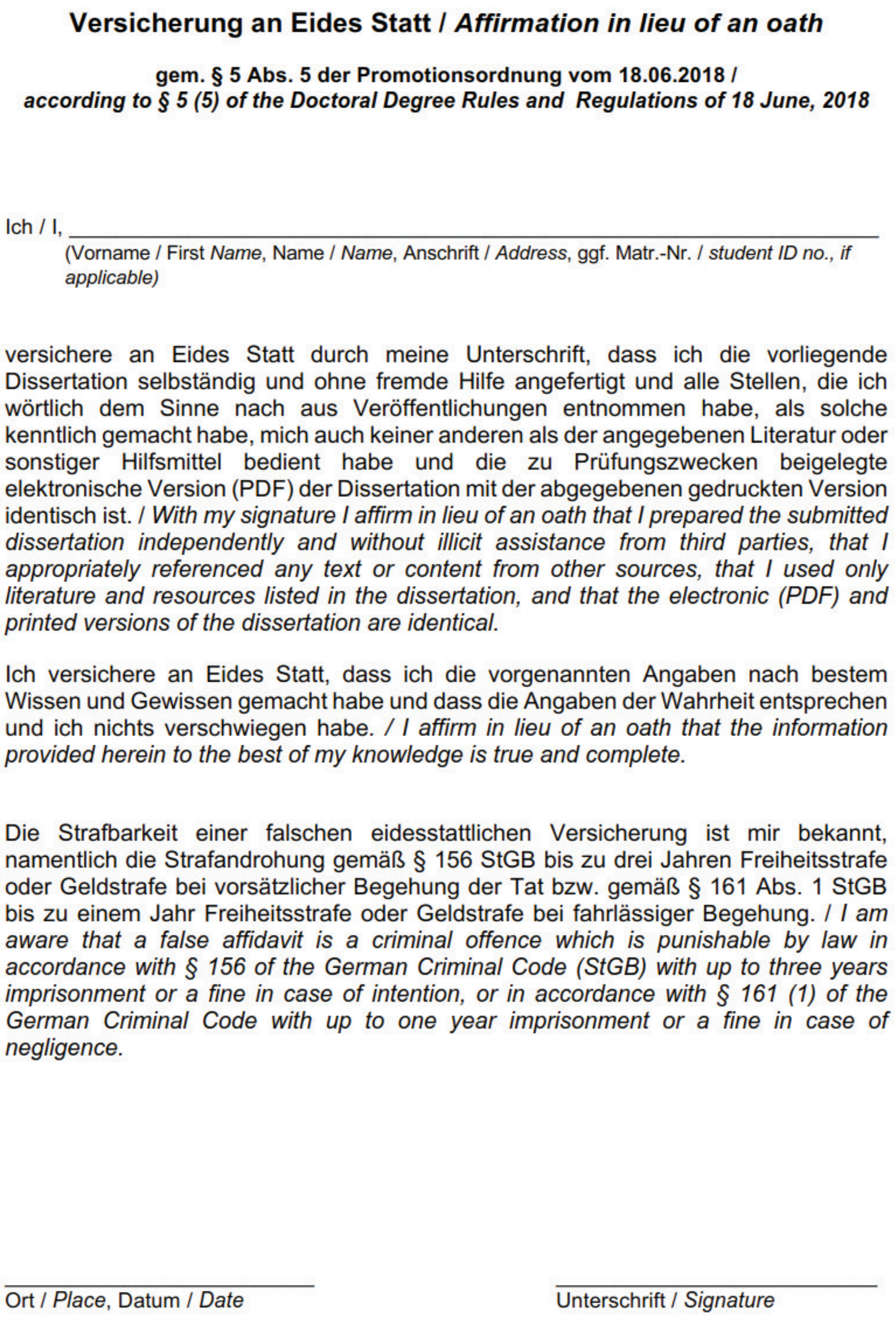

Versicherung an Eides Statt / *Affirmation in lieu of an oath*

gem. § 5 Abs. 5 der Promotionsordnung vom 18.06.2018 /
according to § 5 (5) of the Doctoral Degree Rules and Regulations of 18 June, 2018

Ich / I, ____

(Vorname / First *Name*, Name / *Name*, Anschrift / *Address*, ggf. Matr.-Nr. / *student ID no., if applicable)*

versichere an Eides Statt durch meine Unterschrift, dass ich die vorliegende Dissertation selbständig und ohne fremde Hilfe angefertigt und alle Stellen, die ich wörtlich dem Sinne nach aus Veröffentlichungen entnommen habe, als solche kenntlich gemacht habe, mich auch keiner anderen als der angegebenen Literatur oder sonstiger Hilfsmittel bedient habe und die zu Prüfungszwecken beigelegte elektronische Version (PDF) der Dissertation mit der abgegebenen gedruckten Version identisch ist. / *With my signature I affirm in lieu of an oath that I prepared the submitted dissertation independently and without illicit assistance from third parties, that I appropriately referenced any text or content from other sources, that I used only literature and resources listed in the dissertation, and that the electronic (PDF) and printed versions of the dissertation are identical.*

Ich versichere an Eides Statt, dass ich die vorgenannten Angaben nach bestem Wissen und Gewissen gemacht habe und dass die Angaben der Wahrheit entsprechen und ich nichts verschwiegen habe. */ I affirm in lieu of an oath that the information provided herein to the best of my knowledge is true and complete.*

Die Strafbarkeit einer falschen eidesstattlichen Versicherung ist mir bekannt, namentlich die Strafandrohung gemäß § 156 StGB bis zu drei Jahren Freiheitsstrafe oder Geldstrafe bei vorsätzlicher Begehung der Tat bzw. gemäß § 161 Abs. 1 StGB bis zu einem Jahr Freiheitsstrafe oder Geldstrafe bei fahrlässiger Begehung. / *I am aware that a false affidavit is a criminal offence which is punishable by law in accordance with § 156 of the German Criminal Code (StGB) with up to three years imprisonment or a fine in case of intention, or in accordance with § 161 (1) of the German Criminal Code with up to one year imprisonment or a fine in case of negligence.*

______________________________	______________________________
Ort / *Place*, Datum / *Date*	Unterschrift / *Signature*

Abbreviations sorted by subject (most important ones)

Intercoast	*Integrated Coastal Zone And Shelf-Sea Research*
IC	*Intercoast*
DFG	*Deutsche Forschungsgeschellschaft*
Dgebo	*Deutsche Forschungsgesellschaft Für Bodenmechanik*
MARUM	*Centre Of Marine Environmental Sciences*
CPTu	*Cone Penetration Tests With Pore Pressure Mesurements*
CPT	*Cone Penetration Tests*
SPT	*Standard Penetration Tests*
SCPT	*Seismic Cone Penetration Test*
FFCPTu	*Free Fall Piezocone Tests*
Q_c	*Resistance Force At The Cone*
F_s	*Resistance Force At The Sleeve*
F_T	*Total Resistance Force*
A_s	*The Area Of The Sleeve*
A_c	*The Area Of The Cone*
F_b	*Buoyancy Force*
F_d	*Drag Force*
q_c	*Cone Resistance*
q_t	*Pore Pressure Corrected Cone Resistance*
$q_{c\text{-}qst}$	*Quasi Static Cone Resistance*
$q_{c\text{-}dy}$	*Dynamic Cone Resistance*
Q_t	*Normalized Cone Resistance*
q_{net} /q_n	*Net Cone Resistance*
q_u	*Ultimate Bearing Capacity*
q_{ud}	*Ultimate Dynamic Bearing Capacity*
q_{scb}	*The Quasi Static Bearing Capacity*
FF	*The Factor Of Firmness*
σ_{v0}	*The Vertical Overburden Stress*
σ'_{v0}	*The Effective Vertical Overburden Stress*
s_u	*Undrain Shear Strength*
c_p	*Consolidation Pressure*
f_s	*Sleeve Friction*
R_f	*Friction Ratio*
pwp	*Pore Water Pressure*
u	*Pore Pressure*
u_i	*The Initial Pore Pressure*
u_0	*The Equilibrium Pore Pressure*
u_{hy}	*The Hydrostatic Pore Pressure*
Δu	*Excess Pore Water Pressure*

U	The Normalised Excess Pore Water Pressure
B_q	Normalised (vb Q_n) Pore Water Pressure
U_d	Alternative Definition Of The Excess Pore Water Pressure After Jang Et Al. 2015
u_d	The Alternative Excess Pore Water Pressure After Jang Et Al. 2015

PRC	Penetration Rate Correction
PRF/SRF	Penetration /Strain Rate Factor
SRE	Strain Rate Effects
SSRC	Soil Specific Rate Coefficient

t	Time
t_p	The Total Penetration Time
T^*	The Modified Theoretical Time-Factor At 50% Dissipation
T	The Theoretical Time-Factor At 50% Dissipation

V_{st} / v_{st}	Standard Penetration Velocity
V or v	Penetration Velocity

dec	Deceleration
a_{max}	The Maximum Acceleration Of The Instrument
g	The Gravitational Constant (9.81 M/S^2)

d	The Penetration Depth
d_n	Normalised Embedded Depth
z	Embedded Depth
D	Diameter Of The Cone
r / R_c	The Cone Radius
R_p / r_p	The Plastic Deformation Radius

e	The Void Ratio
Λ	Plastic Volumetric Strain
γ	Specific Unit Weight
m_v	The Coefficient Of Volume Compressibility
κ	The Coefficient Of Permeability
c_h	The Coefficient Of Consolidation

LL	Liquid Limit
PL	Plastic Limit
SL	Shrinking Limit
I_p	Plasticity Index
I_S	Shrinking Index
C_C	Compression Index
C_R	Recompression Index
C_S	Swelling Index

m	Mass
ρ	Density

V	*Volume*
C_D	*Drag Coefficient*
J_0 and Y_0	*The Bessel Function Of The First And Second Kind Of The Order Zero*
α	*A Modelling Parameter (In The Range 1 To* 10^3*)*
κ	*Modelling Parameter (*$K>0$*) For The Model After Jang Et Al. 2015*
α_j	*The Y-Intercept For The Model After Jang Et Al. 2015*
ε	*The Slope For The Model After Jang Et Al. 2015*
λ	*The Modelling Parameter*
D	*The Y-Intercept For The Model After Jang Et Al. 2015*
N	*The Slope For The Model After Jang Et Al. 2015*
SSR	*Least Square Error*
SER	*Standard Error Of Regression*

Appendix M.1

For Appendix M.1 I would like to illustrate how the free fall calibration test was configured. Therefore, the following figures show: The design of the experimental container (size, height, and wall thickness), the calculations of the plastic deformation zone, the characterisation of the Hermmilger soil and its alteration to fit the experimental needs. Also shown are the consolidation phase via the hydraulic pump of the working group from Prof. Dr. Tobias Mörz (*Marine Engineering Geology*) and the penetration via the laboratory free fall tower utilised from the work of Stephan (2015).

Free Fall calibration test configuration

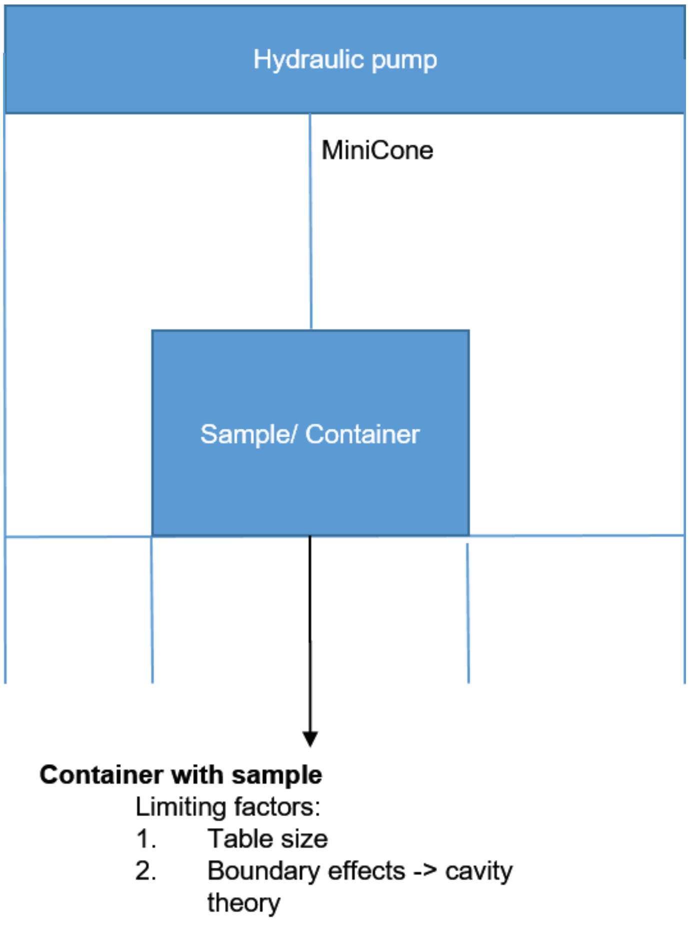

A.M.1 Figure 1 Side view of the calibration chamber table form the working group Prof. Dr. Tobias Mörz Marine Engineering Geology, and its hydraulic pump. Pointed out are the limiting factors for the experimental specimen container such as table size and the boundary effect of the plastic deformation zone from the cavity expansion theory.

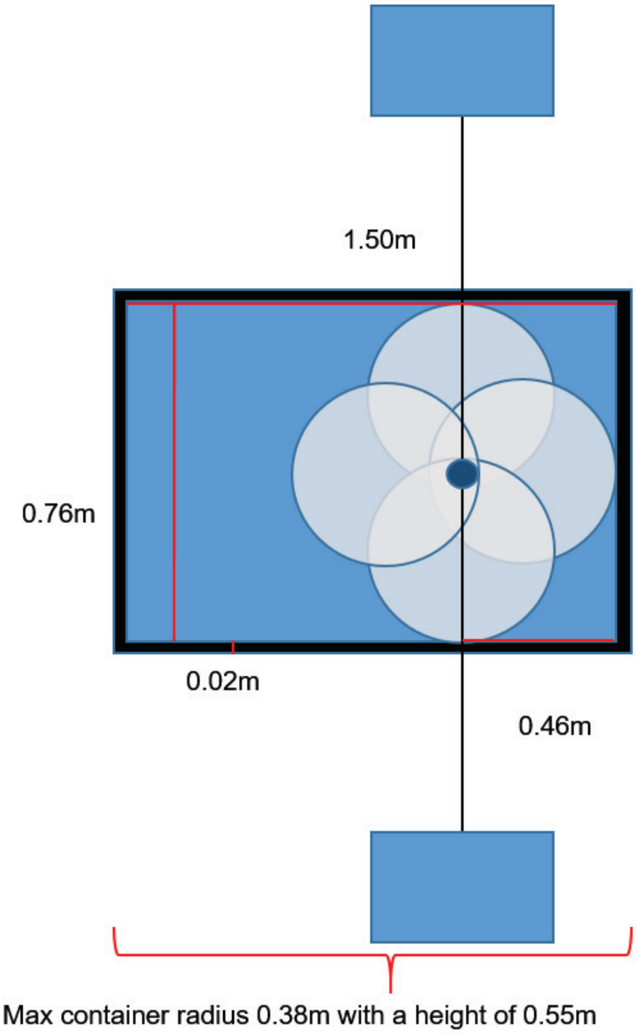

A.M.1 Figure 2 Top view of the calibration chamber table to configure the container size. The objective wa incorporate as many tests pushes/ drops in one container as possible to ensure repeatability

M.1 Table 3 Calculation for container wall thickness to hold up consolidation pressure.

Material : Pomm

Parameters:	Symbols	SI Unit	Values:
Resistance value	K	N/mm² = MPa	13
Safety value	S	-	1,5
weld efficiency factor	v	-	0,75
Tolerance corrosion	c1	mm	0,6
Tolerance erosion	c2	mm	1
Applied pressure	p	bar	0,63
outer diameter	d	mm	500
wall thickness	s	mm	4,011

d*p	315
K/S	8,66666667
K/S*V	6,5
20*K/S*V	130
(20*K/S*V)+p	130,63
(d*p)/(20*K/S*V)+p	2,41139095
(d*p)/(20*K/S*V)+p +c1 +c2	4,01139095

$$s = \frac{d \cdot p}{20 \cdot \frac{K}{S} \cdot v + p} + c_1 + c_2$$

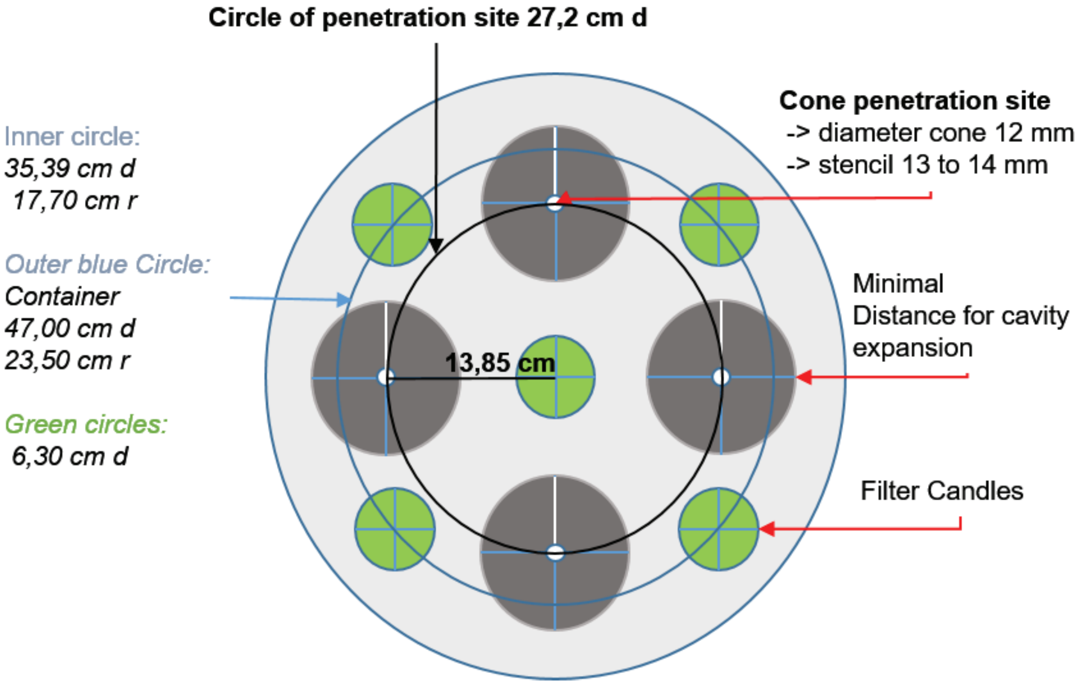

A.M.1 Figure 3 Geometrical considerations to estimate the maximum amount of test sides in the experimental container. Included are considerations for the plastic deformation zone analysis via cavity expansion theory to estimate needed distance between push sides and vertical drainages position/filter candles (green).

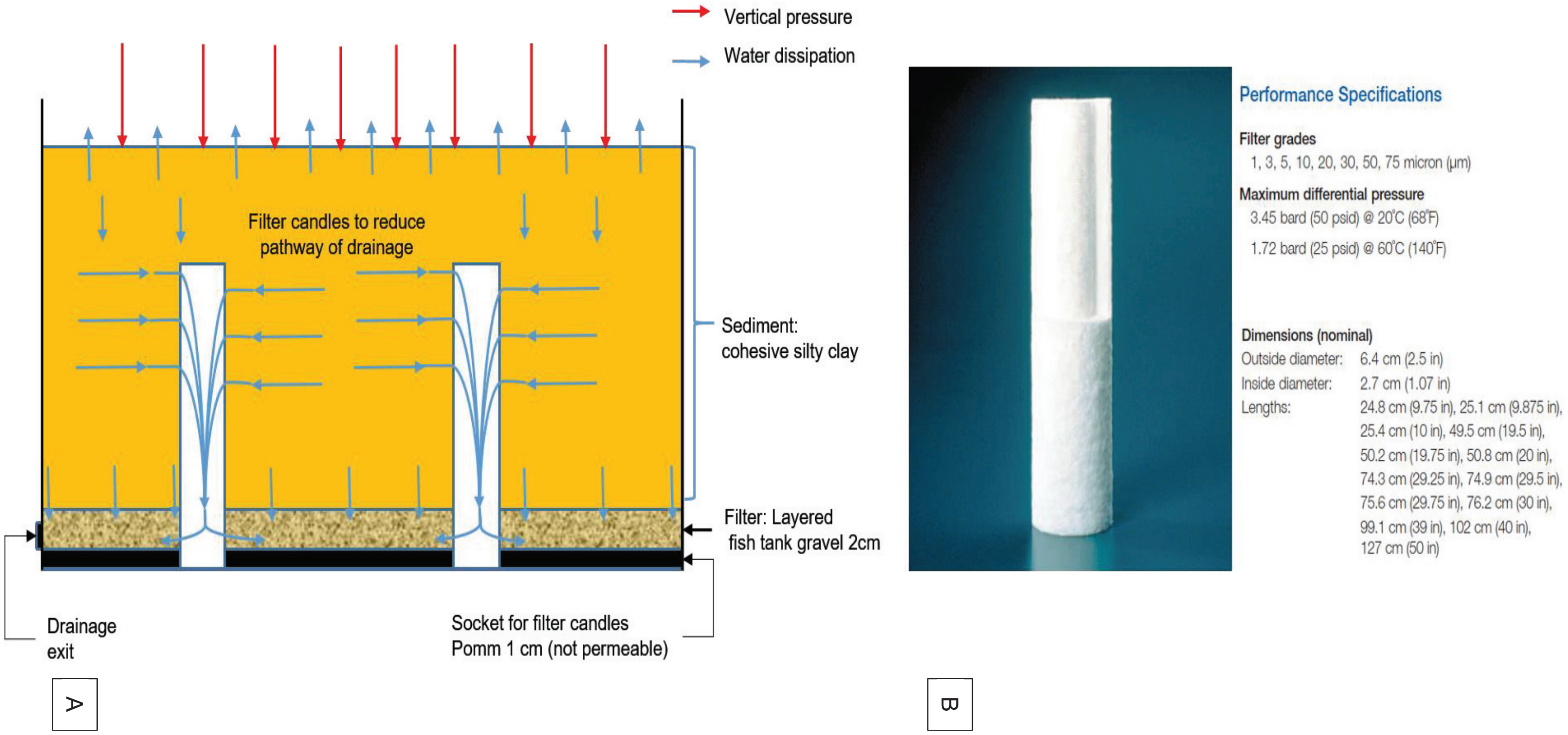

Performance Specifications

Filter grades
1, 3, 5, 10, 20, 30, 50, 75 micron (µm)

Maximum differential pressure
3.45 bard (50 psid) @ 20°C (68°F)
1.72 bard (25 psid) @ 60°C (140°F)

Dimensions (nominal)

Outside diameter:	6.4 cm (2.5 in)
Inside diameter:	2.7 cm (1.07 in)
Lengths:	24.8 cm (9.75 in), 25.1 cm (9.875 in), 25.4 cm (10 in), 49.5 cm (19.5 in), 50.2 cm (19.75 in), 50.8 cm (20 in), 74.3 cm (29.25 in), 74.9 cm (29.5 in), 75.6 cm (29.75 in), 76.2 cm (30 in), 99.1 cm (39 in), 102 cm (40 in), 127 cm (50 in)

A.M.1 Figure 4 Considerations for the vertical drainages to decrease consolidation time. The vertical drainages reduced the theoretical container size and therefore the consolidation time. Panel A: Schematic display of the theoretical function of the vertical drainages. Panel B: The performance specification from the bought vertical drainages from http://www.par-group.co.uk/site-content/1/Docs/updates/3-engineering-plastics/3.73-vyon-f-6mm-tds.pdf, 08.11.2016, 13:45.

Example calculation
for pre-consolidation:

Searching for needed pressure p!

P = g*p*h

g = 9,81 m/s²

p = 2197 kg/m³

h = 1.5 - 3 m

P ~ 31500 - 63000 kg/ms²
= 31500 - 63000 N/m²
= 31 - 63 kPa

-> 3150 - 6300 kg/m²
-> 522,9 - 1045,8 kg/ 0.166 m²

Sample configuration:
D = 0.47m
H = 0.47m
Penetration H = 0.35m
V = 81 l
Density = 1700 kg/m³
M = 138 kg

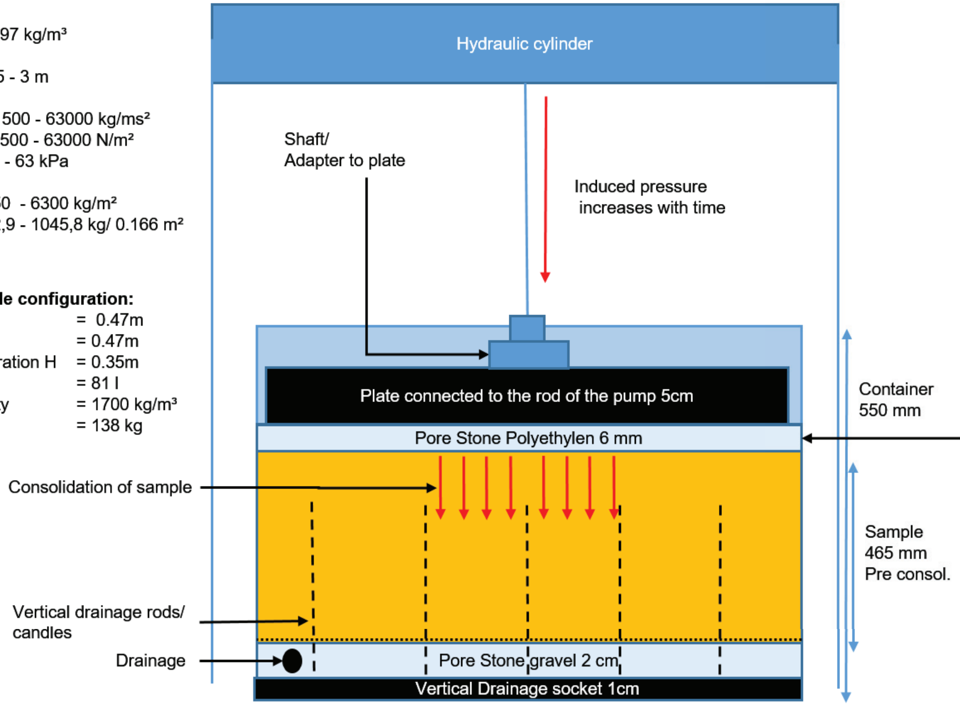

Pore pressure filter plate configuration acquired at par-group
k_f = 0.5 – 1.5
Pore size = 30 – 60
Porosity = 35%
D = 465
H = 6

http://www.par-group.co.uk/site-content/1/Docs/updates/3-engineering-plastics/3.73-vyon-f-6mm-tds.pdf

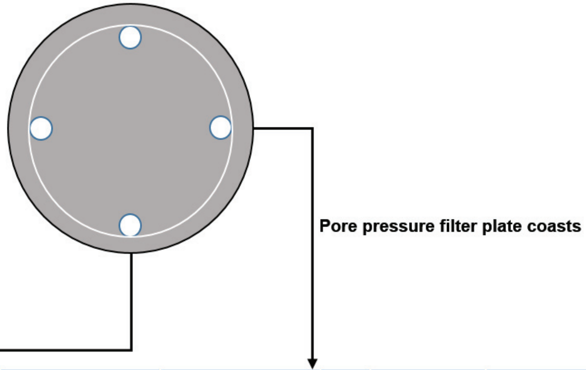

Code	Description	Qty	UOM	Each
NS1	470Øx6mm Vyon F	2	Each	£199.00
EXPORT-ADMIN-FEE	Banking and Admin Fees (per transaction)	1	Each	£35.00
SHIP-EURO	Carrier to Germany (4/5 days transit)	1	Each	£38.50
Total				£471.50
VAT(20%)				£0.00
Total to Pay				£471.50

A.M.1 Figure 5 Puts all the consideration from above together in one schematic overview for the experimental container. Here, included is also the vertical layering of the experimental container. From bottom to top: Vertical drainage socket, to hold the vertical drainages at place. The horizontal gravel pore filter layer. The metal grid to separate the cohesive soil from the gravel. The soil specimen with the vertical drainages, including red arrows, which symbolise the sediment consolidation pressure. The polyethylene pore filter plate. The pressure plate, which connects to the pressure adapter from the hydraulic pump. Also included are example calculation for the consolidation pressure and sample configurations and the coasts for the pore filter plate.

Soil specimen descriptions and characterisation

Sample Hemmerlinger Marsch
GPS: 34.83.780 RW
5877.395 HW

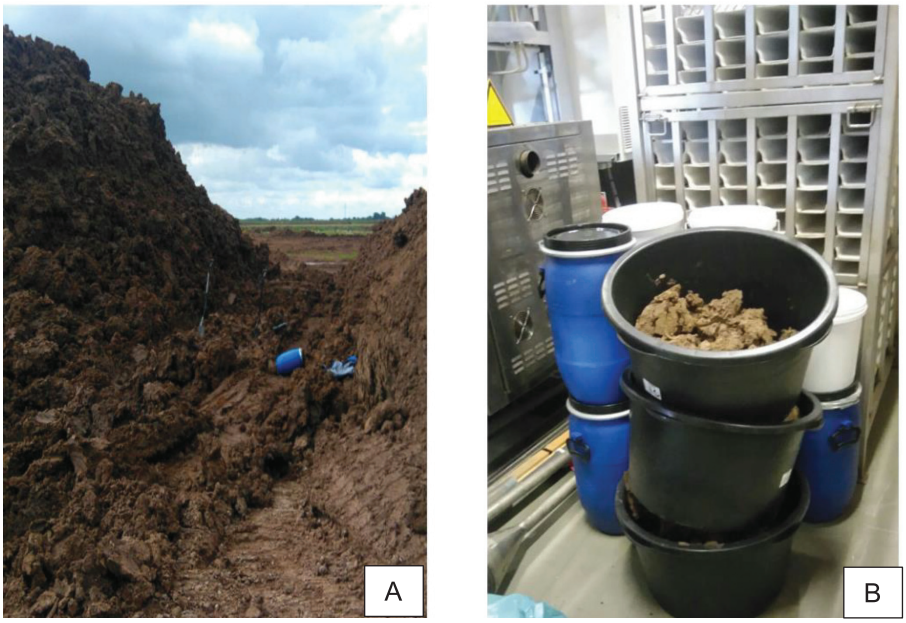

Description Site:

Northern side deposition/fill of loam

Description Sediment

Cohesive soil
Some sand
Very few smaller pebbles
Congregation loam/clay
Clayey material
Moist
Remoulded
Very hard if try
Crunchy -> silt
Colour burnish reddish
No vegetation

A.M.1 Figure 6 Panel A (left): The side of the Hemmerlinger Marsch sediment (GPS data is given in the figure). Panel B (right): The total amount of sediment sampled from the side with sediment description.

A.M.1 Table 1 The experimental table for estimating the atterberg limits of the Hermmerlinger Marsch soil.

	Data (measured)		Calculation		Final Output			
	liquid limit					plastic limit		
N°	1.	2.	3.	4.	5.	1.	2.	3.
N	16	43	30	34				
m_c [g]	1.1485	1.1435	1.1523	1.1523		1.1495	1.1854	1.1519
m_1 [g]	15.4590	15.8810	15.1785	15.8652		5.3372	4.6927	4.0810
m_2 [g]	10.1057	10.6633	10.2923	10.6209		4.6975	4.1904	3.7037
m_d [g]	8.96	9.52	9.14	9.47	0.00	3.55	3.01	2.55
m_w [g]	5.35	5.22	4.89	5.24	0.00	0.64	0.50	0.38
w [%]	59.77	54.81	53.46	55.39	#DIV/0!	18.03	16.72	14.79

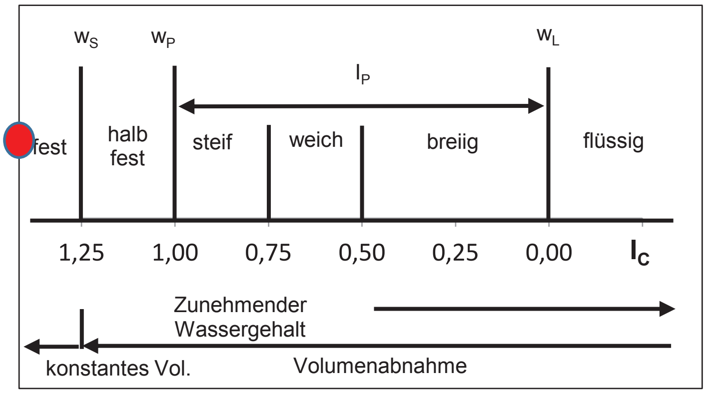

A.M.1 Figure 7 Display of the plastic index for the Hemmerlinger Marsch. The Marsch is identified as a very firm soil.

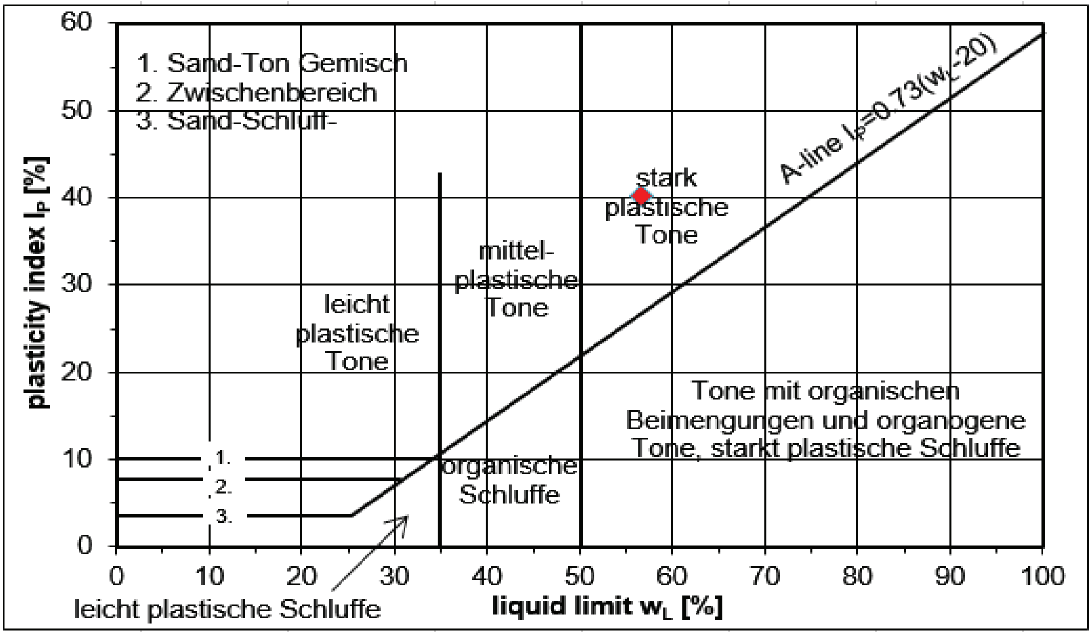

A.M.1 Figure 8 Plot of the plasticity index over the liquid limit to characterise the soil with the Atterberg limits. The Hemmerlingeer Marsch soil is identified as a strong plastic clay.

Direct shear test

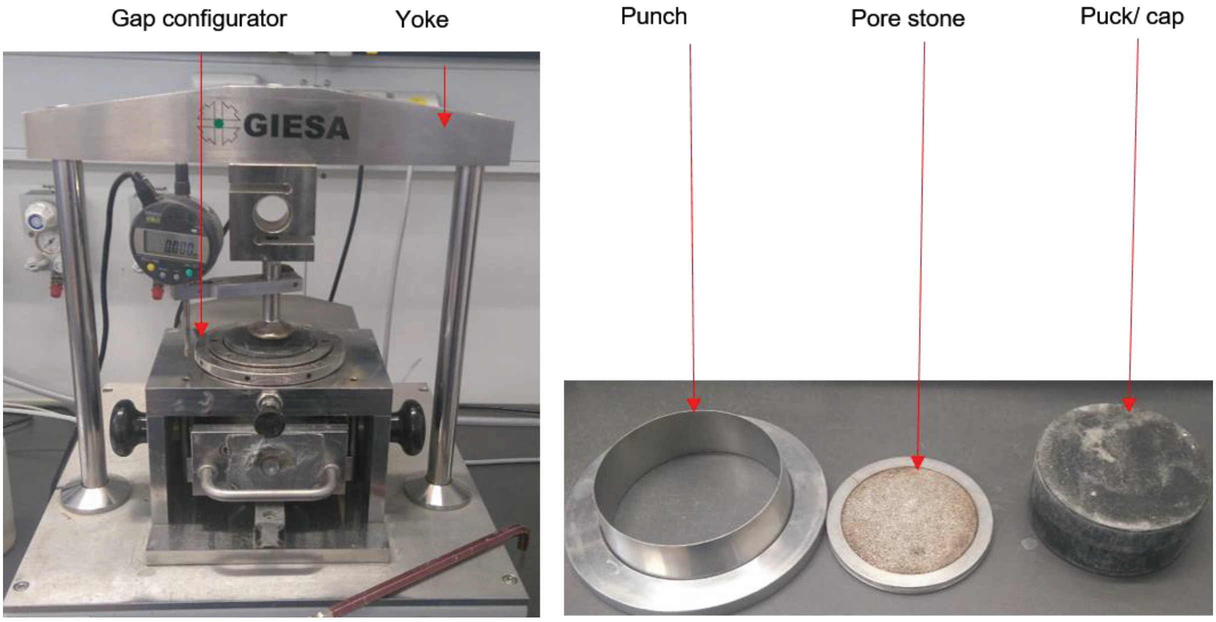

A.M.1 Figure 9 The direct shear device from the workig goup of Prof. Dr. Mörz Marine Engineering Geology. Identified are the most important parts oft he device in ordert o initiate a direct shear test.

Instructions for the direct shear test in the laboratory of Prof. Dr. Mörz Marine Engineering Geology

Determine Shear velocity

- Needs plasticity index
- Atterberg limits
- Or educated guess: 0.04 m/min -> shear path 1 cm -> 250 min

Needed configuration on the PC, connected to the direct shear test device:

- Program: GeoLab
- System /configurations/ choose come via *Gisa* in scroll down manue
- Restart GeoLab
- Project/New/ Project ’Project Name’
- Project/New/Test(Versuch)
- Messung/Load as % at 0.1% to connect load stamp with sample then 5% (of 5 kN/40cm² -> 1250 kPa -> 63 = 5.04%)
- Messung/sample interval 10 to 20 sec
- Data export via plot data which is exported must be in the interval lines
- Outputs needed: load, settlement, shear path and shear stress

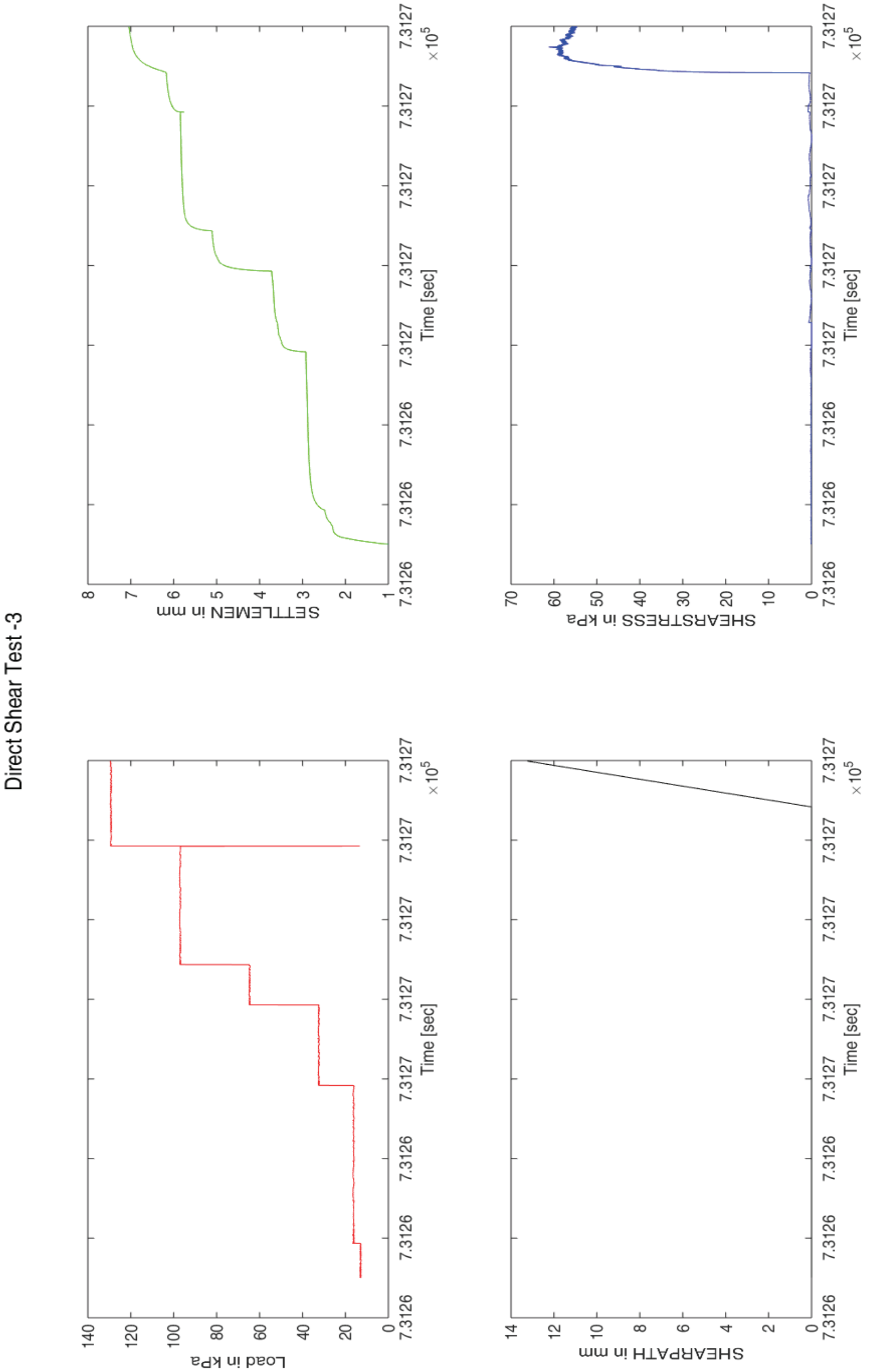

A.M.1 Figure 10 Measurements of the direct shear test, shown are The load, settlement, shear path and shear stress over time in seconds.

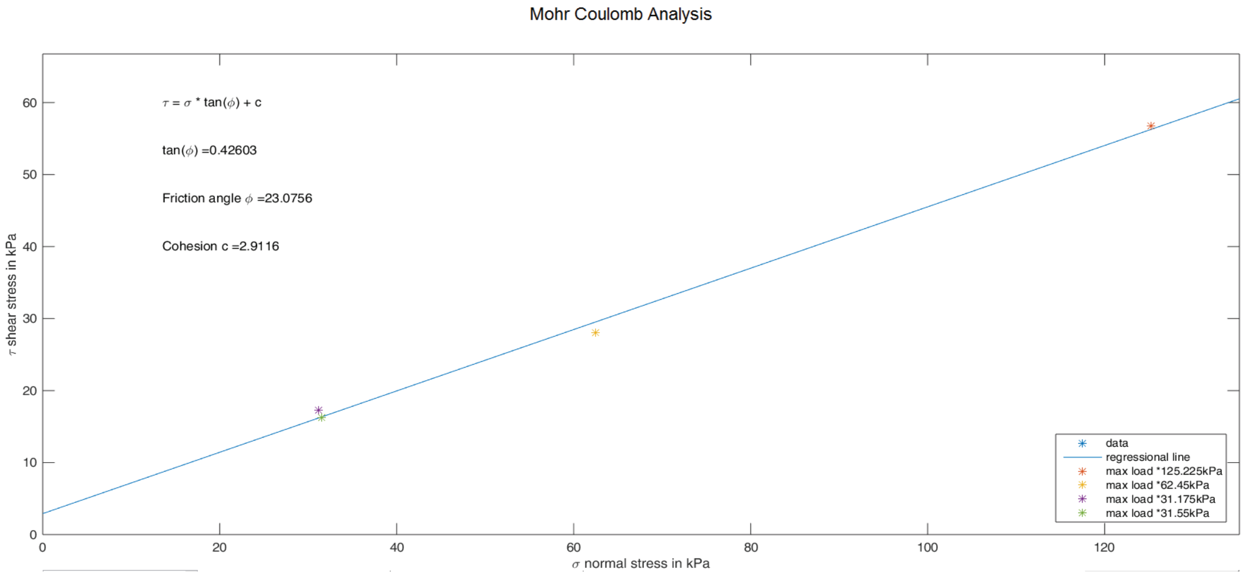

A.M.1 Figure 11 The Mohr Coulomb analysis via three different consolidation pressures and one repeatability test (~32 kPa) to estimate the friction angle and cohesion of the soil

Oedometer test

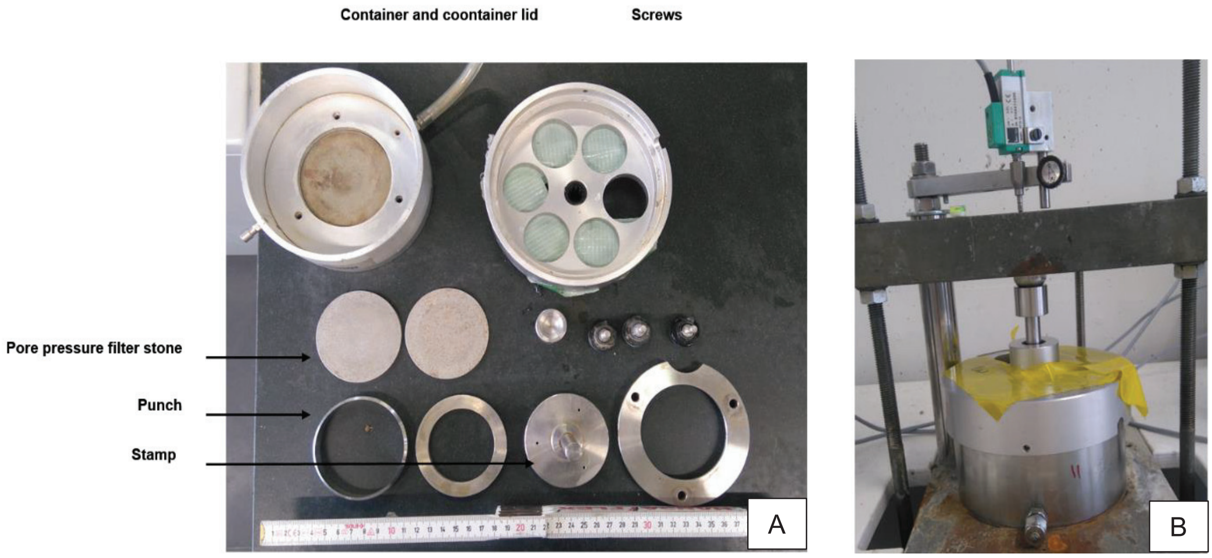

A.M.1 Figure 12 Panal A: Dissembled oedometer device from the working group of Prof. Dr. Mörz Marine Engineering Geology. Panel B: The assembled oedometer device.

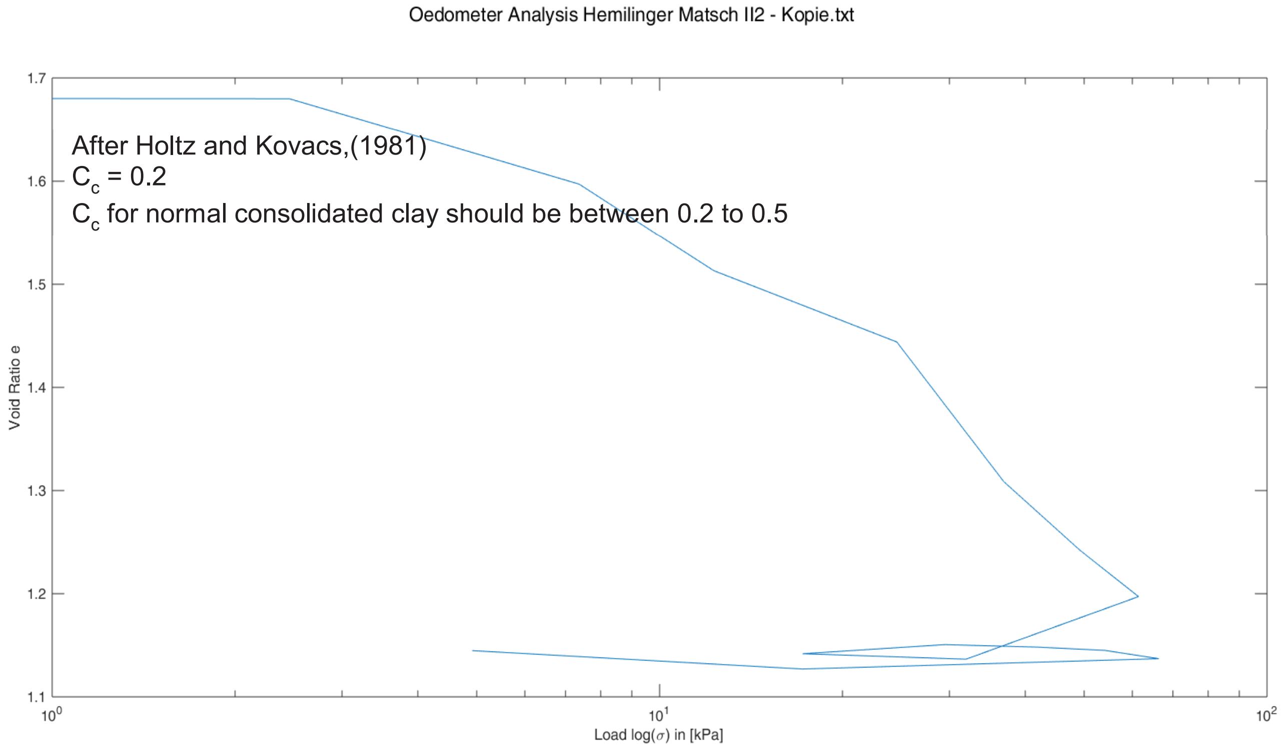

A.M.1 Figure 13 Void ratio over vertical overburden stress (in log display) and its analysis for the compression index C_C.

Specimen preparation and alteration to fit consolidation criteria

A.M.1 Figure 14 The alteration of the Hemmliger Marsch soil by adding synthetic grains to the Hemmlinger Marsch soil, done by the student helper Awais Saeed.

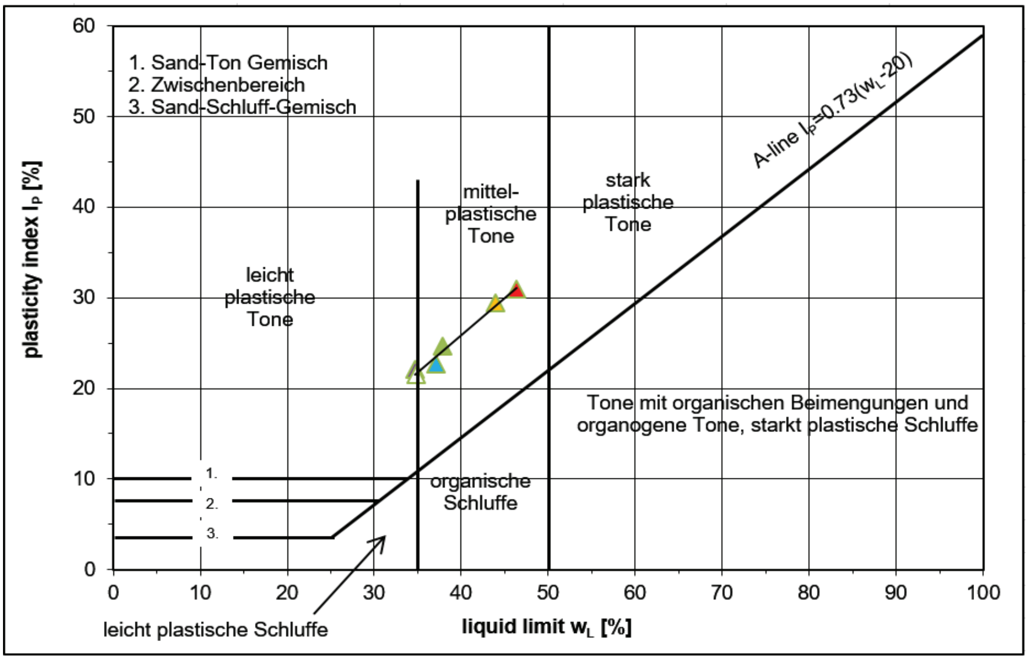

A.M.1 Figure 15 The analysis of the alteration of the Hermmerliger Marsch soil to fit a plasticity index around 20 so that the coefficient of consolidation and therefore the consolidation time reduces.

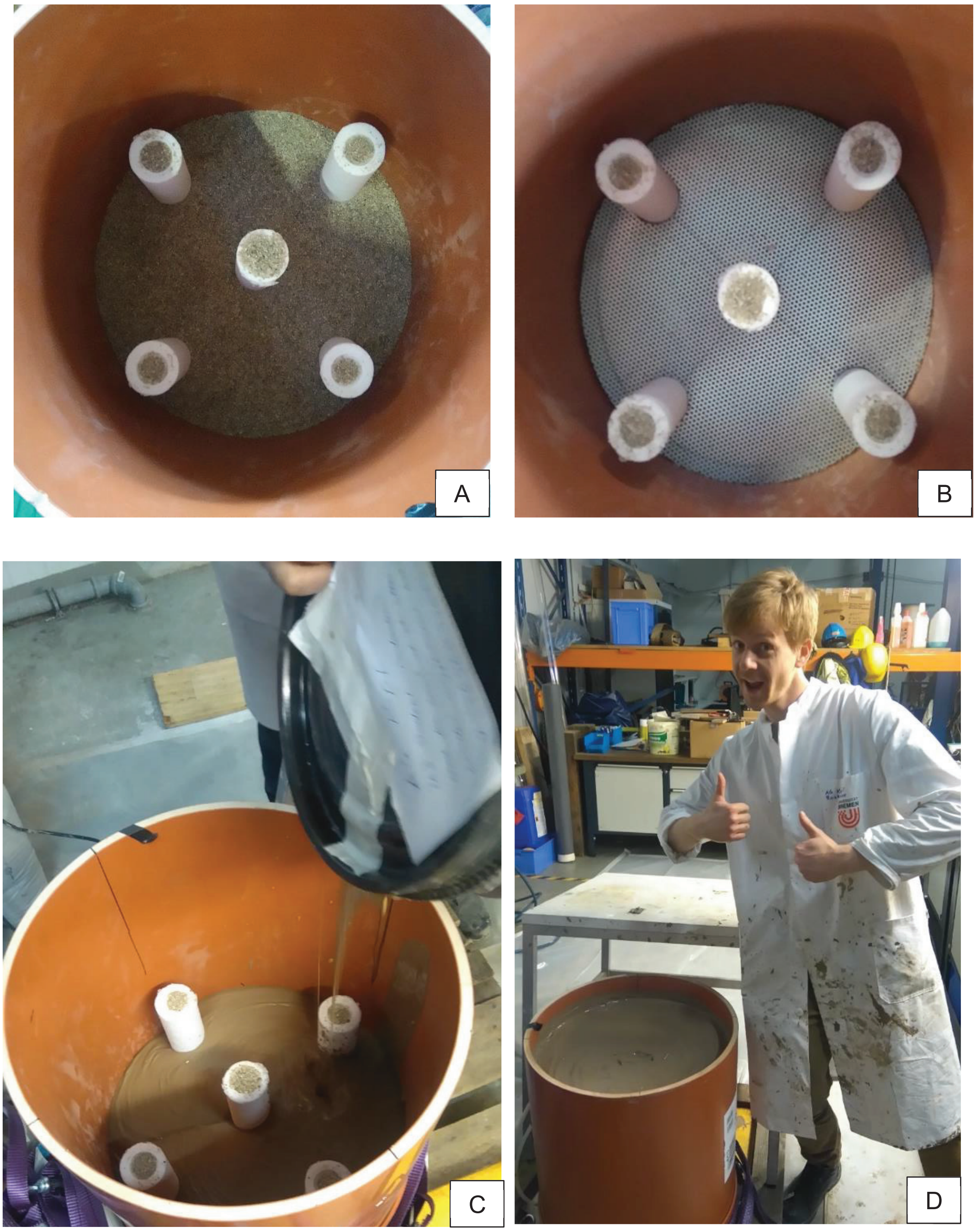

A.M.1 Figure 16 Documentation of the filling from the experimental container of the free fall calibration test. Panel A: Coarse gravel layer, which serves as a filter drainage for the consolidation phase. Also already shown are the hollow vertical drainages, which are also filled with the same gravel. Panel B: Metal grid at place to separate the soil specimen from the filter layer. Panel C: Filling of the container with the alternated soil specimen. To guarantee a homogeneous specimen the soil was built in close to its liquid limit. Panel D: Satisfied doctoral student Robert Roskoden after the first filling of the experimental container.

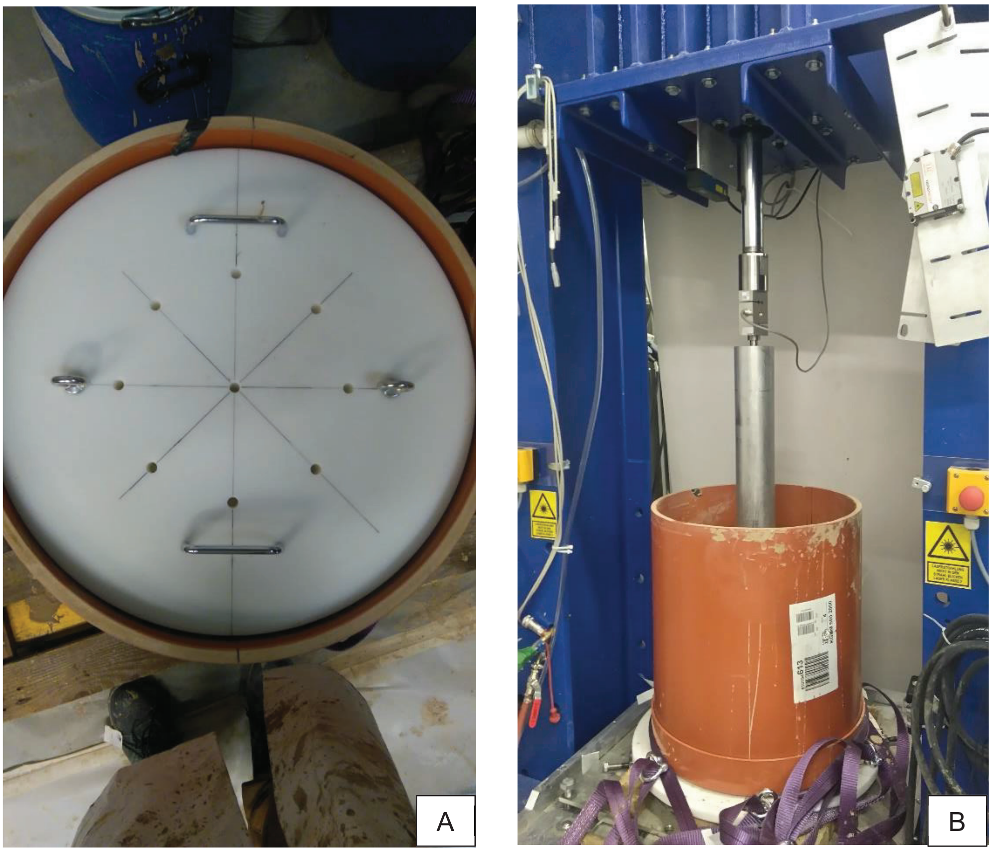

A.M.1 Figure 17 Panel A Top view on the experimental container, showing the pressure plate, which equally distributes the applied pressure from the hydraulic pump. Panel B: Shown here is the consolidation phase of the soil specimen via the hydraulic pump.

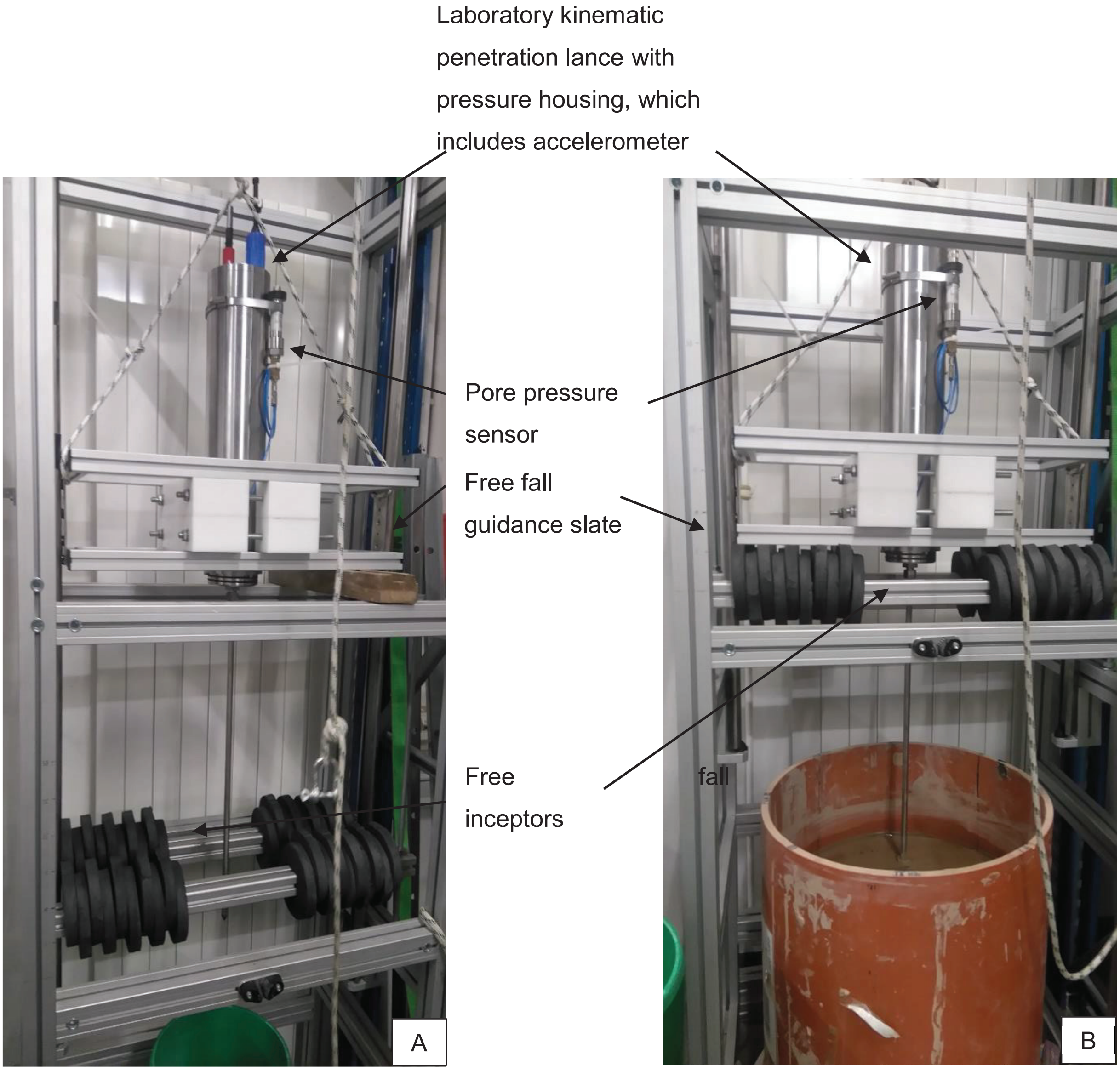

A.M.1 Figure 18 Laboratory free fall calibration tower. Panel A:The laboratory kinematic penetration lance with the pore pressure sensor on its site, built into the free fall slate. The slate ensures the unerring of the laboratory lance. Panel B: The laboratory lance after penetration, slate lays on top of the free fall inceptors

A.M.1 Figure 19 Experimental container with the consolidated and penetrated specimen.

References Appendix M.1

1. Stephan, S., 2015. A Rugged Marine Impact Penetrometer for Sea Floor Assessment. Bremen, Universität Bremen, Diss., 2015.

Appendix M.2

The appendix for the Manuscript 2 includes two tables which hold the exact geographical locations of the Nimrod penetration sites and one single figure, which unfortunately could not be published but is shown here as a tribute to Dean Sandwell and Nicola Lovett who went head deep into the mud of the Firth of Thames to collect the data and samples with me together.

A.M.2 Table 1 Positions of the Boat Transect. The data was collected on the 09.11.2017.

	Latitude	Longitude
1	-3.720.638.397	175.444.383
2	-3.720.646.603	1.754.447
3	-3.720.645.497	175.444.654
4	-3.720.637.701	175.444.627
5	-3.720.601.198	175.444.549
6	-3.720.615.196	175.444.574
7	-3.720.654.901	175.444.739
8	-3.720.661.003	175.444.783
9	-3.720.657.399	175.444.775
10	-3.720.670.399	175.444.737
11	-3.720.674.498	175.444.845
12	-3.720.669.804	175.444.825
13	-3.720.695.604	175.444.846
14	-3.720.645.103	175.444.696
15	-3.720.635.799	175.444.608
16	-3.720.629.403	175.444.701
17	-3.720.627.702	175.444.592
18	-3.720.615.598	175.444.797
19	-3.720.537.001	175.444.111
20	-3.720.495.201	175.443.737
21	-3.720.366.396	175.443.244
22	-3.720.084.496	175.441.475
23	-3.719.569.000	175.439.232
24	-3.719.499.397	175.438.702
25	-3.719.465.802	175.438.634

A.M.2 Table 2 Positions of the Mangrove Transect. The data was collected on the 04.12.2017

	Latitude	Longitude
1	-372.071.540.169.418	175.445.016.995.072
2	-372.072.019.614.279	175.445.130.988.955
3	-372.076.260.019.094	175.445.310.026.407
4	-372.080.809.716.135	175.445.676.986.128
5	-372.078.166.666.667	175.445.400.000.000
6	-372.081.330.232.322	175.445.828.028.023
7	-372.134.459.763.765	175.448.370.007.798
8	-372.134.469.822.049	175.448.361.039.162
9	-372.136.059.869.081	175.448.686.005.548

A.M.2 Figure 1 Final figure of the data acquisition in the Firth of Thames. From left to right: The amazing technician Mr. Dean Sandwell, a very satisfied doctoral student Robert Roskoden, and the best field helper one could hope for Nicola Lovett.

Appendix M.4 and M.5

As mentioned in the prefix of *Manuscript 4*, the *Manuscript 4* and *5* used to be one, therefore all data and figures not presented in these two manuscripts are presented here together. Shown are the model predictions for the three different literature models Burns and Mayne (2002), Krage et al. (2014) and Jang et al. (2015) as well as the predictions of the *ad hoc model* for all the measured dissipation test at Bramley Drive. The order of presentation is: ~19, ~23, ~27m. ~22m is not presented here, since it is already shown and analysed in the *Manuscript 4*.

Burns and Mayne (2002)

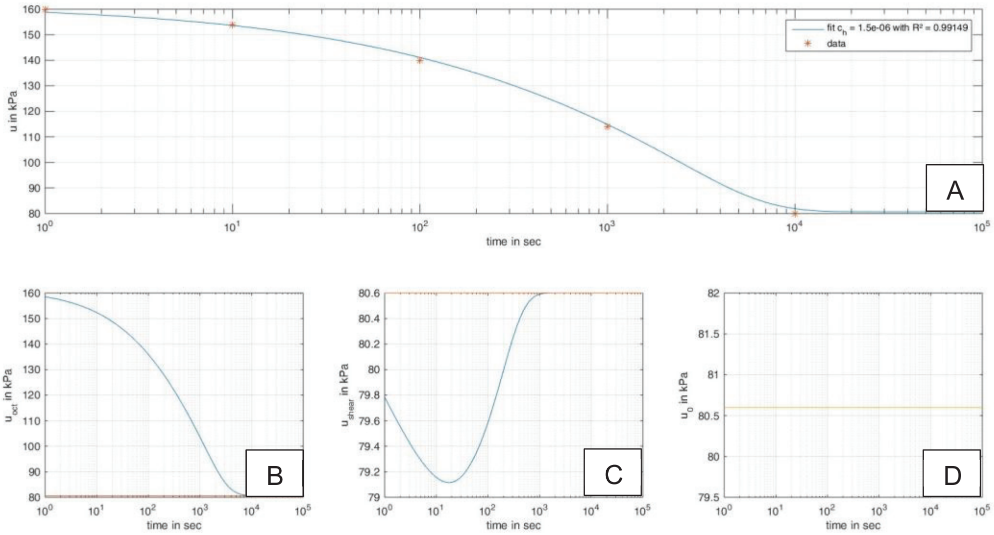

A.M.4.5. Figure 1 A representation of the model of Burns and Mayne (2002) with synthetic data. This figure was programmed to test if the in matlab simulated model of Burns and Mayne (2002) works before it was applied to the Manuscript 4 and 5. Therefore, all three components of the model are here presented singly. Panel A: The composition of the shear, octahedral and hydrostatic induced pore water pressure in [kPa] over time in seconds. Panel B: Just the octahedral introduced pore water pressure over time. Panel C: Just the shear induced pore water pressure over time. Panel D: Just the hydrostatic introduced pore water pressure over time.

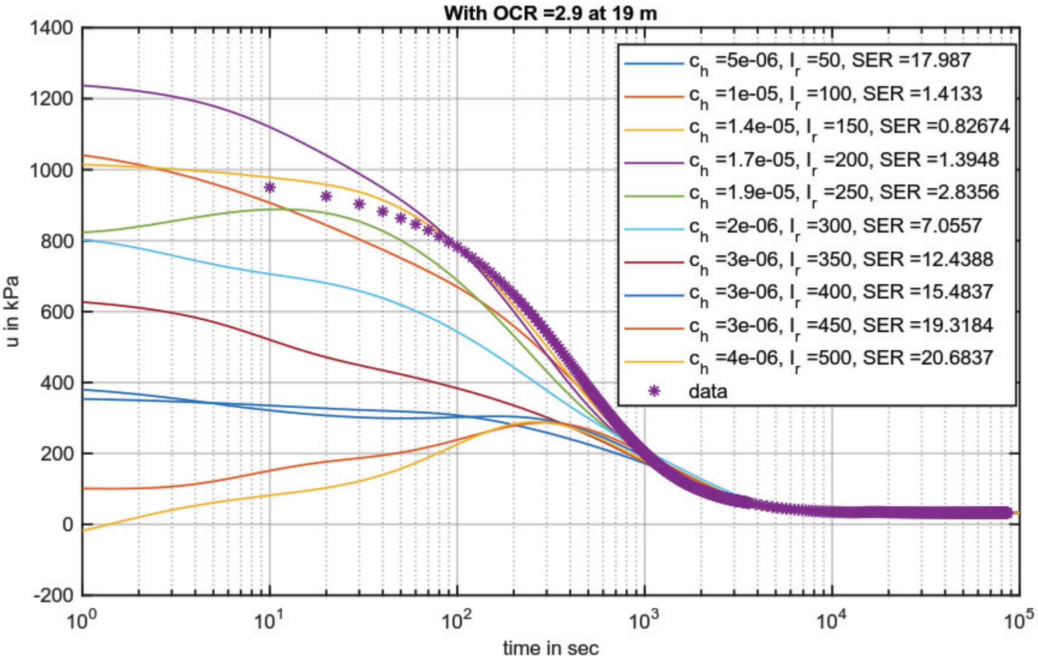

*A.M.4.5. Figure 2 Pore water pressure u in [kPa] plotted over time in seconds. Here displayed and simulated is the dissipation test from the Bramley Drive slide at ~19m. The best fit was achieved with an OCR = 2.9, c_h = 1.5*10^{-5} and an I_r = 150.*

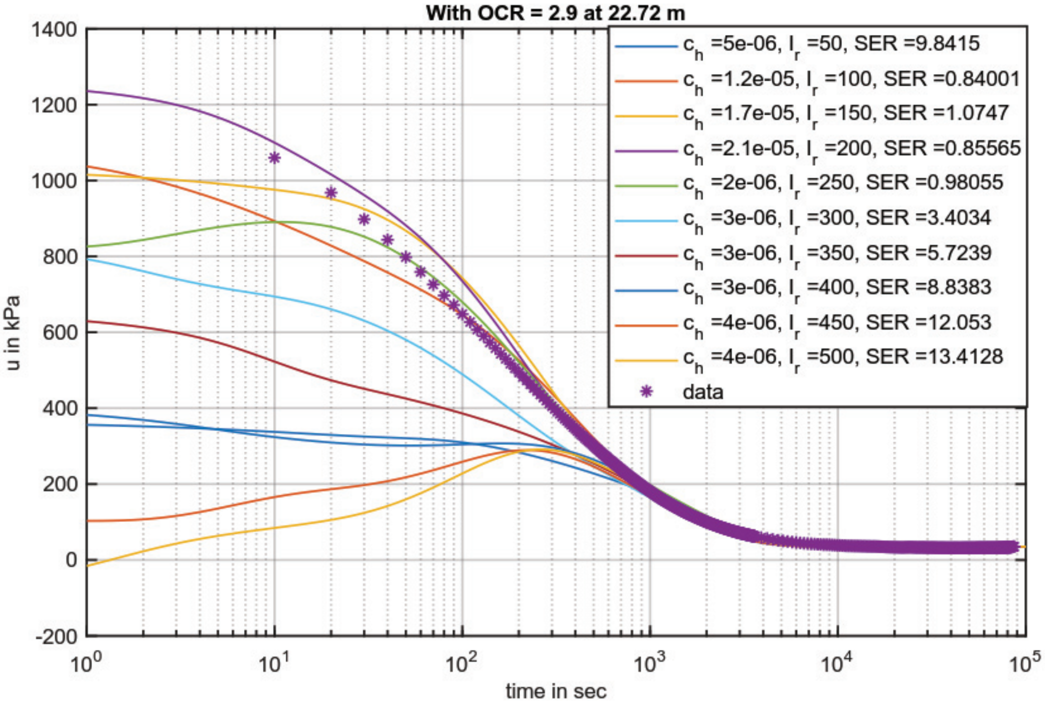

A.M.4.5. Figure 3 Pore water pressure u in [kPa] plotted over time in seconds. Here displayed and simulated is the dissipation test from the Bramley Drive slide at ~23m. The best fit was achieved with an OCR = 2.9, $c_h = 2.1*10^{-5}$, and an $I_r = 200$.

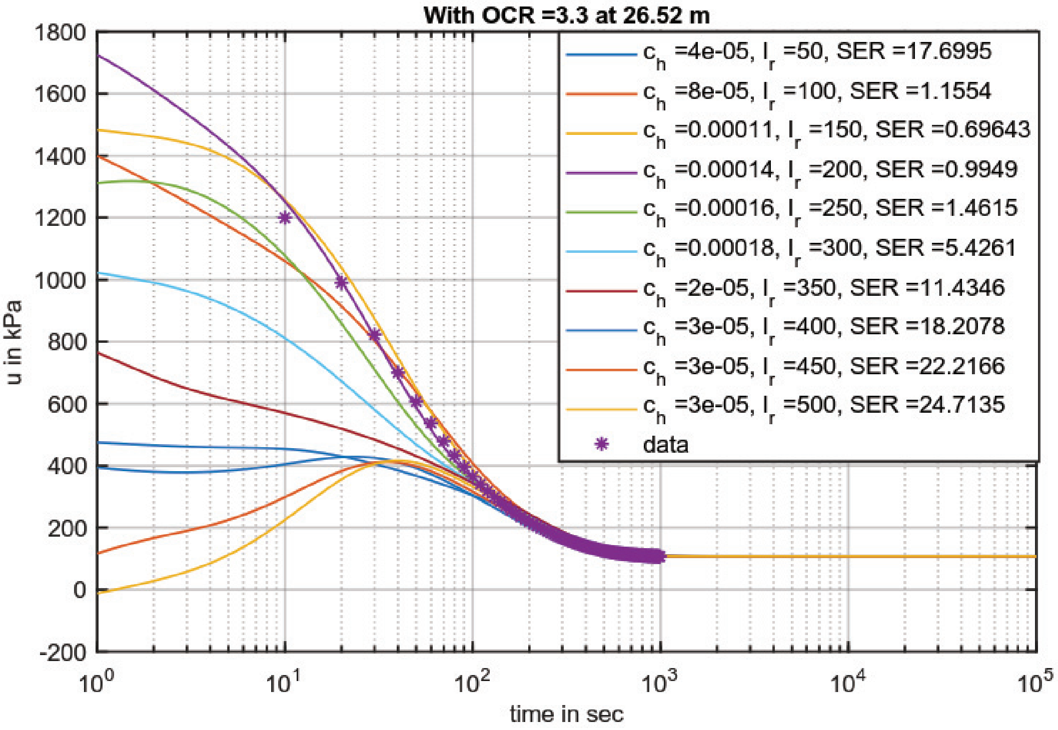

*A.M.4.5. Figure 4 Pore water pressure u in [kPa] plotted over time in seconds. Here displayed and simulated is the dissipation test from the Bramley Drive slide at ~27m. The best fit was achieved with an OCR = 3.3, c_h = 1.1*10^{-4} and an I_r = 150.*

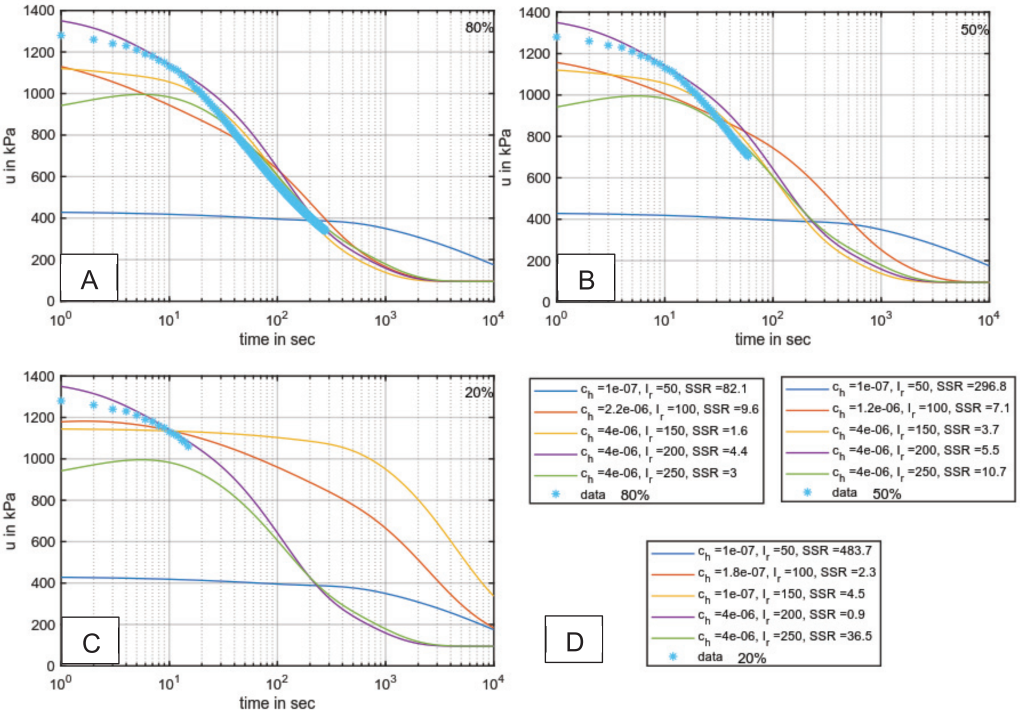

A.M.4.5. Figure 5 Pore water pressure u in [kPa] plotted over time in seconds. Panel A to C show how the model of Burns and Mayne (1998) reacts to different truncated data sets. The greater the truncation the more unstable the model gets. However, in all three cases the same c_h could be achieved ~ $4*10^{-6}$ but with different I_r (150 to 200). Panel A: Truncation ~ 20%, hence 80% residuals. Panel B: Truncation ~ 50%, hence 50% residuals. Panel C: Truncation ~ 80%, hence 20% residuals. Panel D: Corresponding legends to the amount of the residuals.

Krage et al. (2014)

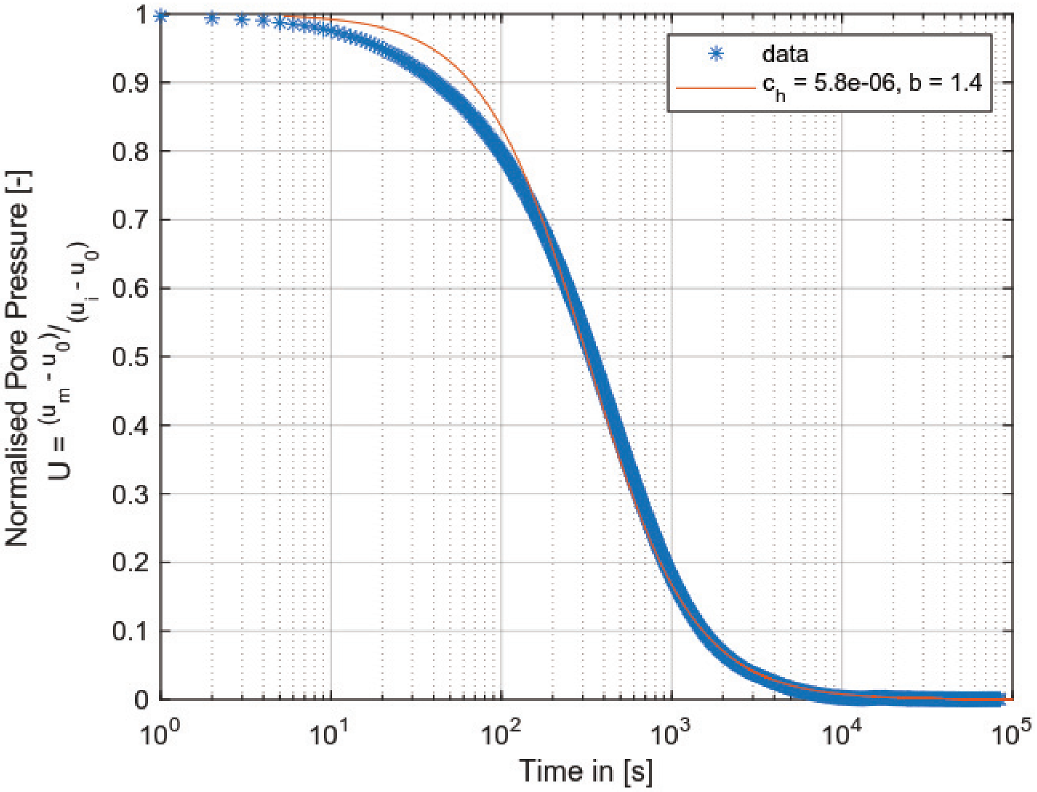

A.M.4.5. Figure 6 The model prediction of Krage et al. (2014) for the dissipation test at Bramley Drive at ~19 m plotted is the normalised pore pressure over time in seconds. The predicted $c_h = 5.8*10^{-6}$*, the assumed* $I_r = 250$*.*

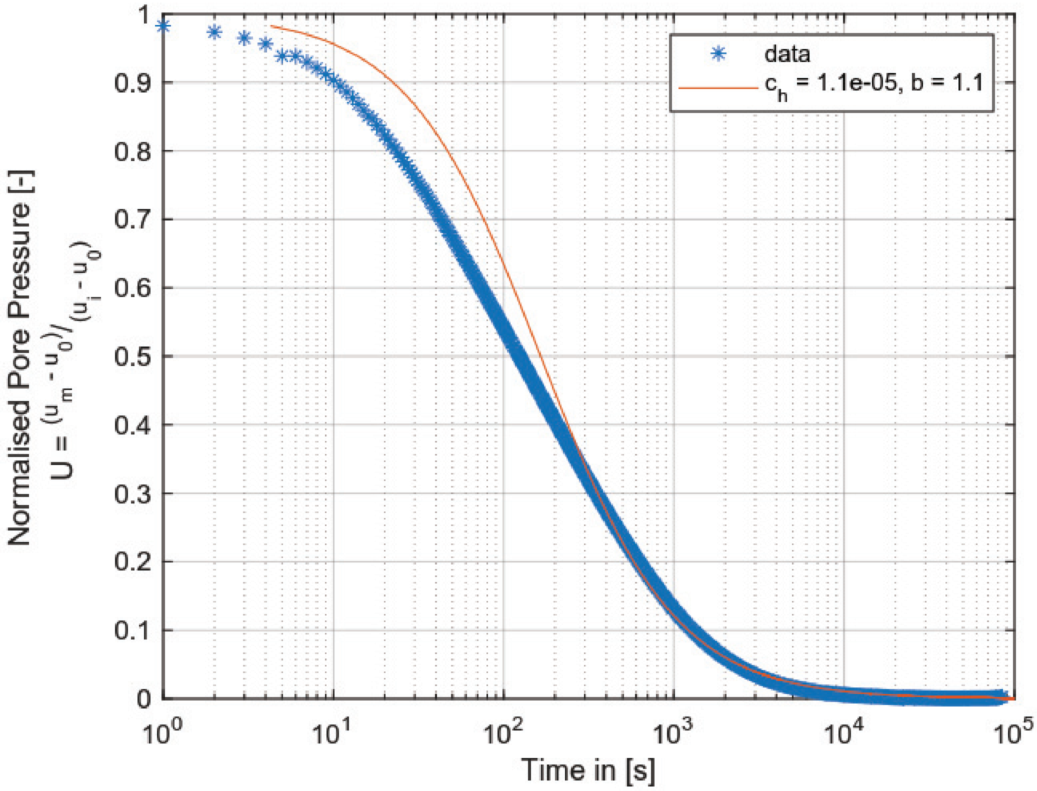

A.M.4.5. Figure 7 The model prediction of *[Krage et al. (2014)](#)* *for the dissipation test at Bramley Drive at ~23 m plotted is the normalised pore pressure over time in seconds. The predicted* $c_h = 1.1*10^{-5}$*, the assumed* $I_r = 250$*.*

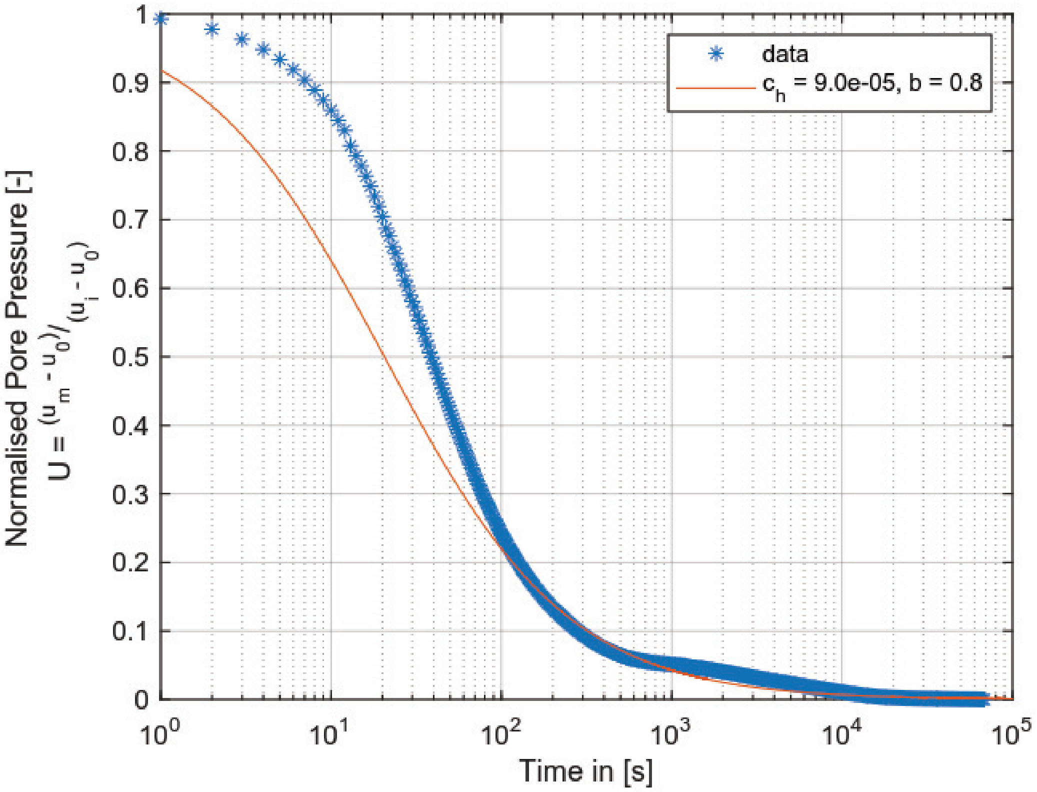

A.M.4.5. Figure 8 The model prediction of Krage et al. (2014) for the dissipation test at Bramley Drive at ~27 m plotted is the normalised pore pressure over time in seconds. The predicted c_h = $9*10^{-5}$, the assumed I_r = 250.

Jang et al. (2015)

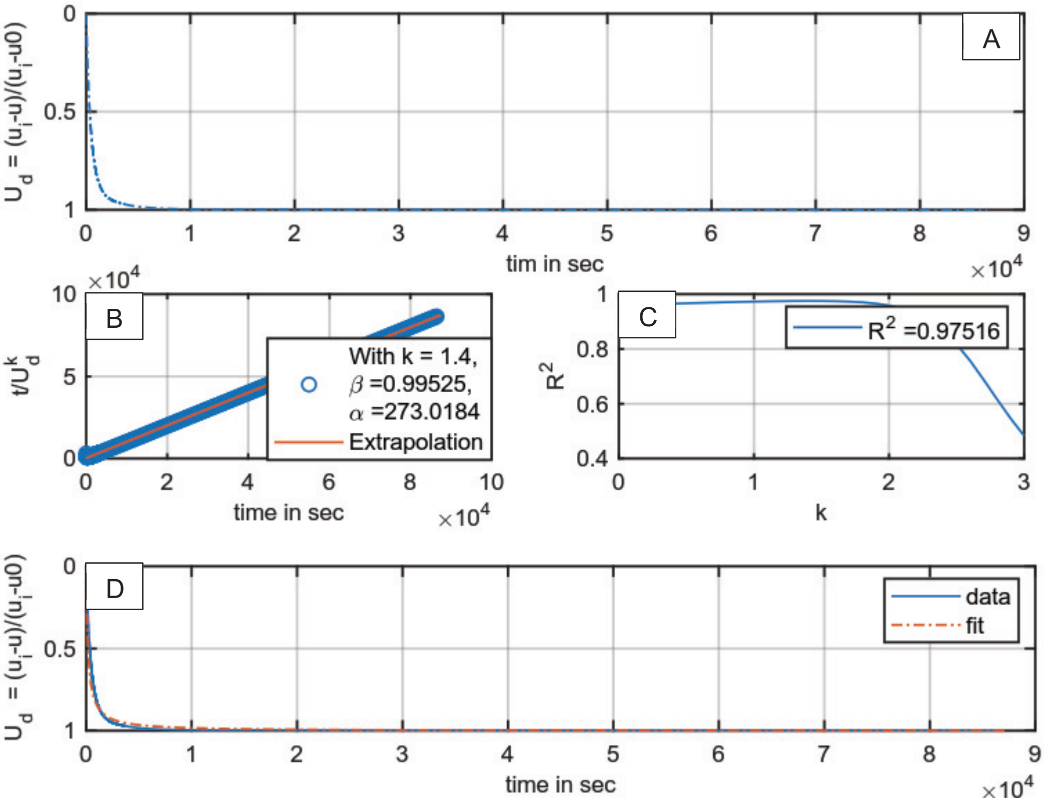

A.M.4.5. Figure 9 Model predictions after Jang et al. (2015) for the Bramley Drive slide at ~ 19m. Panel A: Alternative normalised pore pressure over time in seconds. Panel B: Linear regression of the ratio time to alternative pore pressure over time in seconds plotted over time in seconds. Panel C: Linear goodness of fit R² plotted over the modelling parameter k to find the best k in the ratio time over the alternative normalised pore pressure. Panel D: Alternative normalised pore pressure over time in seconds. Here the predicted data is compared with the measured to predicted data. Yielded $c_h = 4.5*10^{-6}$.

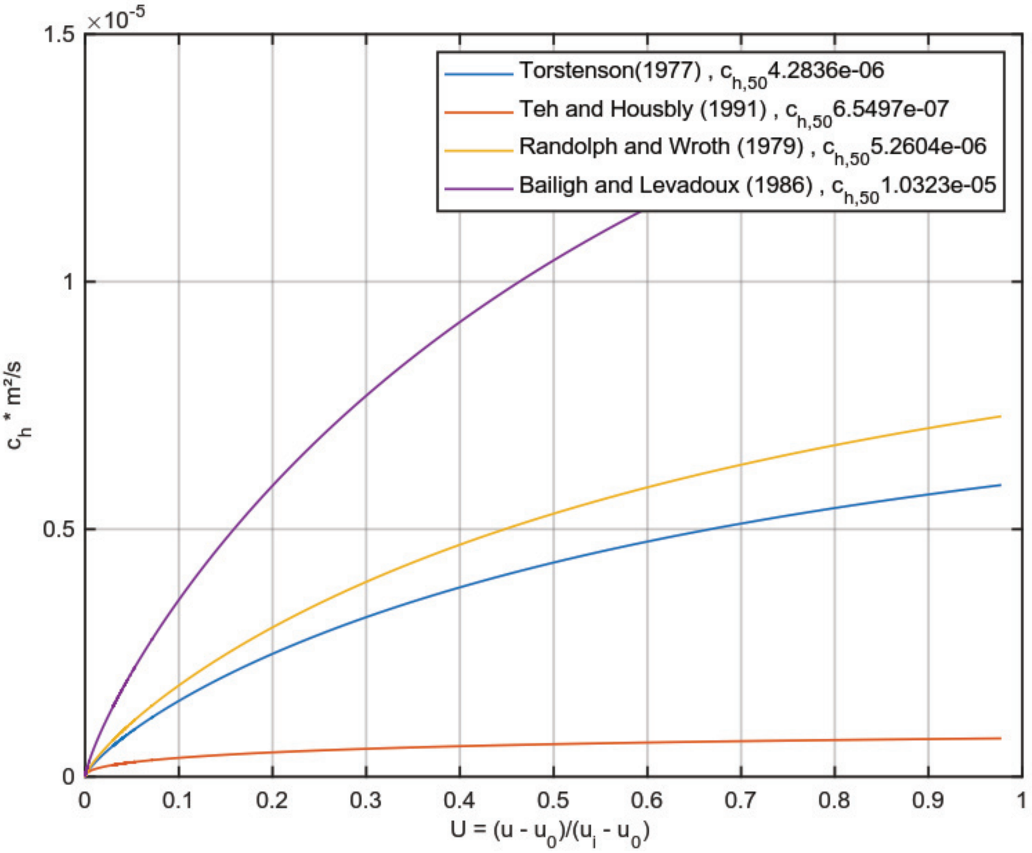

A.M.4.5. Figure 10 The coefficient of consolidation plotted over the normalised pore pressure for the different theoretical reference dissipation tests. The coefficients for 50% pore pressure dissipation are given in the legend and are averaged to yield here the utilised coefficient of consolidation. For further details see Jang et al. (2015). Yielded (averaged) $c_h = 4.5*10^{-6}$.

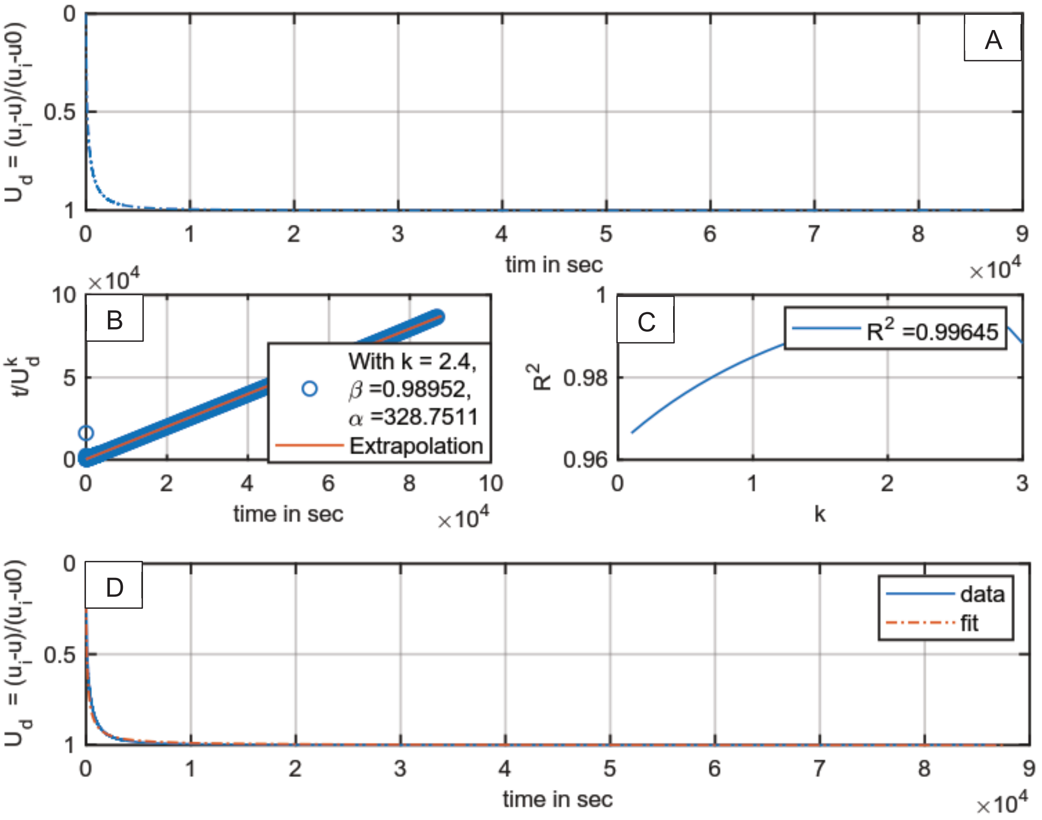

A.M.4.5. Figure 11 Model predictions after Jang et al. (2015) for the Bramley Drive slide at ~ 23m. Panel A: Alternative normalised pore pressure over time in seconds. Panel B: Linear regression of the ratio time to alternative pore pressure over time in seconds plotted over time in seconds. Panel C: Linear goodness of fit R² plotted of the modelling parameter k to find the best k in the ratio time over the alternative normalised pore pressure. Panel D: Alternative normalised pore pressure over time in seconds. Here the predicted data is compared with the measured to predicted data. Yielded $c_h = 1.4*10^{-5}$.

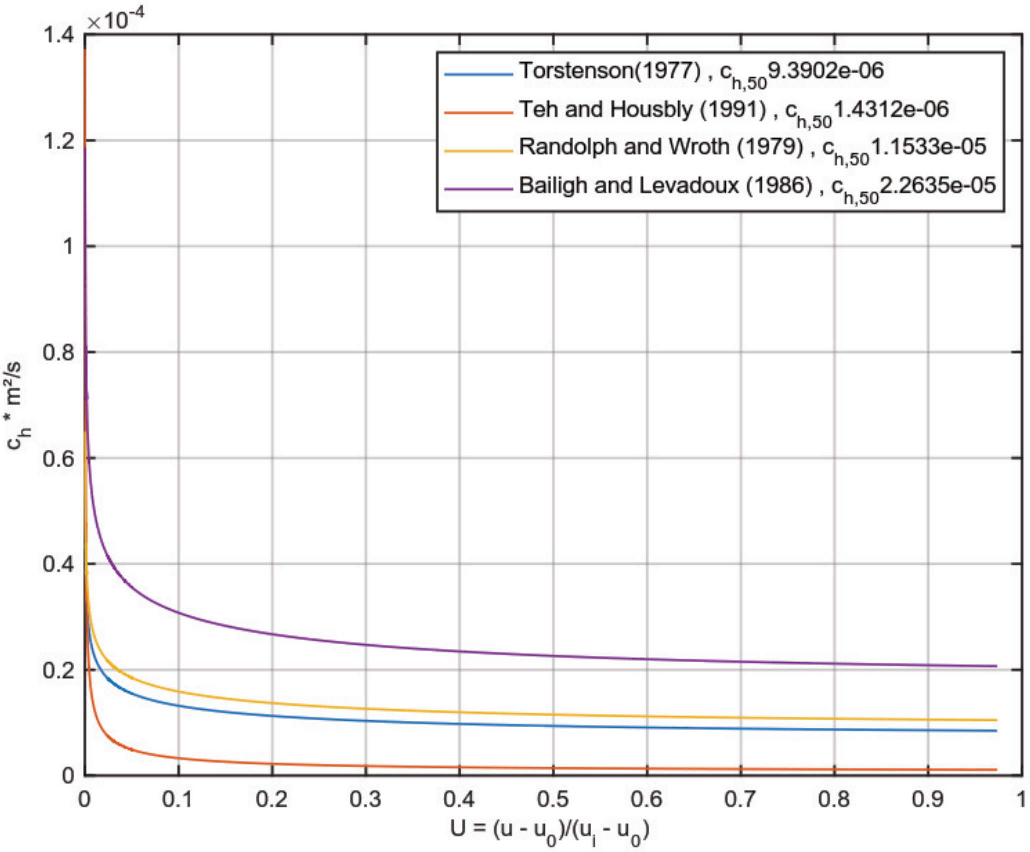

A.M.4.5. Figure 12 The coefficient of consolidation plotted over the normalised pore pressure for the different theoretical reference dissipation tests. The coefficients for 50% pore pressure dissipation are given in the legend and are averaged to yield here the utilised coefficient of consolidation. For further details see Jang et al. (2015). Yielded (averaged) $c_h = 1.4*10^{-5}$.

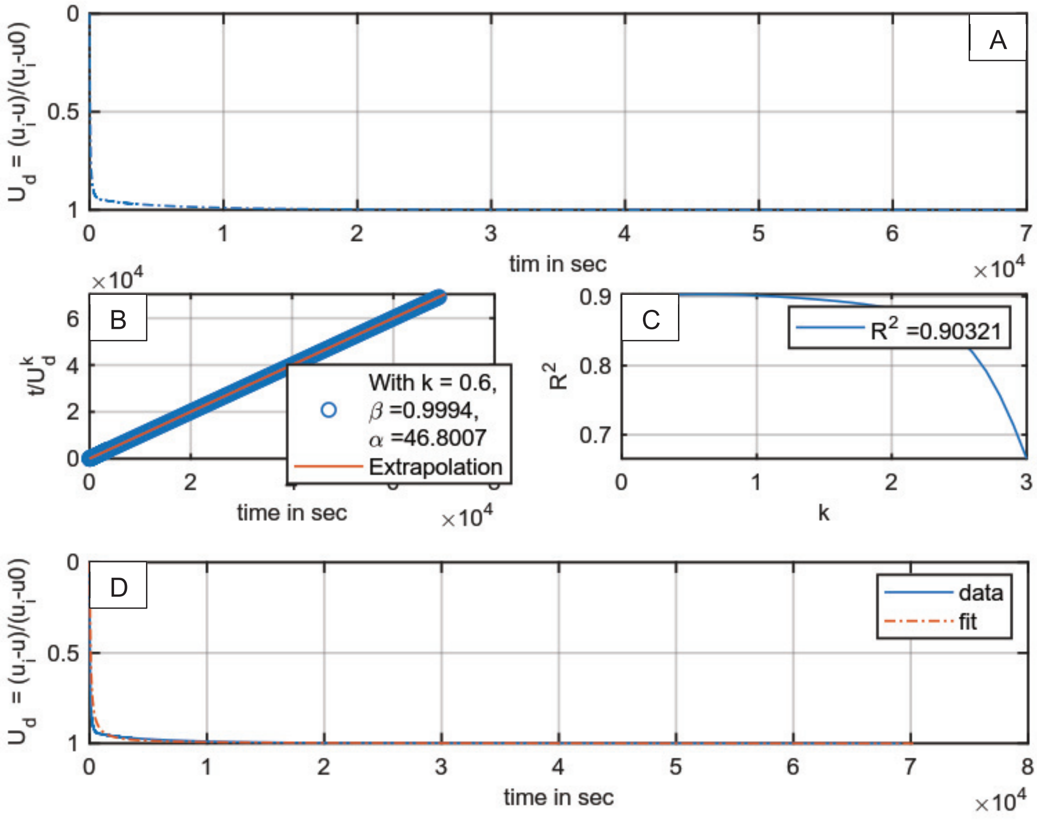

A.M.4.5. Figure 13 Model predictions after Jang et al. (2015) for the Bramley Drive slide at ~ 27m. Panel A: Alternative normalised pore pressure over time in seconds. Panel B: Linear regression of the ratio time to alternative pore pressure over time in seconds plotted over time in seconds. Panel C: Linear goodness of fit R² plotted of the modelling parameter k to find the best k in the ratio time over the alternative normalised pore pressure. Panel D: Alternative normalised pore pressure over time in seconds. Here the predicted data is compared with the measured to predicted data. Yielded $c_h = 2.4*10^{-5}$.

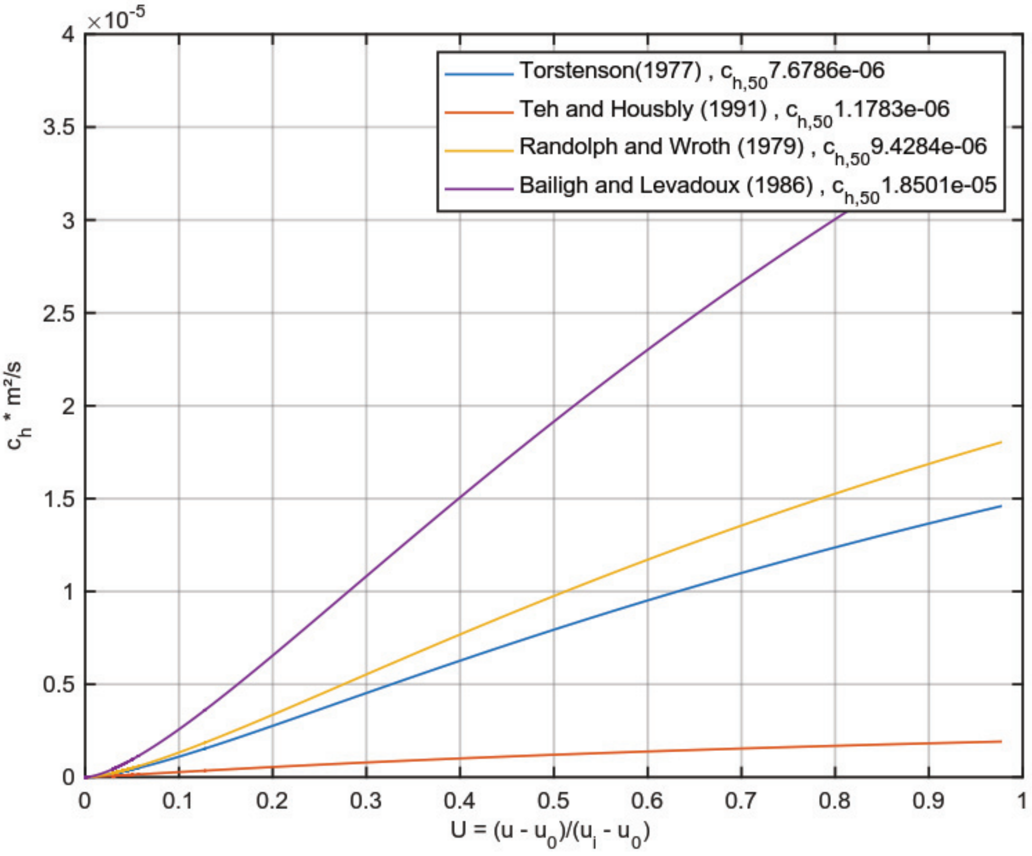

A.M.4.5. Figure 14 The coefficient of consolidation plotted over the normalised pore pressure for the different theoretical reference dissipation tests. The coefficients for 50% pore pressure dissipation are given in the legend and are averaged to yield here the utilised coefficient of consolidation. For further details see Jang et al. (2015). Yielded (averaged) $c_h = 2.4*10^{-5}$.

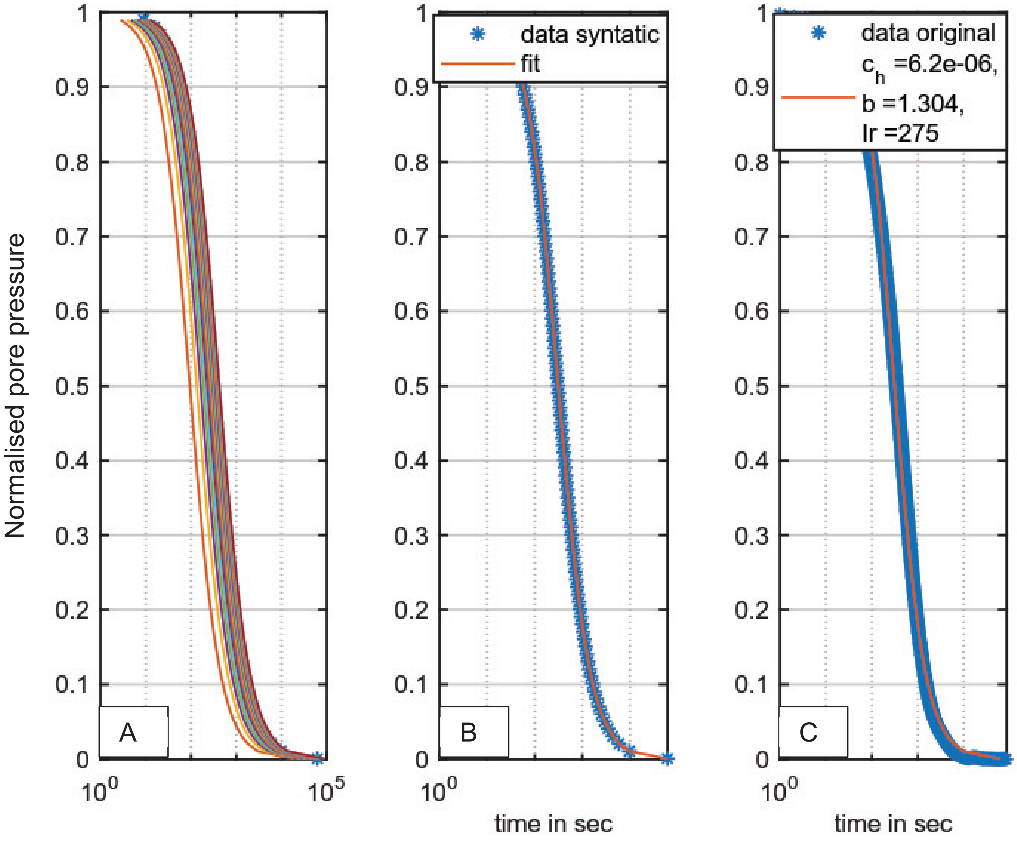

A.M.4.5. Figure 15 Model predication via the ad hoc model for the Bramley Drive slide at ~ 19m. Each panel plot the normalised pore pressure overtime in seconds. Panel A: I_r iteratively changed until the best fit is found. Panel B the step after the measured dissipation data was simulated by the model of Krage et al. (2014) forwarded to and simulated by Jang et al. (2015). (Panel C).

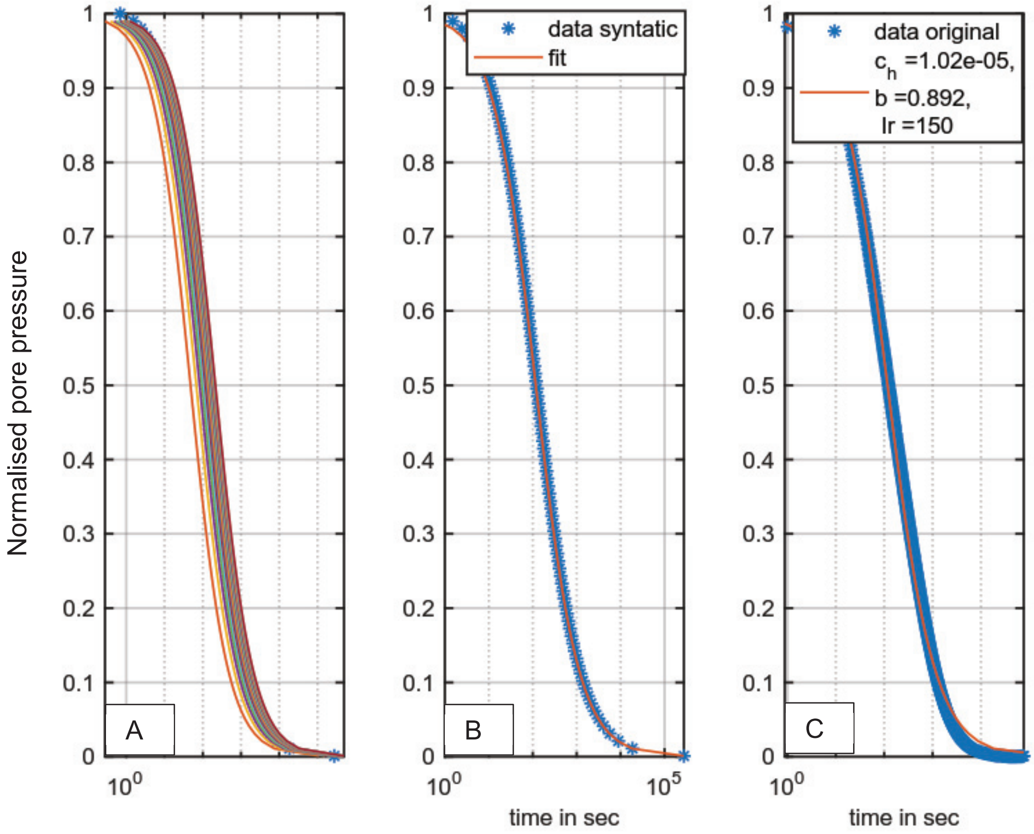

A.M.4.5. Figure 16 Model predication via the ad hoc model for the Bramley Drive slide at ~ 23m. Each panel plot the normalised pore pressure overtime in seconds. Panel A: $\mathrm{I_r}$ *iteratively changed until the best fit is found. Panel B the step after the measured dissipation data was simulated by the model of Krage et al. (2014) forwarded to and simulated by Jang et al. (2015). (Panel C).*

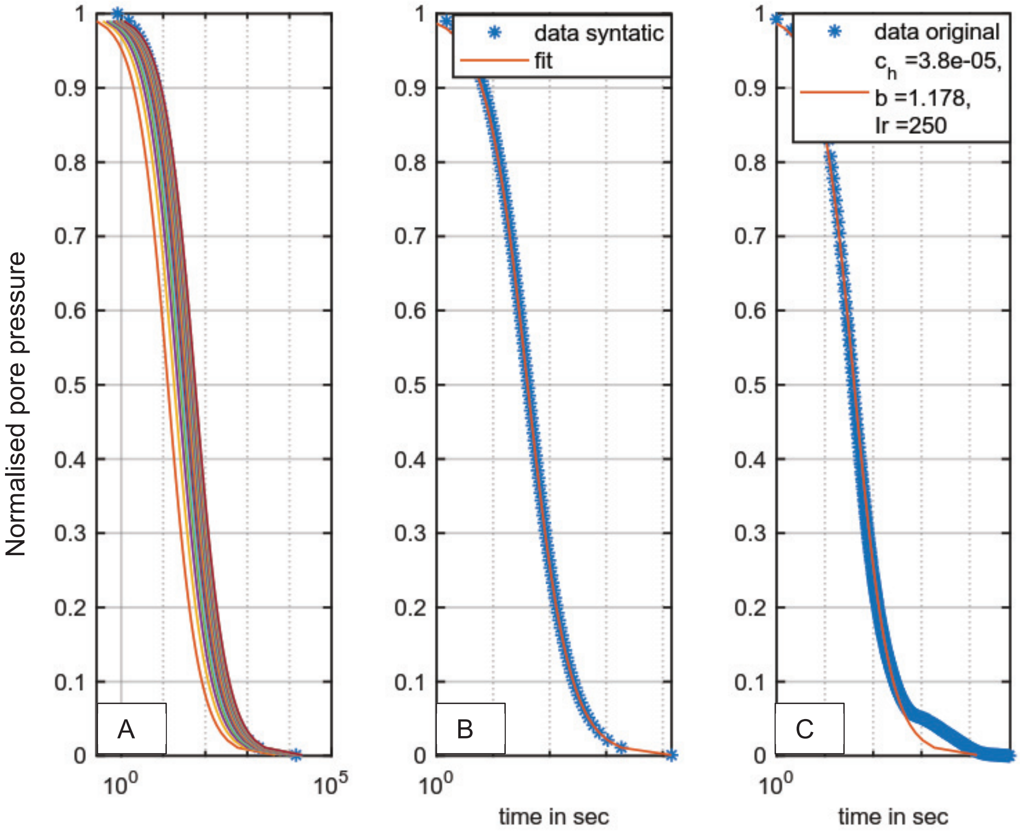

A.M.4.5. Figure 17 Model predication via the ad hoc model for the Bramley Drive slide at ~ 27m. Each panel plot the normalised pore pressure overtime in seconds. Panel A: I_r *iteratively changed until the best fit is found. Panel B the step after the measured dissipation data was simulated by the model of Krage et al. (2014) forwarded to and simulated by Jang et al. (2015). (Panel C).*

A.M.4.5. Table 1 Comparison of the different estimated, predicted or yielded coefficients of consolidation compared with the reference method from The and Houlsby (1991). Furthermore, the coefficient was not only yielded via I_r 250 for the reference method, but also the predicted I_r values from the ad hoc model have been utilised in the reference method to estimate the influence of the rigidity index on the coefficient of consolidation (column 11). Column 12 yields the coefficient of consolidation with the normal T factor and not rigidity index. Clear visible is that the ad hoc model shows the smallest average deviation from the ad hoc model.

Depth		**Coefficient of consolidation from the Laboratory**			**Burns and Mayne (2002)**	**Krage et al. (2014)**	**Jang et al. (2015)**	**Ad hoc.**	**Teh and Houlsby (1991)**		
Core	**CPTu**	**c_v**	**$c_{h,rotated}$**	**$c_{h,remoulded}$**	**OCR 2.9 I_r 150. OCR 2.9 I_r 200. OCR 2.6 I_r 200. OCR 3.3 I_r 150 $I_{r,avg}$ 175**	**I_r 250**		**I_r 275; 175; 150; 250 $I_{r,avg}$ 212**	**c_h via T* I_r 250**	**I_r 275; 175; 150; 250**	**c_h via T**
19.0	19.0	1E-06	1E-07	1E-07	1.4E-05	5.8E-06	4.5E-06	6.2E-06	4.9E-06	5.1E-06	2.1E-07
22.2	22.1		1E-07	1E-07	4.0E-06	2.2E-05	1.4E-05	2.5E-05	2.8E-05	2.4E-05	1.0E-06
23.0	22.7		1E-05	1E-07	2.2E-05	1.1E-05	5.4E-06	1.2E-05	1.3E-05	1.0E-05	5.7E-07
27.6	26.5		1E-05	1E-06	1.1E-04	9.0E-05	2.4E-06	3.8E-05	6.2E-05	6.2E-05	2.6E-06
					187.7%	19.2%	7.5%	27.4%	0.0%	4.9%	95.8%
					85.9%	22.7%	50.8%	12.1%	0.0%	16.3%	96.3%
					64.2%	56.7%	59.7%	12.7%	0.0%	22.5%	95.8%
					78.4%	46.0%	96.1%	38.4%	0.0%	0.0%	95.8%
		Average Deviation			**104.0%**	**36.1%**	**53.5%**	**22.6%**	**0.0%**	**10.9%**	**95.9%**

The Bramley Drive CPTu pushes and dissipation tests

Due to reasons for completeness, I will present screenshots from the CPTit – reports for the yet unpublished and also not yet interpreted *CPTu* pushes and their dissipation tests (if available) in this section (note that dissipation tests have been already interpreted in *Manuscript 4* and *5*). The original reports only exits in PDF-files and will be part of the digital appendix. A.M.4.5. Figure 18 and A.M.4.5. Table 2 give the geographical relation from the five *CPTu* pushes at the study area Bramley Drive, Omokoroa, New Zealand. Exact geographical location of the *CPTu* pushes is given in their headlines and on the screenshots.

Note: Penetration 1 and 2 form the outer parts of the *CPTu* study transect to better identify the failure prone layer so that the dissipation tests depths for the *CPTu* pushes 3, 4, and 5 could be determined.

A.M.4.5. Figure 18 Google earth screenshot showing the CPTu transect in relation to the already installed geoscientific observatories such as piezometers at 12 m, 21 m, and 27.5 m, which have been logging continuously since May 2013, as well as waves, wind and rainfall surveillances.

A.M.4.5. Table 2 summary of all CPTu push meta data such as penetration depth, distance to the fence in A.M.4.5. Figure 18 etc.

CPTu push number	1	2	3	4	5
Penetration depth [m]	31	28	26	30	19
Distance to the fence [m]	15.10	02.38	11.50	08.74	5.56
Distance to the next CPTu push		3.18	4	2.76	3.18
Dissipation Depth [m]	-	-	26	21 and 22	19
Dissipation Time [h]	-	-	22	0.5 and 24	24
Installed w.t. tubes	x	x		x	

CPT01 S 37° 37.830' / E 176° 02.750' Penetration depth 31 m

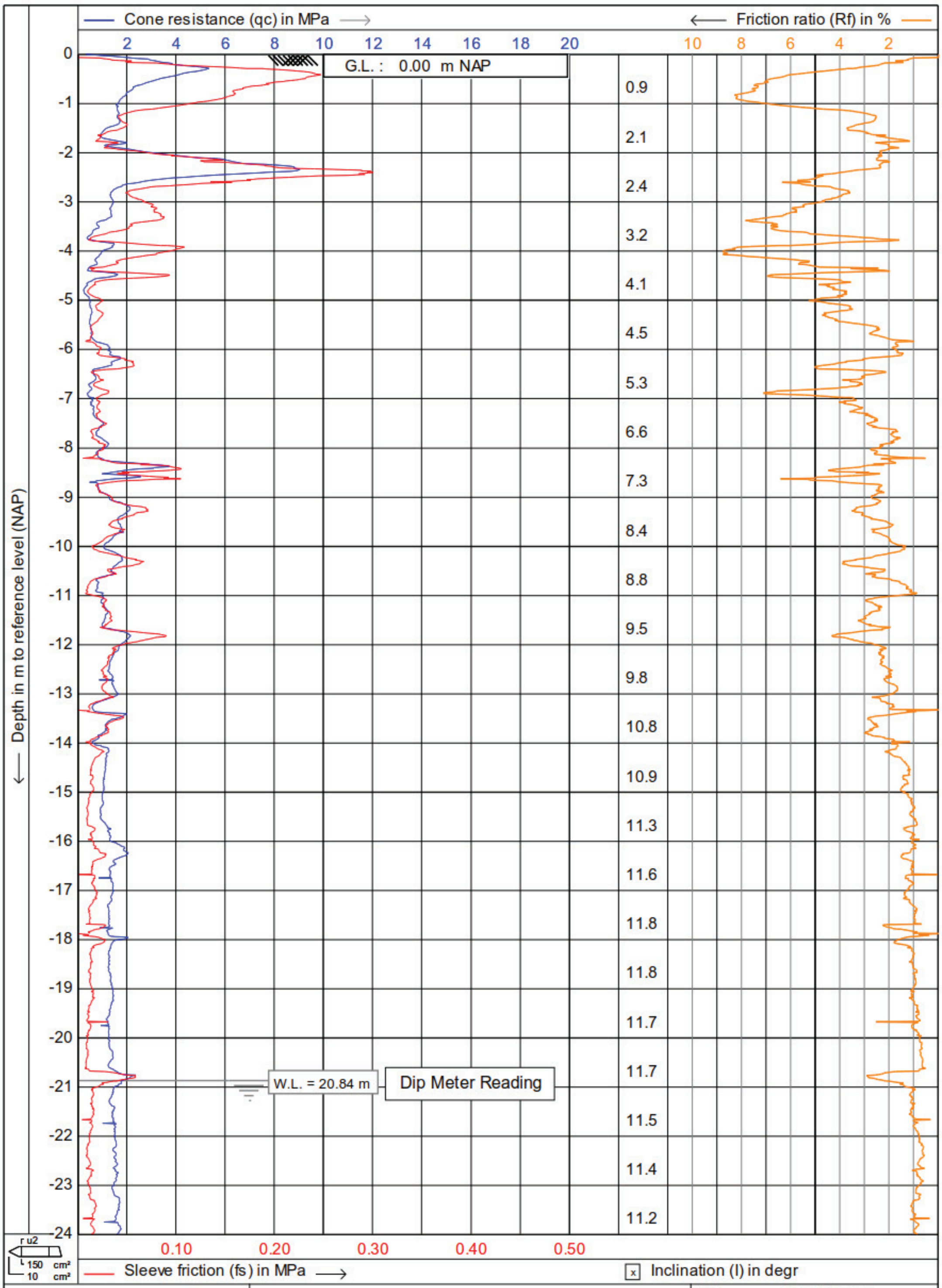

CPT it CONE PENETROMETER TESTING

ISO 22476-1:2012 Application class 2 Test type TE2

Project : **PROJECT DISSIPATION TEST**

Location: **OMOKOROA SLIP**

Position: **0, 0**

Date : **15/12/2017**

Cone no. : **S10CFIIP.S16082**

Project no. : **17052 / PDT**

CPT no. : **CPT01** **1/30**

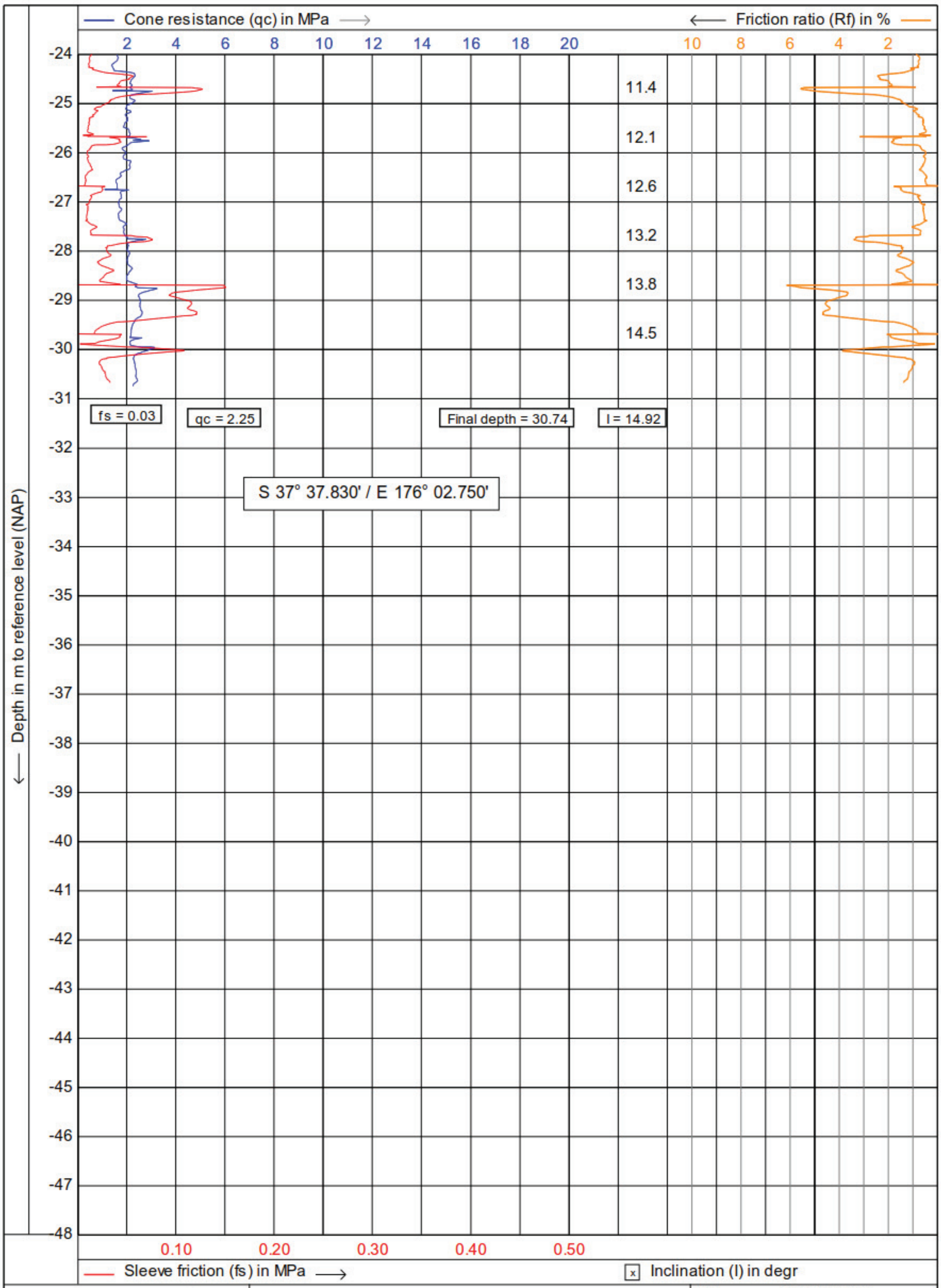

CPT it
CONE PENETROMETER TESTING

ISO 22476-1:2012 Application class 2 Test type TE2

Project : **PROJECT DISSIPATION TEST**
Location: **OMOKOROA SLIP**
Position: **0, 0**

Date : **15/12/2017**
Cone no. : **S10CFIIP.S16082**
Project no. : **17052 / PDT**
CPT no. : **CPT01** **2/30**

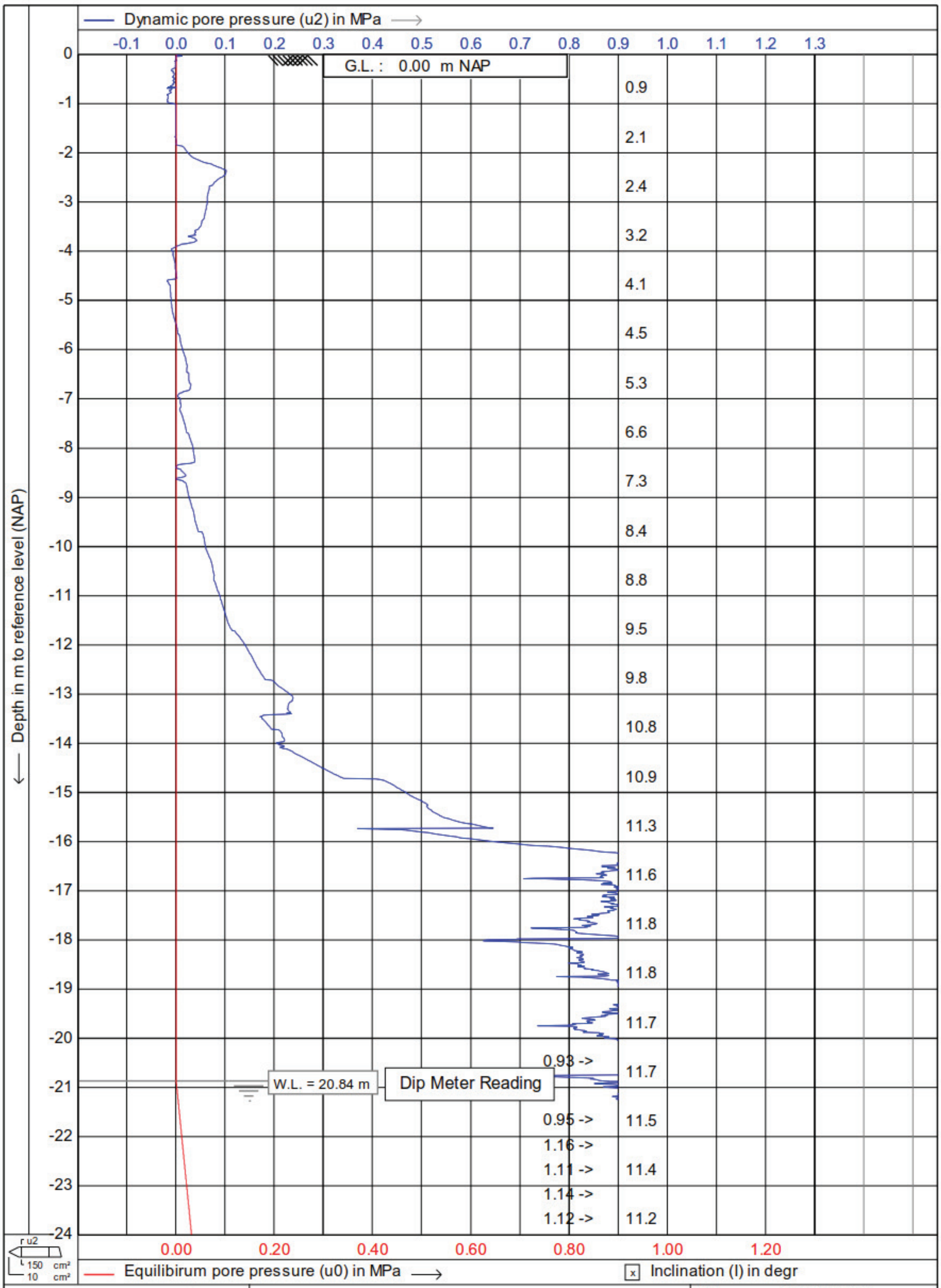

CONE PENETROMETER TESTING

ISO 22476-1:2012 Application class 2 Test type TE2

Project : **PROJECT DISSIPATION TEST**

Location: **OMOKOROA SLIP**

Position: **0, 0**

Date : **15/12/2017**

Cone no. : **S10CFIIP.S16082**

Project no. : **17052 / PDT**

CPT no. : **CPT01** **3/30**

1.47

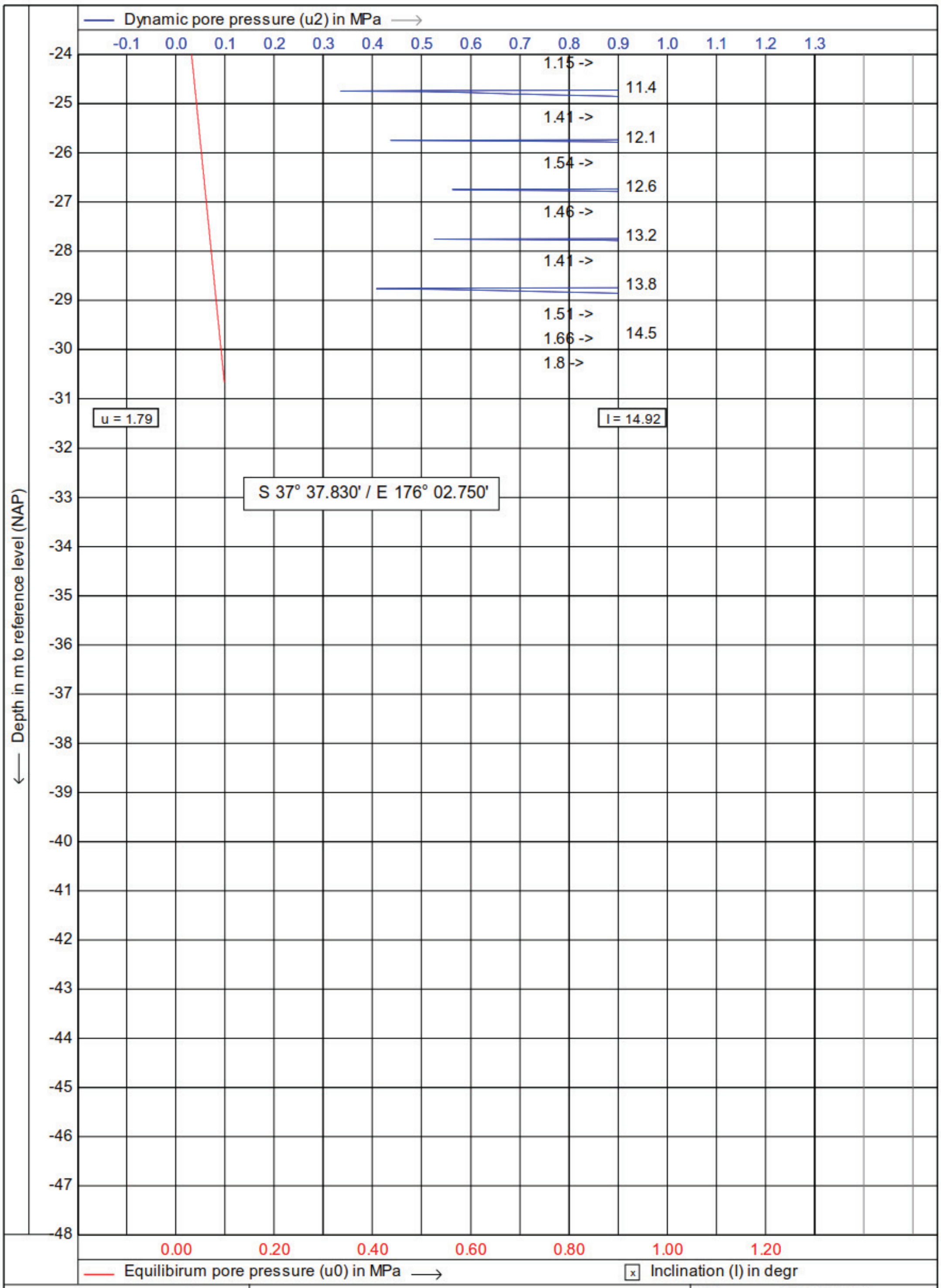

ISO 22476-1:2012 Application class 2 Test type TE2

Project : **PROJECT DISSIPATION TEST**
Location: **OMOKOROA SLIP**
Position: **0, 0**

Date : **15/12/2017**
Cone no. : **S10CFIIP.S16082**
Project no. : **17052 / PDT**
CPT no. : **CPT01** **4/30**

CPT02 S 37° 37.833' / E 176° 02.758' Penetration depth 28 m

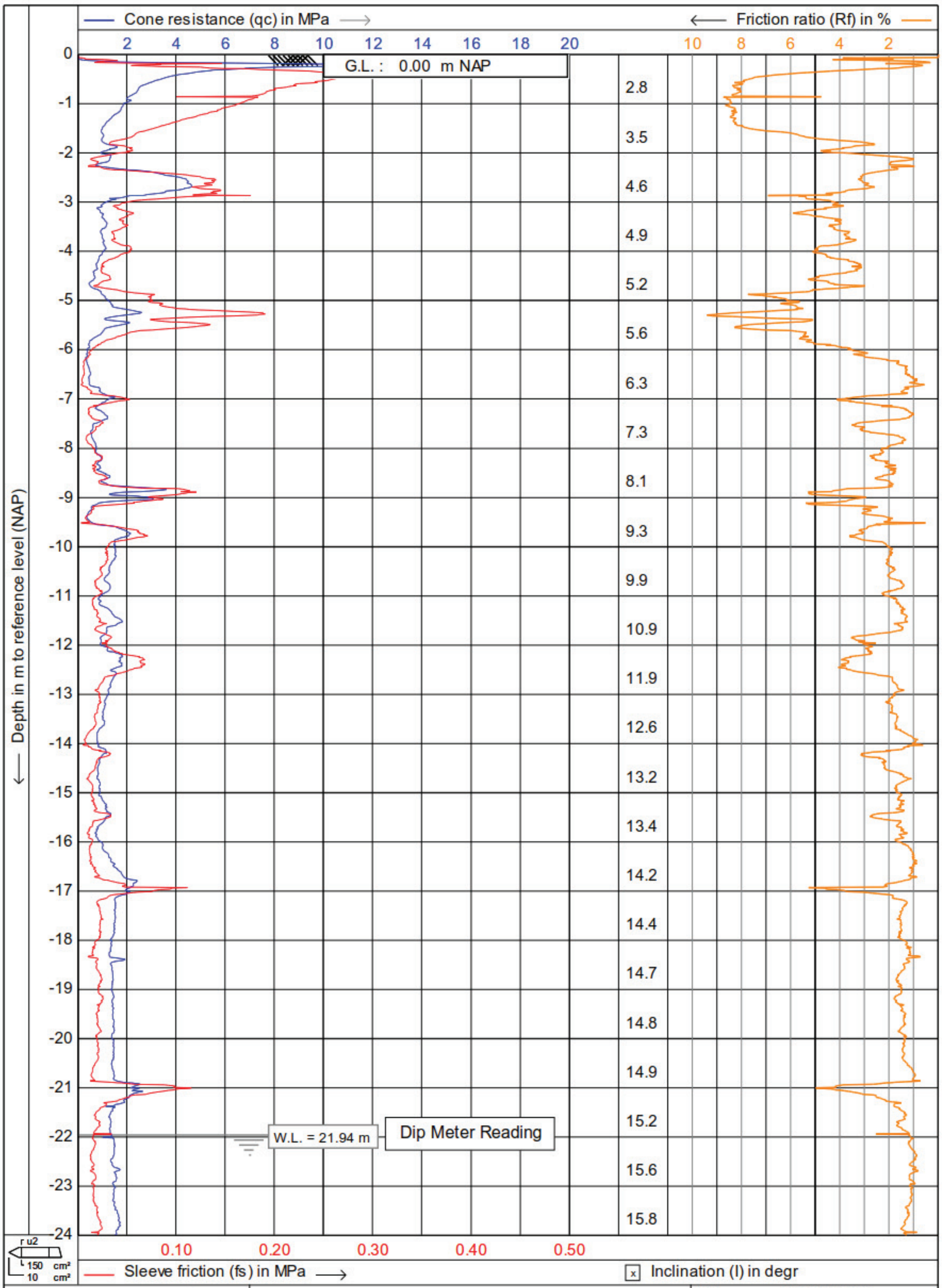

CONE PENETROMETER TESTING

ISO 22476-1:2012 Application class 2 Test type TE2

Project : **PROJECT DISSIPATION TEST**
Location: **OMOKOROA SLIP**
Position: **0, 0**

Date : **15/12/2017**
Cone no. : **S10CFIIP.S16082**
Project no. : **17052 / PDT**
CPT no. : **CPT02** **1/30**

1.47

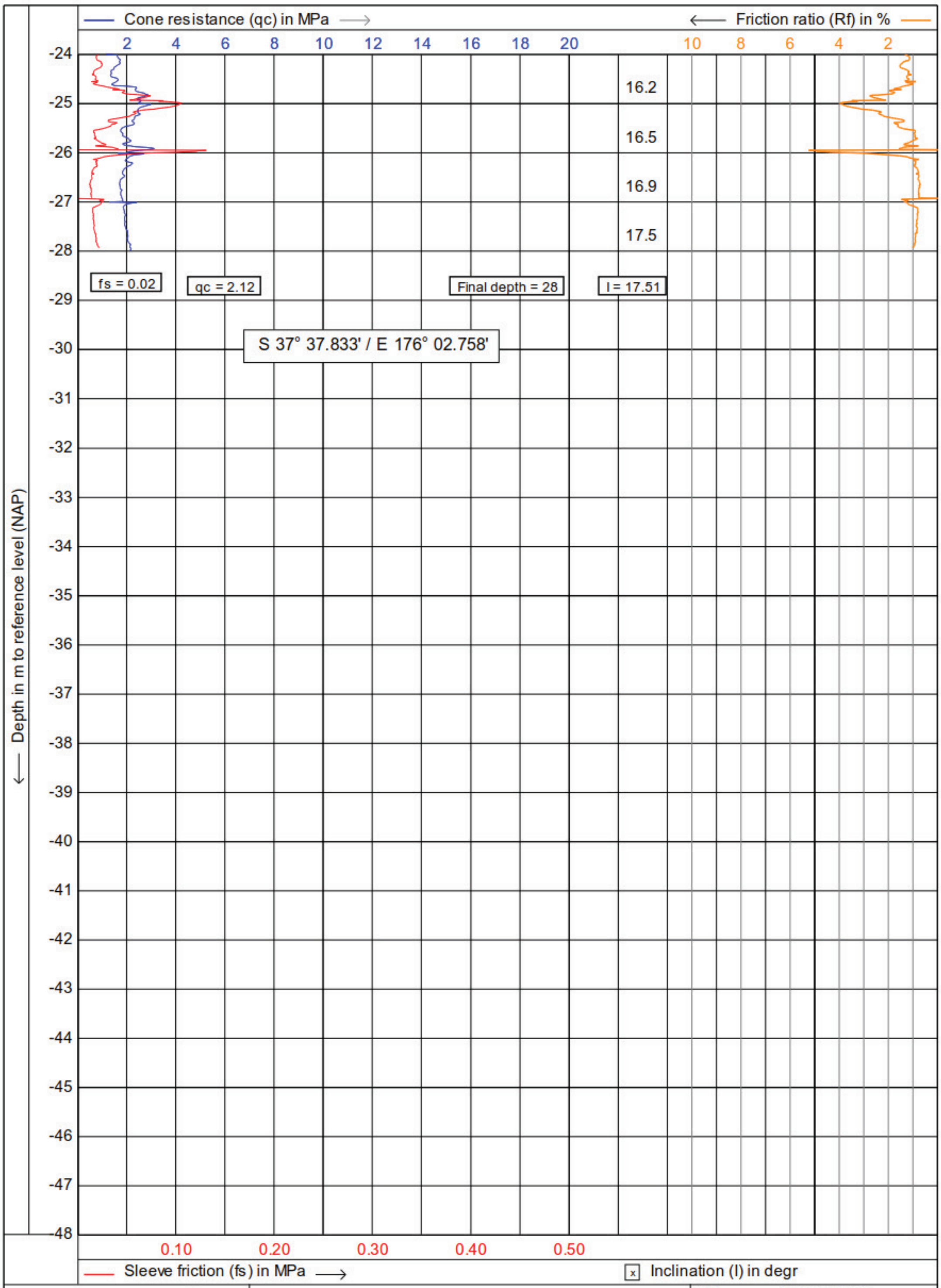

ISO 22476-1:2012 Application class 2 Test type TE2

Project : **PROJECT DISSIPATION TEST**
Location: **OMOKOROA SLIP**
Position: **0, 0**

Date : **15/12/2017**
Cone no. : **S10CFIIP.S16082**
Project no. : **17052 / PDT**
CPT no. : **CPT02** **2/30**

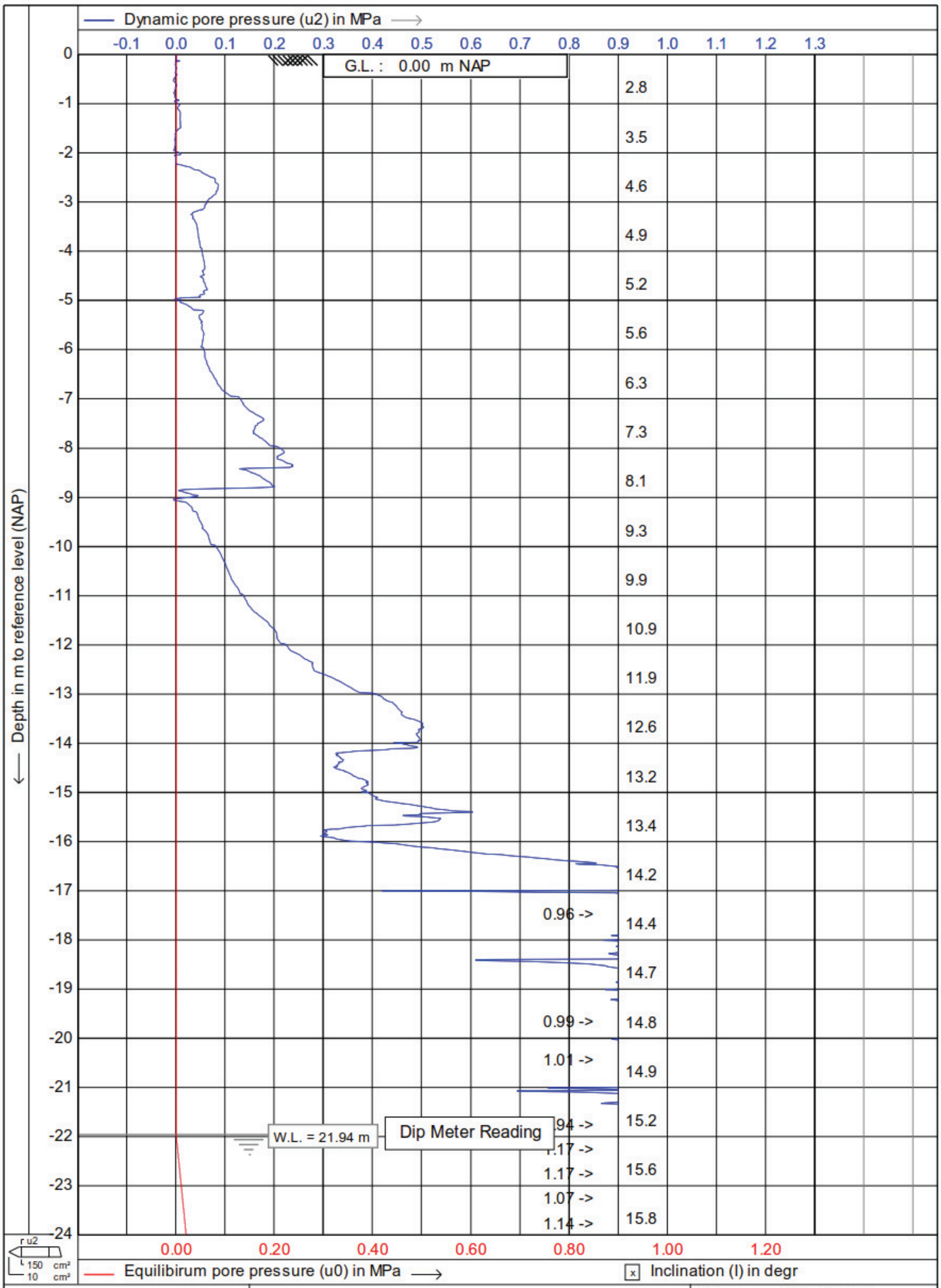

ISO 22476-1:2012 Application class 2 Test type TE2

Project : **PROJECT DISSIPATION TEST**

Location: **OMOKOROA SLIP**

Position: **0, 0**

Date : **15/12/2017**

Cone no. : **S10CFIIP.S16082**

Project no. : **17052 / PDT**

CPT no. : **CPT02** **3/30**

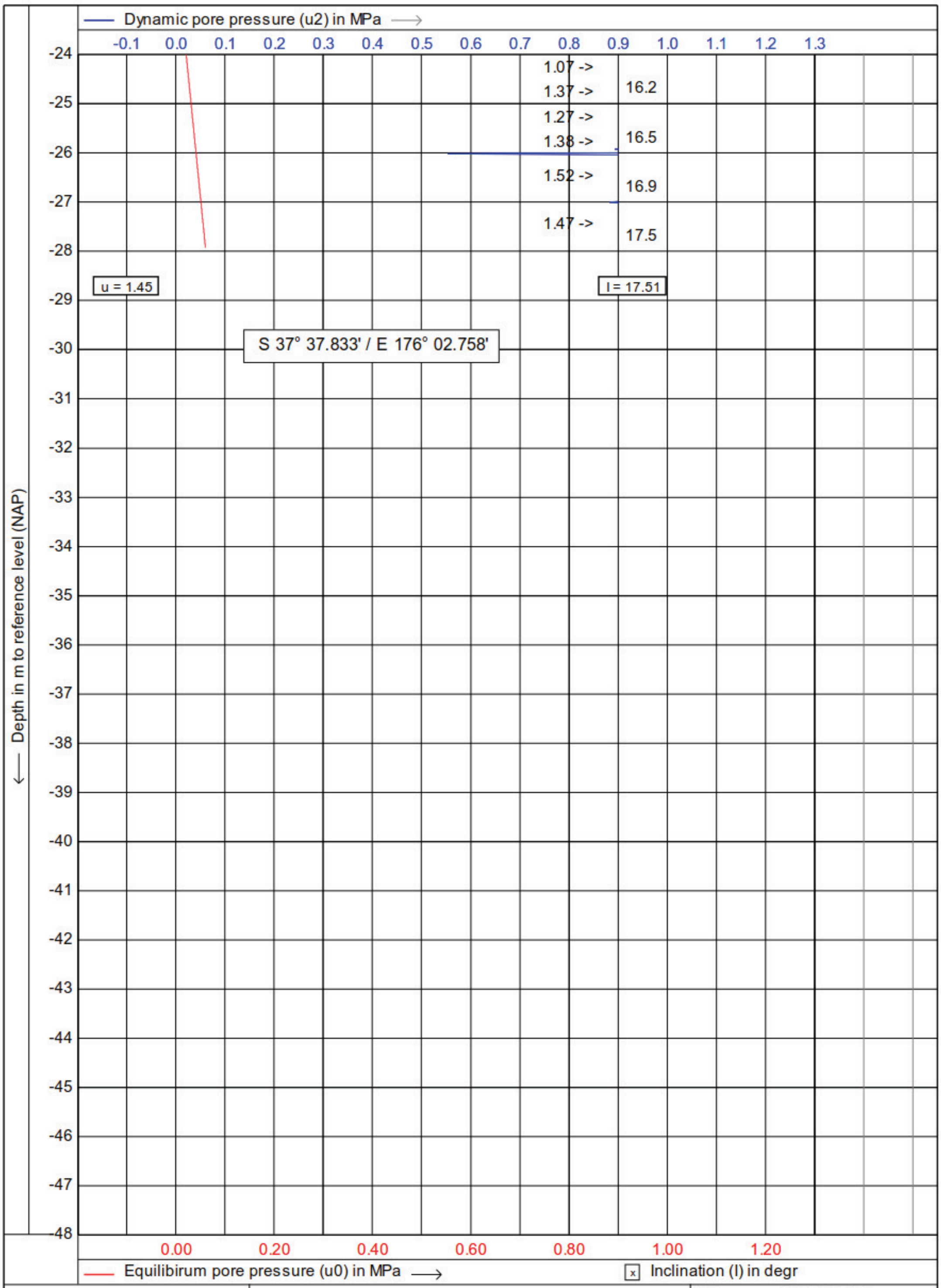

ISO 22476-1:2012 Application class 2 Test type TE2

Project : **PROJECT DISSIPATION TEST**
Location: **OMOKOROA SLIP**
Position: **0, 0**

Date : **15/12/2017**
Cone no. : **S10CFIIP.S16082**
Project no. : **17052 / PDT**
CPT no. : **CPT02** **4/30**

CPT03 S 37° 37.831' / E 176° 02.753' Penetration depth 26.52 m

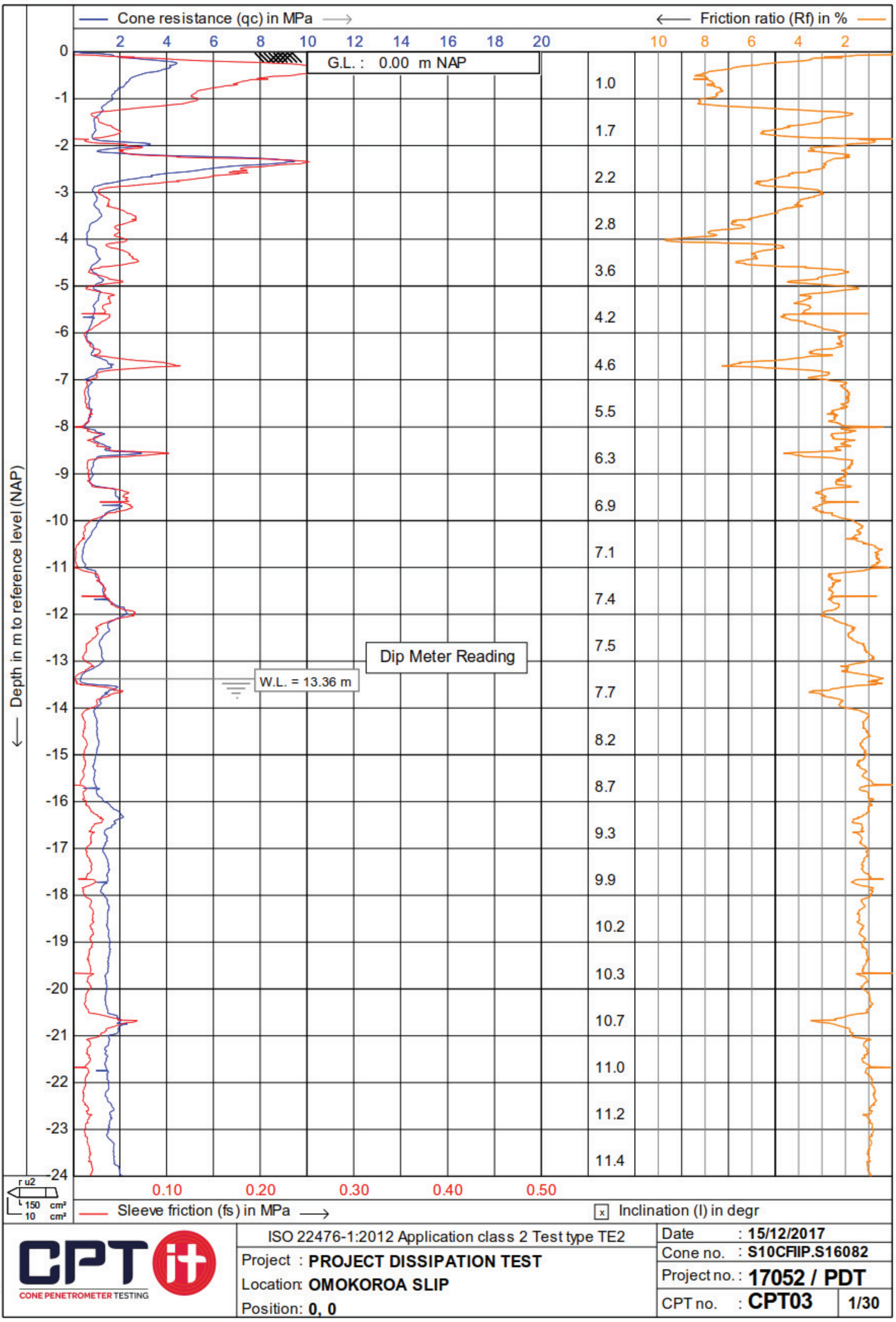

ISO 22476-1:2012 Application class 2 Test type TE2

Project : **PROJECT DISSIPATION TEST**

Location: **OMOKOROA SLIP**

Position: **0, 0**

Date : **15/12/2017**

Cone no. : **S10CFIIP.S16082**

Project no. : **17052 / PDT**

CPT no. : **CPT03** **1/30**

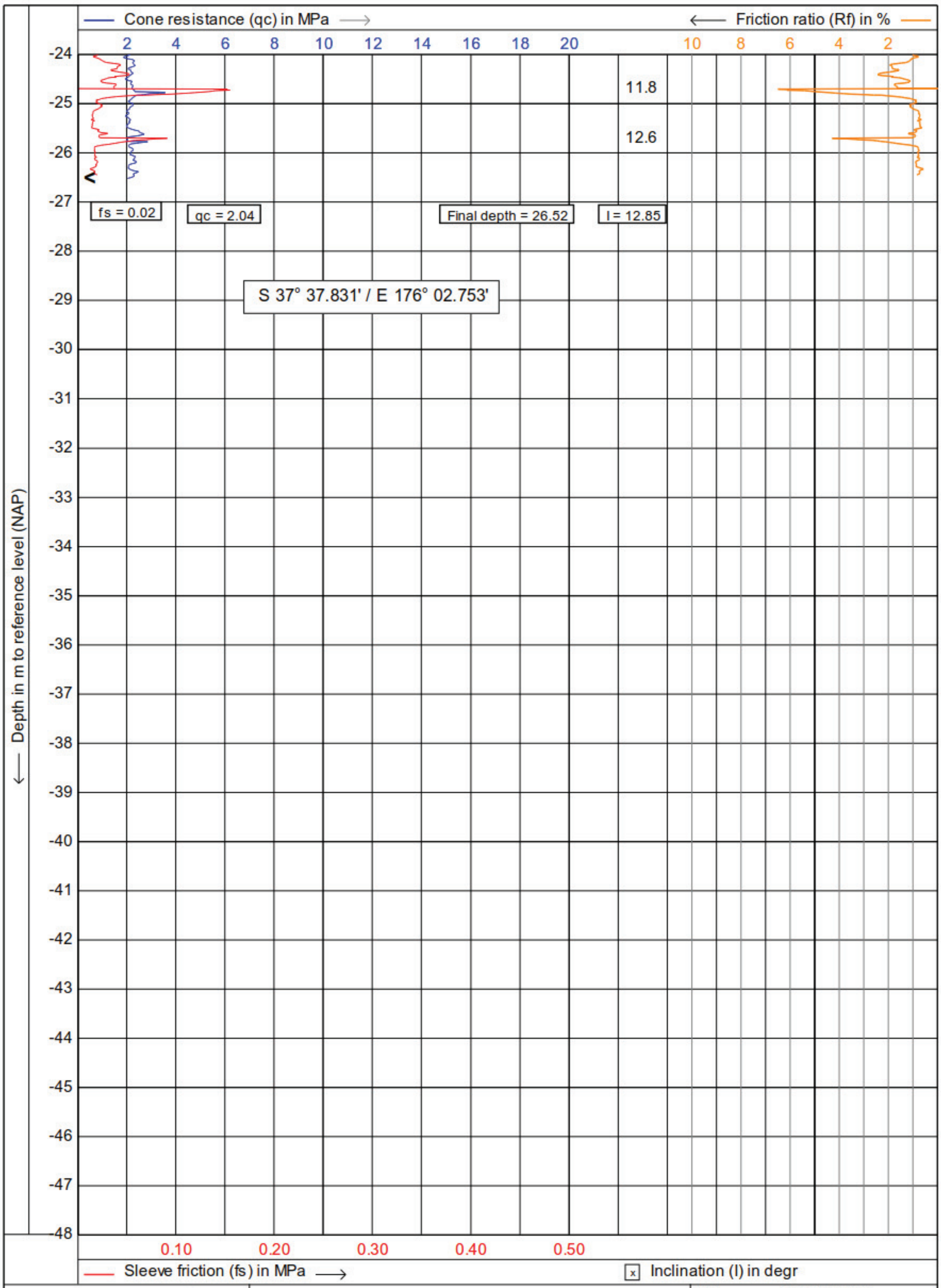

CPT it
CONE PENETROMETER TESTING

ISO 22476-1:2012 Application class 2 Test type TE2

Project : **PROJECT DISSIPATION TEST**
Location: **OMOKOROA SLIP**
Position: **0, 0**

Date : **15/12/2017**
Cone no. : **S10CFIIP.S16082**
Project no. : **17052 / PDT**
CPT no. : **CPT03** **2/30**

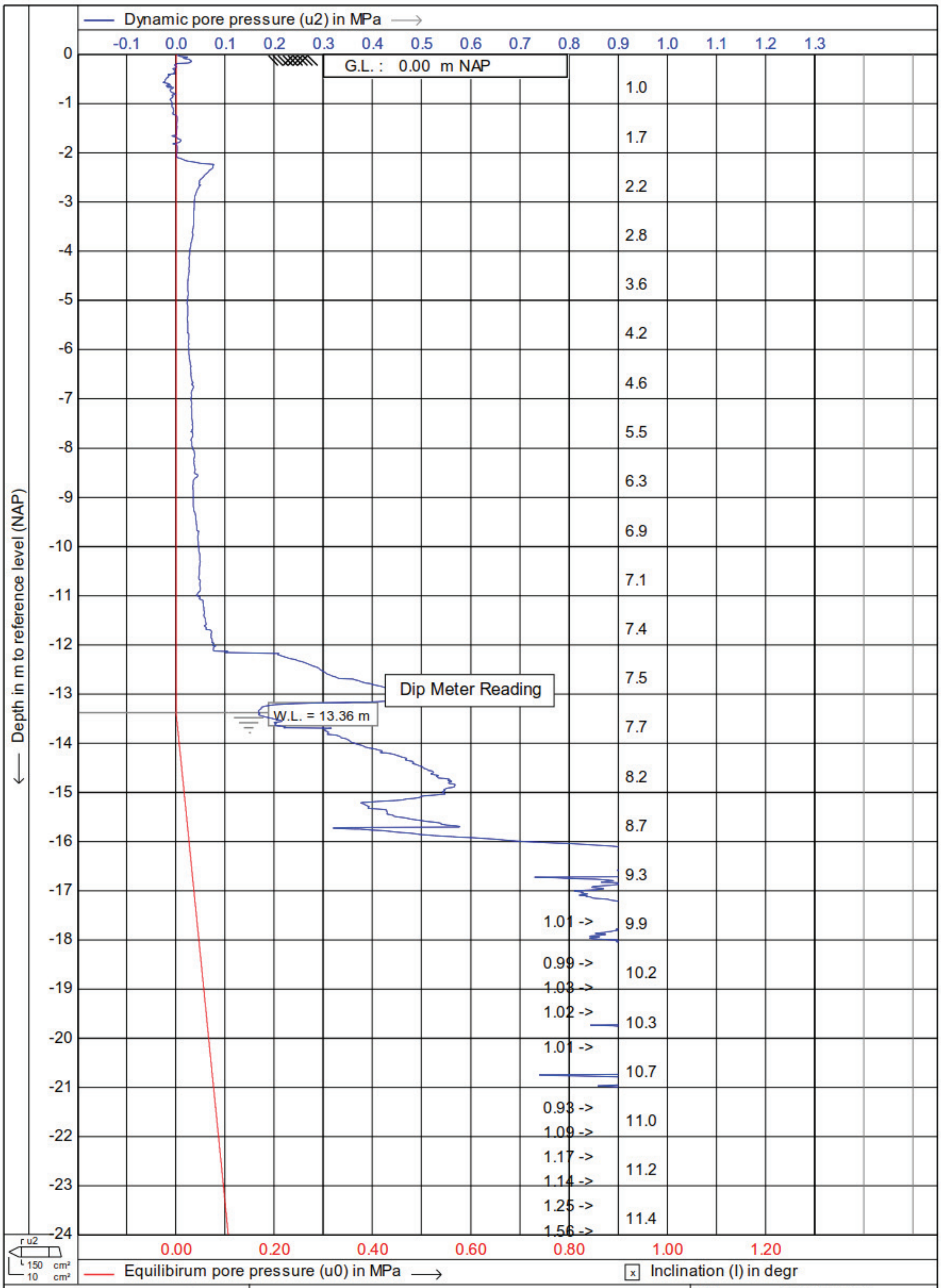

CPT it CONE PENETROMETER TESTING

ISO 22476-1:2012 Application class 2 Test type TE2

Project : **PROJECT DISSIPATION TEST**

Location: **OMOKOROA SLIP**

Position: **0, 0**

Date : **15/12/2017**

Cone no. : **S10CFIIP.S16082**

Project no. : **17052 / PDT**

CPT no. : **CPT03** **3/30**

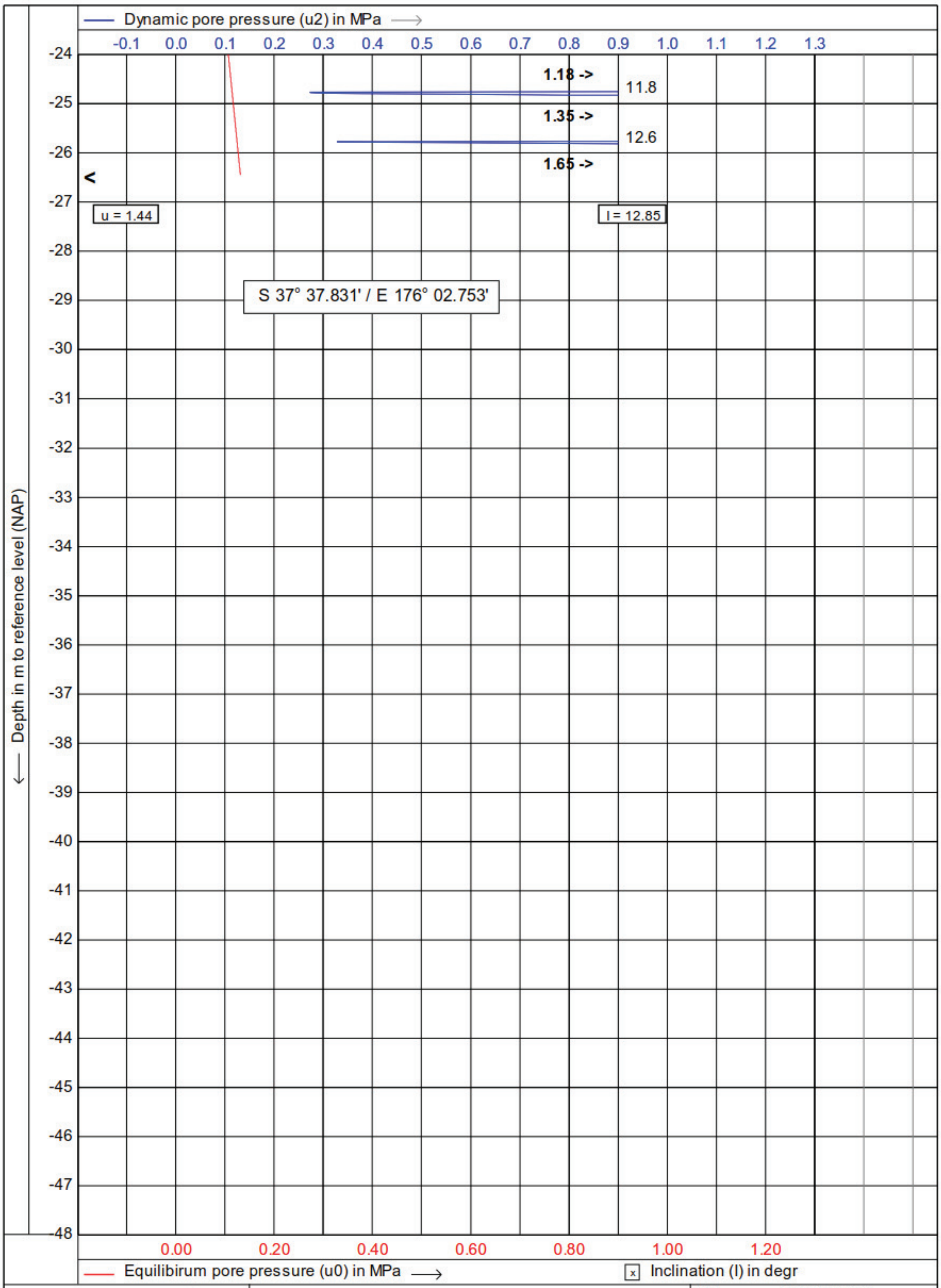

CONE PENETROMETER TESTING

ISO 22476-1:2012 Application class 2 Test type TE2

Project : **PROJECT DISSIPATION TEST**
Location: **OMOKOROA SLIP**
Position: **0, 0**

Date : **15/12/2017**
Cone no. : **S10CFIIP.S16082**
Project no. : **17052 / PDT**
CPT no. : **CPT03** **4/30**

Test number 1

Ubegin : 1.392 MPa

Uo : 0.132 MPa

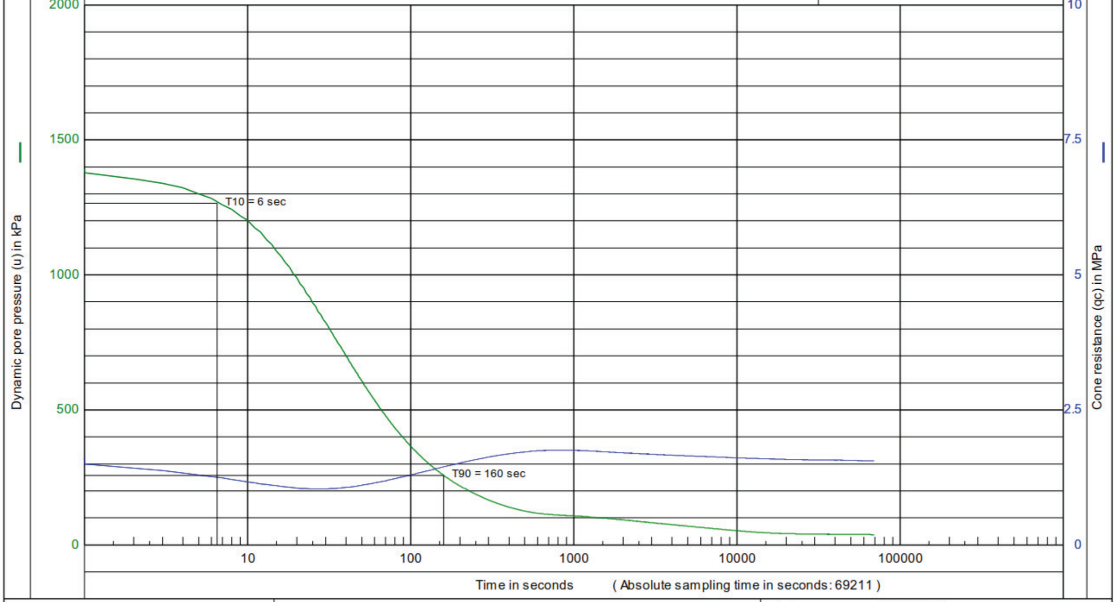

CONE PENETROMETER TESTING

ISO 22476-1:2012 Application class 2 Test type TE2

Project : PROJECT DISSIPATION TEST

Location : OMOKOROA SLIP

Date : 15/12/2017
Project no. : 17052 / PDT
CPT no. : CPT03
Test depth : 26.52 [m] - G.L.
Water level : -13.36 [m] - G.L.

CPT04 S 37° 37.831' / E 176° 02.755' Penetration depth 30.83 m

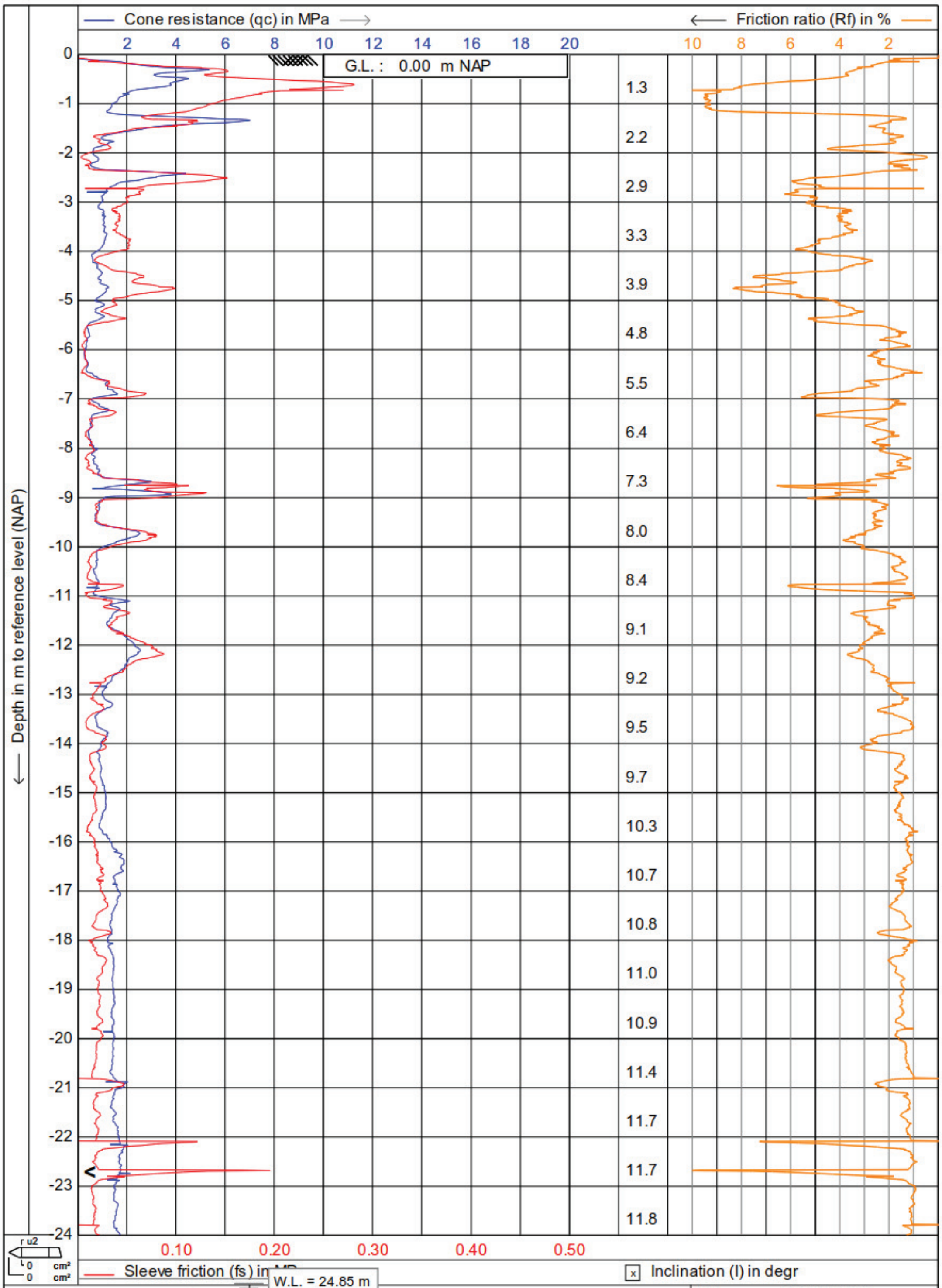

ISO 22476-1:2012 Application class 2 Test type TE2

Project : **PROJECT DISSIPATION TEST**
Location: **OMOKOROA SLIP**
Position: **0, 0**

Date : **16/12/2017**
Cone no. : **S10CFIIP.S16082**
Project no. : **17052 / PDT**
CPT no. : **CPT04** **1/30**

CPT it
CONE PENETROMETER TESTING

1.47

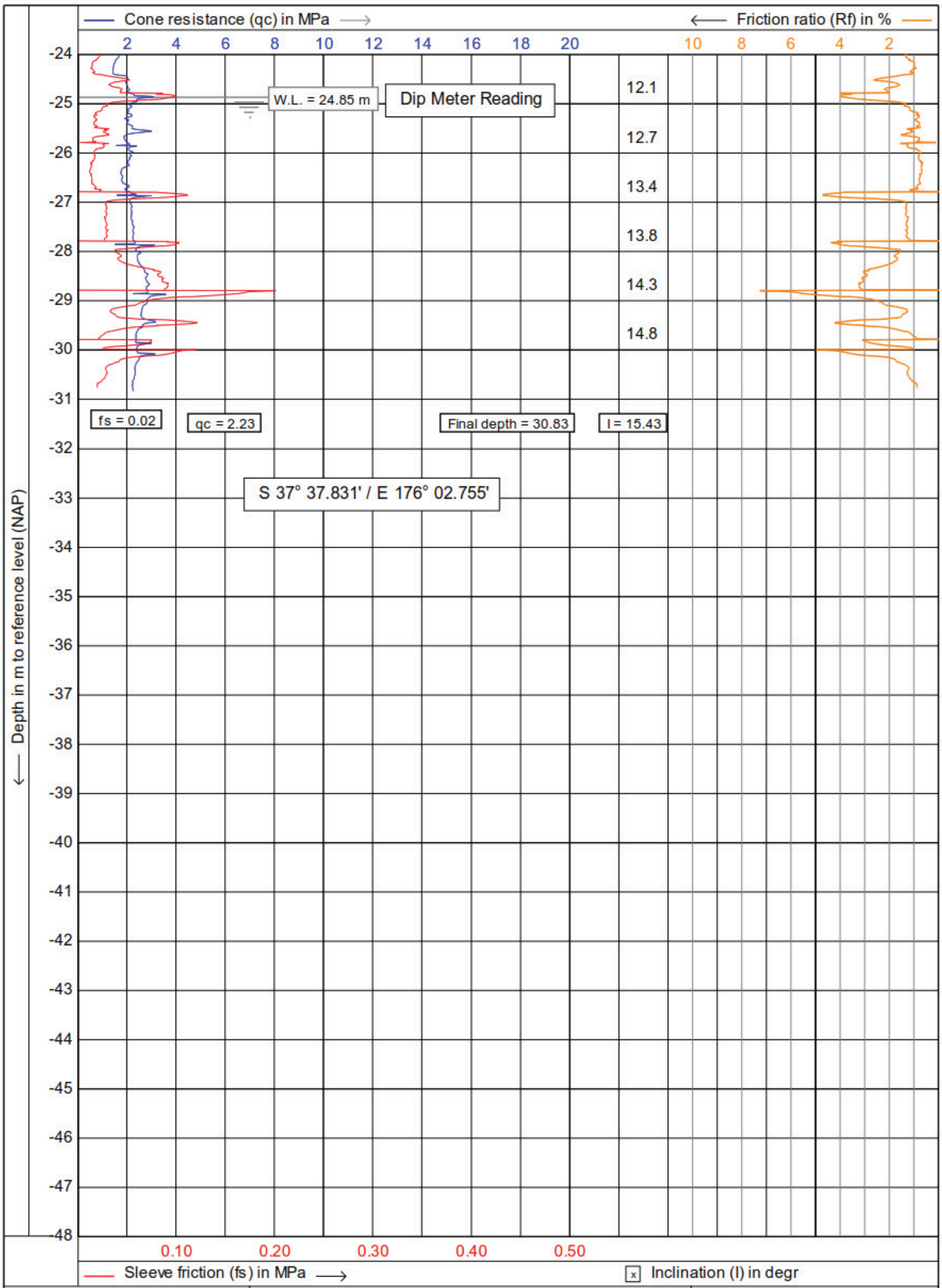

CONE PENETROMETER TESTING

ISO 22476-1:2012 Application class 2 Test type TE2

Project : **PROJECT DISSIPATION TEST**

Location: **OMOKOROA SLIP**

Position: **0, 0**

Date : **16/12/2017**

Cone no. : **S10CFIIP.S16082**

Project no. : **17052 / PDT**

CPT no. : **CPT04** **2/30**

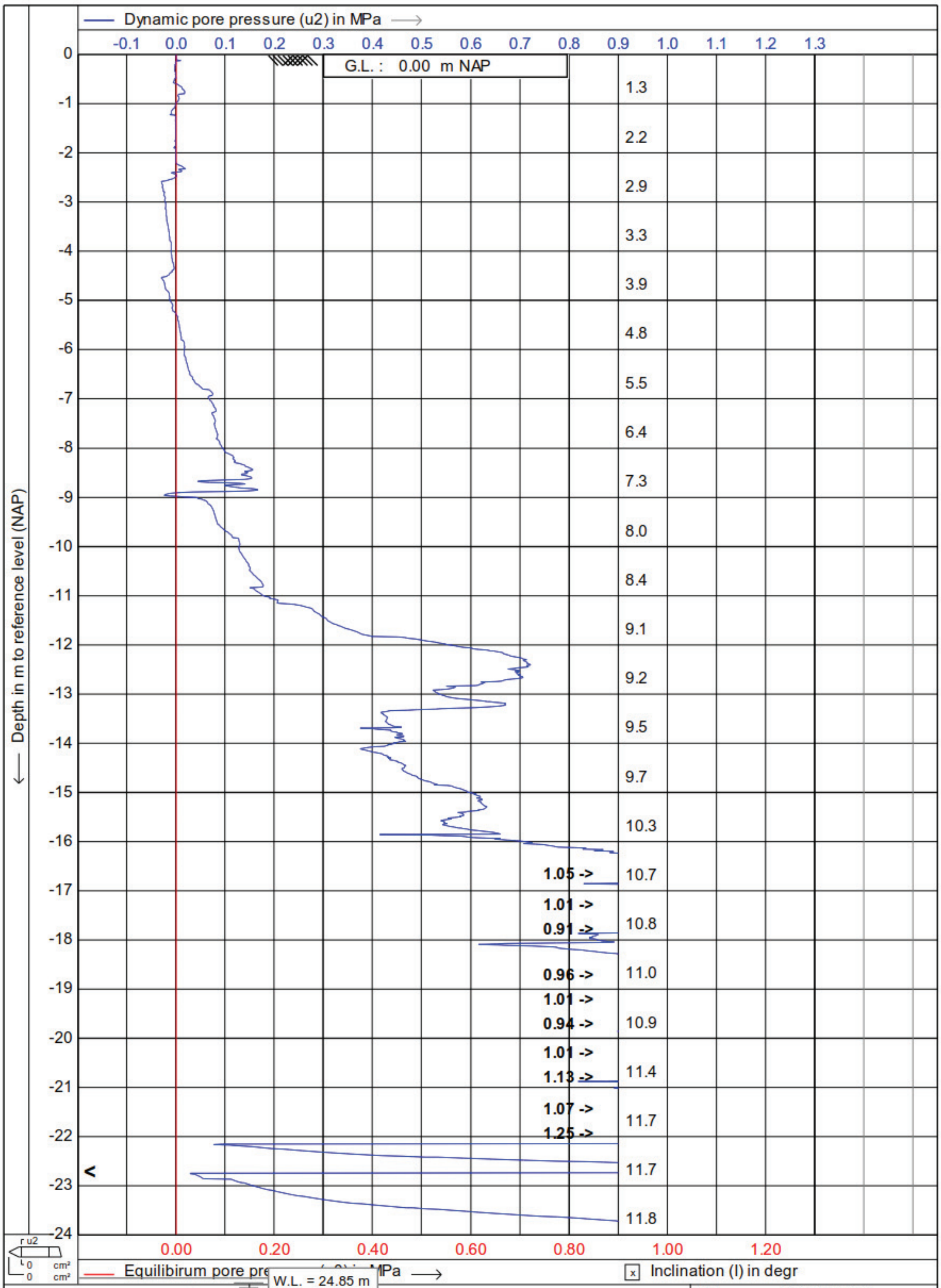

ISO 22476-1:2012 Application class 2 Test type TE2

Project : **PROJECT DISSIPATION TEST**
Location: **OMOKOROA SLIP**
Position: **0, 0**

Date : **16/12/2017**
Cone no. : **S10CFIIP.S16082**
Project no. : **17052 / PDT**
CPT no. : **CPT04** **3/30**

1.47

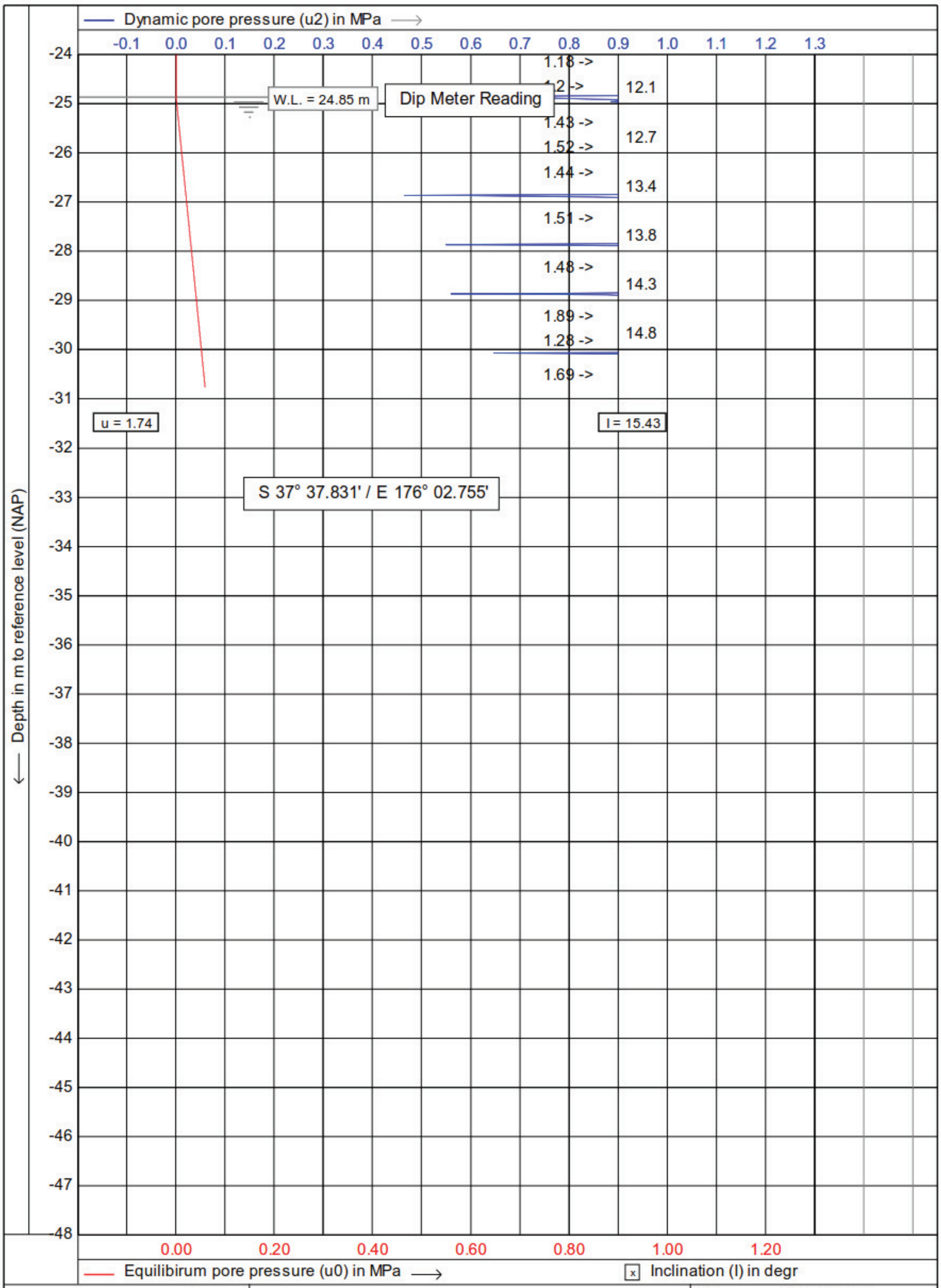

CPT it CONE PENETROMETER TESTING

ISO 22476-1:2012 Application class 2 Test type TE2

Project : **PROJECT DISSIPATION TEST**	Date : **16/12/2017**		
Location: **OMOKOROA SLIP**	Cone no. : **S10CFIIP.S16082**		
	Project no. : **17052 / PDT**		
Position: **0, 0**	CPT no. : **CPT04**	**4/30**	

Test number 02

Ubegin : 1.166 MPa
Uo : -0.021 MPa

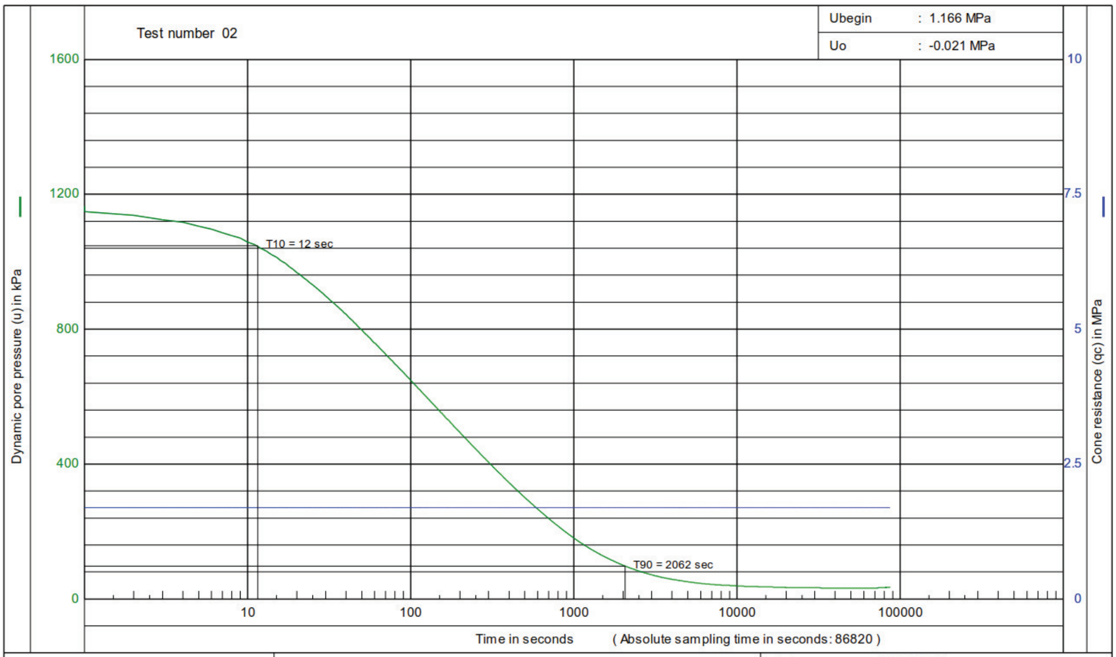

ISO 22476-1:2012 Application class 2 Test type TE2

Project : PROJECT DISSIPATION TEST
Location : OMOKOROA SLIP

Date : 16/12/2017
Project no. : 17052 / PDT
CPT no. : CPT04
Test depth : 22.72 [m] - G.L.
Water level : -24.85 [m] - G.L.

CPT05 S 37° 37.830' / E 176° 02.757' Penetration depth 19.77 m

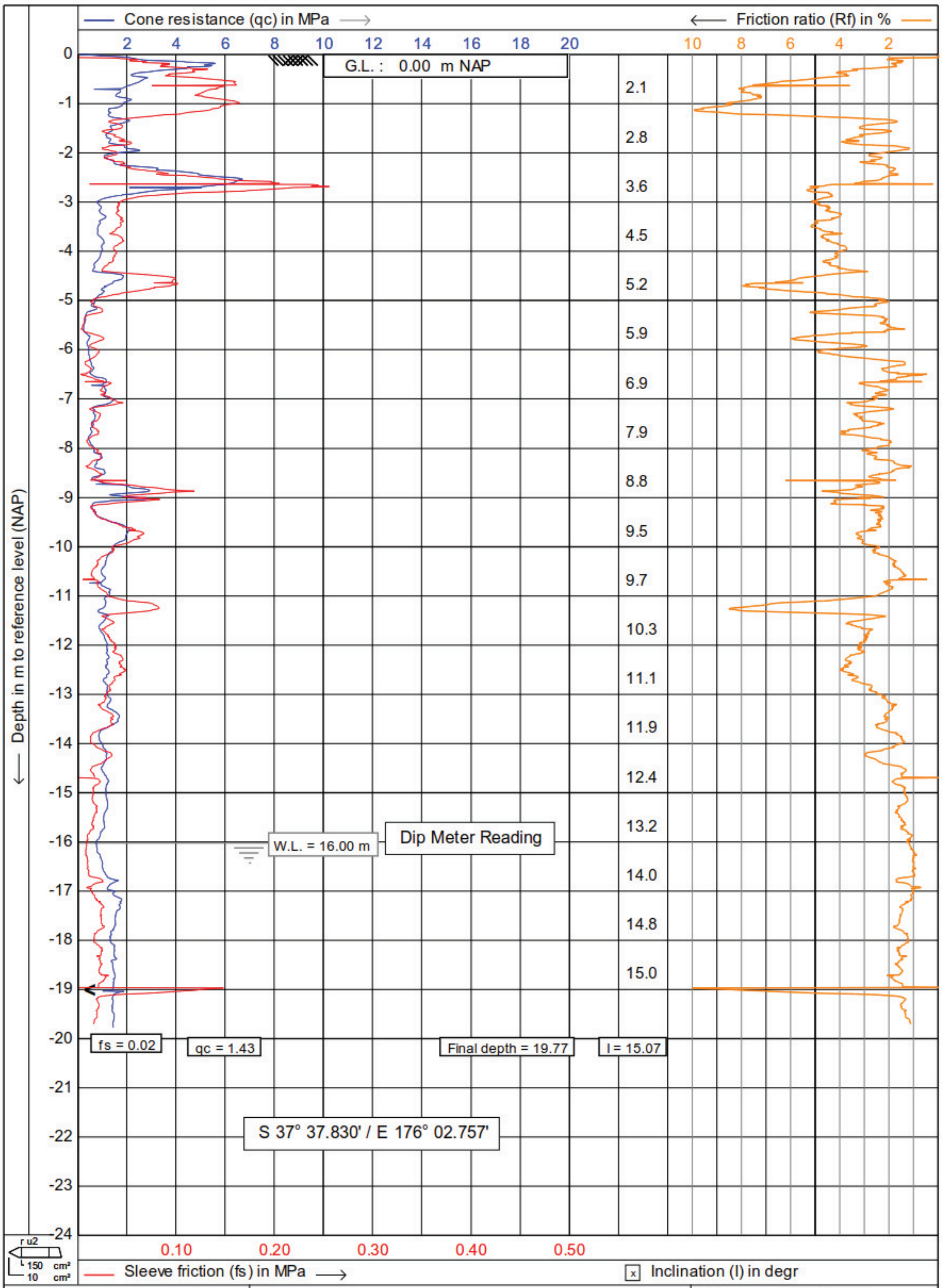

CPT it CONE PENETROMETER TESTING

ISO 22476-1:2012 Application class 2 Test type TE2

Project : **PROJECT DISSIPATION TEST**
Location: **OMOKOROA SLIP**
Position: **0, 0**

Date : **17/12/2017**
Cone no. : **S10CFIIP.S16082**
Project no. : **17052 / PDT**
CPT no. : **CPT05** **1/15**

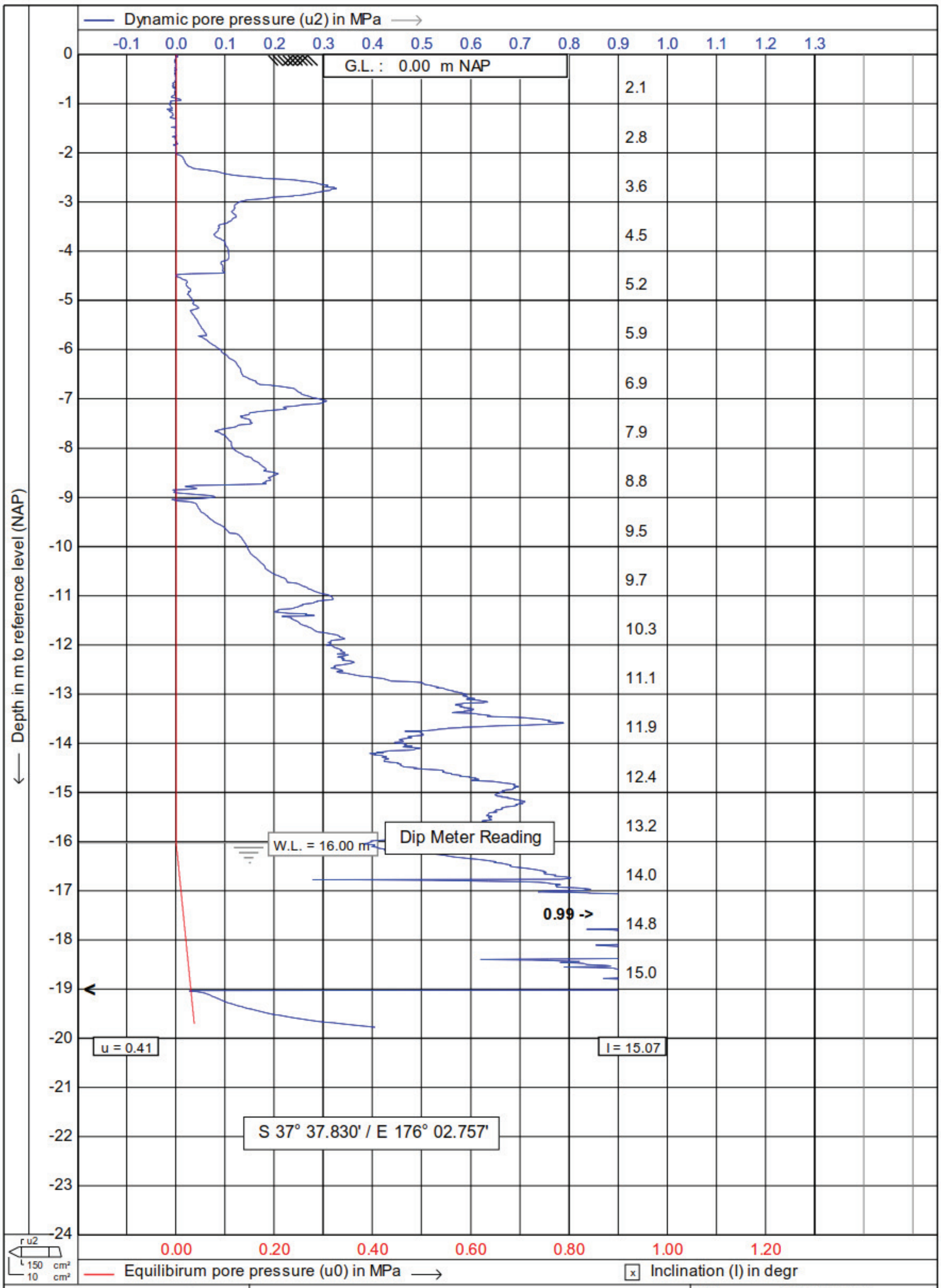

CPT it CONE PENETROMETER TESTING

ISO 22476-1:2012 Application class 2 Test type TE2

Project : **PROJECT DISSIPATION TEST**
Location: **OMOKOROA SLIP**
Position: **0, 0**

Date	: **17/12/2017**
Cone no.	: **S10CFIIP.S16082**
Project no. :	**17052 / PDT**
CPT no.	: **CPT05** **2/15**

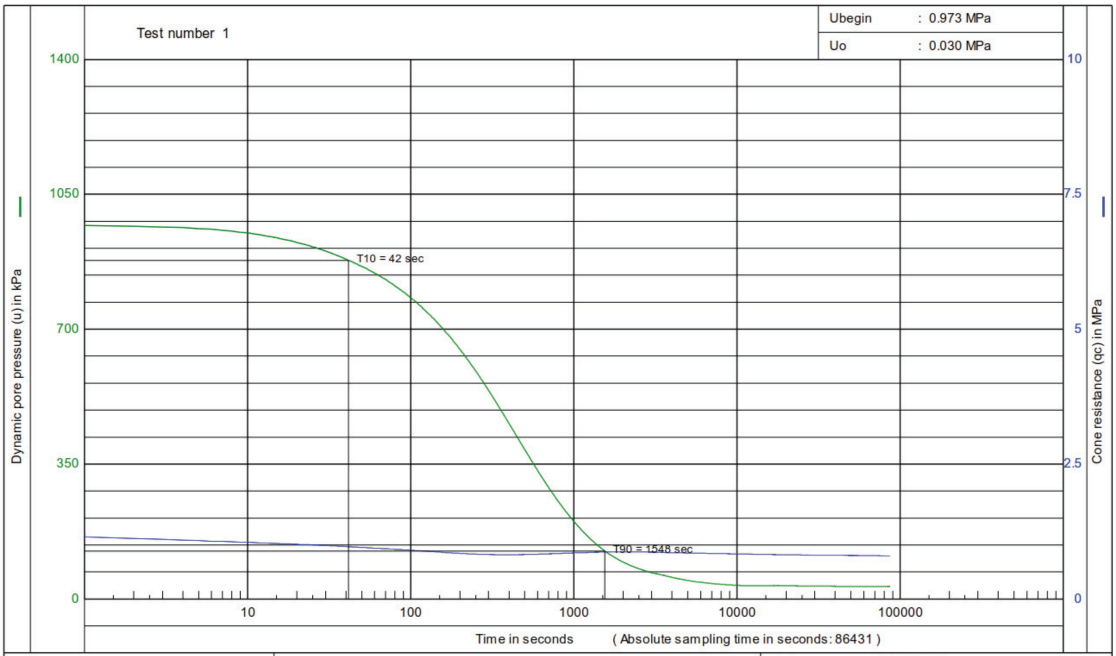

ISO 22476-1:2012 Application class 2 Test type TE2

Project : PROJECT DISSIPATION TEST
Location : OMOKOROA SLIP

Date : 17/12/2017
Project no. : 17052 / PDT
CPT no. : CPT05
Test depth : 19.02 [m] - G.L.
Water level : -16.00 [m] - G.L.

References

1. 18122, D., 2000. Din Deutsche Institut Für Normung E. V., Zustandsgrenzen (Konsitenzgrenzen). Beuth, Berlin.

2. Albatal, A., Stark, N., 2017. Rapid Sediment Mapping and in Situ Geotechnical Characterization in Challenging Aquatic Areas. Limnology and Oceanography: Methods, V. 15, No. 8, p. 690-705, doi# doi.org/10.1002/lom3.10192.

3. Alongi, D.M., 2008. Mangrove Forests: Resilience, Protection from Tsunamis, and Responses to Global Climate Change. Estuarine, Coastal and Shelf Science, V. 76, No. 1, p. 1-13, doi# doi.org/10.1016/j.ecss.2007.08.024.

4. Aubeny, C., Shi, H., 2006. Interpretation of Impact Penetration Measurements in Soft Clays. Journal of geotechnical and geoenvironmental engineering, V. 132, No. 6, p. 770-777, doi# doi.org/10.1061/(ASCE)1090-0241(2006)132:6(770).

5. Baligh, M.M., Levadoux, J.-N., 1986. Consolidation after Undrained Piezocone Penetration. Ii: Interpretation. Journal of Geotechnical Engineering, V. 112, No. 7, p. 727-745, doi# doi.org/10.1061/(ASCE)0733-9410(1986)112:7(727).

6. Barentsen, P., 1936. Short Description of a Field Testing Method with Cone-Shaped Sounding Apparatus, Proceedings 1st International Conference on Soil Mechanics and Foundation Engineering, pp. 6-10.

7. Begemann, H., 01 August 2018. The Friction Jacket Cone as an Aid in Determining the Soil Profile, Proceedings of the 6th International Conference on Soil Mechanics and Foundation Engineering, ICSMFE, Montreal, September. Springer, Cham, pp. 8-15.

8. Begemann, H., 1953. Improved Method of Determining Resistance to Adhesion by Sounding through a Loose Sleeve Placed Behind the Cone, Proceedings of the 3rd International Conference on Soil Mechanics and Foundation Engineering, ICSMFE, August, Zurich, pp. 213-217.

9. Bennett, R.H., Hulbert, M.H., Meyer, M.M., Lavoie, D.M., Briggs, K.B., Lavoie, D.L., Baerwald, R.J., Chiou, W.A., 1996. Fundamental Response of Pore-Water Pressure to Microfabric and Permeability Characteristics: Eckernförde Bay. Geo-Marine Letters, V. 16, No. 3, p. 182-188, doi# 10.1007/bf01204507.

10. Bergen, K.J., Johnson, P.A., Maarten, V., Beroza, G.C., 2019. Machine Learning for Data-Driven Discovery in Solid Earth Geoscience. Science, V. 363, No. 6433, p., doi# doi.org/10.1126/science.aau0323

11. Biscontin, G., Pestana, J.M., 2001. Influence of Peripheral Velocity on Vane Shear Strength of an Artificial Clay. Geotechnical Testing Journal, V. 24, No. 4, p. 423-429, doi# doi.org/10.1520/GTJ11140J.

12. Bishop, R., Hill, R., Mott, N., 1945. The Theory of Indentation and Hardness Tests. Proceedings of the Physical Society, V. 57, No. 3, p. 147, doi# doi.org/10.1088/0959-5309/57/3/301.

13. Burns, S., Mayne, P., 1998. Monotonic and Dilatory Pore-Pressure Decay During Piezocone Tests in Clay. Canadian Geotechnical Journal, V. 35, No. 6, p. 1063-1073, doi# doi.org/10.1139/cgj-35-6-1063.

14. Burns, S.B., Mayne, P.W., 2002. Analytical Cavity Expansion-Critical State Model for Piezocone Dissipation in Fine-Grained Soils. Soils and Foundations, V. 42, No. 2, p. 131-137, doi# doi.org/10.3208/sandf.42.2_131.

15. Cahoon, D.R., Perez, B.C., Segura, B.D., Lynch, J.C., 2011. Elevation Trends and Shrink–Swell Response of Wetland Soils to Flooding and Drying. Estuarine, Coastal and Shelf Science, V. 91, No. 4, p. 463-474, doi# doi.org/10.1016/j.ecss.2010.03.022.

16. Casagrande, A., Fadum, R.E., 1940. Notes on Soil Testing for Engineering Purposes, in: Havard Graduate School of Engineering, S.M. (Ed.), Cambridge, Mass., p. 268.

17. Casagrande, A., Wilson, S., 1951. Effect of Rate of Loading on the Strength of Clays and Shales at Constant Water Content. Géotechnique, V. 2, No. 3, p. 251-263, doi# doi.org/10.1680/geot.1951.2.3.251.

18. Chilingar, G.V., 1964. Relationship between Porosity, Permeability, and Grain-Size Distribution of Sands and Sandstones, Developments in Sedimentology. Elsevier, p. 71-75, doi.org/10.1016/S0070-4571(08)70469-2.

19. Chow, S., O'Loughlin, C., Randolph, M., 2014. Soil Strength Estimation and Pore Pressure Dissipation for Free-Fall Piezocone in Soft Clay. Géotechnique, V. 64, No. 10, p. 817-827, doi# doi.org/10.1680/geot.14.P.107.

20. Chow, S., O'Loughlin, C., White, D., Randolph, M., 2017. An Extended Interpretation of the Free-Fall Piezocone Test in Clay. Géotechnique, V. 67, No. 12, p. 1090-1103, doi# doi.org/10.1680/jgeot.16.P.220.

21. Christophers, A.J., 2015. Paleogeographic Reconstruction of the Omokoroa Domain, Bay of Plenty, New Zealand. University of Waikato, p. 194.

22. Chung, S., Kweon, H., Jang, W., 2013. Hyperbolic Fit Method for Interpretation of Piezocone Dissipation Tests. Journal of geotechnical and geoenvironmental engineering, V. 140, No. 1, p. 251-254, doi# doi.org/10.1061/(ASCE)GT.1943-5606.0000967.

23. Cudmani, R., Osinov, V., 2001. The Cavity Expansion Problem for the Interpretation of Cone Penetration and Pressuremeter Tests. Canadian Geotechnical Journal, V. 38, No. 3, p. 622-638, doi# doi.org/10.1139/t00-124.

24. Dahdouh-Guebas, F., Jayatissa, L.P., Di Nitto, D., Bosire, J.O., Seen, D.L., Koedam, N., 2005. How Effective Were Mangroves as a Defence against the Recent Tsunami? Current biology, V. 15, No. 12, p. R443-R447, doi# doi.org/10.1016/j.cub.2005.06.008.

25. Dayal, U., Allen, J.H., 1973. Instrumented Impact Cone Penetrometer. Canadian Geotechnical Journal, V. 10, No. 3, p. 397-409, doi# doi.org/10.1139/t73-034.

26. Dayal, U., Allen, J.H., 1975. The Effect of Penetration Rate on the Strength of Remolded Clay and Sand Samples. Canadian Geotechnical Journal, V. 12, No. 3, p. 336-348, doi# doi.org/10.1139/t75-038.

27. de Ruiter, J., 1971. Electric Penetrometer for Site Investigations. Journal of the Soil Mechanics and Foundations Division, V. 97, No. 2, p. 457-472, doi# -.

28. DeJong, J.T., Randolph, M., 2012. Influence of Partial Consolidation During Cone Penetration on Estimated Soil Behavior Type and Pore Pressure Dissipation Measurements. Journal of geotechnical and geoenvironmental engineering, V. 138, No. 7, p. 777-788, doi# doi.org/10.1061/(ASCE)GT.1943-5606.0000646.

29. DIN, 2012. Din Deutsche Institut Für Normung E. V. Eindimensionaler Kompressionsversuch. Beuth, Berlin.

30. Dushi, A., 2006. Refurbishment of Louisiana State University Calibration Chamber. Louisiana State University and Agricultural and Mechanical College, p. 122.

31. Eyring, H., 1936. Viscosity, Plasticity, and Diffusion as Examples of Absolute Reaction Rates. The Journal of chemical physics, V. 4, No. 4, p. 283-291, doi# doi.org/10.1063/1.1749836.

32. Fiot, J., Gratiot, N., 2006. Structural Effects of Tidal Exposures on Mudflats Along the French Guiana Coast. Marine Geology, V. 228, No. 1-4, p. 25-37, doi# doi.org/10.1016/j.margeo.2005.12.009.

33. Gilman, E.L., Ellison, J., Duke, N.C., Field, C., 2008. Threats to Mangroves from Climate Change and Adaptation Options: A Review. Aquatic botany, V. 89, No. 2, p. 237-250, doi# doi.org/10.1016/j.aquabot.2007.12.009.

34. Gopinath, G., 2016. Application of Electric Cone Penetration Test in Unconsolidated and Consolidated Sediments. Procedia Technology, V. 24, No. -, p. 271-279, doi# doi.org/10.1016/j.protcy.2016.05.036.

35. Greenberg, J., 2017. Big Metadata, Smart Metadata, and Metadata Capital: Toward Greater Synergy between Data Science and Metadata. Journal of Data and Information Science, V. 2, No. 3, p. 19, doi# doi.org/10.1515/jdis-2017-0012.

36. Grey, C.E., Cooper, S.S., Malone, P.G., 1993. Method and Apparatus for in-Situ Detection and Determination of Soil Contaminants, https://patents.google.com/patent/US5246862A/en#patentCitations US Secretary of Army

37. Hamilton, E.L., 1964. Consolidation Characteristics and Related Properties of Sediments from Experimental Mohole (Guadalupe Site). Journal of Geophysical Research, V. 69, No. 20, p. 4257-4269, doi# doi.org/10.1029/JZ069i020p04257.

38. Hampton, M.A., Lee, H.J., Locat, J., 1996. Submarine Landslides. Reviews of Geophysics, V. 34, No. 1, p. 33-59, doi# doi.org/10.1029/95rg03287.

39. ISO, 2017. International Organization for Standardization Geotechnical Investigation and Testing - Laboratory Testing of Soil - Part 5: Incremental Loading Oedometer Test (Iso 17892-5:2017); , Geotechnical investigation and testing–Laboratory.

40. Jang, W., Chung, S., Kweon, H., 2015. Estimation of Coefficients of Consolidation and Permeability Via Piezocone Dissipation Tests. KSCE Journal of Civil Engineering, V. 19, No. 3, p. 621-630, doi# doi.org/10.1007/s12205-013-1418-2.

41. Jorat, M., Kreiter, S., Mörz, T., Moon, V., De Lange, W., 2014. Utilizing Cone Penetration Tests for Landslide Evaluation, Submarine Mass Movements and Their Consequences. Springer, Cham, p. 55-71, doi.org/10.1007/978-3-319-00972-8_6.

42. Jorat, M., Mörz, T., Schunn, W., Kreiter, S., Moon, V., de Lange, W., 2014a. Geotechnical Off-Shore Seabed Tool (Gost): Cptu Measurements and Operations in New Zealand CPT'14, V. -, No. -, p. 217-223, doi# -.

43. Jorat, M., Mörz, T., Schunn, W., Kreiter, S., Moon, V.G., de Lange, W.P., 2014b. Geotechnical Offshore Seabed Tool (Gost): Cptu Measurements and Operations in New Zealand, CPT'14. 3rd International Symposium on Cone Penetration Testing, pp. 217-223.

44. Joussein, E., Petit, S., Churchman, J., Theng, B., Righi, D., Delvaux, B., 2005. Halloysite Clay Minerals–a Review. Clay minerals, V. 40, No. 4, p., doi# doi.org/10.1180/0009855054040180.

45. Kantorowicz, J., 1990. The Influence of Variations in Illite Morphology on the Permeability of Middle Jurassic Brent Group Sandstones, Cormorant Field, Uk North Sea. Marine and Petroleum Geology, V. 7, No. 1, p. 66-74, doi# doi.org/10.1016/0264-8172(90)90057-N.

46. Karpatne, A., Ebert-Uphoff, I., Ravela, S., Babaie, H.A., Kumar, V., 2018. Machine Learning for the Geosciences: Challenges and Opportunities. IEEE Transactions on Knowledge and Data Engineering, V. 31, No. 8, p. 1544 - 1554 doi# doi.org/10.1109/TKDE.2018.2861006.

47. Kathiresan, K., Rajendran, N., 2005. Coastal Mangrove Forests Mitigated Tsunami. Estuarine, Coastal and Shelf Science, V. 65, No. 3, p. 601-606, doi# doi.org/10.1016/j.ecss.2005.06.022.

48. Keaveny, J., 1985. In-Situ Determination of Drained and Undrained. University of California, Berkeley.

49. Kluger, M., Kreiter, S., Moon, V., Orense, R., Mills, P., Mörz, T., 2019. Undrained Cyclic Shear Behaviour of Weathered Tephra. Géotechnique, V. 69, No. 6, p. 489-500, doi# doi.org/10.1680/jgeot.17.P.083.

50. Kluger, M., Moon, V., Kreiter, S., Lowe, D., Churchan, G., Hepp, D., Seibel, D., Jorat, M., Moerz, T., 2017. A New Attraction-Detachment Model for Explaining Flow Sliding in Clay-Rich Tephras. Geology, V. 42, No. 2, p. 131-134, doi# doi:10.1130/G38560.1.

51. Kluger, M.O., Jorat, M.E., Moon, V.G., Kreiter , S., de Lange, W., Mörz, T., Robertson, T., Lowe, D.J., 2019. Rainfall Threshold for Initiating Effective Stress Decrease and Failure in Weathered Tephra Slopes. Landslides, V. doi:10.1007/s10346-019-01289-2, No., p. 1-15, doi# doi:10.1007/s10346-019-01289-2.

52. Koizumi, Y., Lee, J., Yokota, Y., Yamamoto, T., Fujisawa, K., 2010. Numerical Analysis of Landslide Behavior Induced by Tunnel Excavation, ISRM International Symposium-EUROCK 2010. International Society for Rock Mechanics and Rock Engineering, Lausanne, Switzerland.

53. Kopf, A., Stegmann, S., Krastel, S., Förster, A., Strasser, M., Irving, M., 2007. Marine Deep-Water Free-Fall Cpt Measurements for Landslide Characterisation Off Crete, Greece (Eastern Mediterranean Sea) Part 2: Initial Data from the Western Cretan Sea, Submarine Mass Movements and Their Consequences. Springer, p. 199-208, doi.org/10.1007/978-1-4020-6512-5_21.

54. Krage, C., DeJong, J., Schnaid, F., 2014. Estimation of the Coefficient of Consolidation from Incomplete Cone Penetration Test Dissipation Tests. Journal of geotechnical and geoenvironmental engineering, V. 141, No. 2, p., doi# doi.org/10.1061/(ASCE)GT.1943-5606.0001218.

55. Krastel, S., Braeunig, A., Feldens, P., Georgiopoulou, A., Jaehmlich, H., Lange, M., Lindhorst, K., Llopart, J., Mader, S., Mehringer, L., Merl, M., Muecke, I., Renkl, C., Roskoden, R., Schoenke, M., Schulten, I., Schwarz, J.-P., Stevenson, C., Vallee, M., Wegener, B., Wiesenberg, L., 2016. Geomorphology, Processes and Geohazards of Giant Submarine Landslides and Tsunami Generation Capacity, as Recorded in the Sedimentary Record of the Only Historic Slide of This Kind: The 1929 Grand Banks Landslide of the Canadian Atlantic Continental Margin - Cruise No. Msm47 - September 30 - October 30, 2015 - St. John's (Canada) - Ponta Delgada, Azores (Portugal). MARIA S. MERIAN-Berichte, V. doi.org/10.2312/cr_msm47 No., p. 55, doi# doi.org/10.2312/cr_msm47

56. Kurup, P., Voyiadjis, G., Tumay, M., 1994. Calibration Chamber Studies of Piezocone Test in Cohesive Soils. Journal of Geotechnical Engineering, V. 120, No. 1, p. 81-107, doi# doi.org/10.1061/(ASCE)0733-9410(1994)120:1(81).

57. Lary, D.J., Alavi, A.H., Gandomi, A.H., Walker, A.L., 2016. Machine Learning in Geosciences and Remote Sensing. Geoscience Frontiers, V. 7, No. 1, p. 3-10, doi# doi.org/10.1016/j.gsf.2015.07.003.

58. Leroueil, S., Kabbaj, M., Tavenas, F., Bouchard, R., 1985. Stress–Strain–Strain Rate Relation for the Compressibility of Sensitive Natural Clays. Géotechnique, V. 35, No. 2, p. 159-180, doi# doi.org/10.1680/geot.1985.35.2.159.

59. Lohr, S., 2013. The Origins of ‘Big Data': An Etymological Detective Story, The New York Times. Arthur Ochs Sulzberger.

60. Lovelock, C.E., Cahoon, D.R., Friess, D.A., Guntenspergen, G.R., Krauss, K.W., Reef, R., Rogers, K., Saunders, M.L., Sidik, F., Swales, A., 2015. The Vulnerability of Indo-Pacific Mangrove Forests to Sea-Level Rise. Nature, V. 526, No. 7574, p. 559, doi# doi.org/10.1038/nature15538

61. Lu, Q., Randolph, M., Hu, Y., Bugarski, I., 2004. A Numerical Study of Cone Penetration in Clay. Géotechnique, V. 54, No. 4, p. 257-267, doi# doi.org/10.1680/geot.2004.54.4.257.

62. Lucking, G., Stark, N., Lippmann, T., Smyth, S., 2017. Variability of in Situ Sediment Strength and Pore Pressure Behavior of Tidal Estuary Surface Sediments. Geo-Marine Letters, V. doi.org/10.1007/s00367-017-0494-6, No. 37, p. pages441–456 doi# doi.org/10.1007/s00367-017-0494-6.

63. Lunne, T., Powell, J.J., Robertson, P.K., 2002. Cone Penetration Testing in Geotechnical Practice. CRC Press.

64. Lunne, T., Powell, J.J.M., Robertson, P.K., 1997. Cone Penetration Testing in Geotechnical Practice. Taylor & Francis.

65. Lunne, T., Robertson, P., Powell, J., 1997. Cone Penetration Testing. Taylor & Francis.

66. Massarsch, K., 2014. Cone Penetration Testing—a Historic Perspective, Proceedings 3rd international symposium on cone penetration testing. , Las Vegas, Nevada, USA, pp. 97-134.

67. May, R.E., 1987. A Study of the Piezocone Penetrometer in Normally Consolidated Clay. University of Oxford, Oxford, p. 264.

68. McIvor, A., Spencer, T., Möller, I., Spalding, M., 2013. The Response of Mangrove Soil Surface Elevation to Sea Level Rise, Natural Coastal Protection Series: Report 3. Cambridge Coastal Research Unit Working Paper 42. .

69. Mesri, G., Godlewski, P.M., 1977. Time and Stress-Compressibility Interrelationship. ASCE J Geotech Eng Div, V. 103, No. 5, p. 417-430, doi# doi.org/10.1016/0148-9062(77)91005-1.

70. Mills, P., Moon, V., 2016. Static Failure Mechanisms in Sensitive Volcanic Soils in the Tauranga Region, New Zealand, 11th Australia and New Zealand Young Geotechnical Professionals Conference, Queenstown, New Zealand.

71. Mitchell, J.K., 1964. Shearing Resistance of Soils as a Rate Process. Journal of Soil Mechanics & Foundations Div, V. 90, No. SM1, p. 29-61, doi# Accession Number: 00264432.

72. Mitchell, J.K., Soga, K., 2005. Fundamentals of Soil Behavior. John Wiley and Sons, Inc, United States of America

73. Moernaut, J., Wiemer, G., Reusch, A., Stark, N., De Batist, M., Urrutia, R., de Guevara, B.L., Kopf, A., Strasser, M., 2017. The Influence of Overpressure and Focused Fluid Flow on Subaquatic Slope Stability in a Formerly Glaciated Basin: Lake Villarrica (South-Central Chile). Marine Geology, V. 383, No., p. 35-54, doi# doi.org/10.1016/j.margeo.2016.11.012.

74. Montgomery, J., Bryan, K., Horstman, E., Mullarney, J., 2018. Attenuation of Tides and Surges by Mangroves: Contrasting Case Studies from New Zealand. Water, V. 10, No. 9, p. 1119, doi# doi.org/10.3390/w10091119.

75. Moon, V., 2016. Halloysite Behaving Badly: Geomechanics and Slope Behaviour of Halloysite-Rich Soils. Clay minerals, V. 51, No. 3, p. 517-528, doi# doi.org/10.1180/claymin.2016.051.3.09.

76. Moon, V.G., Cunningham, M.J., Wyatt, J.B., Lowe, D.J., Morz, T., Jorat, M., 2013. Landslides in Sensitive Soils, Tauranga, New Zealand. Proc. 19th NZGS Geotechnical Symposium, V. 19, No. -, p., doi# -.

77. Moon, V.G., de Lange, W.P., Garae, C., Morz, T., Jorat, M., Kreiter, S., 2015. Monitoring the Landslide at Bramley Drive, Tauranga, Nz, 12th Australia New Zealand Conference on Geomechanics: ANZ 2015 Changing the Face of the Earth-Geomechanics and Human Influence, Wellington, New Zealand.

78. Moon, V.G., Lowe, D.J., Cunningham, M.J., Wyatt, J., Churchman, G., de Lange, W., Mörz, T., Kreiter, S., Kluger, M.O., Jorat, M.E., 2015. Sensitive Pyroclastic-Derived Halloysitic Soils in Northern New Zealand: Interplay of Microstructure, Minerals, and Geomechanics. Volcanic Rocks and Soils., V. 10.1201/b18897-3, No., p. 3-21, doi# 10.1201/b18897-3.

79. Morrisey, D.J., Swales, A., Dittmann, S., Morrison, M.A., Lovelock, C.E., Beard, C.M., 2010. The Ecology and Management of Temperate Mangroves. Oceanography and marine biology, V. 48, No., p. 43-160, doi# doi.org/10.1201/EBK1439821169-c2.

80. Mulhearn, P., 2002. Influences of Penetrometer Probe Tip Geometry on Bearing Strength Estimates for Mine Burial Prediction. Defence Science and Technology Organisation Canberra (australia), Fishermans Bend, Victoria 3207 Australia p. 27.

81. Mulukutla, G.K., Huff, L.C., Melton, J.S., Baldwin, K.C., Mayer, L.A., 2011. Sediment Identification Using Free Fall Penetrometer Acceleration-Time Histories. Marine Geophysical Research, V. 32, No. 3, p. 397-411, doi# doi.org/10.1007/s11001-011-9116-2.

82. Mumtaz, M.B., 2018. Investigation of Pore Pressures During High-Velocity Impact by a Free Fall Penetrometer. Virginia Tech, p. 73.

83. Neuzil, C., 1986. Groundwater Flow in Low-Permeability Environments. Water Resources Research, V. 22, No. 8, p. 1163-1195, doi# doi.org/10.1029/WR022i008p01163.

84. Nordlund, R., 1963. Bearing Capacity of Piles in Cohesionless Soils. Journal of the Soil Mechanics and Foundations Division, V. 89, No. 3, p. 1-36, doi# -.

85. Pallatt, N., Wilson, J., McHardy, B., 1984. The Relationship between Permeability and the Morphology of Diagenetic Illite in Reservoir Rocks. Journal of Petroleum Technology, V. 36, No. 12, p. 2,225-222,227, doi# doi.org/10.2118/12798-PA.

86. Pandit, N.S., Chaney, R.C., Fang, H.-Y., 1985. Review of Cavity Expansion Models in Soil and Its Applications. Current Practice in Geo. Engng, International Book Traders, Delhi, V. -, No., p. 35-53, doi# -.

87. Paniagua, P., Carroll, R., L'Heureux, J.-S., Nordal, S., 2016. Monotonic and Dilatory Excess Pore Water Dissipations in Silt Following Cptu at Variable Penetration Rate. 5th INTERNATIONAL CONFERENCE ON GEOTECHNICAL AND GEOPHYSICAL SITE CHARACTERISATION (ISC5), V. 5, No. 5, p., doi# hdl.handle.net/11250/2491806.

88. Parkes, E., 2019. Scientific Progress Is Built on Failure. nature https://www.nature.com/articles/d41586-019-00107-y.

89. Perlow, M., Richards, A.F., 1977. Influence of Shear Velocity on Vane Shear Strength. Journal of the Geotechnical Engineering Division, V. 103, No. 1, p. 19-32, doi# -.

90. Pfender, M., Villinger, H., 2002. Miniaturized Data Loggers for Deep Sea Sediment Temperature Gradient Measurements. Marine Geology, V. 186, No. 3-4, p. 557-570, doi# doi.org/10.1016/S0025-3227(02)00213-X.

91. Power, W., Downes, G., McSaveney, M., Beavan, J., Hancox, G., 2005. The Fiordland Earthquake and Tsunami, New Zealand, 21 August 2003, Tsunamis. Springer, p. 31-42, doi.org/10.1007/1-4020-3331-1_2.

92. Ramsey, N., 2002. A Calibrated Model for the Interpretation of Cone Penetration Tests (Cpts) in North Sea Quaternary Soils, Offshore Site Investigation and Geotechnics' Diversity and Sustainability'; Proceedings of an International Conference. Society of Underwater Technology, London, pp. 341-356.

93. Randolph, M., Hope, S., 2004. Effect of Cone Velocity on Cone Resistance and Excess Pore Pressures, Proc., Int. Symp. on Engineering Practice and Performance of Soft Deposits. Yodagawa Kogisha Co., Ltd., Osaka, Japan, pp. 147-152.

94. Randolph, M.F., Wroth, C., 1979. An Analytical Solution for the Consolidation around a Driven Pile. International Journal for Numerical and Analytical Methods in Geomechanics, V. 3, No. 3, p. 217-229, doi# doi.org/10.1002/nag.1610030302.

95. Raschke, S.A., Hryciw, R.D., 1997. Vision Cone Penetrometer for Direct Subsurface Soil Observation. Journal of geotechnical and geoenvironmental engineering, V. 123, No. 11, p. 1074-1076, doi# doi.org/10.1061/(ASCE)1090-0241(1997)123:11(1074).

96. Rattley, M., Richards, D., Lehane, B., 2008. Uplift Performance of Transmission Tower Foundations Embedded in Clay. Journal of geotechnical and geoenvironmental engineering, V. 134, No. 4, p. 531-540, doi# doi.org/10.1061/(ASCE)1090-0241(2008)134:4(531).

97. Richardson, A.M., Whitman, R.V., 1963. Effect of Strain-Rate Upon Undrained Shear Resistance of a Saturated Remoulded Fat Clay. Géotechnique, V. 13, No. 4, p. 310-324, doi# doi.org/10.1680/geot.1963.13.4.310.

98. Riggs, C., 1982. A Proposed Standard Test Method for a Free Fall Penetration Test. Geotechnical Testing Journal, V. 5, No. 3/4, p. 89-92, doi# doi.org/10.1520/GTJ10808J

99. Robertson, P., 2009. Interpretation of Cone Penetration Tests—a Unified Approach. Canadian Geotechnical Journal, V. 46, No. 11, p. 1337-1355, doi# doi.org/10.1139/T09-065.

100. Robertson, P., Cabal, K., 2010. Guide to Cone Penetration Testing. Gregg Drilling & Testing Inc, Signal Hill, California 90755.

101. Robertson, P., Sully, J., Woeller, D.J., Lunne, T., Powell, J., Gillespie, D., 1992. Estimating Coefficient of Consolidation from Piezocone Tests. Canadian Geotechnical Journal, V. 29, No. 4, p. 539-550, doi# doi.org/10.1139/t92-061.

102. Robertson, P.K., 1990. Soil Classification Using the Cone Penetration Test. Canadian Geotechnical Journal, V. 27, No. 1, p. 151-158, doi# doi.org/10.1139/t90-014.

103. Robertson, P.K., Campanella, R., Gillespie, D., Greig, J., 1986. Use of Piezometer Cone Data, Use of in situ tests in geotechnical engineering. ASCE, pp. 1263-1280.

104. Roskoden, R., 2016. Cone Penetration Tests the Soil Classification and Analytic Assessments of Dynamic and Static Penetrometer Test Data. Universität Bremen, Master Thesis, 2016, Bremen.

105. Roskoden, R., Kopf, A., Moon, V., Moerz, T., Kluger, M., unpublished. Evaluation of a New Dissipation Test Model with Field Data from a Slide Prone Coastal Area.

106. Roskoden, R., Kopf, A., Mörz, T., Kreiter, S., 2018. Analysis of Acceleration and Excess Pore Pressure Data of Laboratory Impact Penetrometer Tests in Remolded Overconsolidated Cohesive Soils, Cone Penetration Testing 2018. CRC Press, p. 545-550, -.

107. Roskoden, R., Moerz, T., Kluger, M., Moon, V., Kopf, A., under review. Evaluation of a New Dissipation Test and Model with Field Data from the Bramley Drive Landslide Area, Omokoroa, New Zealand.

108. Roskoden, R.R., Bryan, K.R., Schreiber, I., Kopf, A., 2019. Rapid Transition of Sediment Consolidation across an Expanding Mangrove Fringe in the Firth of Thames, New Zealand. V. -, No. 40, p. 295-308, doi# doi.org/10.1007/s00367-019-00589-9.

109. Salgado, R., Prezzi, M., Kim, K., Lee, W., 2013. Penetration Rate Effects on Cone Resistance Measured in a Calibration Chamber, 4th International Conference on Site Characterization, ISC'4, pp. 1025-1030

110. Sandven, R., 2010. Influence of Test Equipment and Procedures on Obtained Accuracy in Cptu, 2nd International Symposium on Cone Penetration Testing.

111. Sanglerat, G., 1973. The Penetrometer and Soil Exploration. Soil Science, V. 116, No. 2, p. 131, doi# -.

112. Schofield, A., Wroth, P., 1968. Critical State Soil Mechanics. McGraw-Hill London.

113. Seifert, A., 2011. In Situ Detection and Characterisation of Fluid Mud and Soft Cohesive Sediments by Dynamic Piezocone Penetrometer Testing, Marine Geotechnics. Bremen University Bremen, p. 180.

114. Seifert, A., Stegmann, S., Mörz, T., Lange, M., Wever, T., Kopf, A., 2008. In Situ Pore-Pressure Evolution During Dynamic Cpt Measurements in Soft Sediments of the Western Baltic Sea. Geo-Marine Letters, V. 28, No. 4, p. 213-227, doi# doi.org/10.1007/s00367-008-0102-x.

115. Shepherd, R.G., 1989. Correlations of Permeability and Grain Size. Groundwater, V. 27, No. 5, p. 633-638, doi# doi.org/10.1111/j.1745-6584.1989.tb00476.x.

116. Smalley, I., Ross, C.W., Whitton, J., 1980. Clays from New Zealand Support the Inactive Particle Theory of Soil Sensitivity. Nature, V. -, No. -, p. 576–577, doi# doi.org/10.1038/288576a0.

117. Stark, N., 2011. Geotechnical Investigation of Sediment Remobilization Processes Using Dynamic Penetrometers, Marine Geotechnics. Universität Bremen, Bremen, p. 309.

118. Stark, N., Hay, A.E., Trowse, G., 2014. Cost-Effective Geotechnical and Sedimentological Early Site Assessment for Ocean Renewable Energies, Oceans-St. John's, 2014. IEEE, pp. 1-8.

119. Stark, N., Kopf, A., 2011. Detection and Quantification of Sediment Remobilization Processes Using a Dynamic Penetrometer, OCEANS'11 MTS/IEEE KONA. IEEE, pp. 1-9.

120. Stark, N., Kopf, A., Hanff, H., Stegmann, S., Wilkens, R., 2009. Geotechnical Investigations of Sandy Seafloors Using Dynamic Penetrometers, OCEANS 2009. IEEE, pp. 1-10.

121. Stark, N., Wever, T.F., 2009. Unraveling Subtle Details of Expendable Bottom Penetrometer (Xbp) Deceleration Profiles. Geo-Marine Letters, V. 29, No. 1, p. 39-45, doi# doi.org/10.1007/s00367-008-0119-1.

122. Stark, N., Ziotopoulou, K., 2017. Undrained Shear Strength of Offshore Sediments from Portable Free Fall Penetrometers: Theory, Field Observations and Numerical Simulations, Offshore Site Investigation Geotechnics 8th International Conference Proceeding. Society for Underwater Technology, pp. 391-399.

123. Stegmann, S., 2007. Design of a Free-Fall Penetrometer for Geotechnical Characterisation of Saturated Sediments and Its Geological Application, Marine Geotechnics. Universität Bremen, p. 181.

124. Stegmann, S., Mörz, T., Kopf, A., 2006. Initial Results of a New Free Fall-Cone Penetrometer (Ff-Cpt) for Geotechnical in Situ Characterisation of Soft Marine Sediments. Norwegian Journal of Geology/Norsk Geologisk Forening, V. 86, No. 3, p. 199-208, doi# PANGAEA reference ID: 27196 Serial: RCOM0398.

125. Steiner, A., 2013. Sub-Seafloor Characterization and Stability of Submarine Slope Sediments Using Dynamic and Static Piezocone Penetrometers, Marine Geotechnics. Universität Bremen, Bremen, p. 325.

126. Steiner, A., L'Heureux, J.-S., Kopf, A., Vanneste, M., Longva, O., Lange, M., Haflidason, H., 2012. An in-Situ Free-Fall Piezocone Penetrometer for Characterizing Soft and Sensitive Clays at Finneidfjord (Northern Norway), Submarine Mass Movements and Their Consequences. Springer, Dordrecht, p. 99-109, doi.org/10.1007/978-94-007-2162-3_9

127. Stephan, S., 2015. A Rugged Marine Impact Penetrometer for Sea Floor Assessment. Universität Bremen, , Bremen,, p. 268.

128. Stoll, R.D., Akal, T., 1999. Xbp- Tool for Rapid Assessment of Seabed Sediment Properties. Sea technology, V. 40, No. 2, p. 47-52, doi# ISI:000079003400006.

129. Stoll, R.D., Sun, Y.-F., Bitte, I., 2007a. Seafloor Properties from Penetrometer Tests. IEEE Journal of Oceanic Engineering, V. 32, No. 1, p. 57-63, doi# doi.org/10.1109/joe.2007.890943.

130. Stoll, R.D., Sun, Y.F., Bitte, I., 2007b. Seafloor Properties from Penetrometer Tests. IEEE Journal of Oceanic Engineering, V. 32, No. 1, p. 57-63, doi# 10.1109/Joe.2007.890943.

131. Strout, J.M., Tjelta, T.I., 2005. In Situ Pore Pressures: What Is Their Significance and How Can They Be Reliably Measured? Marine and Petroleum Geology, V. 22, No. 1-2, p. 275-285, doi# doi.org/10.1016/j.marpetgeo.2004.10.024.

132. Sully, J.P., Robertson, P.K., Campanella, R.G., Woeller, D.J., 1999. An Approach to Evaluation of Field Cptu Dissipation Data in Overconsolidated Fine-Grained Soils. Canadian Geotechnical Journal, V. 36, No. 2, p. 369-381, doi# doi.org/10.1139/t98-105.

133. Swales, A., Bentley Sr, S.J., Lovelock, C.E., 2015. Mangrove-Forest Evolution in a Sediment-Rich Estuarine System: Opportunists or Agents of Geomorphic Change? Earth Surface Processes and Landforms, V. 40, No. 12, p. 1672-1687, doi# doi.org/10.1002/esp.3759.

134. Swales, A., Denys, P., Pickett, V.I., Lovelock, C.E., 2016. Evaluating Deep Subsidence in a Rapidly-Accreting Mangrove Forest Using Gps Monitoring of Surface-Elevation Benchmarks and Sedimentary Records. Marine Geology, V. 380, No., p. 205-218, doi# doi.org/10.1016/j.margeo.2016.04.015.

135. Teh, C.I., Houlsby, G.T., 1991. An Analytical Study of the Cone Penetration Test in Clay. Géotechnique, V. 41, No. 1, p. 17-34, doi# doi.org/10.1680/geot.1991.41.1.17.

136. Terzaghi, K., 1943. Theoretical Soil Mechanics. JohnWiley & Sons, New York.

137. Terzaghi, K., Peck, R.B., Mesri, G., 1996. Soil Mechanics in Engineering Practice. John Wiley & Sons, United States of America

138. Torstensson, B.-A., 1977. The Pore Pressure Probe. Nordiske Geotekniske M* te, V., No., p. 1-15, doi#.

139. Tsaparas, I., Rahardjo, H., Toll, D.G., Leong, E.C., 2002. Controlling Parameters for Rainfall-Induced Landslides. Computers and geotechnics, V. 29, No. 1, p. 1-27, doi# doi.org/10.1016/S0266-352X(01)00019-2.

140. Vesic, A.S., 1972. Expansion of Cavities in Infinite Soil Mass. Journal of Soil Mechanics & Foundations Div, V. 98, No. 3, p. 265-290, doi# Accession Number: 00236349.

141. Wesley, L., 1977. Shear Strength Properties of Halloysite and Allophane Clays in Java, Indonesia. Géotechnique, V. 27, No. 2, p. 125-136, doi# doi.org/10.1680/geot.1977.27.2.125.

142. Young, A.G., Bernard, B.B., Remmes, B.D., Babb, L., Brooks, J.M., 2011. Cpt Stinger-an Innovative Method to Obtain Cpt Data for Integrated Geoscience Studies, Offshore Technology Conference. Offshore Technology Conference, -, pp. 1-10.

143. Zhou, Z., van der Wegen, M., Jagers, B., Coco, G., 2016. Modelling the Role of Self-Weight Consolidation on the Morphodynamics of Accretional Mudflats. Environmental Modelling & Software, V. 76, No. -, p. 167-181, doi# doi.org/10.1016/j.envsoft.2015.11.002.